Exon, N.F., Kennett, J.P., Malone, M.J., et al., 2001
Proceedings of the Ocean Drilling Program, Initial Reports Volume 189

3. SITE 1168[1]

Shipboard Scientific Party[2]

PRINCIPAL RESULTS

Site 1168 is located in middle bathyal water depths (2463 m) on the 4° slope of the western margin of Tasmania (70 km from coast) in a 25-km-wide strike-slip basin between upthrown northwest-trending ridges of Cretaceous rocks. The western Tasmania onshore margin was uplifted during the late Paleocene and early Eocene (O'Sullivan and Kohn, 1997), and this uplift and the strike-slip motion were probably coeval. The site is 80 km southeast of Deep Sea Drilling Project (DSDP) Site 282, which is located in deeper water and on a structural high. It lies north of the oceanographic Subtropical Front. Site 1168 was planned to penetrate marine rift to open-margin sediments deposited from the Eocene onward as Australia moved northward from Antarctica. Initially, the site was at the far eastern end of the restricted Australo-Antarctic Gulf and separated from the Pacific Ocean by the Tasmanian land bridge. Plate movements and related margin subsidence led to its Neogene location in open water facing a broad Southern Ocean. The primary objectives were to core and log (1) a prograding detrital sequence, formed during Eocene opening of the ocean south of Australia, for its paleoceanographic, paleoclimatic, and biotic history, (2) an Oligocene to present-day pelagic carbonate sequence for better understanding of the evolution of the Southern Ocean during its expansion in the Cenozoic and for high-resolution paleoclimatic studies, and (3) a Cenozoic sequence for high-resolution biostratigraphic studies.

Seismic profiles suggest that the site was subject to downslope sediment movement to the northwest in the Paleogene but was protected from downslope movement from the east in much of the Neogene by the upslope high (Fig. F1). The Paleocene and Eocene sediments prograde to the northwest, and the drilled late Eocene is hummocky in the southwest–northeast section, with ridges and troughs 0.5–1 km across,

F1. Postdrilling interpretation for local seismic profile SO36-47, across Site 1168, showing broad ages and lithostratigraphic units, p. 57.

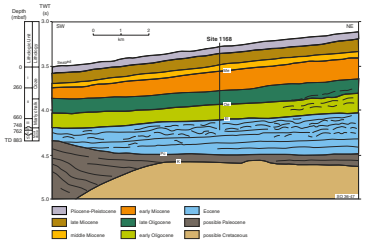

[1]Examples of how to reference the whole or part of this volume.
[2]Shipboard Scientific Party addresses.

Ms 189IR-103

suggesting deltaic lobes. Younger sequences are poorly parallel bedded and almost transparent seismically.

We cored two advanced hydraulic piston corer/extended core barrel corer (APC/XCB) holes, and a third hole with just the APC, at Site 1168. Hole 1168A reached 883.5 mbsf with 98% recovery (Table T2, p. 94, in the "Leg 189 Summary" chapter). Hole 1168B was APC cored to 108.4 mbsf with 98.3% recovery, and Hole 1168C reached 290.5 mbsf with 85.4% recovery. Wireline logging was conducted in Hole 1168A with the triple-combination (triple-combo) tool string (877 to 101 mbsf) and the geological high-sensitivity magnetic tool (GHMT)-sonic tool string (730 to 102 mbsf). A bridge prevented running the GHMT-sonic tool string to the base of the cored interval, and we chose not to run the Formation MicroScanner (FMS) because of the poor hole conditions.

Construction of a composite section of the triple-cored portion of the sedimentary sequence (~110 mbsf) indicates that there are no stratigraphic gaps to that depth. Beyond that, there are limited gaps, but overall core recovery averaged 93%, producing an excellent record of near-continuous deposition since the early late Eocene. Biostratigraphy indicates no major time breaks. Sedimentation rates were relatively low throughout (6.9–1.5 cm/k.y.) for a margin setting close to land. The drilled sequence broadly consists of 260 m of nannofossil ooze of middle Miocene and younger age (lithostratigraphic Unit I); 400 m of clayey chalk, nannofossil siltstone, and sandstone of early Miocene and Oligocene age (Unit II); and 220 m of shallow-marine carbonaceous mudstone and sandstone (Units III–V) of late Eocene age.

Lithostratigraphic Unit I (0–260 mbsf) was subdivided into two subunits: Subunit IA to 45 mbsf and Subunit IB to 260 mbsf. Subunit IA is light greenish gray foraminifer-bearing nannofossil ooze with minor calcareous turbidite sands, and Subunit IB is white nannofossil ooze. Carbonate content averages 90 wt%, and magnetic susceptibility and organic carbon content are both very low. Calcareous microfossils are abundant and little altered, benthic foraminifers are always present, dinoflagellate cysts are absent only in the middle Miocene, and radiolarians and diatoms are common in the upper Miocene. Microfossil ages (early middle Miocene to Pleistocene) show that average sedimentation rates were low at 1.65 cm/k.y. Deposition was in middle bathyal depths in well-oxygenated bottom waters.

Lithostratigraphic Unit II (260–660 mbsf) has three subunits: Subunit IIA to 410 mbsf, Subunit IIB to 540 mbsf, and Subunit IIC to 660 mbsf. These three olive-gray subunits become darker and more clayey and silty downward. Calcareous microfossils are abundant and little altered in the Miocene and moderately preserved in the upper Oligocene. Dinoflagellates and benthic foraminifers are pervasive, radiolarians are uncommon, and diatoms rarely present. Microfossil ages (late Oligocene to early middle Eocene) show that sedimentation rates were higher, averaging 4.3 cm/k.y. through the Miocene and late Oligocene. Deposition was bathyal with variation in the oxygenation of bottom waters. Visible bubbling in the cores and high methane content in headspace and vacutainer samples indicate production of biogenic gas in the upper part of the unit. An association with reduced pore-water chlorinity may indicate the presence of gas hydrates, but well-log results are inconclusive. Nevertheless, the presence of fluid escape structures (soft-sediment deformation) in Subunit IIA suggests that hydrates may indeed have been present in the past.

Subunit IIA consists of clay-bearing nannofossil chalk to nannofossil claystone. Carbonate content averages 40 wt%, magnetic susceptibility

is moderate, and the organic carbon content is low. Subunit IIB consists of nannofossil claystone and nannofossil-bearing claystone. Carbonate content averages 30 wt%, magnetic susceptibility is moderate, and the organic carbon content is low. Subunit IIC consists of silty nannofossil chalk to nannofossil siltstone. Carbonate content averages 40 wt%, magnetic susceptibility is fairly low, and organic carbon content is low.

Lithostratigraphic Unit III (660–748.6 mbsf) has two subunits: Subunit IIIA to 725 mbsf and Subunit IIIB to 748.6 mbsf. These two olive-gray units become darker downward. They contain calcareous microfossils that are abundant but only moderately preserved. Dinocysts and benthic foraminifers are persistent and radiolarians are uncommon. Microfossil ages indicate very low sedimentation rates in the early Oligocene. The environment of deposition was bathyal marine in a relatively tranquil environment. Carbonate content is variable but averages 20–30 wt%, magnetic susceptibility is moderate, and organic carbon content is low. Subunit IIIA consists of clayey nannofossil chalk to nannofossil-bearing organic clayey siltstone. Subunit IIIB consists of organic-bearing silty claystone and organic clayey siltstone.

Lithostratigraphic Units IV and V (748.6–883.5 mbsf) form an upper Eocene package of related sediments. These two units are dark gray to black. Carbonate content is low, magnetic susceptibility is moderate but variable, and the organic carbon content is as high as 5 wt%. Dinocysts are rare but spores and pollen are abundant, and the abundant dispersed organic matter is dominantly from land plants. Geochemical and micropaleontological evidence suggests periodic brackish conditions, with normal marine salinities at other times. Characterization of the organic matter indicates that it is largely terrigenous in origin and is immature, but with increasing maturity toward the base of the hole (i.e., approaching the oil window).

Two nannofossil datums give average sedimentation rates of 6.9 cm/k.y. Calcareous microfossils are sporadic, rarer downward, and moderately to poorly preserved. Agglutinating benthic foraminifers are sporadic. The environment of deposition was reducing, shelfal marine, and protected from currents and waves. Evidence from palynology suggests a subtropical to temperate climate, with a terrestrial plant assemblage containing abundant ferns. Calcareous nannofossils are represented by a warm-water assemblage containing warmer water elements than those previously found elsewhere at equivalent latitudes in the Southern Ocean. Plate reconstructions suggest that the Kerguelen Plateau may have been shielding the Australo-Antarctic Gulf from cold water from the west so that the only water entering the gulf came from warmer areas north of western Australia.

Lithostratigraphic Unit IV (748.6–762 mbsf) consists of dark gray glauconitic, quartzose sandstone, and clayey siltstone, with interbedded black carbonaceous silty claystone. Thin calcareous stringers contain microfossils. Both glauconite and quartz are fine to very coarse grained, and the quartz is subangular. Microfossil ages within this Eocene–Oligocene transition indicate low sedimentation rates during deposition of glauconite layers because of intensified bottom-water activity leading to winnowing. A condensed section with possible brief hiatuses is indicated.

Lithostratigraphic Unit V (762–883.5 mbsf) consists of black carbonaceous silty claystone and clayey siltstone and is finely laminated in part. Pyritic replacements of burrows and fossils are common. There are rare, thin lenses of rippled fine sand, and thin calcareous stringers contain microfossils.

In summary, the sediment sequence records paleoenvironmental changes, beginning with a shallow-water, nearshore, restricted basinal setting with poor ventilation and siliciclastic sedimentation, low oxygenation, and high organic carbon deposition. Site 1168 Eocene sediments, similar to those at DSDP Site 282 to the northwest and DSDP Site 280 just south of the South Tasman Rise, suggest widespread late Eocene anoxic conditions in the eastern Australo-Antarctic Gulf. Following a transitional phase during the Oligocene, by the Neogene these conditions had been replaced by deposition of carbonate ooze in a well-oxygenated, open ocean on a passive margin at middle bathyal depths.

The succession of sediment, climatic, and biotic changes recorded at Site 1168 reflects the three major steps in Cenozoic climate state determined by earlier researchers: "Greenhouse" in the late Eocene; "Doubthouse" of intermediate mode in the Oligocene through early Miocene; and "Icehouse" since the middle Miocene. Relatively rapid changes mark the boundaries at the Eocene–Oligocene transition and during the middle Miocene at ~14 Ma. The most conspicuous change in the sediment and biotic sequence occurred during the transition from the Eocene to the early Oligocene, with conspicuous reduction in sedimentation rates and deposition of glauconite sands. This transition reflects a transient event associated with temporarily increased bottom-water activity in the basin. The timing of this episode is consistent with the hypothesis linking the initial opening of the Tasmanian Gateway, major cooling of Antarctica and associated cryospheric development. The changes are documented in part by excellent microfossil sequences of calcareous nannofossils, planktonic and benthic foraminifers, and dinocysts after the late Eocene. Spores and pollen are abundant in the upper Eocene, fewer in the lower Oligocene, and intermittently present in younger sequences. Major biostratigraphic achievements will be the first comprehensive Cenozoic zonations for the cool temperate region south of Australia for planktonic foraminifers, calcareous nannofossils, and dinoflagellates.

BACKGROUND AND OBJECTIVES

Site 1168 is located in middle bathyal (2463 m) water depths on the continental slope of western Tasmania (Fig. **F3,** p. 68, in the "Leg 189 Summary" chapter). The site is 70 km to the west of the central Tasmanian coast and 70 km to the east of the boundary of the abyssal plain, which lies at a depth of 4500 m. The site is thus at mid depths between continent and abyssal plain but lies above continental crust. The site was selected at the intersection of reflection seismic lines *Tasmante* 125-52 and *Sonne* SO36B-47 (Fig. **F2**). Site 1168 represents a near-continuous sediment record (883.5 m) from the early late Eocene to the present. This constitutes a moderately transparent sequence of Quaternary to Oligocene calcareous pelagic sediments, seismically 0.8 s thick, and an underlying hummocky sequence of siliciclastic sediments ~0.2 s thick, of which the more uniform upper ~0.12 s was drilled.

The present western Tasmania margin was part of the east Gondwana supercontinent until Australia separated from Antarctica during the Late Cretaceous through early Cenozoic. Early separation from the Cretaceous through the middle Eocene, forming the Australo-Antarctic Gulf, was associated with the movement of the western Tasmania margin in a northwest direction. This was followed by north-south movement that had little effect on the margin on which this site is located.

F2. A portion of the seismic line *Sonne* SO36-47 through Site 1168, p. 58.

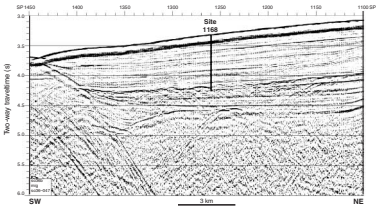

The present structures of the margin were formed by northwest-southeast strike-slip faulting during the Maastrichtian to Paleocene (Hill et al., 1997). A broad epicontinental basin lay between Tasmania and Antarctica from the Cretaceous to the early Paleocene (see Figs. **F24,** p. 90, **F25,** p. 91, **F26,** p. 92, in the "Leg 189 Summary" chapter). The strike-slip motion dissected this basin into a series of narrow northwest-southeast–trending strike-slip basins during the Paleocene. This formed a margin in the Paleogene with characteristics similar to those of the Neogene borderland province of southern California (see Figs. **F6,** p. 71, **F7,** p. 72, in the "Leg 189 Summary" chapter). The Californian borderland is made up of a number of semi-isolated basins interconnected by shallow sills representing the structural highs. There, the inner basins trap much of the coarser sediments derived from the continent so that the outer basins are increasingly less influenced by sediment gravity flows and are starved of coarse siliciclastic sediments. In contrast, the inner basins are increasingly isolated from the open ocean, which reduces ventilation and decreases oxygen concentrations in deep basinal waters.

The seismic stratigraphy of the western Tasmania margin (Fig. **F3**) shows that sedimentation continued within a succession of narrow, fault-bounded basins for much of the remaining Cenozoic (see Fig. **F18**). Site 1168 is located in one such basin, 20 km wide, midway across the continental borderland. Thus, the basin was partially isolated from major terrigenous sediment input and downslope sediment transport during much of the Cenozoic, and it was sufficiently isolated from the open ocean to be poorly ventilated. Seismic evidence indicates that Paleogene sediments sloped gently down toward the northwest as indicated by progradation in the Paleocene–Eocene sequence. The sea would have transgressed southeastward upslope within this basin during the Paleogene. Deposition of the post-Eocene sequence occurred during major subsidence of the western Tasmania margin. This subsidence commenced in the early Oligocene once the southern part of the South Tasman Rise moved sufficiently far north to clear the Antarctic continent. Subsidence has continued during the flight of Australia northward away from Antarctica. Margin subsidence was greater with increasing distance from Tasmania. Basinal filling at Site 1168 occurred during subsidence so that by the latest Neogene sediments moving downslope from shallower waters were no longer blocked by the fault-bounded highs. Site 1168 clearly records Cenozoic subsidence, with sediments deposited in upper bathyal to shelfal depths (>~100 m) in the late Eocene and in middle bathyal depths (~2500 m) in the present day.

The primary objectives of Site 1168 include

1. Coring and logging of a prograding detrital sequence, formed during the Eocene opening of the ocean south of Australia, for its paleoceanographic, paleoclimatic, and biotic history;
2. Coring and logging of an Oligocene to present-day pelagic carbonate sequence for better understanding of the evolution of the Southern Ocean expansion during the Cenozoic and for high-resolution paleoclimatic studies; and
3. Coring of a Cenozoic sequence for high-resolution biostratigraphic studies.

Site 1168 is one of a suite of four sites drilled during Leg 189, designed to advance understanding of circumpolar oceanographic and climatic

F3. Regional cross section through time across Site 1168, p. 59.

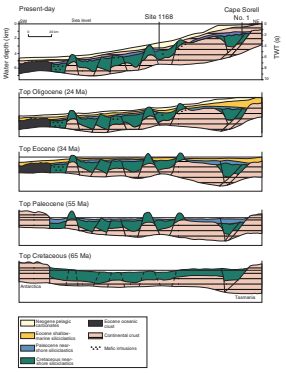

evolution as a result of the northward expansion of the Southern Ocean and the development of the Tasmanian Seaway. This site was selected to provide vitally required information on the changing paleoenvironmental conditions on the northwest side of the Tasmanian gateway as the seaway opened during the Paleogene and then expanded during the rest of the Cenozoic. Its location away from the gateway suggested that, importantly, this site would yield a more complete stratigraphic record than the others. Paleoenvironmental conditions were expected to have undergone dramatic evolution during the Cenozoic in response to plate tectonism. Earlier drilling at DSDP Site 282, just 80 km northwest of Site 1168, revealed an upward progression from a poorly ventilated margin with subdued current activity and dominant terrigenous sedimentation in the upper Eocene section. This changed to increasingly biogenic sedimentation in ventilated conditions during the late Paleogene and early Oligocene, as the margin was influenced by more open ocean conditions. Finally, the sedimentary sequence was exposed to strong current activity with the intensification of the circumpolar circulation. However, much of the Site 282 sequence was poorly cored or absent in unconformities.

It is clear that the western Tasmania margin during the Eocene and early Oligocene was located at the far eastern end of a relatively narrow gulf extending ~2500 km across the full extent of Australia, which we here name the Australo-Antarctic Gulf. The steadily opening gulf was ~800 km wide at the end of the Eocene. Circulation in the eastern Gulf would have been highly restricted, leading to the poorly ventilated margin in which Site 1168 is located. Plate reconstructions show that Site 1168 was at ~60°S in the late Eocene (Cande et al., 2000). This situation contrasts with that of the present-day, in which the margin, at 42°S, is in a fully open ocean, is extremely well ventilated, and faces westward toward the vastness of the northern part of the Southern Ocean. In the last 45 m.y., almost everything has changed drastically on the margin at Site 1168, including tectonism, structure, water depth, ventilation, sediments, biogenic components, water temperature, and geochemistry. Site 1168 was cored to document these changes and provide a basis for understanding their causes.

OPERATIONS

Leg 189 began at 2000 hr on 11 March 2000 when the first line was passed ashore at Macquarie Wharf, Hobart, Tasmania. At 1224 hr on 16 March, after an ~4 day port call, the last line was released from the pier and the ship was maneuvered into the harbor.

Transit from Hobart to Site 1168

The 208-nmi transit to Site 1168 was accomplished at an average speed of 10.6 kt. During this transit there was a moderate amount of rolling caused by a 3- to 4-m westerly swell. Because the vessel pursued a northwest heading to the site, the swell was directly on the port beam and generated rolls as large as 10°. Upon arriving at the coordinates for the site, a beacon was deployed at 0800 hr on 17 March.

Hole 1168A

After the hydrophones and thrusters were extended and the vessel settled on location, the corrected precision depth recorder (PDR) depth referenced to the dual elevator stool was obtained and indicated 2479.4 m below the rig floor (mbrf). Hole 1168A was spudded with the APC at 1715 hr on 17 March. The seafloor depth was calculated from the recovery of the first core and determined to be 2474.2 mbrf, or 2463 mbsl.

Piston coring advanced to 111.8 mbsf. Piston cores were oriented starting with Core 3H, and heat-flow measurements were obtained at 45.3, 64.3, 92.8, and 111.8 mbsf. The average recovery of the piston-cored region was 103%. There were two minor incidents involving the wireline during piston coring in Hole 1168A. When vessel heave caused the overshot shear pin to part, it required an extra wireline trip to recover Core 5H. While attempting to recover Core 10H, the wireline came apart at the rope socket. This required one trip in with a wireline fishing tool, which succeeded in recovering the Tensor tool carrying case and core barrel on the first attempt. Subsequent to a full stroke, the core barrel for Core 12H required drilling over to free the hardware from the sediments.

Consequently, we switched to the XCB system and the hole was deepened from 111.8 mbsf to refusal depth (883.5 mbsf) (Table T1), which was the depth objective of the previously planned rotary hole. The average recovery of the XCB portion was 94%. During XCB coring, coring operations almost had to be stopped on 19 and 20 March when a complex long period (13 s) swell generated vessel-heave values of 6 m or more. Because of the long period of the swell, the passive heave compensator was able to handle the vertical excursions and coring continued.

T1. Coring summary, p. 119.

Throughout most of the XCB coring, the average rate of penetration (ROP) was 31 m/hr. The ROP slowed dramatically below 848 mbsf. From a depth of 848 mbsf to the bottom of the hole at 884 mbsf, the ROP gradually decreased from 6.5 to 2.9 m/hr. Because of the diminishing returns of continued coring, the hole was terminated and preparations were made for logging.

Hole 1168A was logged with the triple combination (triple combo) tool and the GHMT-sonic tool strings. During the triple-combo tool string run, the bit was positioned at 108 mbsf and was raised to 101 mbsf during logging. The first pass covered 877 to 101 mbsf, and a repeat run was made from 301 to 201 mbsf. The data indicated that hole conditions were poor with an uneven and rugged borehole wall. The borehole width commonly exceeded 19 in, but in places was as narrow as 4 in. Because there were many narrow spots, a wiper trip was conducted before the deployment of the second logging tool suite.

During the GHMT-sonic run, the bit was placed at 110 mbsf and was pulled up to 100 mbsf during logging. The main pass of the logging tool covered 730 to 102 mbsf, and a repeat run was conducted from 376 to 245 mbsf. It was not possible to get the tool string past a bridge at 730 mbsf, and as a consequence, the bottom 150 m of the hole could not be logged. In view of the scientific importance of the base of the hole and the poor hole conditions, it was decided that a second attempt to log the lower portion of the hole with the GHMT-sonic was more important than running the FMS. Accordingly, another wiper trip was made and the bit was set at 666 mbsf. Unfortunately, it was still not possible to get any deeper and logging was discontinued. After the logging

equipment was demobilized, the bit was pulled back and cleared the seafloor at 2215 hr on 24 March, ending Hole 1168A.

Hole 1168B

The vessel was offset 20 m north of Hole 1168A, and Hole 1168B was spudded with the APC at 0130 hr on 25 March. Based on recovery of the mudline core, the seafloor depth was estimated to be 2463.6 mbsl, or within 0.2 m of the calculated depth of Hole 1168A. Piston coring advanced to 108.4 mbsf with an average recovery of 98%. Cores were oriented beginning with Core 3H. After Core 12H was obtained, the bit was pulled clear of the seafloor at 1215 hr on 25 March, ending Hole 1168B.

Hole 1168C

After the vessel was offset 20 m north of Hole 1168B, Hole 1168C was spudded with the APC at 1330 hr. Piston coring was initiated and advanced to 114.0 mbsf with an average recovery of 96%. Cores were oriented starting with Core 3H. The hole was deepened with the XCB to 290.5 mbsf when the available operational time expired. The average recovery for Hole 1168C was 85%. The average recovery for the entire site was 93%, representing a total of 1192 m of core.

Following the retrieval of the last core barrel, the drill string was recovered and the bottom-hole assembly was dismantled in anticipation of the transit to Hobart to transfer two personnel and some light cargo. Concurrent with the recovery of the drill string, the beacon was successfully retrieved. After the hydrophones and thrusters were retracted and drilling equipment secured, the vessel was under way at 2100 hr on 26 March.

LITHOSTRATIGRAPHY

A nearly continuous 883.5-m-thick section, drilled at three holes at Site 1168, contains a wide range of sediment types, from calcareous biogenic ooze and chalk to siliciclastic claystone and siltstone (Fig. F4). The calcareous biogenic components (nannofossils and foraminifers) predominate from the surface to 260 mbsf (Core 189-1168A-28X), where siliciclastic clay-sized particles first appear. These clays are associated with siliciclastic silty particles below 530 mbsf (Core 189-1168A-56X). Below 750 mbsf (Core 189-1168A-79X), the sediment consists essentially of siliciclastic silt and clay particles.

The sedimentary sequence has been divided into five units, based on lithologic variability. Lithostratigraphic units (Fig. F5) were defined by consideration of core features, smear slides, thin sections, coulometric carbonate analyses, reflectance spectrophotometry, and magnetic susceptibility data. A significant correlation exists between spectrophotometry data (lightness) and coulometric carbonate contents (Fig. F6), indicating that the color of the sediment at Site 1168 is strongly linked to its content in calcareous biogenic, organic, and siliciclastic particles. Although correlation between coulometric analysis and smear-slide observations proved adequate for predominantly calcareous biogenic and siliciclastic sediments, in transitional carbonate sediments an offset exists between quantitative carbonate content and smear-slide estimates (which underestimate the amount of clay-sized siliciclastics). Coulom-

F4. Lithologic units and chronology, p. 60.

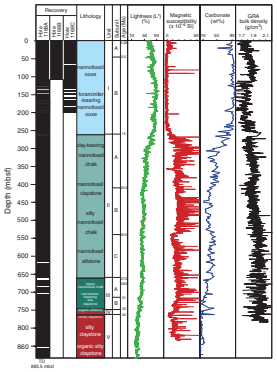

F5. Lithostratigraphic summary, p. 61.

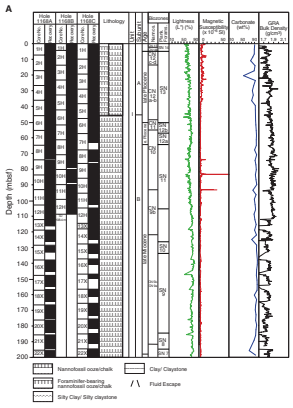

F6. Correlation between lightness and coulometric carbonate data, Hole 1168A, p. 66.

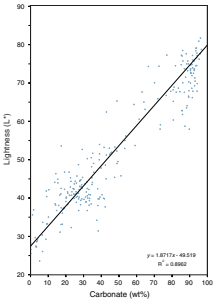

etric carbonate data and visual inspection of the cores provide basic information for determining units and subunits. Smear-slide observations (Fig. F7) were used to describe the lithology from the barrel sheets. Lithostratigraphic units of Site 1168 are compared to those of DSDP Site 282, drilled nearby (Kennett, Houtz, et al., 1975).

Lithostratigraphic Unit I, 260 m thick, is composed of biogenic ooze and chalk divided into two subunits. Subunit IA, 45 m thick, is composed of light greenish gray nannofossil ooze and foraminifer-bearing nannofossil ooze containing macrofossil bioclasts and layers of foraminiferal sand. Carbonate content varies from 75 to 90 wt%. This subunit ranges in age from late Pliocene to the Pleistocene and may correspond to Unit I of DSDP Site 282. Subunit IB, 215 m thick, consists of white nannofossil ooze and foraminifer-bearing nannofossil ooze to chalk, with 85 to 97 wt% carbonate. This subunit ranges in age from middle Miocene to early Pliocene and may correlate to Unit II of DSDP Site 282.

Unit II, 400 m thick, is characterized by siliciclastic clay particles increasing downhole and significant occurrences of silt particles and contains three subunits. Subunit IIA, 150 m thick, ranges from greenish gray clay-bearing nannofossil chalk to nannofossil claystone. Its carbonate content decreases from 75 wt% in the upper part to 30 wt% in the lower part of the subunit. Subunit IIA is early to middle Miocene in age and may correspond to Unit III of DSDP Site 282. Subunit IIB, 130 m thick, includes mostly nannofossil claystone and nannofossil-bearing claystone and is greenish gray to dark greenish gray in color. The carbonate content varies from 10 to 35 wt%. This subunit is late Oligocene in age and may correlate to Unit IV of DSDP Site 282. Subunit IIC, 120 m thick, ranges from silty nannofossil chalks to nannofossil siltstone. The color varies from greenish gray and dark greenish gray to dark gray and olive gray. The carbonate content fluctuates from 18 to 42 wt%. This subunit is early to late Oligocene in age and may correlate to Unit V of DSDP Site 282.

Unit III, 88.6 m thick, is characterized by a variety of pure and mixed siliciclastic sediments and is divided into two subunits. Subunit IIIA, 54 m thick, is early Oligocene in age and varies from clayey nannofossil chalk to nannofossil-bearing silty claystone and nannofossil-bearing organic clayey siltstone. The carbonate content ranges from 0 to 35 wt%, and the color ranges from greenish gray to dark greenish gray. Subunit IIIB, 34.6 m thick, is early Oligocene in age and consists of organic-bearing silty claystone, organic clayey siltstone, and sandy claystone. Sandy layers, shell debris, and pyrite concretions are locally present. The carbonate contents vary from 2 to 18 wt%, and color ranges from dark olive gray and dark gray brown to black. Unit III may correspond to Unit VI of DSDP Site 282.

Unit IV, 13.4 m thick, is latest Eocene to earliest Oligocene in age and is composed of alternating dark grayish brown organic-bearing silty claystone and dark greenish gray glauconite-rich clayey siltstone. This unit is characterized by distinct fluctuations of the carbonate content, from 3 to 38 wt%.

Unit V, 121.5 m thick, is characterized by abundant organic matter and very low carbonate contents (below 8 wt%). This unit ranges from nannofossil-bearing silty claystone to organic silty claystone and clayey siltstone. Unit V is of late Eocene age and may correlate to Unit VII of DSDP Site 282.

Sediments of Site 1168 are generally slightly to moderately disturbed by the drilling process in the APC section. Additional sediment distur-

F7. Sediment composition, Hole 1168A, p. 67.

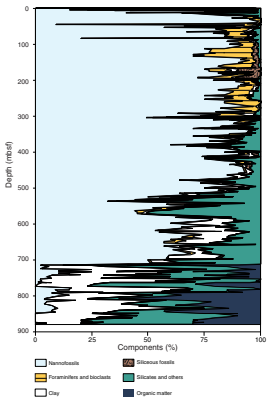

bance is common, as breccia at the top of each core and as biscuits in the XCB section of the holes.

Unit I

Depth: 0 to 260 mbsf
Age: middle Miocene to Pleistocene
Intervals: Cores 189-1168A-1H through 28X; Cores 189-1168B-1H through 12H; and Cores 189-1168C-1H through 28X
Thickness: 260 m

The sediments of Unit I are predominantly calcareous biogenic oozes. Unit I is divided into two subunits based on carbonate content, color, and compositional changes.

Subunit IA

Depth: 0 to 45 mbsf
Age: late Pliocene to Pleistocene
Intervals: Cores 189-1168A-1H through 5H; Cores 189-1168B-1H through 6H; and Cores 189-1168C-1H through 5H
Thickness: 45 m

The sediments of Subunit IA consist of light greenish gray (10GY 8/1) to greenish gray (5GY 6/1) nannofossil ooze and foraminifer-bearing nannofossil ooze and contain abundant bioclast fragments. They are characterized by a high proportion of biogenic carbonates (75 to 90 wt%). Bioturbation is occasional and is rare to present in intensity.

As a minor lithology, thin greenish gray (5GY 6/1) layers (1 to 2 cm thick) and clasts of foraminifers are present throughout this subunit (Fig. F8) (interval 189-1168B-3H-5, 16–30 cm).

An apparent color cyclicity of lighter and darker horizons is observed from spectrophotometer data and visual observation. The basal surface of the darker intervals is typically sharp and contains increased contents of foraminifers. Lightness (L*) was measured on all three holes of Site 1168 in 2-cm resolution. Because of the sampling density of the spectrophotometer, the data include minor sedimentary color changes (e.g., darker bands with a high content of pyritized particles). To investigate possible cyclicity in Subunit IA, moving averages of 10 points and 50 points resolution were calculated (Fig. F9). Both smoothed data sets reveal a strong cyclic pattern, which seems to have very constant cycle lengths. The raw lightness data L* vs. mbsf were then used to perform a spectral analysis applying the Blackman and Tukey method of a Fourier transformation included in the Analyseries software (Paillard et al., 1996). The magnetic susceptibility data set was treated with the same method and parameters. The results imply three major cycle lengths—3.71/3.58 m, 1.85/1.79 m, and 0.40/0.55 m—which are detected in both parameters (Fig. F10). At this stage we can only speculate about the length in time of the cycles. There is a possibility that these three cycles represent a 200, a 100, and a 40-k.y. cyclicity. The 200-k.y. cycle and minor peaks then could be explained as a result of interference and harmonic effects. If this is correct, the resulting sedimentation rate in the core interval from 2–23 mbsf of Hole 1168A would then be 1.85 cm/k.y., close to the 1.47 cm/k.y. sedimentation rate deduced from micropaleontological data.

F8. Close-up photograph of greenish gray sandy layers in the light greenish gray nannofossil ooze of Subunit IA, p. 68.

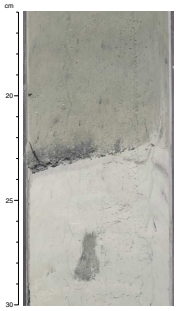

F9. High-resolution lightness data presumably of Pliocene–Pleistocene age, Hole 1168A, p. 69.

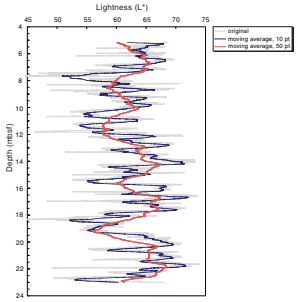

F10. Power spectra of the interval from 2 to 23 mbsf, Hole 1168A, p. 70.

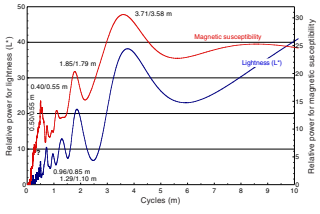

Subunit IB

Depth: 45 to 260 mbsf
Age: middle Miocene to early Pliocene
Intervals: Cores 189-1168A-6H through Section 28X-l; Cores 189-1168B-6H through 12H; and Cores 189-1168C-6H through 28X
Thickness: 215 m

Subunit IB essentially consists of white (N 8) to light greenish gray (10Y 8/1, 10Y 8/2, and 10Y 7/1) nannofossil and foraminifer-bearing nannofossil ooze and chalk. Its carbonate content is very high, between 85 and 97 wt%.

In addition to the major lithology, two minor lithologies are recognized. Light greenish gray (10Y 7/1) to greenish gray (5G 6/1 and 5GY 6/1) layers of nannofossil foraminifer ooze, nannofossil-bearing foraminifer ooze, and foraminifer ooze are found in Cores 189-1168A-6H through 8H and in Core 10H. A foraminifer- and spicule-bearing nannofossil chalk is present in Cores 189-1168A-19X and 21X.

Light greenish gray (5GY 8/1) laminae and clasts enriched in foraminifers are frequent throughout Subunit IB, as well as thin dark beds (N 6/1), nodules, and stains of pyrite. In the lower part of this subunit, infrequent to rare silt-sized calcite suggests that some diagenesis has occurred. Occasional bioturbation is rare to common in intensity and is observed principally as a pale yellow (5Y 7/4) mottled appearance.

An apparent cyclicity of lighter and darker intervals is observed in the lower part of the subunit (Cores 189-1168A-27X and 28X) from spectrophotometer analysis and core description. Major cycles are 1.20 and 2.40 m long.

Unit II

Depth: 260 to 660 mbsf
Age: early Oligocene to middle Miocene
Intervals: Cores 189-1168A-29X through 70X and Cores 189-1168C-29X through 31X
Thickness: 400 m

Unit II is characterized by significant occurrences (20% to 75%) of siliciclastic clay particles increasing with depth in its upper part, in association with siliciclastic silty particles in its lower part. Unit II is divided into three subunits.

Subunit IIA

Depth: 260 to 410 mbsf
Age: early Miocene to middle Miocene
Interval: Cores 189-1168A-29X through 44X and Cores 189-1168C-29X through 31X
Thickness: 150 m

Subunit IIA consists of light greenish gray (5GY 7/1) to dark greenish gray (10GY 4/1) clay-bearing nannofossil chalk to nannofossil claystone. The claystone is partially lithified. Color alternations are observed through this subunit although they vary in length. The carbonate content decreases with depth from 75 to 30 wt%, whereas the clay content

increases. Occasional rare to common silt-sized calcite grains suggest possible diagenesis of calcareous biogenic material.

Lenses and thin layers of very fine sandy material are occasionally present. Pyrite is present commonly as nodules, laminations, and staining from Core 189-1168A-30X downhole. Alternating beds, light gray (5Y 7/2) and light olive gray (5Y 6/2) to light greenish gray (5GY 7/1) in color, are within Cores 189-1168A-30X and 31X and are identified by both the magnetic susceptibility and photospectrometer in the yellow wavelength (550 nm; Fig. **F11**). These changes may indicate oscillations in the oxidation levels in the environment. Bioturbation is very frequent, is moderate to common in intensity, and includes *Zoophycos* and *Chondrites* burrows.

More clayey intervals are present in Cores 189-1168A-32X, 33X, and 35X. Clays are especially abundant in the darker intervals of Core 189-1168A-33X, where the carbonate content drops to 18 wt% and which correlate with strong increases of the magnetic susceptibility. Both dissolution episodes and increased terrigenous supply may account for the significant clay increase.

The sediments of this subunit are often dominated by a cyclic pattern, as illustrated in the reflectance (Fig. **F12**). Magnetic susceptibility also shows this cyclicity and is in good agreement with lightness data (Fig. **F13**). Spectral analysis indicates that the wavelengths of the cycles in both the reflectivity and magnetic susceptibility are in good agreement (Fig. **F14**).

Prominent fluid-escape structures in Core 189-1168A-36X are closely associated with brecciated sediments up to Core 35X and interrupt a faintly laminated sequence (Fig. **F15;** interval 189-1168A-36X-3, 35–75 cm). In addition, smaller fluid-escape structures associated with slumps are present in Cores 189-1168A-39X, 41X, and 42X. The soft sediment deformation is very similar to that drilled in the Miocene silty mudstone off Peru during Leg 112 (Lindsey-Griffin et al., 1990). In the upper Miocene Sisquoc Formation of California, similar soft-sediment deformation has been interpreted as resulting from the dissociation of methane hydrates (Kennett and Fackler-Adams, 2000).

Subunit IIB

Depth: 410 to 540 mbsf
Age: late Oligocene
Interval: Cores 189-1168A-45X through 57X
Thickness: 130 m

In Subunit IIB, the sediment is greenish gray (5GY 5/1 and 10Y 5/1) to dark greenish gray (5GY 4/1 and 10Y 4/1) in color. It mostly varies from nannofossil claystone to nannofossil-bearing claystone, is partially lithified, and its carbonate content fluctuates from 10 to 35 wt%.

Nodules of pyrite, clay concretions, and mud clasts are occasionally present. Convoluted bedding and laminations have been observed locally, but most of this subunit is moderately to abundantly bioturbated. *Zoophycos* and *Chondrites* are the most frequently recognized ichnofossils.

F11. Comparison of the B chromaticity coordinate and magnetic susceptibility, Hole 1168A, p. 71.

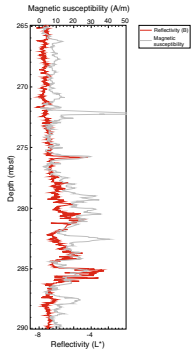

F12. High-resolution record of lightness, Hole 1168A, p. 72.

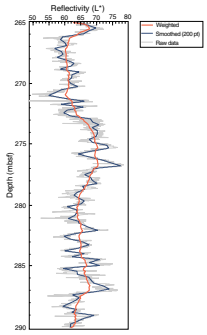

F13. Comparison of lightness and magnetic susceptibility, Hole 1168A, p. 73.

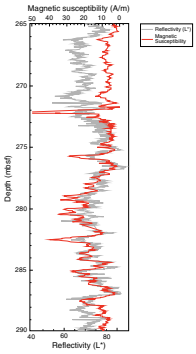

F14. Power spectra of intervals, Hole 1168A, p. 74.

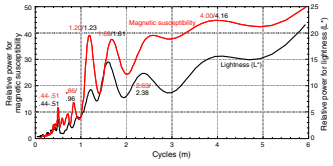

Subunit IIC

Depth: 540 to 660 mbsf
Age: early Oligocene to late Oligocene
Interval: Cores 189-1168A-58X through 70X
Thickness: 120 m

The sediment in Subunit IIC varies from silty nannofossil chalk to partially lithified nannofossil siltstone. Its carbonate content is slightly increased by comparison with Subunit IIB and fluctuates from 18 to 42 wt%. Subunit IIC shows a wide range of colors, from greenish gray (10GY 5/1 and 10Y 5/1) and dark greenish gray (10Y 4/1 and 10Y 3/1) to dark gray (5Y 4/1) and dark olive gray (5Y 3/2).

Laminations are commonly observed in this subunit. Convolute bedding and cross bedding have been locally observed. Mud clasts and nodules of pyrite are observed occasionally with the concentration of pyrite nodules increasing in Core 189-1168A-66X. A fluid escape structure and slumps are in Core 189-1168A-65X. Gastropods, bivalves, and undifferentiated mollusc shells are observed in Cores 189-1168A-56X and 58X to 60X. Rare to common bioturbation is present in the upper part (Cores 189-1168A-58X through 61X) and in the lower part (Cores 189-1168A-66X through 70X) of the subunit.

Unit III

Depth: 660 to 748.6 mbsf
Age: early Oligocene
Interval: Cores 189-1168A-70X through 79X
Thickness: 88.6 m

Unit III is characterized by a variety of pure and mixed siliciclastic sediments and by the occurrence of organic matter in significant amounts. Unit III is divided into two subunits.

Subunit IIIA

Depth: 660 to 714 mbsf
Age: early Oligocene
Interval: Cores 189-1168A-70X through 75X
Thickness: 54 m

The sediment varies from clayey nannofossil chalk and nannofossil-bearing silty claystone to organic clayey siltstone and sandy claystone and is partially lithified. The carbonate content fluctuates from 0 to 35 wt%. Its color ranges from greenish gray (10Y 5/1) to dark greenish gray (5GY 4/1 and 10Y 4/1) and very dark greenish gray (10Y 3/1). Rhythmic changes of color are visible.

Some laminations are observed, especially within darker strata. Small nodules of pyrite are present throughout the subunit. Undifferentiated molluscan shells are found in Core 189-1168A-71X. Bioturbation is rare to abundant and mostly consists of *Chondrites* burrows. Indurated (2.5Y 7/2) clay clasts are observed throughout this subunit. An indurated fine sandstone is observed in interval 189-1168A-75X-6, 56–72 cm.

F15. Photograph showing a fluid escape structure and associated brecciated sediments, p. 75.

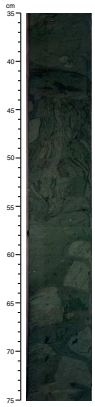

Subunit IIIB

Depth: 714.0 to 748.6 mbsf
Age: early Oligocene
Interval: Cores 189-1168A-76X through 79X
Thickness: 34.6 m

The sediment in Subunit IIIB consists of partially lithified organic-bearing silty claystone, organic clayey siltstone, and sandy claystone. This subunit is characterized by low carbonate content, between 2 and 18 wt%. Color varies from yellowish brown (2.5Y 3/2 and 5Y 3/1) and dark olive gray (5Y 3/2) to dark gray brown (2.5Y 4/2), very dark greenish brown (2.5Y 3/2), and black (5Y 2.5/1).

As a minor lithology, yellowish brown (2.5Y 3/2 and 5Y 3/1) to dark reddish brown (7.5YR 3/2) sandy layers are present in Section 189-1168A-76X-3 downcore and in Core 79X.

Laminations are visible where bioturbation is absent. Pyrite and coarse sand grains are scattered throughout the subunit, as well as shell debris. Occasional bioturbation is rare to abundant in intensity, with compressed burrows being visible in Cores 189-1168A-77X and 78X.

Unit IV

Depth: 748.6 to 762.0 mbsf
Age: latest Eocene to earliest Oligocene
Interval: Cores 189-1168A-79X and 80X
Thickness: 13.4 m

This unit is characterized by alternating dark grayish brown (2.5Y 3/2) organic-bearing silty claystone and dark greenish gray (5GY 3/1 and 5GY 4/1) clayey siltstone. The latter lithology also contains abundant coarse glauconite grains and some sand-sized siliciclastic particles (glauconitic clayey siltstone) (Fig. **F16;** interval 189-1168A-79X-6, 25–50 cm). High concentrations of authigenic glauconite are an indicator of low sedimentation rates and sediment-starved depositional environments (McRae, 1972). The frequency and thickness of the dark greenish gray glauconitic clayey siltstone beds decrease with depth in the unit. The dark grayish brown organic-bearing silty claystone contains small grains of pyrite scattered throughout. The carbonate content in Unit IV shows distinct fluctuations, from 3 to 38 wt%. Rare to common bioturbation is visible in Sections 189-1168A-80X-4 to 80X-7. The boundary between Unit III and Unit IV is marked by a sharp contact, whereas the transition to Unit V is gradational.

F16. Photograph showing layers of glauconitic clayey siltstone in Unit IV, p. 76.

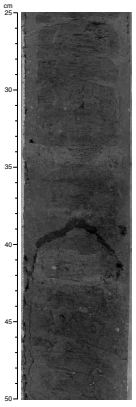

Unit V

Depth: 762.0 to 883.5 mbsf
Age: late Eocene
Interval: Cores 189-1168A-81X through 95X
Thickness: 121.5 m

Unit V consists of silty claystone and nannofossil-bearing organic silty claystone, alternating with organic-bearing clayey siltstone and silty claystone. These lithologies grade to organic clayey siltstone downhole. The sediment of Unit V is partially lithified. The siliciclastic particles are mostly quartz and clay. Very dark brown (10YR 2/2 and 2.5Y 3/

2), dark grayish brown (2.5Y 4/2), and very dark grayish brown (2.5Y 4/1 and 10YR 3/1) sediments alternate with black (5Y 2.5/1, 10YR 2/1, and N 3/0) deposits.

Siliciclastic material (mostly very coarse sand to fine gravel) is scattered throughout the unit and is present as occasional layers. Several thin, coarsening upward successions with sharp basal contacts are observed in Core 189-1168A-83X. Sporadic glauconite and pyrite grains are in the upper part of the unit. Laminations are visible in very dark brown to very dark grayish brown sediments, whereas black sediments are generally massive. Where present, laminated sediments consist of darker and lighter layers and contain very small percentages of nannofossils. Shell fragments are present in the upper part of the unit, where gastropods have been recognized, and in Core 189-1168A-92X. Bioturbation is generally absent. However, rare to abundant bioturbation is sporadically observed within small intervals as well as in Cores 189-1168A-91X to 93X.

Clay Mineralogy

The purpose of this study is to recognize major paleoenvironmental variations at Site 1168, as expressed by the changing nature and abundance of clay minerals. Forty-three samples have been analyzed, at a resolution of one sample for every two cores.

Results

The clay minerals are dominated by smectite, illite, and kaolinite. Chlorite and random mixed-layered clays, occasionally present in minor amounts, are not included in the percentage estimates. Five units of clay associations were determined for Site 1168, based on the abundances of the minerals. These are designated Units C1 through C5 (Fig. F17).

F17. Clay mineral units, p. 77.

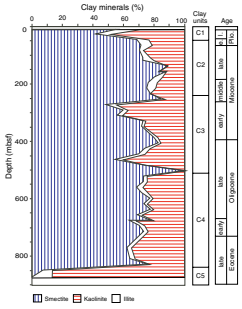

Unit C1, which extends from the seafloor to 45 mbsf, has a clay association that consists of abundant smectite (40% to 60%) and kaolinite (30% to 50%), accompanied by 10% illite. This unit ranges in age from late Pliocene to the Pleistocene and correlates to lithostratigraphic Subunit IA. Unit C2 extends from 45 to 260 mbsf and is largely dominated by smectite (70% to 90%), with common kaolinite (10% to 25%) and sporadic low contents of illite (0% to 10%). Low clay content in some samples results from greater dilution of the fine siliciclastic fraction by biogenic carbonates. This unit is middle Miocene to early Pliocene in age, and it correlates to lithostratigraphic Subunit IB. Unit C3 extends from 260 to 540 mbsf and is characterized by large fluctuations of the clay association. Smectite (45% to 100%) predominates over kaolinite (0% to 45%), whereas illite is episodically present in minor amounts (0% to 10%). This unit is late Oligocene to middle Miocene in age and correlates to lithostratigraphic Subunits IIA and IIB. Unit C4 extends from 540 to 830 mbsf and contains a clay association dominated by smectite (60% to 75%) decreasing with depth, kaolinite (25% to 35%), and very low amounts of illite (0% to 5%). This unit is late Eocene to late Oligocene in age and encompasses the range of lithostratigraphic Subunit IIIC, Unit IV, and part of Unit V. Unit C5 extends from 830 mbsf to the bottom of Hole 1168A at 883.5 mbsf. Kaolinite (85%) largely dominates the clay association and is associated with illite (5% to 15%) and very low amounts of smectite (0% to 5%). Unit C5 is late Eocene in age.

Paleoenvironmental Interpretation of Clay Assemblages

The extreme dominance of kaolinite in Unit C5 suggests that warm climatic conditions, with high precipitation during at least part of the year, prevailed in the source area of the particles during the late Eocene. In the modern environment, this mineral is typical of tropical to subtropical humid areas with good drainage conditions (Weaver, 1989). This pattern of clay mineral association is unusual for this time interval in most oceanic areas where it is generally marked by largely dominant to exclusive smectite (Chamley, 1989; Robert and Chamley, 1992), including at the adjacent Tasman Sea Sites 592 and 593 (Robert et al., 1985). However, kaolinite has already been observed in the late Eocene at southern high latitudes, in the Atlantic sector (Robert and Kennett, 1992), and in the Prydz Bay sector (Hambrey et al., 1991) of the Southern Ocean. Site 1168 is located on a deltaic lobe, and its late Eocene sediments are predominantly siliciclastic. The clay particles are most probably of local origin, supplied through runoff from the adjacent drainage basin. Identical clay associations in similar sedimentological settings have been observed in the South Atlantic during warm Cretaceous intervals of tectonic activity related to the early stages of ocean opening (Robert, 1987). In these areas, precipitation over steep continental relief ensures continuous leaching of chemical elements from the substrates and intensive chemical weathering and erosion. It is therefore highly probable that the clay association in Unit C5 derives from weathering and erosion of steep continental relief in the adjacent drainage basin during the stage of Eocene tectonic activity that preceded final separation of Tasmania from Antarctica.

The base of Unit C4 is characterized by a drastic increase of smectite and a corresponding decrease of kaolinite. The siliciclastic sediment is still deltaic, and the clay particles are most probably derived from the adjacent drainage basin, as in Unit C5. The clay association becomes very similar to those of late Eocene age observed in most oceanic areas of passive margins, including the adjacent Tasman Sea (Robert et al., 1985; Robert and Chamley, 1992). Smectite dominance still corresponds to warm climatic conditions and intense chemical weathering on the adjacent continent. However, this mineral prevails in areas of low relief with alternating periods of precipitation and aridity, its formation being intensified on volcanic substrates (Chamley, 1989; Weaver, 1989). The transition to predominant smectite at the lower part of Unit C4 therefore suggests that continental relief strongly decreased and the morphology of the adjacent drainage basin drastically changed during the late Eocene. A similar evolution of the clay association is observed in Cretaceous sediments from the South Atlantic, where it is related to the phase of subsidence and transgression of the continental margins that follows the early stages of ocean opening (Robert, 1987). At Site 1168, the transition to dominant smectite is probably related to tectonic relaxation and subsidence of the western Tasmania margin as ocean opening progressed. The content of smectite increased slightly in the upper part of Unit C4 in relation to the continuing subsidence of the passive western Tasmania margin.

Unit C3 is mainly marked by distinct fluctuations of the clay association—smectite increases drastically at ~503 mbsf (NP25, late Oligocene), whereas kaolinite increases at 464 mbsf (NP25, late Oligocene) and from 310 mbsf to 272 mbsf (NN2 to NN4, early Miocene). As the Southern Ocean was already largely open south of Tasmania, the siliciclastic fraction of the sediment decreased progressively through time, as

shown from lithostratigraphic Unit III. The clay fraction decreases in abundance, and clay particles most probably originate from different areas of the Australian margin, transported by marine currents to Site 1168. With the subsidence of the passive margin well advanced, the clay association of oceanic margins and basins mostly reflects variations of climate and circulation (Robert, 1987). It is assumed that in Unit C3 at Site 1168, the fluctuations of the clay association mainly result from climatic variability. In the upper Oligocene section, strong increases of smectite and kaolinite in nannofossil Zone NP25 represent intensified chemical weathering in the source areas. Coeval increases of kaolinite have already been observed in different oceanic areas from both hemispheres, where they have been interpreted as intervals of intensified precipitation on most continental areas (Robert and Chamley, 1987). A further increase of kaolinite is in the early Miocene section from Zone NN2 to NN4. Coeval but smaller increases of kaolinite are observed in the adjacent Tasman Sea at DSDP Sites 590, 591, and 592 (Robert et al., 1985; Stein and Robert, 1985). However, such intervals of increased kaolinite have not been observed yet in the North and South Atlantic, where kaolinite decreases in the lower Miocene (Robert and Chamley, 1987). This increase of kaolinite seems of regional importance and may reflect increased warmth and intensified precipitation at middle to high latitudes of the Southwest Pacific. It immediately precedes the development of the East Antarctic Ice Sheet between 14 and 15 Ma (Kennett, 1977).

Unit C2 shows higher contents of smectite, the maximum abundance being recorded between 157 and 138 mbsf (i.e., from Zone NN9 to the lower NN11). Warm climates with alternating intervals of precipitation and aridity prevailed by this time in the source areas of particles (i.e., most probably the southern Australian and the western Tasmanian margins).

Unit C1 is marked by increased contents of kaolinite, beginning during nannofossil Zone NN16 in the late Pliocene. At the same time, the clay content of the predominantly calcareous biogenic sediment slightly increases (Subunit IA). This is probably an interval of intensified erosion of the continental margins. However illite does not increase, which is unusual at this time of further development of physical weathering in most areas. The late Pliocene to Pleistocene clay association of Site 1168 could come from erosion of the central Australian desert by wind activity. At this time in the Tasman Sea, wind supply from arid areas reached its maximum extension to the south (Stein and Robert, 1985). In this case, particles may have been transported to Site 1168 by northwesterly winds similar to those associated with modern nonprecipitating cold fronts (Pye, 1987). However, the clay association derived from central Australia, as observed in the Lord Howe Rise sediments, contains higher proportions of illite (Stein and Robert, 1985). During the late Pliocene, kaolinite increased in several oceanic areas (e.g., at the middle latitudes of the Atlantic and of the North Pacific), whereas it decreased off the northwest African deserts. Differences in the evolution of the clay association have been interpreted as resulting from intensified humidity at middle latitudes of both hemispheres and increased meridional zonation of climate (Robert and Chamley, 1987). At present, both hypotheses may account for the late Pliocene increase of kaolinite at Site 1168, and a higher resolution is necessary to further investigate the climatic processes.

Paleoenvironment

Seismic profiles indicate that the whole area where Site 1168 has been drilled consisted of small sedimentary basins separated by basement highs often capped with Cretaceous or Paleocene poorly sorted sediments (Hill et al., 1997). The Cretaceous to early Eocene sediments were deposited in prograding deltaic environments that kept up with the subsidence caused by crustal thinning as Australia and Antarctica started to rift apart. Unit V of Site 1168 is seismically represented by a body of chaotic reflectors typical of deltaic systems, which give way to well-defined, parallel reflectors to the northwest. The positions of basement highs and sedimentary basins suggest that the late Eocene western Tasmania area consisted of a succession of parallel, most probably subaerial, crests of northwest-southeast orientation separated by troughs of varying depths. At DSDP Site 282 to the west, seismic profiles and sedimentary sequences indicate significantly greater oceanic influence with pillow basalt, dipping reflectors, marine biogenic components, and very low sedimentation rates typical of starved margins. To the southeast, the succession of sedimentary troughs within one of which Site 1168 is located corresponds to a shallow, brackish to marine deltaic setting in the late Eocene, deepening to the northwest (Fig. **F18**). Subaerial areas were probably located on local basement highs as well as to the east on the Tasmania-Antarctica land bridge, which was exposed to tectonic activity during ocean opening. Apatite fission-track dating indicates tectonic uplift and erosion of western Tasmania during the late Paleocene to early Eocene (O'Sullivan and Kohn, 1997). During the Oligocene, the whole area tilted to the west, possibly in relation to extended subsidence, and siliciclastic sediment supply decreased.

In the lowermost part of the drilled section (lithostratigraphic Unit V), of late Eocene age, an anoxic environment is indicated by the black to very dark gray color of the sediment, abundance of organic remains, and the highest total organic carbon (TOC) values (4 to 5 wt%) for Site 1168. The sediment is predominantly siliciclastic siltstones and claystones, derived from erosion of onshore areas. The organic matter is characterized by a low hydrogen index (HI) from 100 to 200 and a high C/N ratio (25 to 50), representative of terrestrially derived organic matter (see **"Organic Geochemistry,"** p. 37). Throughout the whole unit, abundant sporomorphs and plant tissue suggest a nearshore setting, whereas the poorly diversified dinoflagellates are consistent with eutrophic conditions and varying salinity in normal marine to brackish water. The benthic foraminifers present have agglutinated tests typical of highly stressed nearshore, low-oxygen environments (see **"Biostratigraphy,"** p. 21).

Below 830–840 mbsf, massive siltstone and claystone deposits dominate the sequence. The clay mineral assemblage, dominated by kaolinite, suggests a warm climate and significant precipitation in the source area during at least part of the year (Chamley, 1989; Weaver, 1989). Such assemblages are typically derived from steep continental relief and may correspond to the stage of tectonic activity that preceded the separation of Tasmania from Antarctica. High C/S ratios (2 to 6) are characteristic of a brackish environment. The massive black deposits are sporadically intercalated with very dark gray intervals of alternating dark and light laminations, where the lighter laminae contain abundant nannofossils indicative of open-ocean salinities and showing dissolution traces. These laminated intervals of suboxic conditions most

F18. Late Eocene paleogeography and paleoenvironment, p. 78.

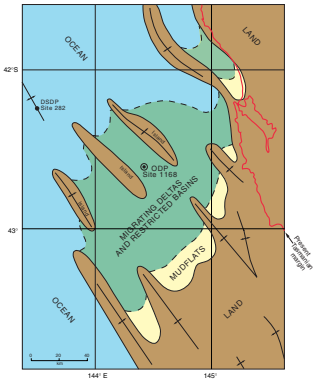

probably correspond to marine incursions and improved oxygenation in the restricted eastern end of the Australo-Antarctic Gulf.

Above 830–840 mbsf, the very dark, predominantly siliciclastic sediment includes episodic occurrences of coarse sand and fine gravel, indicative of intensified erosion in upstream continental areas. The clay mineral assemblage dominated by smectite indicates a warm climate with alternating intervals of humidity and aridity (Chamley, 1989; Weaver, 1989). Such an assemblage is typically derived from continental areas of low relief and is consistent with tectonic relaxation and subsidence associated with passive margin development off Tasmania. Slightly decreased TOC values (between 1.5 and 4.5 wt%), together with fluctuating HI and C/N values, suggest intermittent decreases in terrestrially derived organic components. Lower C/S ratios (1 to 3) indicate brackish to marine conditions (see **"Organic Geochemistry,"** p. 37). Foraminifers and nannofossils, as well as laminated intervals, are more frequent than in the lowermost part of the unit.

To summarize, the lower section of upper Eocene Unit V was deposited near a tectonically active hinterland of steep morphology, characteristic of the early stages of ocean opening. Overall, a warm climate with significant precipitation and runoff prevailed in this area, driving erosion of organic and siliciclastic terrigenous particles. This erosion produced sedimentation rates of ~8 cm/k.y. in a restricted basin at the southeastern boundary of the Australo-Antarctic Gulf, where eutrophism and suboxic conditions prevailed. Marine incursions resulted in temporary more oxygen-rich conditions that allowed preservation of marine calcareous planktonic microorganisms (nannofossils). In the upper part of Unit V, intense erosion persisted in upstream areas of the adjacent drainage basin, whereas areas of low-relief increased along the passive margin. Overall, a warm climate persisted, with sporadic or seasonal aridity. Eutrophism and suboxic conditions still prevailed, but oxic marine incursions increased in frequency.

The sediment of the corresponding interval of Site 282 (Kennett, Houtz, et al., 1975), drilled 80 km northwest of Site 1168, overlies pillow basalt, but interpretation of more recent seismic profiles suggests it is possibly on continental crust (Hill et al., 1997). The dominantly siliciclastic sediment of Site 282 is also deposited in comparable suboxic environment, but the clayey silt and silty clay there include up to 20% each of sponge spicules and nannofossils, indicative of greater marine influence than at Site 1168. The Site 282 sedimentation rate of 2.5–3 cm/k.y. is much lower than at the more proximal Site 1168, which has a sedimentation rate of ~8 cm/k.y.

The very dark gray sediment in lithostratigraphic Unit IV, of latest Eocene age, is still dominated by a siliciclastic component and contains organic remains, suggesting the persistence of suboxic conditions. TOC values of ~2 wt% are associated with low HI (150) and relatively high C/N (20) values, which imply predominance of terrestrial organic matter (see **"Organic Geochemistry,"** p. 37). Sporomorphs dominate the pollen association and indicate the persistence of a nearshore environment. The low diversity dinocyst assemblage supports eutrophic conditions with varying salinity, and the C/S ratio of ~3 may reflect a somewhat brackish environment. The sediment is sporadically truncated by dark grayish green intervals with abundant glauconite and coarse sand, suggesting low sedimentation rates and active, well-oxygenated bottom currents. Assemblages of nannofossils and planktonic foraminifers also suggest that Unit IV is a condensed section or contains one or several hiatuses (see **"Biostratigraphy,"** p. 21).

The depositional environment of Unit IV remained suboxic part of the time, with terrestrial input to the restricted basin. Marine incursions were associated with significant current activity, sufficient to produce winnowing, and possibly hiatuses, as marked by intervals of coarse deposits and glauconite formation. These intervals of intensified current activity increased near the Eocene/Oligocene boundary in the upper part of Unit IV. No equivalent of Unit IV has been found at Site 282. However, in DSDP Core 29-282-15 lenses of glauconite have been found near the Eocene/Oligocene boundary and may be the result of downslope transport. It is hypothesized that a shallow connection to the open ocean may have occurred as subsidence progressed in the western Tasmania area.

In the early Oligocene Unit III, an evolving environment is indicated by very dark sediment colors grading to greenish gray, and TOC values decreasing from 2 to 0.5 wt% upsection. The sediment is predominantly siliciclastic in the lower part of the unit (Subunit IIIB), but the particles decrease in size and abundance in the upper part of the unit (Subunit IIIA), suggesting decreased contribution from continental areas. The clay mineral assemblage contains increasing smectite and is indicative of continued subsidence of the passive margin (Chamley, 1989). The continuously decreasing trend of the C/S (from 3 to below 1) and C/N (from 25 to below 10) ratios reflect a transition to more marine conditions (see **"Organic Geochemistry,"** p. 37), whereas benthic foraminifer faunas indicate shelf to bathyal water depths but continued low oxygenation (see **"Biostratigraphy,"** p. 21).

The predominantly siliciclastic sediments of Subunit IIIB show very dark colors and fluctuating TOC values (between 0.5 and 2 wt%) suggesting suboxic to unstable restricted conditions. Dominance of sporomorphs and plant tissue over pollens is consistent with the persistence of a nearshore environment. Transition to more marine conditions is deduced from the C/S ratio decrease to values between 3 and near 0 (see **"Organic Geochemistry,"** p. 37). Some alternating intervals of laminated and bioturbated sediments indicate transient suboxic to oxic conditions.

A major step in the paleoceanographic evolution of the western Tasmania margin is present within Subunit IIIA (early Oligocene) where the dominant color of the sediment turns to greenish gray and TOC values decrease below 1 wt%. At the same time, C/N values below 10 and C/S values below 1 suggest the dominance of marine organic matter over terrestrially derived organic components as normal salinity seawater prevailed on the margin (see **"Organic Geochemistry,"** p. 37). In most of Subunit IIIA, the sediment is bioturbated with rare laminated intervals. Foraminifers and nannofossils increase in abundance; however, the productivity and/or preservation remain low. Estimated sedimentation rates average 4.3 cm/k.y. and are characteristic of a starved continental margin.

At the beginning of the early Oligocene, marine influences on the western Tasmania margin are more important than in the late Eocene, but poorly oxygenated conditions generally persist at Site 1168. Subunit IIIA of early Oligocene age marks a transition to an increasingly oceanic oligotrophic environment. In the equivalent lower Unit VI of Site 282, a spicule and nannofossil clayey silt indicates greater influence of marine biogenics and less terrestrial contribution than at Site 1168. Intervals of lighter sediment interpreted as being more pelagic represent more open ocean biogenic productivity at Site 282. At this time the sediments of Sites 282 and 1168 converge in composition and include

abundant biogenics within dominant siliciclastic clayey silt and silty clay. Similar sedimentation rates and environmental conditions were present in both areas.

The biogenic content of the sediment increases at Site 1168 in Unit II, which consists of nannofossil claystone, siltstone, and chalk, through intensified productivity and/or carbonate preservation. TOC values are low (below 1 wt%) and the organic matter is predominantly of marine origin, as indicated by C/N values below 15. Predominantly marine conditions are deduced from C/S values generally below 2 (see "Organic Geochemistry," p. 37) and from the benthic foraminifer assemblage, which indicates well-oxygenated conditions at bathyal depths (see "Biostratigraphy," p. 21).

In Subunit IIC (early to late Oligocene), siliciclastic components are still dominant. Slightly bioturbated sediments alternate with rare laminated intervals that, together with occasional C/S values between 2 and 3, suggest temporary development of suboxic conditions. In the corresponding Unit V of Site 282, similar sediment includes an interval of silty clay enriched in glauconite, indicative of low sedimentation rate and intensified current activity.

Beginning in Subunit IIB in the late Oligocene, the continuous decrease in abundance and size of the siliciclastic component suggests a decreasing influence of erosion and continental processes. This siliciclastic decrease is associated with increasingly abundant calcareous biogenics, which became predominant during the Miocene. Benthic foraminifers suggest increasing water depths and, together with very frequent bioturbation, indicate the persistence of well-oxygenated bottom waters and intensified circulation through time (see "Biostratigraphy," p. 21).

From the late Oligocene to the Pleistocene, open marine conditions prevailed on the western Tasmania margin and nannofossil chalks and oozes predominate. In the corresponding interval of Site 282, slow sedimentation of biogenic-rich clays and biogenic oozes alternates with several hiatuses spanning parts of the late Oligocene, the early Miocene, and most of the middle Miocene–Pleistocene interval. The hiatuses were caused by dissolution related to strong bottom circulation (Kennett, Houtz, et al., 1975).

BIOSTRATIGRAPHY

Microfossils belonging to seven major groups were recovered from the sedimentary succession at Site 1168 off west Tasmania. The combined results suggest that there are no major time breaks in the sequence from the late Quaternary to late Eocene (Fig. F19). The site may prove to be a standard reference section for the marine sequences of southern Australia. Of the siliceous groups, diatoms are generally rare and sporadic and with moderate preservation, whereas radiolarians are generally rare but occasionally are abundant with poor to good preservation. Calcareous microfossils (foraminifers and nannofossils) are generally abundant with preservation ranging from poor to good; the best preservation is in the Pleistocene to upper Oligocene. Well-preserved organic walled dinoflagellate cysts (dinocysts) are abundant throughout the succession of Hole 1168A, except for the middle Miocene and upper Eocene intervals where they are common. Benthic foraminifers are present throughout the entire sequence, with the upper Eocene showing low abundances and diversity of mainly agglutinating species. Mod-

F19. Age-depth plot and linear sedimentation rates, p. 79.

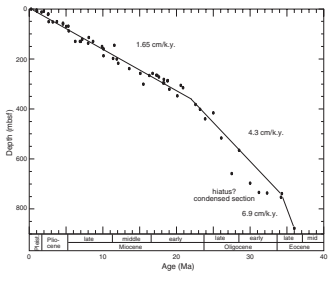

erately preserved sporomorphs dominate the palynomorph samples from the lower part of Hole 1168A assigned to the late Eocene. Sedimentation rates were relatively low, ranging from 1.65 to 6.9 cm/k.y. (Fig. F19).

The Pliocene/Pleistocene boundary is placed between Samples 189-1168A-2H-CC and 3H-CC on nannofossil evidence; definite Pleistocene foraminifers are present only in Sample 189-1168B-1H-CC. The upper/lower Pliocene boundary is placed between Samples 189-1168A-6H-CC and 7H-CC on nannofossil evidence; planktonic foraminiferal Subzone SN12b, which contains this boundary, is present only in Samples 189-1168A-6H-CC and 189-1168C-6H-CC. The Miocene/Pliocene boundary is placed at the base of planktonic foraminiferal Subzone SN12a, which is present between Samples 189-1168A-7H-CC and 8H-CC; nannofossil evidence, however, suggests that this is present between Samples 189-1168A-9H-CC and 10H-CC. The upper/middle Miocene boundary falls within planktonic foraminiferal Zone SN8 and nannofossil Zone CN6 and, therefore, cannot be located with accuracy on the basis of the present set of samples; however, it must be above Sample 189-1168A-21X-CC. Late Miocene radiolarians and mixed assemblages of diatoms are present in Samples 189-1168A-12H-CC, 13H-CC, and 14H-CC with radiolarians continuing down to Sample 189-1168A-20X-CC. The middle/lower Miocene boundary is placed just above the base of planktonic foraminiferal Zone SN5, just below the top of nannofossil Zone CN3, and again cannot be precisely located. Planktonic foraminiferal Zone SN5 is based on the presence of *Praeorbulina suturalis* below the first occurrence (FO) of *Orbulina suturalis;* this zone has not been recognized, but the two species coexist in Sample 189-1168A-28X-CC. This suggests that the boundary may be present within Core 189-1168A-29X.The Miocene/Oligocene boundary falls within the uppermost part of planktonic foraminiferal Subzone SP14b (but is normally placed for convenience at the base of Zone SN1) and at the base of nannofossil Subzone CN1a. Planktonic foraminifers indicate the presence of this boundary between Samples 189-1168A-42X-CC and 43X-CC; nannofossil evidence, however, indicates its occurrence between Samples 189-1168A-46X-CC and 47X-CC.

Bolboformids typical of the late Miocene are recorded only from Samples 189-1168A-16X-CC and 17X-CC. The few available dinocyst and siliceous microfossil datums are in broad agreement with the age assignments presented above. There is evidence that Paleogene dinocysts have been reworked into the Pliocene.

The Neogene dinocyst assemblages are generally represented by relatively warm water, oligotrophic (oceanic) forms. Influence of colder water masses is only evident in the uppermost interval (late Pliocene/Pleistocene). The other microfossil groups suggest temperate to cool-temperate conditions throughout this interval.

The upper/lower Oligocene boundary coincides with the base of planktonic foraminiferal Subzone SP14b. The base of SP14b is defined by the last occurrence (LO) of *Chiloguembelina cubensis,* which is recorded between Samples 189-1168A-59X-CC and 60X-CC. In terms of planktonic foraminifers, the Eocene/Oligocene boundary in temperate regions is considered to fall within the upper part of Zone SP12. This zone is defined by the total range of *Subbotina brevis,* but since this species is very rare in this region, it cannot be used. For convenience, the LO of *Globigerinatheka index* is used as a proxy marker; this species is found between Samples 189-1168A-78X-CC and 79X-CC.

The LO of the nannofossil *Discoaster saipanensis,* which marks the top of Zone CP15, is dated at 34.2 Ma, which is located just below the Eocene/Oligocene boundary. This event is recorded between Samples 189-1168A-79X-CC and 82X-2, 21 cm.

The stratigraphic distribution of dinocysts and the few siliceous microfossils present in this interval are broadly in support of this age assessment. There is evidence that middle Eocene and Cretaceous dinocysts have been reworked into the upper Eocene.

Late Eocene to early Oligocene nannofossil assemblages exhibit distinctly warmer water characteristics than other comparable paleolatitude sites in the Southern Hemisphere. Dinocyst assemblages are dominated by relatively warm water, neritic, eutrophic forms; typical antarctic dinocyst species are conspicuously absent. Sporomorphs increase in relative abundance downhole, indicating decreasing terrigenous influence from the early to late Oligocene.

The upper Eocene planktonic foraminiferal assemblages continue to exhibit low species diversity, and their downhole distribution is patchy, with several samples being barren. In general, there is nannofossil and dinocyst evidence for a continued warm-water influence throughout the early Oligocene and Eocene. Dinocyst assemblages are poorly diversified and suggestive of eutrophic conditions and fluctuating salinity, from neritic open marine to brackish conditions. This is supported by the dominance of sporomorphs in the palynological associations in this part of the sequence.

The benthic foraminiferal record indicates an increase in paleodepth from neritic to upper bathyal in the late Eocene to lower bathyal to upper abyssal in the Neogene (Fig. **F20**). Changes coincide with all major stratigraphic boundaries. At the same time, the assemblages suggest a link between increasing water depth and improved bottom-water oxygenation.

F20. Paleodepth and bottom-water conditions, based largely on benthic foraminifers, p. 80.

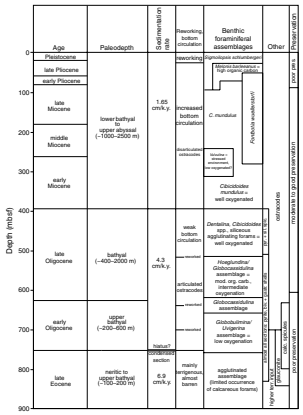

Calcareous Nannofossils

All core-catcher samples plus additional samples from some critical intervals were examined for calcareous nannofossils at Site 1168. Calcareous nannofossils are generally abundant and well to moderately preserved throughout the cored interval (Table **T2**), with a few samples from the upper Eocene yielding few or no nannofossils. The nannofossil biostratigraphy (Table **T3**) established to date the upper Eocene through the Pliocene is believed to be the most detailed among the Southern Hemisphere sites of similar or higher paleolatitudes. The sequence will serve as an important reference section for the Southern Hemisphere.

The FO of *Emiliania huxleyi,* which defines the base of nannofossil Zone CN15 at 0.26 Ma, was found between Samples 189-1168B-1H-1, 55 cm, and 1H-1, 72 cm (Table **T4**). The LO of *Calcidiscus macintyrei* was found in Sample 189-1168A-2H-CC. This datum at 1.67 Ma can generally be used to approximate the Pliocene/Pleistocene boundary outside tropical temperate areas, where discoasters are generally rare or absent.

The LO of *Discoaster surculus* is located between Samples 189-1168A-2H-CC and 3H-CC. This provides a useful datum at 2.55 Ma for subdividing the late Pliocene nannofossil Zone CN12. Further subdividing this zone relies on other discoaster markers, which were not found in the samples examined. The LO of *Reticulofenestra pseudoumbilicus* (3.75 Ma) was found between Samples 189-1168A-6H-CC and 7H-CC, marking the lower Pliocene/upper Pliocene boundary.

T2. Identification and abundance of nannofossils, p. 122.

T3. Calcareous nannofossil datum levels and their assigned age estimates, p. 130.

T4. Calcareous nannofossil datum levels, p. 131.

Rare specimens of *Amaurolithus* were first observed in Sample 189-1168A-7H-CC. This suggests that the base of nannofossil Zone CN11 at 4.6 Ma is between Samples 189-1168A-6H-CC and 7H-CC. *Ceratolithus acutus* was recorded in Samples 189-1168A-8H-CC and 9H-CC. This indicates an age interval of 5.05–5.37 Ma for these two cores. The Miocene/Pliocene boundary is generally located slightly below the FO of *C. acutus,* that is, below Core 189-1168A-9H.

The FO of *Amaurolithus* (*A. primus*) is recorded between Samples 189-1168A-13X-CC and 14X-CC. This datum (7.2 Ma) marks the boundary between nannofossil Subzones CN9a and CN9b. The LO of *Cyclicargolithus floridanus* (11.9 Ma) is located between Samples 189-1168A-21X-CC and 22X-CC. This datum generally lies below the upper Miocene/middle Miocene boundary. A succession of nannofossil datums was recognized in the rest of the middle Miocene and lower Miocene—the LO of *Sphenolithus heteromorphus* (CN5/CN6 boundary at 13.6 Ma) between Samples 189-1168A-31X-CC and 32X-CC; the FO of *Calcidiscus premacintyrei* (17.4 Ma) between Samples 28X-CC and 29X-CC; the FO of *S. heteromorphus* (18.2 Ma) between Samples 31X-CC and 32X-CC; the LO of *Sphenolithus belemnos* (18.3 Ma) between Samples 31X-CC and 32X-CC; and the FO of *S. belemnos* (CN1/CN2 boundary at 20.6 Ma) between Samples 32X-CC and 33X-CC.

The LO of *Reticulofenestra bisecta* is located between Samples 189-1168A-46X-CC and 47X-CC. This marks the Oligocene/Miocene boundary. The following nannofossil datums were found that help date the Oligocene: the LO of *Chiasmolithus altus* (26.1 Ma) between Samples 189-1168A-54X-CC and 55X-CC; the LO of *Sphenolithus distentus* (27.5 Ma) between Samples 69X-CC and 70X-CC; the LO of *Reticulofenestra umbilica* (31.2 Ma) between Samples 77X-CC and 78X-1, 38 cm; and the LO of *Isthmolithus recurvus* (32.3 Ma) between Samples 78X-2, 10 cm, and 78X-2, 144 cm. The LO of *Discoaster saipanensis* (34.2 Ma) was recorded between Samples 189-1168A-79X-CC and 82X-2, 21 cm. This suggests that the Eocene/Oligocene boundary lies above this horizon. The last three datums span 3 m.y. and are within a 20-m sediment interval. This indicates a condensed section and/or one or more disconformities within this interval. The precise location of any disconformity within this interval, however, cannot be located or inferred based on the available data.

Samples 189-1168A-91X-CC through 95X-CC yielded generally rare specimens of nannofossils that do not provide useful age information. Examination of several samples from Core 189-1168A-94X, however, revealed abundant and diverse assemblages of nannofossils. They contain, among other Eocene nannofossils, *I. recurvus* and *Reticulofenestra reticulata*. The overlap of these two taxa suggests an age of ~36 Ma (Wei and Wise, 1992). This age inference is further supported by the fact that some specimens of the latter species are larger than 11 µm.

Nannofossil assemblages from the late Eocene through the early Oligocene show distinctly warmer water characteristics than those from comparable paleolatitude sites in the Southern Hemisphere, such as Sites 699, 703, 747, 748 (47°–58°S) in the South Atlantic and Indian Ocean sectors of the Southern Ocean. This is demonstrated by significantly higher abundance of low-latitude taxa, such as discoasters, *Coccolithus formosus,* and lower abundance of high-latitude taxa, such as chiasmoliths and *Reticulofenestra daviesii,* at Site 1168 than at the aforementioned Southern Ocean sites. Detailed quantitative analysis of the nannofossil assemblages from this interval should allow a detailed delineation of the changes through time in biogeographic gradients be-

tween Site 1168 and the other Southern Ocean sites and, thus, help paleoceanographic reconstruction.

Planktonic Foraminifers

Shipboard examination of all core-catcher samples revealed that a relatively complete marine sequence spanning the uppermost Eocene to the Holocene was recovered at Site 1168. The planktonic foraminiferal biostratigraphic succession seen at Site 1168 is typical of temperate sequences at these latitudes. All biozones belonging to the temperate latitude biostratigraphic scheme of Jenkins (1985, 1993a, 1993b) and Stott and Kennett (1990) are identified, with the notable exception of the *Praeorbulina curva* Zone (see Table T5). The distribution of species in these samples is given in Table T6.

T5. Planktonic foraminifer bioevents and their ages, p. 132.

T6. Range chart of planktonic foraminifers, p. 133.

Quaternary sediments appear to be confined within the uppermost core of all holes drilled at Site 1168 (Cores 189-1168A-1H, 189-1168B-1H, and 189-1168C-1H). The base of the *Globorotalia truncatulinoides* Zone (SN14), which approximates the Pleistocene lower boundary, is defined by the FO of the nominate taxon (1.96 Ma). This zone (SN14) was recorded only in Sample 189-1168B-1H-CC. Thus, the FO of *G. truncatulinoides* is constrained between the core depths of 3.89 and 7.24 mbsf at Site 1168. Rare specimens of *Globorotalia tosaensis* (0.65–2.9 Ma) were also found within two samples (Samples 189-1168B-1H-CC and 189-1168C-1H-CC).

Pliocene

The Pliocene is well represented in all three holes drilled at Site 1168. The base of the *Globorotalia inflata* Zone (SN13) is demarcated by the lowermost stratigraphic occurrences of the nominate taxon (3.2 Ma). This biostratigraphic datum was recorded in the following samples of each hole: Samples 189-1168A-5H-CC (45.96 mbsf), 189-1168B-6H-CC (51.51 mbsf), and 189-1168C-5H-CC (47.45 mbsf).

Continuing downsection, the *G. inflata* Zone is succeeded by the *Globorotalia puncticulata* Subzone (SN12b). The base of the *G. puncticulata* Zone is defined by the LO of *Globorotalia pliozea* (4.6 Ma). The *G. puncticulata* Zone is present in Samples 189-1168A-6H-CC (55.24 mbsf) and 189-1168C-6H-CC (56.26 mbsf). Subzone SN12b was not noted in Hole 1168B, but this is probably because of its probable position between Samples 189-1168B-5H-CC (51.51 mbsf) and 6H-CC (61.32 mbsf).

The base of the *G. pliozea* Zone, which coincides with the Miocene/Pliocene boundary, is defined by the FO of *G. puncticulata* (5.3 Ma). Of all three holes, the lowermost occurrences of *G. puncticulata* are in Sample 189-1168C-7H-CC at an average core depth of 63.09 mbsf. Planktonic foraminiferal assemblages are generally well preserved throughout the Pliocene, although intervals of shell fragmentation and moderate dissolution punctuate this portion of the record.

Miocene

The absence of *G. puncticulata* combined with the presence of *Globorotalia conomiozea* defines the top of the uppermost planktonic foraminiferal zone of the late Miocene, the *G. conomiozea* Zone (SN11). This zone represents a long interval ranging from Samples 189-1168B-8H-CC through 189-1168A-14X-CC. The base of the *G. conomiozea*

Zone is denoted by the FO of the nominate taxon (6.9 Ma). Specimens of *G. conomiozea* are first recorded at ~125 mbsf at Site 1168 (Samples 189-1168A-14X-CC and 189-1168C-14X-CC). Thus, the base of Zone SN11 is constrained to the stratigraphic interval bounded by Samples 189-1168A-14X-CC and 15X-CC. Hole 1168B terminates within the *G. conomiozea* Zone. It should also be noted that the stratigraphic position of the *G. conomiozea* FO is rendered somewhat subjective because of the morphological intergradation of this taxon with ancestral *Globorotalia conoidea*.

The *Globorotalia miotumida* Zone (SN10) is a gap zone bounded by the FO of *G. conomiozea* at its top (6.9 Ma) and the LO of *Paragloborotalia continuosa* at its base (8.0 Ma). The uppermost stratigraphic occurrence of *P. continuosa* was found to be within Sample 16X-CC in both Holes 1168A and 1168C. As a consequence, the base of this gap zone is constrained to the stratigraphic interval between Samples 189-1168A-15X-CC and 16X-CC.

The base of the *P. continuosa* Zone (SN9) is by definition the uppermost stratigraphic occurrence of *Paragloborotalia nympha* (10.1 Ma). The LO of *P. nympha* was identified in Samples 189-1168A-19X-CC and 189-1168C-20X-CC. This limits the possible stratigraphic range for the base of the *P. continuosa* Zone to the interval ranging from 173.37 to 175.23 mbsf.

The downhole stratigraphic sequence is continued with the lowermost zone of the late Miocene, the *P. nympha* Zone (SN8). The lower boundary of the *P. nympha* Zone is delimited by the LO of *Paragloborotalia mayeri* (11.4 Ma). The *P. mayeri* LO was identified in Samples 189-1168A-22X-CC and 189-1168C-22X-CC. Thus, the base of the *P. nympha* Zone is constrained to core depths spanning 194.62–203.67 mbsf. Preservation throughout the upper Miocene is generally good with only minor dissolution and etching of planktonic foraminiferal shells.

Middle Miocene

The uppermost zone of the middle Miocene is the *P. mayeri* Zone (SN7). The base of the *P. mayeri* Zone (12.1 Ma) is defined by FO of the nominate taxon. The lowermost stratigraphic occurrence of *P. mayeri* was recorded in Sample 189-1168A-23X-CC, whereas Hole 1168B terminated in sediments postdating the *P. mayeri* FO. Based on the section recovered from Hole 1168A, it appears that the base of the *P. mayeri* Zone is restricted to core depths of 214.69 to 224.27 mbsf.

The biostratigraphic succession continues uninterrupted downsection with the presence of the *Orbulina suturalis* Zone (SN6). The base of the *O. suturalis* Zone (15.1 Ma) is defined by the FO of the nominate taxon. The FO of *O. suturalis* was identified in Sample 189-1168A-28X-CC. Thus, the lower boundary of the *O. suturalis* Zone is constrained to the stratigraphic interval spanning 260.29 to 272.34 mbsf.

The *Praeorbulina curva* Zone (SN5) was not recognized in the series of core-catcher samples examined. However, specimens of *P. curva* were found co-occurring with *O. suturalis,* particularly in the lower part of the *O. suturalis* Zone. It is suspected that the FO of *P. curva* (16.3 Ma) was not identified because of the low sampling density. It is possible that the *P. curva* Zone is present within the stratigraphic interval bounded by Samples 189-1168A-28X-CC and 29X-CC (260.29–272.34 mbsf). Preservation throughout the middle Miocene is generally good, although chalky layers are present.

Early Miocene

The later parts of the early Miocene are represented by the *Globigerinoides trilobus* Zone (SN4) at Site 1168. The lower boundary of this biozone is delimited by the FO of the nominate taxon (18.8 Ma). This zonal boundary was identified in Sample 189-1168A-30X-CC and not in 31X-CC. Thus, the precise stratigraphic position of this datum is confined to the 281.48–291.59 mbsf interval.

The *Globoturborotalita connecta* Zone (SN3), which predates the *G. trilobus* Zone, begins with the FO of the nominate taxon (20.9 Ma). The marker species *G. connecta* is present in Sample 189-1168A-34X-CC but not in 35X-CC. Therefore, the stratigraphic range for the lower boundary of the *G. connecta* Zone is constrained to 309.97–319.45 mbsf.

The downsection sequence continues uninterrupted with the presence of the *Globoturborotalita woodi* Zone (SN2). The lower boundary of this biozone is demarcated by the FO of the nominate taxon (22.6 Ma). The presence of *G. woodi* in Sample 189-1168A-40X-CC and its absence in 41X-CC restricts the lower boundary of the *G. woodi* Zone to the interval bounded by 376.54–387.07 mbsf.

The base of the *Globoquadrina dehiscens* Zone (SN1), which also corresponds to the Oligocene/Miocene boundary, is defined as the FO of the nominate taxon (23.2 Ma). The marker species *G. dehiscens* was recorded in Sample 189-186-1168A-42X-CC and absent in 43X-CC. Thus, the base of the *G. dehiscens* Zone, and Oligocene/Miocene boundary, is located within the 396.61–406.01 mbsf stratigraphic interval.

Preservation of planktonic foraminifers varies throughout the lower Miocene. In general, the assemblages are moderately to well preserved with restricted intervals of increased shell fragmentation and dissolution.

Late Oligocene

The *Turborotalia euapertura* Subzone (SP14b) is the only biozone of the late Oligocene recognized at this site. The lower boundary of this biozone is delimited by the LO of *Chiloguembelina cubensis* (28.5 Ma). This datum was difficult to determine with confidence because of the erratic stratigraphic distribution and relatively small size of *C. cubensis*. The uppermost stratigraphic occurrence of *C. cubensis* is tentatively placed within Sample 189-1168A-60X-CC. Thus, the lower boundary of the *T. euapertura* Zone is confined to the stratigraphic interval between 396.61 and 406.01 mbsf.

Planktonic foraminifers contained within the upper Oligocene section are only moderately preserved. Strong diagenetic overprinting is conspicuous at some sample horizons. Many specimens suffer from secondary calcite infilling and pyritization.

Early Oligocene

The uppermost biozone of the early Oligocene is the *C. cubensis* Subzone (SP14a). The base of the *C. cubensis* Subzone is delimited by the LO of *Subbotina angiporoides* (30 Ma). The *S. angiporoides* LO was identified within Sample 189-1168A-74X-CC. Therefore, the lower boundary of the *C. cubensis* Subzone lies within the 691.62–702.34 mbsf interval.

The downsection sequence is continued with the presence of the *S. angiporoides* Zone (SP13). The lower boundary of the *S. angiporoides* Zone is delimited by the LO of *S. brevis* (33 Ma). Poor preservation and

unfavorable paleoenvironmental conditions complicated determination of this taxon's stratigraphic distribution. The uppermost stratigraphic occurrence of *S. brevis* is tentatively placed in Sample 189-1168A-77X-CC. The lack of *S. brevis* in the overlying sample (189-1168A-76X-CC) constrained the base of the *S. angiporoides* Zone to the 722.84–733.41 mbsf interval.

Preservation deteriorates downhole, decreasing from moderate to poor. Planktonic foraminifers are infilled with secondary calcite and pyritized. Planktonic foraminifers become rarer downsection, particularly below Sample 189-1168A-70X-CC.

Eocene/Oligocene Boundary

The uppermost stratigraphic occurrence of the late Eocene marker species *Globigerinatheka index* (34.3 Ma) was identified in Sample 189-1168A-79X-CC. The absence of *G. index* in Sample 189-1168A-78X-CC suggests that the Eocene/Oligocene boundary is within the interval spanning 743.28–752.53 mbsf. Specimens of *Subbotina linaperta* and *S. brevis* were found to coexist with *G. index* in Sample 189-1168A-79X-CC. The overlapping stratigraphic ranges of these taxa suggest that the boundary between the *S. brevis* Zone (SP12) and the underlying *S. linaperta* Zone (SP11) is complete, although likely condensed (see Fig. **F19**). However, the degree of completeness of the Eocene/Oligocene boundary at Site 1168 remains equivocal and warrants more detailed investigation.

The presence of the calcareous nannofossil marker species, *I. recurvus,* in Sample 189-1168A-94X-CC suggests the possibility that rare *Acarinina aculeata* (the marker for the top of the Zone SP10) may also be present at the base of this hole, although paleoenvironmental conditions appear to have precluded its presence.

Preservation is generally poor and planktonic foraminifers are commonly infilled with secondary calcite. All samples below Sample 189-1168A-88X-CC were deemed barren of planktonic foraminifers.

Benthic Foraminifers, Ostracodes, and Bolboforma

Most of the benthic foraminiferal taxa preserved in the sediments are extant (Fig. **F20**). Their abundances, diversities, and preservation are extremely low in the upper Eocene. With improved bottom-water oxygenation, as indicated by changes in the assemblages, benthic foraminiferal numbers and diversities increase in the Oligocene. The Neogene is characterized by abundant and diverse assemblages of well preserved benthic foraminifers. The suggested oxygen levels increase from very low to well oxygenated at the same time as the paleodepth increases at the major stratigraphic boundaries (i.e., from neritic to upper bathyal; ~100–200 m) in the upper Eocene to lower bathyal/upper abyssal (~1000–2500 m) in the Neogene. Benthic foraminiferal assemblages suggest frequent reworking of the upper Pliocene to Holocene interval and in selected intervals of the Oligocene. The transition from articulated to disarticulated ostracodes at the Oligocene/Miocene boundary indicates an increase in bottom-water circulation at this time.

The lower Oligocene interval is almost entirely dominated by a low-oxygen fauna (*Globobulimina* spp. and *Uvigerina* spp.). Most *Globobulimina* spp. are badly preserved as their thin test shows signs of compaction. A transition from upper bathyal (~200–600 m) to bathyal (~400–2000 m) water depths is marked by the occurrence of *Globocassidulina*

spp., indicating improved oxygenation of bottom waters. This interval is followed by an assemblage marked by the co-occurrence of increased numbers of *Hoeglundina elegans* and *Globocassidulina subglobosa* until ~520 mbsf (Sample 189-1168A-55X-CC). The remaining late Oligocene assemblages consist of calcareous benthic foraminifers together with high abundances of agglutinating foraminifers with a preference for using siliceous spicules in their tests. The entire Neogene interval contains typical open-marine benthic foraminiferal assemblages from bathyal depths (~1000–2500 m) with varying intervals when individual species show higher abundances (e.g., *Vulvulina pennatula* from ~320 mbsf to the lower/middle Miocene boundary at ~250 mbsf and *Fontbotia wuellerstorfi* from ~280–50 mbsf).

Ostracodes were observed in most core-catcher samples from 700 mbsf (189-1168A-73X-CC) to the surface. The lower part of the drilled section (950 to 700 mbsf) is marked by an increased amount of terrigenous input of varying nature and only infrequent traces of ostracodes. We observe a change at 400 mbsf (Sample 189-1168A-43X-CC) from articulated to disarticulated carapaces. This suggests a change from deposition in a tranquil environment with low or no bioturbation to an environment with increased bottom circulation and/or bioturbation. This coincides with an inferred change in sedimentation rate at the Oligocene/Miocene boundary (Fig. **F19**).

Bolboforma capsula was the only bolboformid positively identified. This species is present in Samples 189-1168A-16X-CC and 17X-CC, placing them in Zone NN9 (top of Zone NN8 to bottom of Zone NN10) (Spiegler and von Daniels, 1991) and, thus, being consistent with the nannofossil stratigraphy. *Bolboforma antarctica,* which strongly resembles a hexagonid *Oolina,* was possibly observed in Eocene samples. Bolboformids have been observed from a narrow temperature range of 4°–8°C, so their presence or absence may be a reflection of the sea-surface temperatures at the time.

Radiolarians

Identifiable radiolarians were recovered from Samples 189-1168A-2H-CC and 11H-CC through 20X-CC; Samples 189-1168B-8H-CC, 11H-CC, and 12H-CC; and Samples 189-1168C-8H-CC, 10H-CC, 2H-CC through 20X-CC, and 22X-CC. These samples contain rare to abundant, poor- to well-preserved radiolarians. The radiolarian sequence in this hole cannot be correlated to the antarctic or tropical zonal schemes because of the absence of marker species. Three radiolarian datums were recognized from Hole 1168A (Table **T7**) and one from Hole 1168C (Table **T8**).

T7. Radiolarian datums recognized in Hole 1168A, p. 141.

T8. Radiolarian datum recognized in Hole 1168C, p. 142.

Hole 1168A

Samples 189-1168A-1H-CC through 10H-CC are nearly barren. Sample 189-1168A-2H-CC contains only one identifiable species, *Stylacontarium aquilonarium.*

Radiolarians are consistently present in Samples 189-1168A-11H-CC through 20X-CC. This fauna is characterized by an absence of antarctic taxa including *Antarctissa* and the subfamily Artiscinae. The fauna consist mainly of the actinommid genera *Hexacontium, Thecosphaera,* and *Stylacontarium.* Nassellarians are consistently present but are rare to common. Samples 189-1168A-12H-CC through 16H-CC commonly contain late Miocene radiolarians, including *Carpocanistrum ob, Cycla-*

dophora antiqua, Dictyophimus splendens, Stylacontarium acquilonium, Stylatractus universus, and *Theocorythium trachelium trachelium*. The faunas of this interval consistently contain the deeper dwelling species *Cornutella profunda,* which in the modern ocean lives deeper than 400 m.

Useful datums were recognized from three horizons (Table T7): the FO of *S. aquilonarium* (Hays), estimated at 7.0 Ma in the North Pacific (Motoyama, 1999), is present between Samples 189-1168A-14X-CC and 15X-CC. The LO of *Cyrtocapsella japonica* is placed between Samples 189-1168A-16X-CC and 17X-CC. In the North Pacific this bioevent is dated as 9.9 Ma (Motoyama, 1999). The last abundant occurrence (LAO) of *C. japonica* is estimated at 10.1 Ma in the North Pacific and is placed between Samples 189-1168A-17X-CC and 18X-CC. Samples 189-1168A-21X-CC through 1168A-95X-CC are mostly barren.

The Oligocene samples occasionally contain poorly preserved radiolarian tests. These show dissolved surfaces and are infilled with opaque material. Only one specimen of *Eucyrtidium spinosum,* which appears at ~37.0 Ma, was found in Sample 189-1168A-65X-CC.

Hole 1168B

Samples 189-1168B-1H-CC through 12H-CC are barren or contain rare specimens. Only one species, *S. aquilonarium,* was found in Samples 189-1168B-11H-CC and 12H-CC.

Hole 1168C

Samples 189-1168B-1H-CC through 11H-CC are also barren or contain rare specimens. Of these, Samples 189-1168B-8H-CC and 10H-CC contain rare radiolarians, including *S. aquilonarium*.

Radiolarians are common in Samples 189-1168C-12H-CC through 16X-CC. The fauna of these samples is similar to that of Samples 189-1168A-11H-CC through 20X-CC but differ from the latter by lacking *Botryostrobus* and *Cycladophora*. This fauna consists mainly of *Axoprunum angelinum, C. ob,* the *Eucyrtidium cienkowskii* group, *Lamprocyrtis hannai, Lithelius nautiloides, Sphaeropyle robusta, Stichocorys delmontensis, Stichocorys peregrina, S. acquilonarium,* and *S. neptunus*.

Sample 189-1168C-17X-CC yielded few radiolarians, including *S. aquilonarium*. This sample contains several species that are not utilized for age determination. *C. japonica,* which becomes extinct at 9.9 Ma in the North Pacific (Motoyama, 1999), was found in Samples 189-1168C-18X-CC and 19X-CC. Sample 189-1168C-20X-CC is barren. Sample 189-1168C-21X-CC contains a few broken specimens of *Cyrtocapsella tetrapera*. Samples 189-1168C-22X through 31X-CC are mostly barren.

The LO of *S. delmontensis* is placed between Samples 189-1168C-12H-CC and 13X-CC (Table T8). The age of this datum has been determined as 5.18–6.9 Ma by Morley and Nigrini (1995).

Diatoms, Silicoflagellates, and Sponge Spicules

All core-catcher samples from Holes 1168A, 1168B, and 1168C were analyzed for diatoms, silicoflagellates, and sponge spicules. Preparation followed the procedures outlined in "Biostratigraphy," p. 9, in the "Explanatory Notes" chapter, although additional processing of sediment was necessary for most samples in order to concentrate the siliceous component. In this instance, 5–7 cm^3 of core-catcher sample was

treated with 40% HCl, washed and sieved through a 20-µm mesh. Strewn slides of the >20-µm fraction were prepared on a hot plate.

Diatoms are absent or in trace abundance throughout Site 1168 sediment except for two discrete sections downhole where they are common: Sections 189-1168A-12H-CC through 14X-CC and 61X-CC through 64X-CC (Table T9). Preservation is moderate and diversity is low. Their abundance appears to be controlled by preservation but probably is also a combination of factors including dilution by carbonate and overall low-diatom productivity (oligotrophic conditions?). Their occurrence downhole is directly proportional to the concentration of dissolved silica in the pore waters (sponge spicules comprise the bulk of the siliceous biogenic component, thereby contributing the most to dissolved silica; Fig. F21). Where diatoms are present, they are buffered from postdepositional dissolution where $H_4SiO_4^0$ concentration in pore waters exceeds ~500 µM.

The *Thalassiothrix antarctica-longissima* group dominates the assemblages in Samples 189-1168A-12H-CC and 13H-CC. Separation of the two species was not possible because of the poor preservation of valve poles. Sample 189-1168A-12H-CC contains a mixed signal assemblage: subantarctic taxa (*Actinocyclus ingens, Proboscia barboi,* and one specimen of the endemic antarctic diatom *Eucampia antarctica*), the temperate taxon *Fragilariopsis reinholdii,* and neritic planktonic diatoms (*Chaetoceros* resting spores and *Thalassionema nitzschioides*). Samples 189-1168A-13X-CC and 14X-CC contain a moderate abundance of the marker *Actinocyclus ingens* var. *ovalis* constraining these samples to the late Miocene. Samples 189-1168A-61X-CC through 64X-CC contain moderately preserved specimens of an apparently monospecific assemblage of an unidentified species of *Arachnodiscus*.

Sponge spicules comprise the bulk of the biogenic silica throughout most of Site 1168. However they are noticeably absent in Sections 189-1168A-31X-CC through 41X-CC and 69X-CC to the bottom of the hole. Sponge spicule abundance is directly related to the concentration of dissolved silica in interstitial pore waters (Fig. F21). Silicoflagellates are recorded in low abundance in Samples 189-1168A-13X-CC and 14X-CC only.

T9. Distribution and abundance of diatoms and silicoflagellates, p. 143.

F21. Siliceous microfossil abundance and preservation vs. $H_4SiO_4^0$ in pore water, Hole 1168A, p. 81.

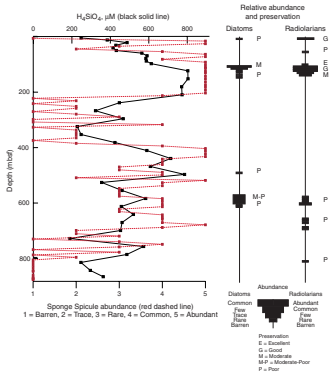

Palynology

Onboard work included palynological analysis of every fourth corecatcher sample at Site 1168 in Hole 1168A. From the uppermost (Sample 189-1168A-1H-CC through 10H-CC) and the lowermost (Sample 189-1168A-74X-CC through 95X-CC) intervals, most available corecatcher samples were analyzed. Recovery of palynomorphs was quite variable. Dinoflagellate cysts (dinocysts) are the most prominent palynomorphs in the upper and middle parts of the succession in Hole 1168A (Table T10). Sporomorphs dominate the lower part of the succession.

T10. Distribution of organic walled dinocysts and sporomorph percentages, Hole 1168A, p. 145.

Dinoflagellate Cysts

Somewhat surprisingly, dinocysts were generally found to be more abundant in parts of the Neogene than in the Paleogene in Hole 1168A (although the interval between Samples 189-1168A-18X-CC to 30X-CC was found to be almost barren; Table T10). Preservation is good in the Neogene to Oligocene section in contrast to the older part of the succession (Sample 189-1168A-75X-CC to the base of the cored interval). Di-

nocyst species in Hole 1168A are largely cosmopolitan and rather long ranging. However, generally their stratigraphic distribution matches that known from the Northern Hemisphere and equatorial regions (calibrated against the calcareous plankton record of Hole 1168A). A few stratigraphically useful events were recorded (viz., the LO of *Amiculosphaera umbracula* and *Invertocysta tabulata* in Sample 189-1168A-6H-CC and the FO of *Achomosphaera andalousiensis* in Sample 189-1168A-14X-CC). The latter event may be taken to approximate the middle/lower Miocene boundary (Table T11). In addition, the LO of *Pyxidinopsis fairhavenensis* and *Glaphyrocysta* spp. appear to be stratigraphically useful events as well, recorded in Samples 189-1168A-34X-CC and 46X-CC, respectively. The available calibration of their tops/bases from the Northern Hemisphere fits well with the results from the onboard calcareous microfossil studies (Table T10; Fig. F19). Curiously, a single specimen of *Diphyes ficusoides* was found in Sample 189-1168A-82X-CC. This taxon is not known to occur outside of the Eocene of the North Sea Basin and surrounding areas, where its LO is near the top of the Lutetian (middle Eocene; e.g., Bujak and Mudge, 1994). The occurrence in Hole 1168A is interpreted to be the result of reworking of upper lower to lower middle Eocene strata into the upper Eocene. Similarly, the occurrence of *Circulodinium distinctum* in Sample 189-1168A-94X-CC is considered to be a result of reworking of (lower?) Cretaceous materials into the upper Eocene. Reworking of Paleogene material into the Pliocene is apparent by the occurrence of *Wetzeliella articulata* in Sample 189-1168A-6H-CC. Several undescribed species were recorded (e.g., new species of *Cerebrocysta, Eocladopyxis,* and *Cannosphaeropsis*); further taxonomic treatment awaits the examination of more specimens.

In the Neogene section, assemblages are marked by an abundance of warm-water species of *Impagidinium,* indicating relatively warm, oligotrophic (oceanic) surface water conditions throughout. In the uppermost samples, a few specimens of the arctic species *Impagidinium pallidum* were recorded. This indicates the influence, albeit limited, of colder water masses in this interval. Occasional abundance of other species in this part of the section, like that of *Operculodinium echigoense,* may be the result of downslope transport. The Oligocene assemblages are dominated by forms like *Spiniferites ramosus, Operculodinium centrocarpum,* and, in particular, *Hystrichokolpoma rigaudiae, Thalassiphora pelagica* and *Systematophora placacantha,* which are tentatively interpreted to reflect increasingly more eutrophic surface conditions, possibly associated with more shallow waters, and/or increased transportation from such settings. The presumed upper Eocene succession is marked by poorly diversified assemblages with sporadic occurrences of *Deflandrea phosphoritica* and *Lejeunecysta* spp. indicating eutrophic conditions with varying salinities, from normal marine to brackish conditions. The dinocyst assemblage in this part of the core is very similar to those recorded elsewhere from ancient delta front deposits.

T11. Selected age-diagnostic dinocyst events, Hole 1168A, p. 149.

Other Palynomorphs

Sporomorphs are frequent in the palynological associations, as are the organic linings of foraminifers. Quite appropriately, sporadic occurrences of representatives of the chlorophyte *Tasmanites* have been recorded in some samples. The percentage of terrestrial palynomorphs is given in Table T10.

The palynological associations of the lower part of Hole 1168A, notably from Sample 189-1168A-75X-CC downward (early Oligocene?–late

Eocene), are dominated by sporomorphs. Long-ranging smooth and verrucate fern spores such as *Verrucosisporites kopukuensis, Cyathidites minor,* and *Crassiretritriletes vanraadshovenii* are particularly common. Pollen are represented by alete bisaccates and *Nothofagidites* spp., notably *N. asperus*. Few specimens of *Acaciapollenites miocenicus* are present in the lower sample suite; their presence may be taken to support the inferred late Eocene age of this interval on the basis of the calcareous microfossil record (following MacPhail, 1999). The abundance of sporomorphs in the lower part of the section (occasionally up to 100% of the palynomorph association), in conjunction with the massive abundance of plant tissue debris in this interval, further supports attribution to delta front environments. A more detailed study of the terrestrial palynomorph assemblages of the lower sequence of Hole 1168A may result in a more definite age assessment of these deposits.

Age Model and Sedimentation Rates

The combined nannofossil, planktonic foraminifer, diatom, radiolarian, and dinocyst biostratigraphy at Site 1168 yielded 51 reliable bioevents with age significance. Principal trends through this essentially continuous section are shown in Figure **F19.** Datums are from the combined microfossil bioevents and 10 magnetic polarity datums. The bioevents are comprised of 23 FO events and 28 LO events and are listed in Table **T12.** All events are plotted according to their observed depths at Site 1168 and by their ages as defined in **"Biostratigraphy,"** p. 9, in the "Explanatory Notes" chapter. First occurrence events may have been estimated to be too shallow and LO events may have been estimated as being deep, based on the limited sampling interval. Stratigraphic position of these datums will be refined with further study. See individual microfossil group discussion for more detailed bioevent data.

T12. Biostratigraphic events, p. 150.

Sedimentation rates increase downcore as biostratigraphic control decreases. The upper 380 mbsf are well constrained by 40 bioevents and 10 magnetic polarity events. The average sedimentation rate of 1.65 cm/k.y. from the Pleistocene to the mid-early Miocene may be low in part because of silica dissolution or other parameters. Silica concentration in pore-water samples (see **"Inorganic Geochemistry,"** p. 42) does increase from ~100 to 225 mbsf and may be a result of increasing amounts of sponge spicules. Event levels between microfossil groups agree rather well, taking into consideration the large sampling interval. Datums that are well out of sequence, such as the FO of diatom *Fragilariopsis reinholdii,* have large ranges on the depth of the event (see Table **T12** for more examples).

Biostratigraphic control degrades downcore, with six bioevents to date the lower Miocene through lowermost Oligocene interval from 380 to 700 mbsf. The average sedimentation rate increased to 4.3 cm/k.y. with an influx of siliciclastic material beginning in Core 189-1168A-44X, the beginning of lithostratigraphic Subunit IIB. Lower sedimentation rates mark the lower Oligocene, but the sequence appears to be continuous.

The uppermost Eocene section from 750 to 880 mbsf is delineated by only a single bioevent. Increasing dissolution of calcareous microfossils downcore coincided with a lithofacies change to sandy and organic-rich claystones (see **"Lithostratigraphy,"** p. 8). Core-catcher samples 189-1168A-90X-CC through 95X-CC were barren of calcareous and siliceous microfossils. Toothpick samples from carbonate rich intervals of Samples 189-1168A-91X to 94X yielded a bottom-hole age of ~36 Ma

based on the FO of *I. recurvus* at Sample 189-1168A-94X-3, 137 cm (see "Calcareous Nannofossils," p. 23). The bottom-hole age is overestimated, and detailed shore-based work may suggest an increase in the average sedimentation rate of 6.9 cm/k.y.

PALEOMAGNETISM

Introduction

The natural remanent magnetization (NRM) and remanent magnetization after alternating-field (AF) demagnetization of the archive-half sections from Holes 1168A and 1168B were measured at 5-cm intervals using the pass-through cryogenic magnetometer. We measured the NRM of all cores up to Core 189-1168A-26X, but the remainder were only measured after 20-mT demagnetization because of time constraints. A nonmagnetic core barrel assembly was used for alternate cores in each hole. In Hole 1168A, even-numbered APC cores were taken with the nonmagnetic core barrel assembly. In Holes 1168B and 1168C, odd-numbered cores were taken, starting with Cores 3H. The comparison between results from cores collected with the nonmagnetic corer and standard cores is discussed (see the "Appendix" chapter), as are results of experiments investigating the effect of core splitting on magnetization and other coring-related magnetic experiments. We note here that a strong overprint was found to be induced by splitting sections from two test cores (Sections 189-1168B-3H-4, 3H-5, and 3H-6; 189-1168B-8H-2, 8H-3, 8H-4, 8H-5, and 8H-6). This was not demagnetized by 20 mT. In Hole 1168C, long-core sections were therefore run as whole cores, rather than as archive halves, to determine if a better magnetostratigraphy could be obtained.

The Tensor tool was used to orient the APC cores beginning with the third core at each hole. The variability in the declination values for Holes 1168A and 1168B precluded the orientation of the cores.

Discrete oriented samples were routinely collected from Hole 1168A; two samples taken from each working-half core. These were used to aid in the interpretation of the long-core record of magnetization by providing additional measurements of polarity and basic magnetic characterization. Most of them were demagnetized at 5, 10, 15, 20, 30, 40, and 50 mT to permit principal component analysis. For rock magnetic characterization, anhysteretic remanent magnetization (ARM) and isothermal remanent magnetization (IRM) were applied, measured, and progressively demagnetized up to 50 mT. A DTECH AF demagnetizer (model D-2000) was used to impart an ARM. A direct-current (DC) field at 0.2 mT combined with an alternating field of 200 mT was used. IRM was given in a DC field of 1 T with an Analytical Service Company (ASC) model IM-10 impulse magnetizer. Some discrete samples were progressively saturated to 1.3 T to study the hardness of the IRM.

Results

Long-Core Measurements

Long-core measurements provided, for the most part, poor records of reversal sequences with shallow inclinations, anomalously long transitions between polarities, and the 0° declination artifact. After demagnetization of coring overprints, the magnetization was on the order 10^{-5}

A/m, which is close to the sensitivity limit of the instrument. Moreover, measurements of empty core liners gave spot readings on the same order of magnitude of the intensity of magnetization. These facts explain the poor quality of the paleomagnetic signal. Hole 1168C sections were measured as whole cores and for the first ~30 mbsf yielded inclinations close to the expected value of 62° for the site latitude of 42°S (Fig. F22). The first 0.25 mbsf was oxidized and strongly remagnetized in the present field direction (see "Physical Properties," p. 45). Five well-defined magnetozones (three normal and two reversed) were identified between 0.25 and 28.1 mbsf. Unfortunately, the correlation with the geomagnetic polarity time scale (GPTS) (Berggren et al., 1995a, 1995b) is not completely satisfactory. Three biostratigraphic datums are available (see "Biostratigraphy," p. 21)—the FO of *E. huxleyi* (0.26 Ma) at 0.64 mbsf, the LO of *C. macintyrei* (1.67 Ma) at 12.12 mbsf, and the LO of *D. surculus* (2.55 Ma) at 21.86 mbsf—to constrain the magnetozones. We interpret the termination of the Jaramillo Subchron (C1r.1n) at 3.75 mbsf, the onset of this subchron at 9 mbsf, and the termination of the Olduvai Subchron (C2n) at 28.1 mbsf.

At greater depth in the core, we attempted to use biostratigraphic markers to constrain the depth of such long chrons as C5n, C6n, C12r, and C13r. In addition, we used the measurements of discrete samples to find depths where a reliable paleomagnetic record was likely to be present. Using these techniques we were able to establish a magnetic polarity record between 250 and 287.6 mbsf; where the magnetization is relatively strong, inclinations approached the expected values, and the numerous biostratigraphic datums allowed us to constrain the correlation with the GPTS (Fig. F23). Magnetozones can be matched to Subchrons C5En, C5Dr, C5Dn, C5Cr, and C5Cn. Around 300 m, the sedimentation rate changes, reaching >40 m/m.y., which makes interpretation of the long positive-magnetization zone below C5Br problematic. However, it appears that C6n is indeed between 321.5 and 347.3 mbsf. Attempts to identify sequences of reversals around other long periods of constant polarity were unsuccessful. In the two depth ranges, within which we established the polarity sequences, the intensity of magnetization measured in the long-core mode was 10^{-3} A/m or more.

Discrete Samples

Examination of discrete samples indicated that the majority of samples carried a poor paleomagnetic record in their NRM and after demagnetization to 20 mT, although there were notable exceptions (Fig. F24). The preliminary rock magnetic analysis in terms of demagnetization of NRM, ARM, and saturation IRMs revealed a range in magnetic characteristics that afforded a basis for interpretation of the paleomagnetic record. For example, in the upper calcareous part of the hole, the ratio of ARM to IRM was high, suggesting the predominance of fine, single-domain material, probably magnetosomes, as the carrier of the paleomagnetic record. There was a particularly striking contrast in the characteristics of samples taken from Cores 189-1168A-30X through 34X compared with 35X and 36X. Cores 189-1168A-30X through 34X carried NRM, which gave principal component analysis (PCA) results with maximum angular deviation (MAD) angles of as low as 3°, indicating that a stable magnetization had been acquired (Fig. F24). In Cores 189-1168A-35X and 36X, the results were so scattered that no PCA could be carried out after the coring contamination had been separated. Figure F25 shows that Cores 189-1168A-30X through 34X have stronger NRM,

F22. Long-core magnetic inclination and intensity for the uppermost 50 mbsf, Holes 1168A, 1168B, and 1168C, p. 82.

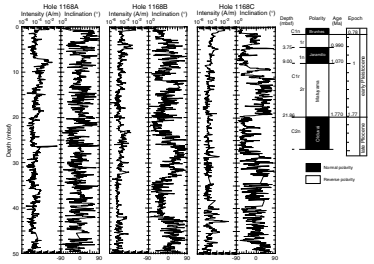

F23. Long-core magnetic inclination and intensity, Hole 1168A between 250 and 350 mbsf, p. 83.

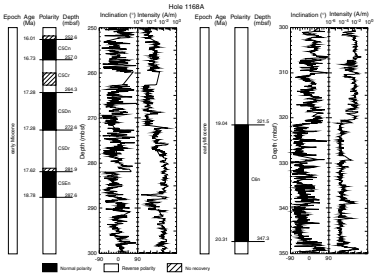

F24. Principal component analysis of NRM of Sample 189-1168A-34X-CC, 25 cm, p. 84.

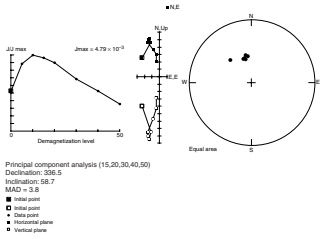

F25. Magnetic characterization of Samples 189-1168A-30X-4, 104 cm, and 36X-6, 145 cm, p. 85.

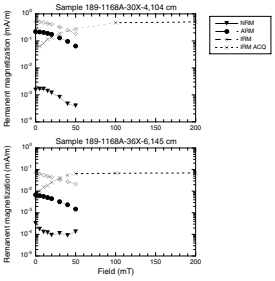

ARM, and IRM ratios of ARM:IRM and have hard IRM relative to Cores 189-1168A-35X and 36X. These results indicate that Cores 189-1168A-30X through 34X have finer magnetic material than Cores 189-1168A-35X and 36X. Whether this reflects better preservation of magnetosomes or secondary fine particles produced in the oxidation region is not initially clear. However, the low ratio of NRM:IRMs suggests that this is not a chemical remanence and that the preservation of magnetosome magnetite may be better in this interval than above. Cores 189-1168A-34X and 36X appear to represent a change in sedimentation associated with coarser magnetic material.

Magnetostratigraphy

As is evident from Figures F22 and F23 and the discussion of long-core measurements above, the magnetostratigraphy of this site is very difficult to establish. The principal problem lies in the weak intensity of magnetization of the sediments, which approaches the noise limit of the instrument. The weak intensity also means that magnetic contamination adding to the signal has a much greater effect than in more strongly magnetized cores. It is for these reasons that we have only given magnetostratigraphic results for the more strongly magnetized parts of the hole. The results obtained are shown in Figures F22 and F23 and in Table T13. They proved to be in good agreement with the biostratigraphic data and were included in the time-depth study. However, whereas the magnetostratigraphy at the top of the core can be recognized independently from the biostratigraphy, the magnetostratigraphy between 250 and 350 mbsf is dependent upon the biostratigraphy for the location of Chron C6n.

T13. Magnetostratigraphic results, Holes 1168A and 1168C, p. 151.

COMPOSITE DEPTHS

Multisensor track (MST) and spectral reflectance (L*) data collected from Holes 1168A, 1168B, and 1168C were used to determine depth offsets in the composite section. Magnetic susceptibility, gamma-ray attenuation (GRA) bulk density, and spectral reflectance measurements were the primary parameters used for core-to-core correlation at Site 1168. GRA bulk density and magnetic susceptibility data were collected at 2-cm intervals on all APC cores recovered from Holes 1168A, 1168B, and 1168C and at 2- to 4-cm intervals on XCB cores from Holes 1168A and 1168C. Spectral reflectance data were collected at 2-cm intervals on cores from Holes 1168A, 1168B, and 1168C. (see "Physical Properties," p. 45, and "Lithostratigraphy," p. 8, for details about MST and spectral reflectance data).

The data used to construct the composite section and determine core overlaps are presented on a composite depth scale in Figure F26. The depth offsets that comprise the composite section for Holes 1168A, 1168B, and 1168C are given in Table T14.

The composite data show that the APC cores from Site 1168 provide a continuous overlap to at least 120 m composite depth (mcd) (base of Core 189-1168B-12H). Below the APC section, most of the XCB cores from Hole 1168C could be tied into XCB cores from Hole 1168A and placed into a composite depth framework. Very few core gaps, however, could be bridged between the XCB cores from the two holes, and an XCB splice could not be constructed.

F26. Smoothed spectral reflectance, magnetic susceptibility, and GRA bulk density data for the upper 130 mcd, p. 86.

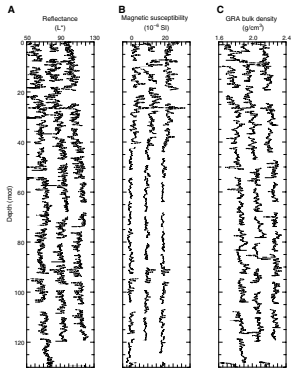

T14. Composite depth section, p. 152.

Stretching and compression of sedimentary features in aligned cores indicate distortion of the cored sequence. Because significant distortion occurred within individual cores on depth scales of <9 m, it was not possible to align every feature in the MST and color reflectance records accurately by simply adding a constant to the mbsf core depth. Core-scale changes will require postcruise processing to align smaller sedimentary features. Only after allowing variable adjustments of peaks within each core can an accurate estimate of core gaps be made.

Following construction of the composite depth section for Site 1168, a single spliced record was assembled for the aligned cores over the upper 120 mcd (base of Core 189-1168A-11H) primarily by using cores from Holes 1168A and 1168B. Intervals having significant disturbance or distortion were avoided. The Site 1168 splice (Table T15) can be used as a sampling guide to recover a single sedimentary sequence between 0 and 120 mcd.

T15. Splice tie points, p. 153.

ORGANIC GEOCHEMISTRY

The shipboard organic geochemistry program at Site 1168 included studies of volatile hydrocarbons, total organic and inorganic carbon, total nitrogen, total sulfur, and hydrogen and oxygen indexes. Rock-Eval pyrolysis, CNS analysis, gas chromatography, and carbon coulometry were performed (see "Organic Geochemistry," p. 20, in the "Explanatory Notes" chapter).

Sedimentary Geochemistry

Results

Carbonate ($CaCO_3$) content for the strata sampled at Site 1168 ranges from 0 to 90 wt% (Fig. F27; Table T16). In general, the profile exhibits an overall increasing upsection trend. Sediments from 878 to ~700 mbsf commonly contain <10 wt% $CaCO_3$, except for several distinct excursions with values of up to 38 wt%. Carbonate content steadily increases between ~700 and 550 mbsf, ranging from ~10 to 40 wt%. From ~550 to 450 mbsf, a broad declining trend in percent carbonate was measured, with values ranging from approximately <10 to 50 wt%. Above this broad decrease is a narrow zone of increasing carbonate content (~20–50 wt%) from 450 to ~370 mbsf, which is overlain by a narrow decrease to ~310 mbsf (carbonate content as low as ~17 wt%). Carbonate content steadily increases from the top of this horizon to ~250 mbsf, where values of ~90 wt% $CaCO_3$ are attained; one region of depressed values exists at ~200 mbsf. From here, carbonate content remains at ~90 wt% until ~40 mbsf, above which the values decrease to ~80 wt% (with a value as low as 50 wt%) to the seafloor.

The total organic carbon content for most intervals at Site 1168 is <1 wt%, although deposits below ~700 mbsf contain up to 5 wt% TOC (Fig. F27; Table T16). Note that TOC values determined by Rock-Eval pyrolysis and CNS analysis provide similar TOC profiles (Fig. F27; Tables T16, T17). Total nitrogen content ranges from 0 to 0.18 wt% (Table T16), with the highest values being between 700 mbsf and the base of Hole 1168A; nitrogen content covaries with TOC content (Fig. F27). From 878 to ~540 mbsf, total sulfur content is generally high, ranging from near 0 to >2 wt% (Fig. F28; Table T16). Above ~540 mbsf, the total sulfur profile shows an overall gradual decrease upsection with occa-

F27. Plots of $CaCO_3$, TOC, and total nitrogen, C/N ratios, and HI values, Hole 1168A, p. 87.

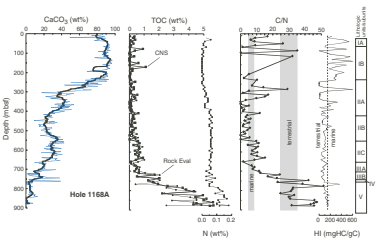

T16. Values for inorganic carbon, calcium carbonate, total carbon, total organic carbon, total nitrogen, total sulfur, and hydrogen in sediments, Hole 1168A, p. 154.

T17. Results of Rock-Eval pyrolysis analyses on sediments, Hole 1168A, p. 158.

F28. Total sulfur contents compared to C/S ratios, Hole 1168A, p. 88.

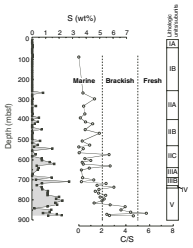

sional values >1 wt% dispersed through the profile. Sulfur standards were inconsistent from ~320 to 680 mbsf. Nonetheless, we calculated C/S ratios assuming that all of the sulfur exists as pyrite within the sediments. C/S values <2 are generally considered representative of marine environments, whereas C/S values >5 indicate freshwater-influenced environments (Berner and Raiswell, 1984).

Organic matter type was assessed using Rock-Eval pyrolysis and CNS analyses. In general, high HI (>~200) and low oxygen index (OI) (<~150) values from Rock-Eval pyrolysis are indicative of marine (Type II) or lacustrine (Type I) organic matter, although lacustrine organic matter generally shows higher HI and lower OI values than marine counterparts (Espitalie et al., 1977; Peters, 1986). In addition, C/N ratios of ~5–8 are generally considered to indicate marine organic matter (Bordovskiy, 1965; Emerson and Hedges, 1988). In contrast, terrestrially derived organic matter from higher plants (Type III) exhibits relatively low HI (<~150), relatively high OI values, and C/N ratios of ~25–35. Oxidized Type I and II organic matter may show HI and OI values similar to those obtained from Type III organic matter, and consistently low HI and OI values are characteristic of Type IV (highly oxidized) organic matter.

Hydrogen index values from Rock-Eval pyrolysis range from 0 to >600 mg of hydrocarbon per gram of TOC at Site 1168 (Fig. **F27;** Table **T17**). The highest HI values are in sediments above 300 mbsf, whereas below 300 mbsf only discrete horizons contain values exceeding 150. Oxygen index values vary between 21 and 5250 mg of CO_2 per gram of TOC. The T_{max} values obtained from Rock-Eval pyrolysis range from 350° to 590°C (Fig. **F29**), although the most reliable T_{max} values cluster between 400° and 430°C. T_{max} values provide an estimate of organic matter thermal maturity, with values <435°C being indicative of immaturity relative to petroleum generation. The "oil window" is generally considered to range between T_{max} values of 435°–465°C, whereas values >465°C are indicative of thermogenic gas zones (Espitalie et al., 1977; Peters, 1986).

The extremely low TOC values obtained from Rock-Eval pyrolysis in the upper 300 m of sediment at Site 1168 must be considered as lowering the reliability of the HI and OI values in this interval. We performed duplicate and triplicate analyses on many of the samples through this section of the core to validate the results. We found a close correspondence between HI values and C/N ratios, which suggests that our results are consistent and valid for interpretation. However, total nitrogen contents through the core are generally low, so C/N ratios must also be considered with care. The generally high OI values through much of the core are here attributed to the thermal degradation of calcium carbonate during pyrolysis and are not considered in this interpretation.

Discussion

The high carbonate content of sediments at Site 1168 mainly reflects the dominance of calcareous nannoplankton and foraminifers (see **"Biostratigraphy,"** p. 21). The overall upward increase in carbonate content through the cored interval is a direct consequence of a change from brackish/shallow-marine to pelagic open-ocean conditions. Within this depositional setting, an overall upward decrease in clastic sediment content was observed (see **"Lithostratigraphy,"** p. 8), indicating an upward decrease in clastic sediment dilution. The implications to interpretations of depositional environment and sequence stratigra-

F29. T_{max} values generated from Rock-Eval pyrolysis analyses of organic matter, Hole 1168A, p. 89.

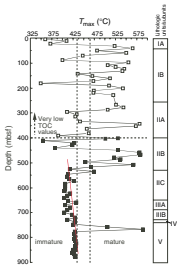

phy of the broad carbonate decline observed from ~530 to 320 mbsf are unclear. However, this zone corresponds to a distinct maximum in Ca^{2+} obtained from sediment pore waters, suggesting this zone may have been subject to preferential dissolution (see "Inorganic Geochemistry," p. 42).

A plot of carbonate content vs. TOC content (Fig. F30) shows that a wide range of percent carbonate values are present in sediments with low TOC values. However, the highest TOC values are only in those sediments with low carbonate content. Sediments with high TOC and low $CaCO_3$ are between ~700 and 878 mbsf, where clastic content is highest. This observation suggests that organic matter content in Hole 1168A is a function of preferential preservation (enhanced burial rate?) or enhanced terrestrial organic matter delivery associated with higher clastic sediment input, or both.

F30. TOC vs. $CaCO_3$ for sediments, Hole 1168A, p. 90.

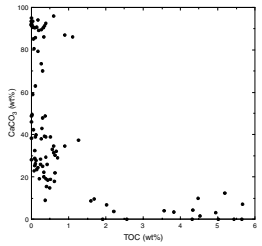

The type of organic matter encountered provides some insight into depositional processes at Site 1168. The basal portion of Hole 1168A from ~700 to 878 mbsf contains strong geochemical evidence for terrestrial organic matter influence on deposition at the site. As described above, this interval contains the lowest percent carbonate and highest TOC values, likely as a function of clastic input. Here, HI values of mostly <150 and C/N ratios >20 indicate terrestrial organic matter preservation, and total sulfur values and C/S ratios suggest dominantly brackish water conditions. Marine incursions into this relatively nearshore setting are indicated by fluctuations to higher HI, lower C/N, and relatively high total sulfur values at discrete horizons through this interval. A shift from terrestrial to marine-influenced conditions is indicated by organic carbon and carbonate preservation between ~700 and 750 mbsf at Site 1168. Here total sulfur and C/S values suggest brackish to marine water conditions. From ~700 to 500 mbsf, TOC content is still relatively high (0.5–1 wt%) but displays an overall decline that is maintained throughout the rest of the core. In this interval, HI values continue to suggest preservation of mostly Type III (terrestrial) organic matter; however, the elevated OI values may represent oxidized organic matter deposition. The C/N values through this interval are closer to marine values (0–15), although the signal is somewhat elevated compared with a typical marine signature. These parameters suggest mixed inputs of terrestrial or oxidized marine with marine organic matter to the seafloor. The percent carbonate begins a steady upward increase through this interval, which generally continues through the rest of the section. The C/S values suggest dominantly marine depositional conditions, with excursions into the brackish water realm. From ~450 to 350 mbsf, carbonate increases to >40 wt%, whereas TOC values decrease significantly to below 1. The C/S ratios indicate marine depositional conditions, with low values attributable to extremely low total sulfur values for those horizons. Discrete horizons containing relatively higher HI values and low C/N ratios indicate marine organic matter preservation, whereas lower HI values likely record seafloor-redox conditions as discussed below.

Above ~300 mbsf, the extremely high carbonate content (up to 95 wt%) represents either a decrease in clastic dilution or enhanced carbonate preservation and may indicate enhanced biogenic productivity. The extremely low TOC values through this interval likely record the settling of organic matter through a well-mixed water column and/or to a well-oxygenated seafloor. HI values vary widely, and the C/N ratios show a wide range of values from 0 to ~35. We suggest that the variations in organic matter type record variations in seafloor redox condi-

tions, although we cannot discount the possibility of limited terrestrial input to the system. In this conceptual model, intervals containing high HI and low C/N values likely record preservation of residual marine organic matter perhaps associated with carbonate producers, or dinocysts (see "Biostratigraphy," p. 21). Relatively high C/N and low HI intervals could represent oxidized marine organic matter in which N- and H-bearing functional groups have been cleaved to produce a more refractory, carbon-rich residuum. The high C/N and low HI units could also represent a total oxidation of labile marine organic matter and subsequent preservation of minor quantities of refractory terrestrial residuum.

The T_{max} values obtained from Rock-Eval pyrolysis are interpreted to represent mostly immature organic matter (Fig. F29). In the upper half of the core, T_{max} values fluctuate through the maximum possible range. This wide range is attributed to extremely low TOC values and the mixed marine to oxidized marine character of organic matter, which can generate an erroneously large range in T_{max} values. In the lower half of the core, by contrast, T_{max} values gradually smooth out and exhibit a sloping linear trend from ~410° to 435°C with depth. We consider these values as valid because they were obtained from horizons containing at least 0.5 wt% TOC composed of Type I organic matter; note, however, that Type I organic matter can generate erroneously low T_{max} values.

Volatile Hydrocarbons

Results

Concentrations of volatile hydrocarbon gases were measured from every core using the standard Ocean Drilling Program (ODP) headspace-sampling technique and gas chromatographic analysis. Profiles of methane content (Fig. F31; Table T18), and various methane, ethane, and propane ratios, are presented in Figure F31. Within the upper ~230 m of the cored sediment section, methane is present only in minor concentrations (2–716 ppmv) except near the surface, where methane content increases to 2400 ppmv (Fig. F31; Table T18). From 350 to ~500 mbsf, methane concentrations show a pronounced peak to ~52,000 ppmv. Below 500 mbsf, methane concentrations decrease relatively, although they remain high (up to >40,000 ppmv) and display a wide range. The ratios of methane vs. ethane plus propane (C_1/C_2+C_3), in contrast, show maximum values at the sediment surface (~8000) while decreasing gradually to 300–500 at ~500–700 mbsf and further to <100 at the base of the hole (Fig. F31). The percent wetness stays below 5% within the entire core, thus falling below the range of values typical for economically viable gas reservoirs (Fig. F31).

F31. Methane concentrations, methane vs. ethane and propane ratios, and percent wetness from headspace gas analysis, p. 91.

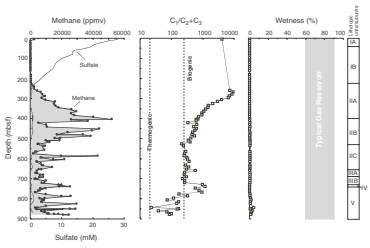

T18. Headspace gas composition, Hole 1168A, p. 160.

Discussion

The mostly low gas content of the uppermost 230 m of Site 1168 is likely a function of two characteristics of the sediment. First, the sediments contain very little organic matter as a source of natural gas. Second, pore-water profiles show that appreciable SO_4^{2-} exists to ~230 mbsf; thus, the sulfate reduction process may be limiting the onset of methanogenesis in this interval (see "Inorganic Geochemistry," p. 42). Below ~230 mbsf, methane content increases to a broad multipeaked zone of high concentrations between ~350 and 450 mbsf. The C_1/C_2+C_3 ratios indicate that this gas has a biogenic origin. The presence of this

peak immediately beneath the zone of sulfate reduction is characteristic of microbially driven diagenetic depth zonation (Claypool and Kaplan, 1974). However, the presence of elevated methane contents within strata generally characterized by TOC values of <0.5 wt% suggests that these lithologies may not be the sole gas source (i.e., the gas has migrated from elsewhere). In this case, the most likely source for the elevated biogenic methane content is the high TOC terrestrial organic matter (gas prone)-containing strata in the older parts of the section. Obviously, if any methane migrates higher in the section (above ~250 mbsf), it is likely oxidized in the sulfate reduction zone. However, this process does not describe the peak in methane content observed at Site 1168, if gas migration has occurred. Therefore, a mechanism must be invoked to trap gas in the strata. No obvious lithostratigraphic traps were recognizable (see **"Lithostratigraphy,"** p. 8). In fact, porosity measurements actually indicate an increase above the high methane content horizon (see **"Physical Properties,"** p. 45). Interestingly, a zone of soft-sediment deformation was observed at ~325 mbsf (see **"Lithostratigraphy,"** p. 8), and degassing intervals were observed during headspace sampling apparently centered on discrete particles at ~330–345 mbsf. These observations were considered as circumstantial evidence for methane clathrates; the bottom of the gas hydrate stability zone was calculated at ~300 mbsf (see **"Inorganic Geochemistry,"** p. 42). A resistivity "spike" at ~250 mbsf (see **"Downhole Measurements,"** p. 47) may also be suggestive of gas hydrates at an interval above the strata with relatively high methane content. If clathrates exist in the subsurface at Hole 1168A, they could prevent methane from migrating higher in the sedimentary sequence.

Beneath the zone of relatively elevated biogenic methane content, methane concentrations and the C_1/C_2+C_3 values show an overall decrease. The C_1/C_2+C_3 ratios approach the thermogenic range near the base of Hole 1168A. A limited number of gas samples were taken with a vacutainer in horizons where gas pockets were visible through the core liner. Vacutainer and headspace samples analyzed on the natural gas analyzer, from horizons between ~480 and 878 mbsf, include some butane (C_4) and pentane (C_5), suggesting a thermogenic origin for at least some of the gas phase (Hunt, 1996). These measurements are consistent with observations of thermogenic gas in shallow areas on the western Tasmania continental slope within ~30 km of Site 1168 (Hinz et al., 1986). In their study, Hinz et al. (1986) postulated an early to middle Eocene source rock, which may exist beneath the upper Eocene sediment at Site 1168.

T_{max} values approaching 435°C are indicative of the top of the "oil window." Of further interest to the thermal maturity of strata is the observation of double S_2 peaks on Rock-Eval pyrograms in cores between ~750 and 830 mbsf from Hole 1168A. Double S_2 peaks have been attributed to in situ organic matter and bitumen existing as a product of hydrocarbon generation from some of the in situ material (Clementz, 1979). Fluorescence was observed in core material treated with acetone between ~700 and 878 mbsf, suggesting the presence of liquid hydrocarbons (Shipboard Scientific Party, 1995), although the fluorescence may have been derived from acetone soluble portions of bitumen. The presence of bitumen and thermogenic gases suggests that the lowermost portions of Hole 1168A have been subject to some degree of thermal maturation. The depths in the core at which this postulated

maturation has occurred are anomalously low, suggesting the possibility of an alternate heat source to burial maturation.

INORGANIC GEOCHEMISTRY

Forty-nine whole-round samples were taken from Hole 1168A for interstitial water (IW) analyses at the following frequency: three per core in the upper 60 m, one per core from 60 to 100 m, and one every third core to total depth. Only 38 of the 47 IW samples were used for shipboard analyses; the balance of samples from the upper 60 mbsf of the hole were archived for shore-based analyses. Results of IW analyses are reported in Table T19 and Figure F32.

T19. Interstitial water data, p. 161.

Chloride, Sodium, and Salinity

The conservative parameters, chloride (Cl^-), sodium (Na^+), and salinity, exhibit little change in the upper 100 mbsf (Fig. F32; Table T19). Chloride increases downhole ~1% in the upper 25 mbsf to 564 mM, returning to seawater values in the underlying 75 mbsf; sodium varies from ~470 to 480 mM through the same interval. From 100 mbsf, Cl^- and Na^+ gradually decrease to 267 mbsf, where a sharp decrease exists to the base of the hole. The less sensitive salinity measurement does not show the same sharp decrease. In the interval of sharply decreasing values, Cl^- and Na^+ profiles covary and are marked by multiple distinct maxima and minima rather than smoothly decreasing values. The maximum dilution relative to seawater is 21% for Cl^- (440 mM), 17% for Na^+ (402 mM), and 28.5% for salinity (25). Previous studies (e.g., McDuff, 1985; Schrag et al., 1996) have attributed increases in Cl^- in the upper 50 mbsf to increases in salinity during the last glacial maximum. The 1% increase in Cl^- centered at 20 mbsf is consistent with this interpretation.

F32. Concentration-depth profiles of interstitial water chemistry with the approximate lithostratigraphic boundaries, p. 92.

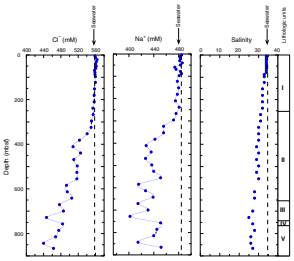

Low Cl^- in marine pore waters has been observed in a variety of environments, ranging from accretionary prisms to passive continental margins. One possible external source of low-Cl^- fluids in passive continental margins is advection of meteoric waters from the continent (e.g., Austin, Christie-Blick, Malone, et al., 1998). However, Site 1168 is located in one of a series of strike-slip basins between upthrown ridges of Cretaceous rocks on the western Tasmania margin (see **"Background and Objectives,"** p. 4). Thus, it seems unlikely that effective conduits for meteoric recharge could be achieved at Site 1168.

Possible internal sources that may provide low-Cl^- fluids are (1) gas hydrate dissociation; (2) dehydration reactions of hydrous minerals, such as clays and biogenic opal; and (3) clay-membrane ion filtration (e.g., Kastner et al., 1991; Hesse and Harrison, 1981; Paull, Matsumoto, Wallace, et al., 1996). The distinct maxima and minima in Cl^- and Na^+ values suggest that the emplacement of "fresher" fluids occurred relatively recently or diffusional processes would have smoothed the profiles. Gas hydrate dissociation is a common cause of such profiles in continental margin settings. Previous legs that have recovered gas hydrates have noted that the Cl^- profile returns to higher concentrations below the gas hydrate stability zone (e.g., Paull, Matsumato, Wallace, et al., 1996). The Cl^- profile at Site 1168 does not return to higher values below the estimated gas hydrate stability zone (GHSZ) or anywhere in the cored interval. Resistivity and sonic logs also do not show character-

istic responses typically associated with the presence of gas hydrates (see "Downhole Measurements," p. 47). In addition, crude estimates of the base of the GHSZ, using the measured geothermal gradient (60°C/km; see "Physical Properties," p. 45) and assuming a pure methane and seawater system, suggest methane hydrates should not be stable below ~300 mbsf at this site. However, the depth of the hydrate stability zone is sensitive to the chemistry of the pore fluids and incorporation of other gases into the hydrate structure (Dickens and Quinby-Hunt, 1997). Therefore, the existence of hydrates cannot yet be discounted, and a more rigorous calculation of gas hydrate stability will be pursued postcruise. With the data available, we cannot completely eliminate any of the possible hypotheses or evaluate if they are occurring in some combination; however, postcruise isotopic analyses may assist in differentiating between possible processes.

Sulfate, pH, Alkalinity, and Ammonium

Sulfate (SO_4^{2-}), titration alkalinity, and ammonium (NH_4^+) exhibit rapid changes in the upper part of the drilled interval (Fig. F32). Sulfate concentrations decrease from near-seawater values at the top of Hole 1168A to complete depletion by 238 mbsf, coincident with a sharp increase in methane (see "Volatile Hydrocarbons," p. 40, in "Organic Geochemistry;" Fig. F31). Alkalinity increases sharply in the upper 200 mbsf (maximum of 9.1 mM) then decreases to 3.9 mM across the lithostratigraphic Unit I/II boundary at 350 mbsf. There appears to be real alkalinity variation at depth, but the low fluid recovery over this depth interval prevented higher resolution alkalinity measurements. Ammonium increases steadily downhole over the entire drilled sequence, reaching a maximum concentration of 2.3 mM. The pH decreases from 7.5 at the top of the hole to ~7.0 in the upper 100 mbsf then increases to 7.6 at 324 mbsf, coincident with the alkalinity minima. Below 324 mbsf, the pH begins to decrease but the measurement became limited by low water content downcore. These major changes reflected in the profiles of SO_4^{2-}, alkalinity, and NH_4^+ are representative of bacterially mediated degradation of organic matter characterized primarily by sulfate reduction followed by methanogenesis (see "Volatile Hydrocarbons," p. 40, in "Organic Geochemistry"). The rate of sulfate reduction appears to be high for the low sedimentation rates noted for the upper 200 mbsf (~1.5 cm/k.y; see "Age Model and Sedimentation Rates," p. 33, in "Palynology").

Strontium, Calcium, and Lithium

Strontium (Sr^{2+}) concentrations increase with depth from the seafloor to a maximum of 909 µM centered at ~180 mbsf, below which values decrease to a minimum of 108 µM at the base of the hole. The calcium (Ca^{2+}) profile is nonsteady state, showing several maxima and minima. Calcium concentrations remain near seawater values for the upper 78 mbsf. Calcium concentration maxima are located at 123 mbsf (11.7 mM) and 468 mbsf (20.1 mM; 1.9 times seawater concentration). Minima in the Ca^{2+} profile are located at 238 mbsf (9.7 mM) and the base of the hole (866 mbsf; 5.8 mM, a 45% decrease from seawater values). Lithium (Li^+) concentrations steadily increase with depth, reaching 890 µM at 554 mbsf, below which values decrease to 277 µM at the base of the cored sequence. It is important to appreciate that the previ-

ously discussed pore-fluid freshening exhibited by the decrease in Cl^- should also affect the ions discussed in this section. Thus, Ca^{2+}, Li^+, and Sr^{2+} have been normalized to Cl^- in Figure **F33** to remove any dilution effect, yet still show nonsteady state trends.

The pronounced increase in Sr^{2+} centered around 200 mbsf is consistent with the release of dissolved Sr^{2+} to pore fluids during the recrystallization of pelagic carbonates (Manheim and Sayles, 1974; Baker et al., 1982). The largest increase in Sr^{2+} is in lithostratigraphic Unit I, which is dominated by calcareous oozes (see **"Lithostratigraphy,"** p. 8). Typically in deep-sea marine pore waters, Sr^{2+} reaches a maximum value at depth, maintaining a plateau concentration that is ultimately limited by celestite solubility (e.g., Baker and Bloomer, 1988). However, the rapid Sr^{2+} decrease with depth at Site 1168 indicates that either carbonate recrystallization is confined solely to the interval of elevated Sr^{2+} or a Sr^{2+} sink exists at depth.

The Ca^{2+} profile appears to be controlled by dissolution (the Ca^{2+} maxima) and precipitation (the Ca^{2+} minima) reactions. The Ca^{2+} maxima at 123 mbsf and minima at 238 mbsf are coincident with the zone of elevated Sr^{2+} values in the calcareous-rich sediments of lithostratigraphic Unit I and, therefore, may be the result of local carbonate dissolution and precipitation. The maximum concentration of Ca^{2+} at 468 mbsf corresponds with lithostratigraphic Unit II in a zone of low carbonate content (Fig. **F34**) and may be the result of intense dissolution of $CaCO_3$ in this interval. However, elevated Sr^{2+} concentrations, which usually accompany increases in dissolution of $CaCO_3$, are conspicuously absent here. The peak Ca^{2+} concentration also corresponds to the interval of increased Li^+ concentration. Increases in Li^+ with depth are often attributed to alteration of biogenic carbonate, biogenic opal, or other silicate phases, including ion-exchange reactions (Gieskes, 1983; DeCarlo, 1992); however with the present data set, we cannot distinguish the source of Ca^{2+} and Li^+ input to the pore fluids centered around 500 mbsf.

Magnesium and Potassium

Magnesium (Mg^{2+}) and potassium (K^+) concentrations gradually and consistently decrease downcore (Fig. **F32**). By the base of the hole, Mg^{2+} has decreased by 74.6% to 13.7 mM, whereas K^+ has decreased 64% to 3.8 mM. Normalizing the profiles to Cl^- (Fig. **F33**) shows these decreases are not attributable to dilution by the low-Cl^- source. The smooth diffusional profiles indicate that Mg^{2+} and K^+ are being consumed in reactions below the cored interval. The decrease in Mg^{2+} and K^+ are highly correlated (r = 0.986), which suggest they are removed by a similar process, probably associated with silicate reaction (i.e., clay diagenesis or alteration of basement) (e.g., Gieskes, 1983).

Silica

Dissolved silica ($H_4SiO_4^0$) concentrations range from ~250 µM to a maximum of ~800 µM, while showing distinct changes downcore. The highest concentrations of $H_4SiO_4^0$ (>600 µM) are found between ~100 to 230 mbsf and ~400 to 500 mbsf; concentrations of ~400–600 µM were observed at 20 to 100 mbsf, 550 to 700 mbsf, and 750 to 800 mbsf. The rest of the hole has $H_4SiO_4^0$ concentrations below ~400 µM.

F33. Concentration-depth profiles of Ca^{2+}, Sr^{2+}, Mg^{2+}, Li^+, and K^+ normalized to Cl^-, p. 95.

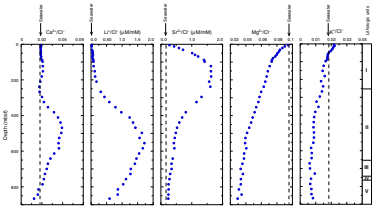

F34. Concentration of Ca^{2+} compared to weight percent $CaCO_3$, p. 96.

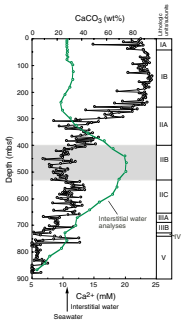

Smear-slide assessments of siliceous sponge spicule abundance (see "Biostratigraphy," p. 21) within the sediments at Site 1168 (>63 µM) covary with the pore fluid $H_4SiO_4^0$ variations (Fig. F35). This observation suggests that most silica dissolution occurs in sediments enriched in biogenic silica. The decreases in dissolved silica may be associated with primary depositional fluctuations or to diagenetic transformation of biogenic silica to opal-CT at depth (e.g., Baker, 1986). Further studies (e.g., X-ray diffraction analyses) may provide additional insight into such "silica diagenetic fronts."

F35. Concentration of dissolved silica within interstitial waters compared to siliceous sponge spicule abundance, Hole 1168A, p. 97.

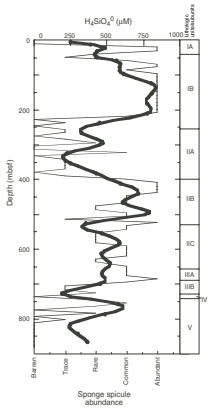

PHYSICAL PROPERTIES

The physical properties program at Site 1168 included MST and thermal conductivity measurements of whole-round cores and compressional wave (*P*-wave) velocity, moisture and density (MAD), and vane shear-strength measurements of split cores. The Adara tool was deployed four times in Hole 1168A for in situ temperature measurements.

Multisensor Track

All core sections from Holes 1168A, 1168B, and 1168C were routinely measured on the MST (for magnetic susceptibility, *P*-wave velocity, GRA density, and natural gamma ray) at 2-cm intervals. *P*-wave velocities were recorded at 2-cm intervals in Hole 1168A sections to a depth of ~111.8 mbsf. *P*-wave velocities were not recorded in the XCB-cored sections. Natural gamma-ray measurements were made on cores from Hole 1168A at 5- to 20-cm intervals down to 291.4 mbsf. Because the counts were barely above the background, these measurements were omitted below 291.4 mbsf.

GRA density data and discrete wet bulk density data both show a gradual downhole increase resulting from sediment compaction and dewatering with increased overburden (Fig. F36A). In addition to the overall downhole trend, the GRA data show distinct variations in relation to the lithologic changes at several stratigraphic boundaries (e.g., Miocene/Pliocene and Oligocene/Miocene boundaries; Fig. F36A).

F36. GRA and wet bulk density vs. depth, Hole 1168A, p. 98.

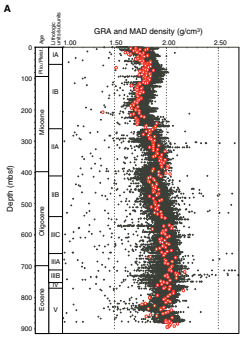

Some offsets, however, are evident between the MST and discrete density data. For example, GRA values are higher than the discrete density values between ~20 and 240 mbsf. The higher GRA values are explained by the relatively high carbonate content, porosity, and moisture content of the sediments for this interval. As the calibration procedure for the MST is optimized for mixed sediments, the GRA method overestimates the density in the carbonate-rich sediments of lithologic Subunits IA and IB.

Magnetic susceptibility (Fig. F36A) is negatively correlated with GRA and wet bulk density (Fig. F36B) in both carbonate- and clay-rich intervals of the hole. A good correlation is observed between magnetic susceptibility and color reflectance measurements, mainly the lightness value (L*) and the chromaticity coordinate b* (see "Lithostratigraphy," p. 8, and "Composite Depths," p. 36). Magnetic susceptibility and color reflectance reveal a pronounced cyclicity, which may be useful to identify astronomically controlled depositional processes in this region.

Velocity

Compressional velocities were obtained on the split-core sections at a sampling interval of one per section down to ~330 mbsf (Figs. F37, F38A). The discrete measurements were performed with the digital sediment velocimeter to a depth of ~240 mbsf. Below ~240 mbsf, we used the modified Hamilton Frame (PSW3) velocimeter. Signals were completely attenuated at a depth of ~350 mbsf, except for some cemented sandstones several centimeters thick in the lowermost part of Hole 1168A (in Sections 189-1168A-75X-6 and 86X-1; Fig. F38B). A comparison of the continuous velocity profile obtained with the MST and the discrete values is shown in Figure F37. As expected for the sediment type encountered at this site, velocities vary between 1550 m/s in the soft-surface sediments and 1900 m/s in the more consolidated sediments (Table T20). Downhole, the PSW3 (x- [across core] direction) velocities increase up to 2100 m/s at ~340 mbsf (Fig. F38A), similar to values seen in the downhole logging data (see "Downhole Measurements," p. 47). The velocity measurements perpendicular (PSW1; z- [along core] direction) and parallel to the bedding (PSW2; y- [perpendicular to the core] direction) show similar readings, indicating that no velocity anisotropies are present in the y- and z-directions of the sediments. There is an offset of PSW1 and PSW2 velocities compared to the PSW3 velocities, which increases sharply below ~100 mbsf. This offset is attributed to tension cracks in the sediments and fine cracks created in the sediments by the insertion of the transducers, thereby reducing *P*-wave propagation and resulting in lower *P*-wave velocities overall than obtained from the PSW3 transducer. The PSW3 transducer is nondestructive and appears to produce more accurate data below ~100 mbsf. PSW3 results are comparable to both MST and downhole logging data.

Thermal Conductivity

Thermal conductivity was measured on Section 3 of each core in Hole 1168A to a depth at which induration prevented insertion of the needles (~112 mbsf; Fig. F39). Values decrease with depth, corresponding to an overall decrease in porosity with depth (Fig. F40).

In Situ Temperature Measurements

The Adara tool was deployed four times in Hole 1168A. The temperature at the seafloor (2.5°C) was determined using the mudline stops. Three of these deployments yielded acceptable temperature records. The temperature record from Core 189-1168A-12H (a typical deployment record) shows a well-developed thermal decay after the penetration (Fig. F41). The successful penetration of the Adara tool into the bottom-hole formation results in an instantaneous rise of temperature as a result of the frictional heating of the penetration, which is followed by a gradual, exponential decrease during the dissipation of the heat.

Heat Flow

The geothermal gradient was determined using the four points of the temperature profile (Fig. F42). They can be reasonably fitted with a linear least-squares regression. The solution gives a geothermal gradient of 58°C/km compared to 27°C/km in the Cape Sorell No. 1 exploration well on the continental shelf 100 km to the northeast (Willcox et al.,

F37. *P*-wave velocities measured for discrete samples and in whole cores vs. depth, Hole 1168A, p. 100

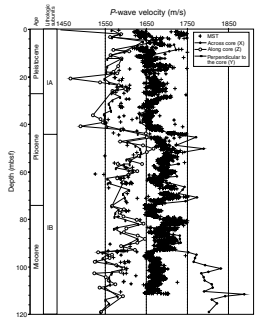

F38. *P*-wave velocities explained and measured for discrete samples vs. depth, p. 101.

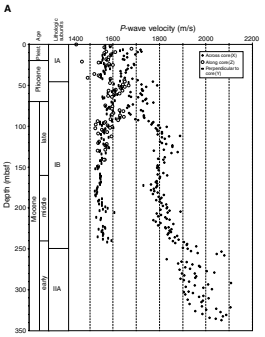

T20. *P*-wave velocities, Hole 1168A, p. 162.

F39. Thermal conductivity vs. depth measured on whole cores, p. 103.

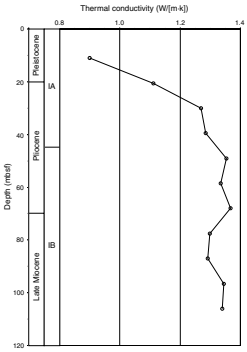

1989). The average of the thermal conductivities measured from 0 through 160 mbsf at Site 1168 is 1.25 W/(m·K) (Table T21). Calculations using the average conductivity and the geothermal gradient yield a heat flow of 72.5 mW/m². This heat-flow value is nearly two times higher than values reported from sedimentary basins and slopes near western Tasmania north of the site and Mesozoic continental margins in the mid-Atlantic (~40 mW/m²; Nagihara et al., 1996; Paull, Matsumoto, Wallace, et al., 1996).

Vane Shear Strength

Vane shear strength was measured once per section on Hole 1168A cores to the depth at which induration prevented insertion of the vane for shear strength (~260 mbsf). The results are displayed in Figure F43 and Table T22. On average, values show a good overall correlation with the GRA density (Fig. F43), indicating a strong relationship between lithology, degree of cementation, and shear strength.

Moisture and Density

Discrete moisture and density measurements are presented in Figure F40 and Table T23. Downhole trends reflect increased compaction and dewatering with depth. All of the first-order variations in moisture and density correlate well with the lithologic and stratigraphic (e.g., mid-Miocene, Oligocene/Miocene boundary, and Eocene–Oligocene transition) units. The discrete density data (Fig. F40) correlate very well with the GRA data and can be used to calibrate and correct GRA density (Fig. F36A).

Wet bulk density and porosity variability correlate well with silica content (see "Biostratigraphy," p. 21, and "Inorganic Geochemistry," p. 42) in lithostratigraphic Subunit IB of Hole 1168A. Water content and porosity mirror magnetic susceptibility (Fig. F36B) in the Oligocene and Eocene sections, reflecting the increased clay content in the deeper intervals at Site 1168. The carbonate-rich lithostratigraphic Subunit IB can be subdivided into an upper interval (from 45 to 125 mbsf) with relatively high density, *P*-wave velocity, shear strength, and thermal conductivity and low porosity and water content, and a lower interval (from 125 to 260 mbsf) characterized by low density, *P*-wave velocity, shear strength, and thermal conductivity but high porosity and water content (cf. Figs. F36A, F38A, F39, F40, F43).

The coring technique was changed from APC to XCB at 112 mbsf, which often results in spurious *P*-wave data because of disturbance resulting from core sampling. The *P*-wave velocity values measured both in downhole logs (starting at 120 mbsf) and on the cores, however, correlate very well around this interval. Therefore, it seems improbable that the drilling and splitting techniques have influenced the quality of the core measurements. The physical properties data for this interval merely reflect carbonate/silica variations in the sedimentary section.

DOWNHOLE MEASUREMENTS

Logging Operations

Downhole logging was performed in Hole 1168A after it had been drilled to a depth of 883 mbsf with a 9.875-in APC/XCB drill bit (see

F40. Wet bulk density, water content, and porosity measured at discrete intervals vs. depth, Hole 1168A, p. 104.

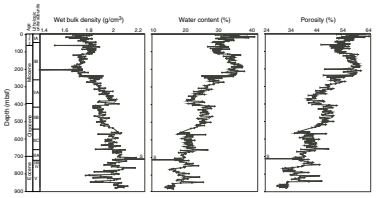

F41. Penetration temperature record from the Adara tool deployment in Core 189-1168A-12H, p. 105.

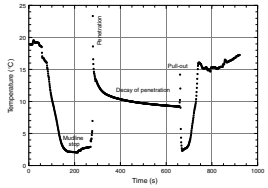

F42. Temperature vs. depth plot, p. 106.

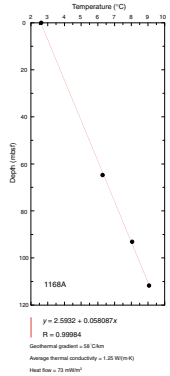

T21. Thermal conductivity measured on whole-core sections, Hole 1168A, p. 164.

F43. Undrained shear strength from miniature vane-shear measurements and GRA density vs. depth, Hole 1168A, p. 107.

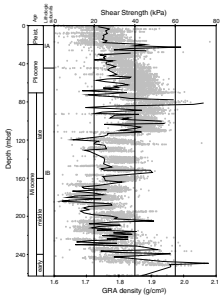

"Operations," p. 6). Two tool-string configurations were run, the triple combo and the GHMT-sonic (see "Downhole Measurements," p. 27, in the "Explanatory Notes" chapter). The dipole shear sonic imager (DSI) on the GHMT-sonic was run in P, S, and upper dipole mode (see Schlumberger, 1995). The weather was good, with a maximum recorded heave of <3 m. The wireline heave compensator was used throughout the logging operations.

Three logging runs were attempted, although the last one was unsuccessful. Details of the intervals logged, together with the position of the drill bit and the depth of the seafloor (calculated from results of the gamma-ray log) are shown in Figure F44. During the first logging run with the triple combo, the passage of the tool string up and down the hole was frequently hindered by bridges in the formation. For this reason a wiper trip was conducted after the first run, with the aim of clearing any constrictions. A wiper trip involves pushing the pipe all the way back to the base of the hole and then pulling the bit back up to the required depth. Despite this action, it was still only possible to reach a depth of 728.5 mbsf with the second tool string, the GHMT-sonic (see Fig. F44).

Because of very poor hole conditions (see "Results/Data Quality," below) it was decided that a second attempt to log the base of the hole with the GHMT-sonic was a higher priority than running the FMS. There were two principal reasons for this: (1) the hole conditions were so poor (see "Results/Data Quality," below) that any FMS data would likely be of limited or no use and (2) the scientifically important Eocene/Oligocene boundary was at ~750 mbsf (see "Biostratigraphy," p. 21), close to the position where logging had stopped during the second run (Fig. F44). A second wiper trip was conducted and the bit was placed at 664.5 mbsf. Unfortunately, it was still not possible to get the tool string past the constriction and no further data were obtained. The principal results are summarized in Figures F45, F46, and F47.

Results/Data Quality

The caliper data show that the borehole was uneven and highly variable in width (from 4 to >19 in), with the greatest rugosity occurring below 250 mbsf (Figs. F45). The poor hole conditions affected the readings from the density and neutron porosity tools the most because the sensors used to make these measurements require good contact against the borehole wall. The frequent association of high caliper readings (>18 in) with density minima and porosity maxima (Fig. F48) provides qualitative evidence of the effect that poor hole conditions had on these log values.

Comparing bulk density values from the high-temperature lithodensity sonde (HLDS) with results from the core (Fig. F49) shows that where hole conditions were poor, densities have been underestimated. This is particularly apparent between 300 and 500 mbsf. The density spike at 712 mbsf is evident in both the core and logging results (Fig. F49), suggesting that there is very little depth mismatch between the two data sets at this point. This density spike is correlative with an 18-cm-thick indurated sandstone bed recovered in the core.

A comparison of density porosity, neutron porosity, and core porosity (Fig. F50) shows that where hole conditions were poor, porosities have been overestimated. Above 300 mbsf, where hole conditions were reasonable, density porosities and core porosities are similar. However, the neutron porosities above 300 mbsf are significantly higher than

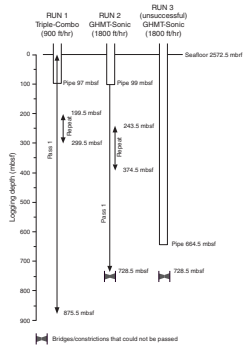

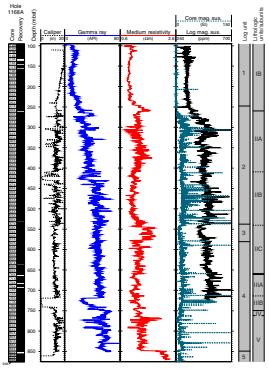

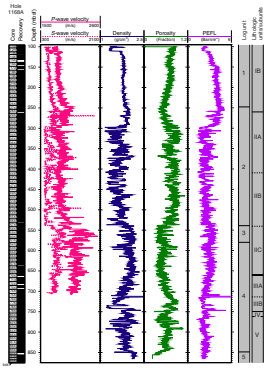

both the density and core values. Because the formation above 300 mbsf has a very similar composition to limestone (grain densities = 2.7 g/cm³; see "Physical Properties," p. 45), the offset between the neutron and density porosities are most likely a result of the effect of bound waters in clays or mica. The 18-cm-thick indurated sandstone bed, evident in the density log, produces minima in density and core porosities at 712 mbsf (Fig. F50).

The resistivity, gamma, and magnetic susceptibility logs are least affected by poor hole conditions and will be most useful for core/log integration and for providing information on fluctuating physical, chemical, and lithologic properties downhole. The sharp decreases in gamma and spectral gamma-ray ratios between 420–430 mbsf and 718–741 mbsf result from the fact that the caliper had to be closed to get past a bridge in the formation; this tool requires the caliper to be open to enable a correction to be made for borehole diameter.

The *P*-wave sonic data are also relatively unaffected by the hole conditions. The same is not true, however, of the shear wave (*S*-wave) data. The *S*-wave velocities between ~197.7 and 527.5 mbsf may be inaccurate because the amplitude of the *S*-wave arrival at the upper dipole was low throughout the logging of this interval. Down to ~240 mbsf, *P*-wave velocities from the DSI compare well with the velocities measured in the PSW-3 direction from core samples (see "Physical Properties," p. 45) (Fig. F51). However below ~240 mbsf, there is an increasing downhole discrepancy between the core and log results (Fig. F51). *P*-wave velocities were used to construct integrated traveltimes for this hole, which enable comparisons with the seismic section (see "Principal Results," p. 1).

Reasonable total field measurements were also recorded by the GHMT tool during the second run and may allow at least a partial magnetic reversal stratigraphy to be generated after shore-based processing. The difficulties encountered in the upper carbonate-rich section (logging Unit 1) by the shipboard paleomagnetists will likely also apply to downhole polarity stratigraphy in this interval.

Log Units

Log units have been defined using mainly resistivity, magnetic susceptibility, and sonic velocity data. These parameters are least affected by poor borehole conditions and tend to show the most variability downhole.

Log Unit 1: Base of the Pipe (97 mbsf) to 247.5 mbsf

Throughout this unit, the mean values of resistivity, magnetic susceptibility, sonic velocity, and natural gamma remain relatively low (0.958 ± 0.076 Ωm, 340 ± 11.8 SI, 1846 ± 43 m/s, and 12.7 ± 3.4 gAPI, respectively) (Figs. F45, F46, F47). Density values are also quite constant (mean = 1.77 ± 0.11 g/cm³), whereas porosities gradually decrease from 84% at the base of the pipe to ~50% at the bottom of this unit. This downhole porosity decrease is most likely caused by sediment compaction. The photoelectric effect (PEFL) values are consistently high between 145 and 247.5 mbsf (average = 4), indicating a high carbonate content, consistent with the calcareous biogenic ooze and chalks that dominate the core material down to 260 mbsf (lithostratigraphic Unit I; see "Lithostratigraphy," p. 8). In addition, the low magnetic susceptibility and natural gamma values suggest the terrige-

F47. Total gamma-ray and spectral gamma-ray values, Hole 1168A, p. 111.

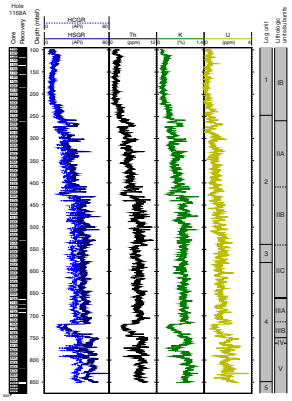

F48. Intervals from the logs where hole conditions were particularly poor, p. 112.

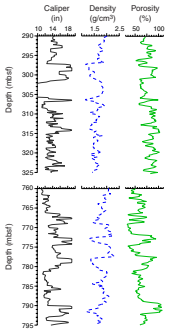

F49. Downhole log bulk density plotted with core bulk density, p. 113.

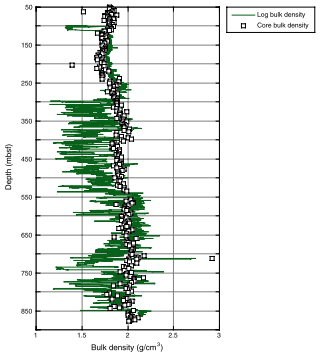

nous component of the sediments is low. The lack of any distinct variability in the other log parameters suggests a relatively uniform lithology throughout the unit.

Log Unit 2: 247.5–540.0 mbsf

Magnetic susceptibility values increase sharply from ~350 ppm at 247.5 mbsf to ~550 ppm at 305 mbsf, implying an increase in the terrigenous component of the formation. Magnetic susceptibilities then remain relatively high through the remainder of the logged section. Similarly, gamma-ray, resistivity, and sonic velocity values all show a stepwise increase near the top of Unit 2 (247.5–305.0 mbsf) consistent with an increased terrigenous fraction and general consolidation of the sediments. The variability in all log parameters is greater throughout this interval and most likely reflects a more lithologically and compositionally varied section relative to the upper portion of the hole.

Log Unit 3: 540.0–580.0 mbsf

At 540 mbsf *P*- and *S*-wave velocities show a marked increase; *P*-wave velocities increase from ~1960 to ~2190 m/s, and *S*-wave velocities increase from ~500 to ~840 m/s. Densities and resistivities also increase within this unit, whereas porosities and magnetic susceptibilities decrease. The decrease in magnetic susceptibility and an associated increase in PEFL values suggest carbonate contents increase relative to the siliciclastic component of the sediment.

Log Unit 4: 580.0–848.0 mbsf

There is a decrease in resistivity (from 1.72 to 1.17 Ωm), *P*-wave velocity (from 2350 to 2050 m/s) and density at the top of this unit. Magnetic susceptibilities are generally higher in Unit 4 than in Unit 3, suggesting a greater terrigenous component.

Log Unit 5: 848 mbsf–Base of the Hole

Resistivities increase very suddenly at 848 mbsf, to maximum values of 2.5 Ωm in this unit. Densities also increase slightly at this depth. Unfortunately, this region is too deep in the section to be captured by most of the other logs.

Core/Log Correlation

The transition between log Units 1 and 2 corresponds with a lithologic transition from calcareous biogenic oozes (75–97 wt% $CaCO_3$) in the upper 260 m of the sequence (lithostratigraphic Unit I) to increasingly siliciclastic sediments below, consistent with the compositional shift inferred from log parameters. The highest values of core magnetic susceptibility below 260 mbsf are associated with clay-rich zones (see **"Lithostratigraphy,"** p. 8, and **"Physical Properties,"** p. 45) implying that magnetic susceptibility is strongly influenced by changes in the siliciclastic fraction of the sediment. However, the presence of pyrite in many intervals must also influence the magnetic susceptibility and may explain some of the differences between the magnetic susceptibility and natural gamma logs. Accurate assessment of the periodicity and ultimate origin of the observed cyclicity in core magnetic susceptibility

F50. Downhole density porosity and neutron porosity plotted with core porosity, p. 114.

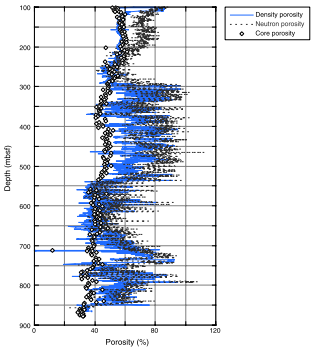

F51. Downhole *P*-wave velocities from the DSI logs plotted with the *P*-wave velocities measured vertically on half cores, p. 115.

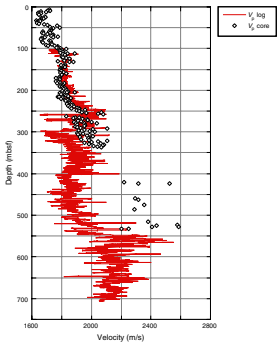

(see "Lithostratigraphy," p. 8) require that a continuous sequence with accurate depth control be used in the analysis. The strong correlation between continuous log and discontinuous core magnetic susceptibility records should allow the recovered XCB sections to be mapped back to their true stratigraphic depths, providing an estimate of the size and location of core gaps and the number of cycles missed. A good example of this is shown in Figure F52.

The zone of increased consolidation inferred from log responses (log Unit 3; 540–580 mbsf) is consistent with the increased lithification observed at 540 mbsf (the top of lithostratigraphic Subunit IIC, see "Lithostratigraphy," p. 8). The relative stabilization of log caliper readings below 540 mbsf is also consistent with an in-formation consolidation at this point.

The top of logging Unit 5 (848 mbsf), defined by the sudden increase in resistivity, corresponds to an observed change in clay mineralogy in the core. Between Cores 189-1168A-90X and 88X, there is an upward transition from predominantly kaolinite to smectite (see "Lithostratigraphy," p. 8). This mineralogic change may be related to an increase in tectonism leading to a sedimentary environment more typical of passively subsiding regions (see "Lithostratigraphy," p. 8). The short interval (<2 m) over which resistivity increases in the log section suggests that this environmental change is confined to a relatively brief depositional period.

One valuable application of the sonic velocity logging is the creation of a curve of depth (in meters below seafloor) vs. two-way traveltime (in seconds). For Hole 1168A, the velocity information from the sonic log was collated with the *P*-wave data from the MST from the top of the hole, where the drill pipe prevented the recording of good log data. The one-way velocities increased steadily down the hole from ~1600 m/s at the top to ~2100 m/s at the base of the log at ~720 m. The cumulative velocities (in two-way traveltime) have been plotted against depth in Figure F53 and are assumed to approximate to seismic velocities. By using the time/depth curve, we can correlate the seismic reflection profiles with well horizons, thus putting Site 1168 into the regional context. Figure F5, p. 70, in the "Leg 189 Summary" chapter, indicates that some major reflectors correspond to various biostratigraphic/lithostratigraphic boundaries; "Me" to the top of the lower Miocene and to the Unit I/II boundary; "El" to the top of the upper Eocene and the Unit III/IV boundary.

F52. Core and log magnetic susceptibility data, Holes 1168A and 1168C, p. 116.

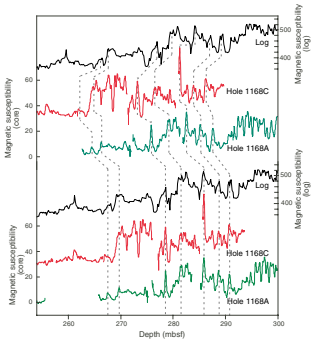

F53. Sonic two-way traveltime curve, p. 117.

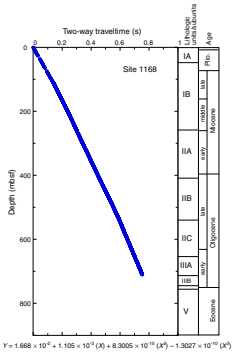

Discussion

Gas Hydrates

Geochemical and lithologic results from the core indicate the possibility of gas hydrates at this site. Headspace measurements show that methane concentrations reach a maximum of ~50,000 ppm at ~400 mbsf (see "Organic Geochemistry," p. 37), and observations of soft-sediment deformation observed in the core at ~325 mbsf may be indicative of the dissociation of methane clathrates (see "Lithostratigraphy," p. 8). At this stage, log measurements are unable to confirm or deny the presence of gas hydrates at Site 1168.

Simple thermodynamic models give a general estimate for the base of the gas hydrate stability zone at ~300 mbsf (see "Inorganic Geochemistry," p. 42). If hydrates were present at this site, then sonic data should show a sharp decrease in *P*-wave velocities at the depth of the

inferred change from gas hydrates to free gas (see Guerin et al., 1999; Paull et al., 1996). There is indeed a sharp decrease in *P*- wave velocities at ~295 mbsf, from ~1940 to 1830 m/s (Fig. F46). Nevertheless, there is also a concomitant decrease in *S*-wave velocities and densities at this point, which should not happen if this zone marks a change from hydrate- to gas-bearing sediments (see Anstey, 1991; Guerin et al., 1999). However, the quality of the *S*-wave and density data are not particularly good in this interval (see "Results/Data Quality," p. 48). Gas hydrates are generally associated with increased resistivity values (e.g., Matthews and von Huene, 1985). There is a slightly anomalous spike in resistivities in Hole 1168A at 257 mbsf (Fig. F45), which could possibly indicate the presence of gas hydrates, although this depth does not correlate with the decrease in sonic velocities. Further postcruise work is required.

Organic-Rich Shales

The spectral gamma-ray values downhole (Fig. F47) show that a good correlation exists between Th and K concentrations. This is commonly observed in ODP holes, as both Th and K tend to be contained within the terrigenous clay component of the sediment (Hassan et al., 1976). At this site, U concentrations vary semi-independently of Th and K and, to a certain extent, of total gamma (HSGR). Increasing U concentrations are generally associated with increasing organic matter within the sediment, and particularly high U concentrations (>~5 ppm) and low Th/U ratios (<~2) are often associated with black shale deposits (Adams and Weaver, 1958; Doveton 1991). The logging results (Fig. F47) show that U concentrations increase steadily downhole from <0.1 ppm in log Unit 1 to >4.5 ppm at the base of the hole. The increasing contribution that U makes toward total gamma-ray radioactivity downhole is illustrated by the increasing offset between the HSGR (Th, K, and U radiation) and HCGR (Th and K radiation) curves (Fig. F47). This increase in U concentrations downhole is consistent with the lithostratigraphic results, which show increasing organic matter with depth. However, although Th/U ratios generally decrease downhole, it seems unlikely that the extremely acidic, reducing conditions necessary for the formation of black shale were ever achieved (Fig. F54).

F54. Downhole Th/U ratios, Hole 1168A, p. 118.

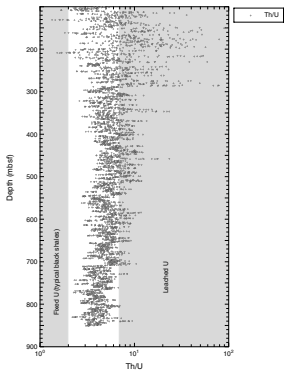

REFERENCES

Adams, J.A.S., and Weaver, C.E., 1958. Thorium-to-uranium ratios as indicators of sedimentary processes: example of concept of geochemical facies. *AAPG Bull.,* 42:387–430.

Anstey, N.A., 1991. Velocity in thin section. *First Break,* 9:449–457.

Austin, J.A., Jr., Christie-Blick, N., Malone, M.J., et al., 1998. *Proc. ODP, Init. Repts.,* 174A: College Station, TX (Ocean Drilling Program).

Baker, P.A., 1986. Pore-water chemistry of carbonate-rich sediments, Lord Howe Rise, Southwest Pacific Ocean. *In* Kennett, J.P., von der Borch, C.C., et al., *Init. Repts. DSDP,* 90 (Pt. 2): Washington (U.S. Govt. Printing Office), 1249–1256.

Baker, P.A., and Bloomer, S.H., 1988. The origin of celestite in deep-sea carbonate sediments. *Geochim. Cosmochim. Acta,* 52:335–339.

Baker, P.A., Gieskes, J.M., and Elderfield, H., 1982. Diagenesis of carbonates in deep-sea sediments: evidence from Sr^{2+}/Ca^{2+} ratios and interstitial dissolved Sr^{2+} data. *J. Sediment. Petrol.,* 52:71–82.

Berggren, W.A., Hilgen, F.J., Langereis, C.G., Kent, D.V., Obradovich, J.D., Raffi, I., Raymo, M.E., and Shackleton, N.J., 1995a. Late Neogene chronology: new perspectives in high-resolution stratigraphy. *Geol. Soc. Am. Bull.,* 107:1272–1287.

Berggren, W.A., Kent, D.V., Swisher, C.C., III, and Aubry, M.-P., 1995b. A revised Cenozoic geochronology and chronostratigraphy. *In* Berggren, W.A., Kent, D.V., Aubry, M.-P., and Hardenbol, J. (Eds.), *Geochronology, Time Scales and Global Stratigraphic Correlation.* Spec. Publ.—Soc. Econ. Paleontol. Mineral. (Soc. Sediment. Geol.), 54:129–212.

Berner, R.A., and Raiswell, R., 1984. C/S method for distinguishing freshwater from marine sedimentary rocks. *Geology,* 12:365–368.

Bordovskiy, O.K., 1965. Accumulation and transformation of organic substances in marine sediment, 2. Sources of organic matter in marine basins. *Mar. Geol.,* 3:5–31.

Bujak, J.P., and Mudge, D.C., 1994. A high-resolution North Sea Eocene dinocyst zonation. *J. Geol. Soc. London,* 151:449–462.

Cande, S.C., Stock, J.M., Muller, R.D., and Ishihara, T., 2000. Cenozoic motion between east and west Antarctica. *Nature,* 404:145–150.

Chamley, H., 1989. *Clay Sedimentology:* Berlin (Springer-Verlag).

Claypool, G.E., and Kaplan, I.R., 1974. The origin and distribution of methane in marine sediments. *In* Kaplan, I.R. (Ed.), *Natural Gases in Marine Sediments:* New York (Plenum), 99–139.

Clementz, D.M., 1979. Effect of oil and bitumen saturation on source-rock pyrolysis. *AAPG Bull.,* 63:2227–2232.

De Carlo, E.H., 1992. Geochemistry of pore water and sediments recovered from the Exmouth Plateau. *In* von Rad, U., Haq, B.U., et al., *Proc. ODP, Sci. Results,* 122: College Station, TX (Ocean Drilling Program), 295–308.

Dickens, G.R., and Quinby-Hunt, M.S., 1997. Methane hydrate stability in pore water: a simple theoretical approach for geophysical applications. *J. Geophys. Res.,* 102:773–783.

Doveton, J.D., 1991. Lithofacies and geochemical facies profiles from nuclear wireline logs: new subsurface templates for sedimentary modeling. *In* Franseen, E.K., Watney, W.L., Kendall, C.J., and Ross, W. (Eds.), *Sedimentary Modeling: Computer Simulations and Methods for Improved Parameter Definition.* Kansas Geol. Soc. Bull., 233:101–110.

Emerson, S., and Hedges, J.I., 1988. Processes controlling the organic carbon content of open ocean sediments. *Paleoceanography,* 3:621–634.

Espitalié, J., Madec, M., and Tissot, B., 1977. Source rock characterization method for petroleum exploration. *Proc. Annu. Offshore Technol. Conf.,* 3:439–443.

Gieskes, J.M., 1983. The chemistry of interstitial waters of deep-sea sediments: interpretation of deep-sea drilling data. *In* Riley, J.P., and Chester, R. (Eds.), *Chemical Oceanography* (Vol. 8): London (Academic), 221–269.

Guerin, G., Goldberg, D., and Meltser, A., 1999. Characterization of in situ elastic properties of gas-hydrate bearing sediments on the Blake Ridge. *J. Geophys. Res.,* 104:17781–17795.

Hambrey, M.J., Ehrmann, W.U., and Larsen, B., 1991. Cenozoic glacial record of the Prydz Bay continental shelf, East Antarctica. *In* Barron, J., Larsen, B., et al., *Proc. ODP, Sci. Results,* 119: College Station, TX (Ocean Drilling Program), 77–132.

Hassan, M., Hossin, A., and Combaz, A., 1976. Fundamentals of the differential gamma ray log: interpretation technique. *Trans. SPWLA 17th Annu. Logging Symp.,* H1–H18.

Hesse, R., and Harrison, W.E., 1981. Gas hydrates (clathrates) causing pore-water freshening and oxygen isotope fractionation in deep-water sedimentary sections of terrigenous continental margins. *Earth Planet. Sci. Lett.,* 55:453–462.

Hill, P.J., Meixner, A.J., Moore, A.M.G., and Exon, N.F., 1997. Structure and development of the West Tasmanian offshore sedimentary basins: results of recent marine and aeromagnetic surveys. *Aust. J. Earth Sci.,* 44:579–596.

Hinz, K., Willcox, J.B., Whiticar, M., Kudrass, H.-R., Exon, N.F., and Feary, D.A., 1986. The West Tasmanian Margin: an underrated petroleum province? *In* Glenie, R.C. (Ed.), *Tech. Papers at 2nd South-Eastern Australia Oil Exploration Symposium,* Melbourne, November 14–15, 1985. Pet. Expl. Soc. Aust., 395–410.

Hunt, J.M., 1996. *Petroleum Geochemistry and Geology* (2nd. ed): New York (W.H. Freeman and Company).

Jenkins, D.G., 1985. Southern mid-latitude Paleocene to Holocene planktic foraminifera. *In* Bolli, H.M., Saunders, J.B., and Perch-Nielsen, K. (Eds.), *Plankton Stratigraphy:* Cambridge (Cambridge Univ. Press), 263–282.

Jenkins, D.G., 1993a. Cenozoic southern mid- and high-latitude biostratigraphy and chronostratigraphy based on planktonic foraminifera. *In* Kennett, J.P., and Warnke, D.A. (Eds.), *The Antarctic Paleoenvironment: A Perspective on Global Change.* Antarct. Res. Ser., 60:125–144.

————, 1993b. The evolution of the Cenozoic Southern high-and mid-latitude planktonic foraminiferal faunas. *In* Kennett, J.P., and Warnke, D.A. (Eds.), *The Antarctic Paleoenvironment: a Perspective of Global Change.* Antarct. Res. Ser., 60:175–194.

Kastner, M., Elderfield, H., and Martin, J.B., 1991. Fluids in convergent margins: what do we know about their composition, origin, role in diagenesis and importance for oceanic chemical fluxes? *Philos. Trans. R. Soc. London A,* 335:243–259.

Kennett, J.P., 1977. Cenozoic evolution of Antarctic glaciation, the circum-Antarctic Ocean, and their impact on global paleoceanography. *J. Geophys. Res.,* 82:3843–3860.

Kennett, J.P., and Fackler-Adams, B.N., 2000. Relationship of clathrate instability to sediment deformation in the upper Neogene of California. *Geology,* 28:215–218.

Kennett, J.P., Houtz, R.E., et al., 1975. *Init. Repts. DSDP,* 29: Washington (U.S. Govt. Printing Office).

Lindsley-Griffin, N., Kemp, A., and Swartz, J.F., 1990. Vein structures of the Peru Margin, Leg 112. *In* Suess, E., von Huene, R., et al., *Proc. ODP, Sci. Results,* 112: College Station, TX (Ocean Drilling Program), 3–16.

MacPhail, M.K., 1999. Palynostratigraphy of the Murray Basin, inland southeastern Australia. *Palynology,* 23:197–240.

Manheim, F.T., and Sayles, F.L., 1974. Composition and origin of interstitial waters of marine sediments, based on deep sea drill cores. *In* Goldberg, E.D. (Ed.), *The Sea* (Vol. 5): *Marine Chemistry: The Sedimentary Cycle:* New York (Wiley), 527–568.

Matthews, M.A., and von Huene, R., 1985. Site 570 methane hydrate zone. *In* von Huene, R., Aubouin, J., et al., *Init. Repts. DSDP,* 84: Washington (U.S. Govt. Printing Office), 773–790.

McDuff, R.E., 1985. The chemistry of interstitial waters, Deep Sea Drilling Project Leg 86. *In* Heath, G.R., Burckle, L.H., et al., *Init. Repts. DSDP,* 86: Washington (U.S. Govt. Printing Office), 675–687.

McRae, S.G., 1972. Glauconite. *Earth-Sci. Rev.,* 8:397–440.

Morley, J.J., and Nigrini, C., 1995. Miocene to Pleistocene radiolarian biostratigraphy of North Pacific Sites 881, 884, 885, 886, and 887. *In* Rea, D.K., Basov, I.A., Scholl, D.W., and Allan, J.F. (Eds.), *Proc. ODP, Sci. Results,* 145: College Station, TX (Ocean Drilling Program), 55–91.

Motoyama, I., 1999. A review of radiolarian biostratigraphy for the oil-bearing Neogene of Japan: advances in biostratigraphic resolution. *J. Jpn. Assoc. Pet. Tech.,* 64:28–39.

Nagihara, S., Sclater, J.G., Phillips, J.D., Behrens, E.W., Lewis, T., Lawver, L.A., Nakamura, Y., Garcia-Abdeslem, J., and Maxwell, A.E., et al., 1996. Heat flow in the western abyssal plain of the Gulf of Mexico: implications for thermal evolution of the old oceanic lithosphere. *J. Geophys. Res.,* 101:2895–2913.

O'Sullivan, P.B., and Kohn, B.P., 1997. Apatite fusion track thermochronology of Tasmania. *Aust. Geol. Surv. Org. Rec.,* 1997/35:61.

Paillard, D., Labeyrie, L., and. Yiou, P., 1996. Macintosh program performs time-series analysis. *Eos,* 77:379.

Paull, C.K., Matsumoto, R., Wallace, P.J., et al., 1996. *Proc. ODP, Init. Repts.,* 164: College Station, TX (Ocean Drilling Program).

Peters, K.E., 1986. Guidelines for evaluating petroleum source rock using programmed pyrolysis. *AAPG Bull.,* 70:318–329.

Pye, K., 1987. *Aeolian Dust and Dust Deposits:* London (Academic Press).

Robert, C., 1987. Clay mineral associations and structural evolution of the South Atlantic: Jurassic to Eocene. *Palaeogeogr., Palaeoclimatol., Palaeoecol.,* 58:87–108.

Robert, C., and Chamley, H., 1987. Cenozoic evolution of continental humidity and paleoenvironment, deduced from the kaolinite content of oceanic sediments. *Palaeogeogr., Palaeoclimatol., Palaeoecol.,* 60:171–187.

————, 1992. Late Eocene–early Oligocene evolution of climate and marine circulation: deep-sea clay mineral evidence. *In* Kennett, J.P., and Warnke, D.A. (Eds.), *The Role of the Southern Ocean and Antarctica in Global Change.* Antarct. Res. Ser., 56:97–117.

Robert, C., and Kennett, J.P., 1992. Paleocene and Eocene kaolinite distribution in the South Atlantic and Southern Ocean: Antarctic climatic and paleoceanographic implications. *Mar. Geol.,*103:99–110.

Robert, C., Stein, R., and Acquaviva, M., 1985. Cenozoic evolution and significance of clay associations in the New Zealand region of the South Pacific, DSDP Leg 90. *In* Kennett, J.P., von der Borch, C.C., et al., *Init. Repts. DSDP,* 90: Washington (U.S. Govt. Printing Office), 1225–1238.

Schlumberger, 1995. *DSI—Dipole Sonic Imager:* Houston (Schlumberger Wireline and Testing), SMP-5128.

Schrag, D.P., Hampt, G., and Murray, D.W., 1996. Pore fluid constraints on the temperature and oxygen isotopic composition of the glacial ocean. *Science,* 272:1930–1932.

Shipboard Scientific Party, 1995. Site 909. *In* Myhre, A.M., Thiede, J., Firth, J.V., et al., *Proc. ODP, Init. Repts.,* 151: College Station, TX (Ocean Drilling Program), 159–220.

Spiegler, D., and von Daniels, C.H., 1991. A stratigraphic and taxonomic atlas of *Bolboforma* (Protophytes, incertae sedis, Tertiary). *J. Foraminiferal Res.,* 21:126–158.

Stein, R., and Robert, C., 1986. Siliciclastic sediments at Sites 588, 590 and 591: Neogene and Paleogene evolution in the Southwest Pacific and Australian climate. *In* Kennett, J.P., von der Borch, C.C., et al., *Init. Repts. DSDP,* 90 (Pt. 2): Washington (U.S. Govt. Printing Office), 1437–1455.

Stott, L.D., and Kennett, J.P., 1990. Antarctic Paleogene planktonic foraminifer biostratigraphy: ODP Leg 113, Sites 689 and 690. *In* Barker, P.F., Kennett, J.P., et al., *Proc. ODP, Sci. Results,* 113: College Station, TX (Ocean Drilling Program), 549–569.

Weaver, C.E., 1989. *Clays, Muds, and Shales:* Amsterdam (Elsevier).

Wei, W., and Wise, S.W., Jr., 1992. Eocene-Oligocene calcareous nannofossil magnetobiochronology of the Southern Ocean. *Newsl. Stratigr.,* 26:119–132.

Willcox, J.B., Baillie, P., Exon, N.F., Lee, C.-S., and Thomas, B., 1989. BMR record 1989/13, Field Excursion Notes. The geology of Western Tasmania and its continental margin–with particular reference to petroleum potential. *Bureau Mineral Resources* (Australia), Record 1989/13.27.

Figure F1. Postdrilling interpretation for local seismic profile SO36-47, across Site 1168, showing broad ages and lithostratigraphic units. The site is on a gentle slope to the west. Note the thick Oligocene sequence. The long-wavelength hummocks in the late Eocene may represent delta distributaries. There is almost no seismic character in the younger sequences, but three age/lithostratigraphic boundaries are marked by reflectors: Me, Oe, and El. Siliciclastic material has been shed from a ridge upslope into the Eocene and Oligocene sequences. TWT = two-way traveltime. TD = total depth (subseabed).

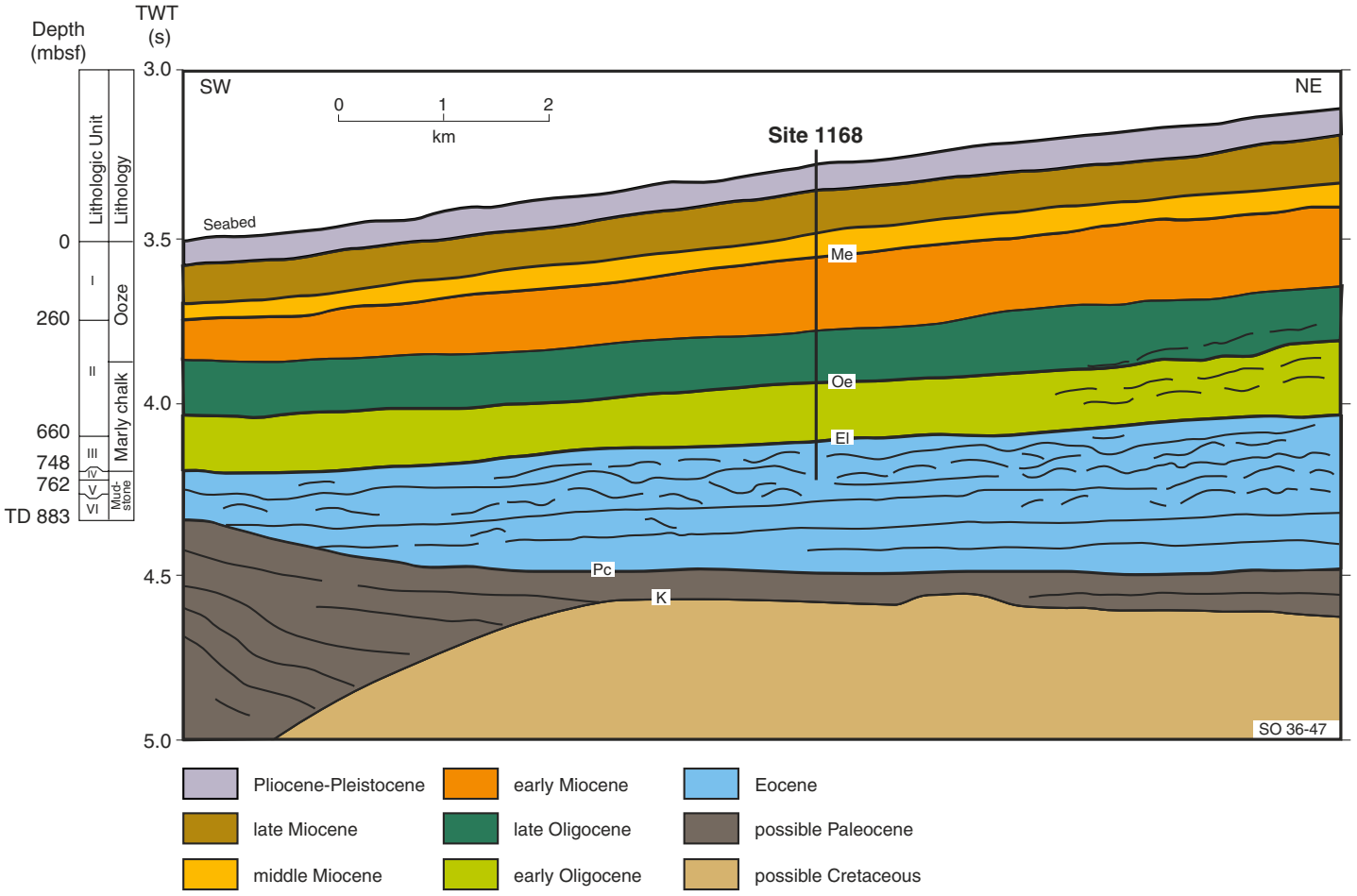

Figure F2. A portion of the seismic line *Sonne* SO36-47 through Site 1168, including the approximate depth of penetration. SP = shotpoint.

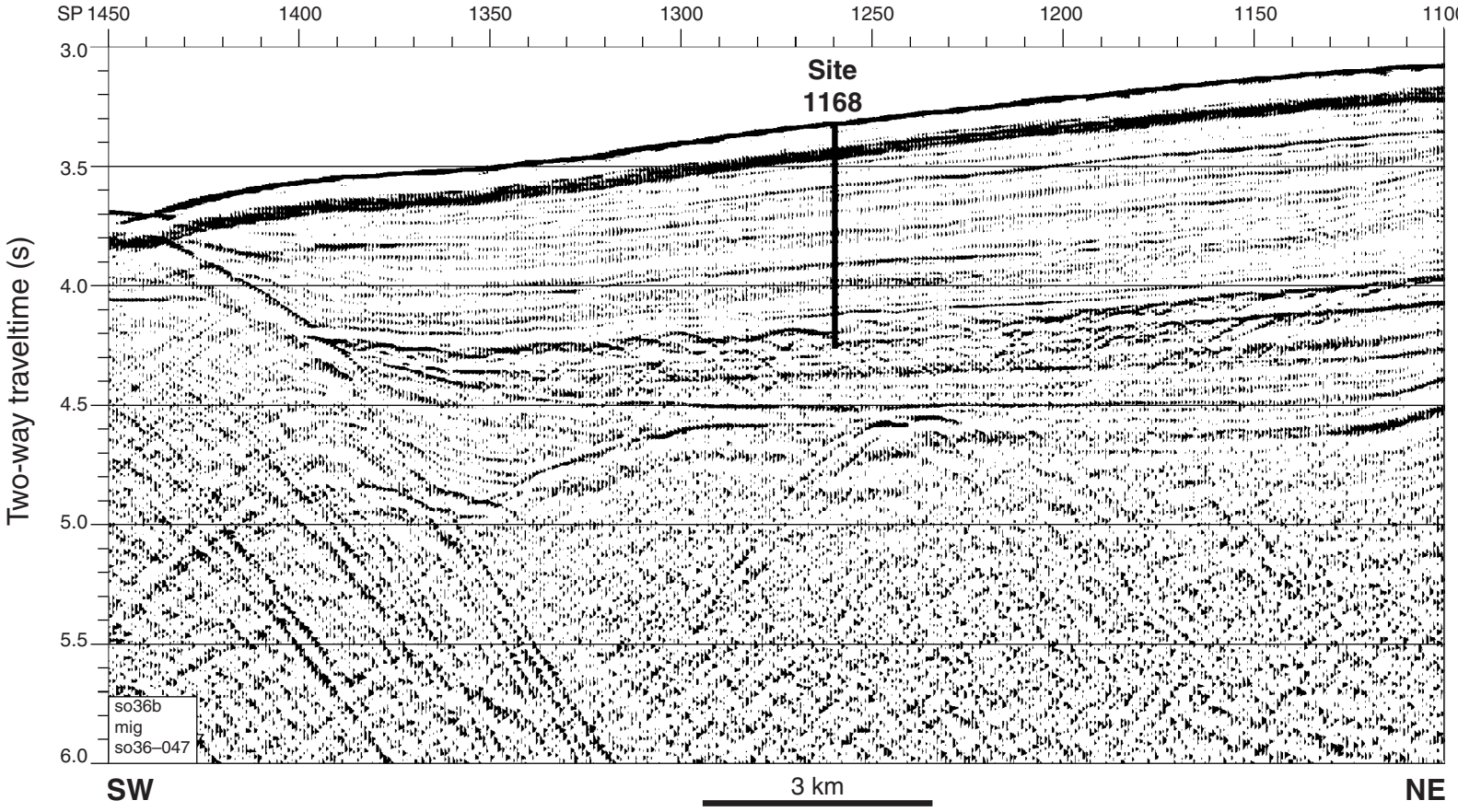

Figure F3. Regional cross section through time across Site 1168, from Tasmania southwest to the abyssal plain, based on seismic profile SO36-47 and other geological information. Note the development of ridges by northwest-southeast strike-slip motion between Australia and Antarctica during the Paleocene, the Eocene departure of Antarctica by strike-slip motion and emplacement of oceanic crust, and the Oligocene collapse of the margin. Cape Sorell drill site No. 1 is located at shallow depth on the transect. TWT = two-way traveltime.

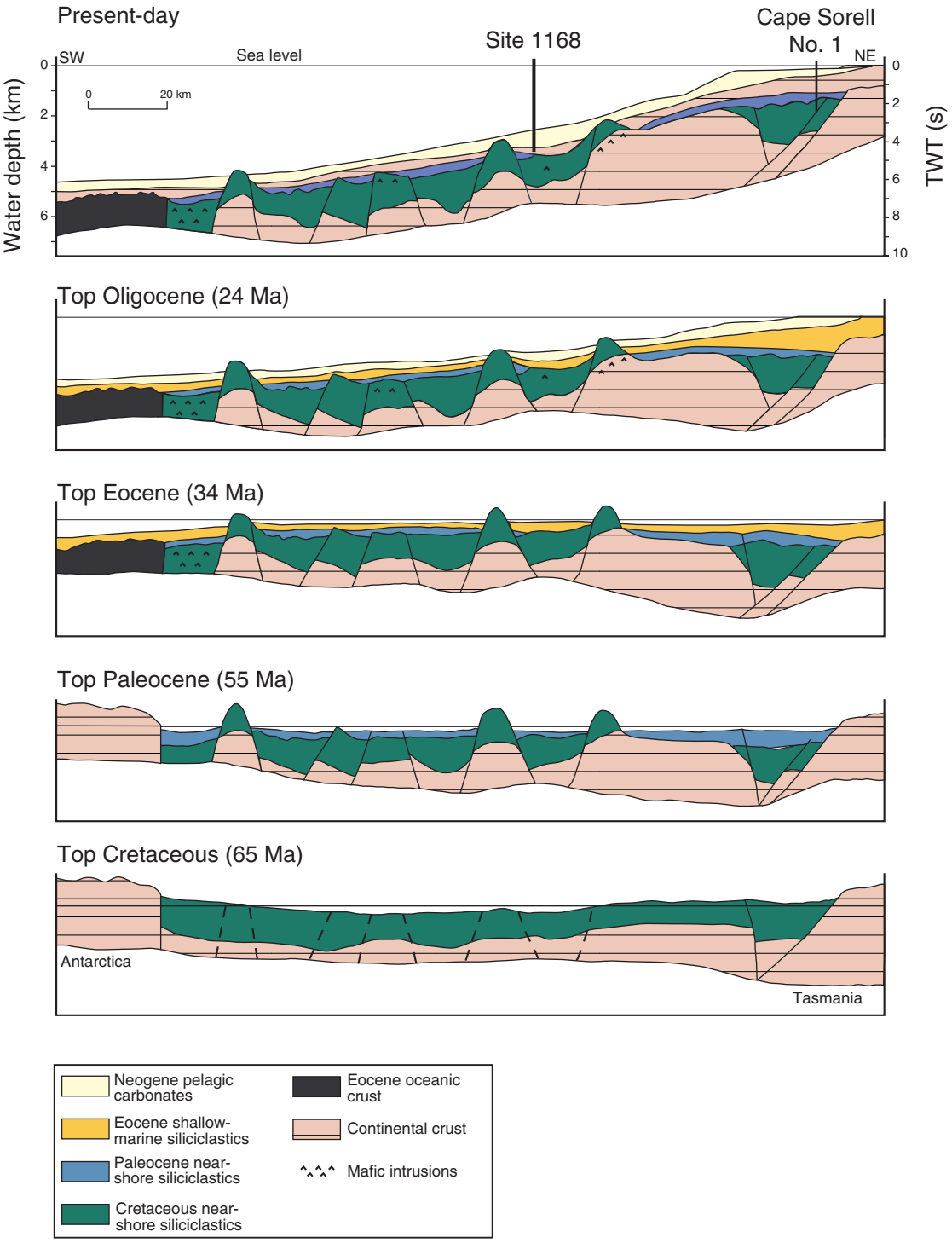

Figure F4. Major lithologic units of Site 1168 and their chronology. GRA = gamma-ray attenuation. TD = total depth.

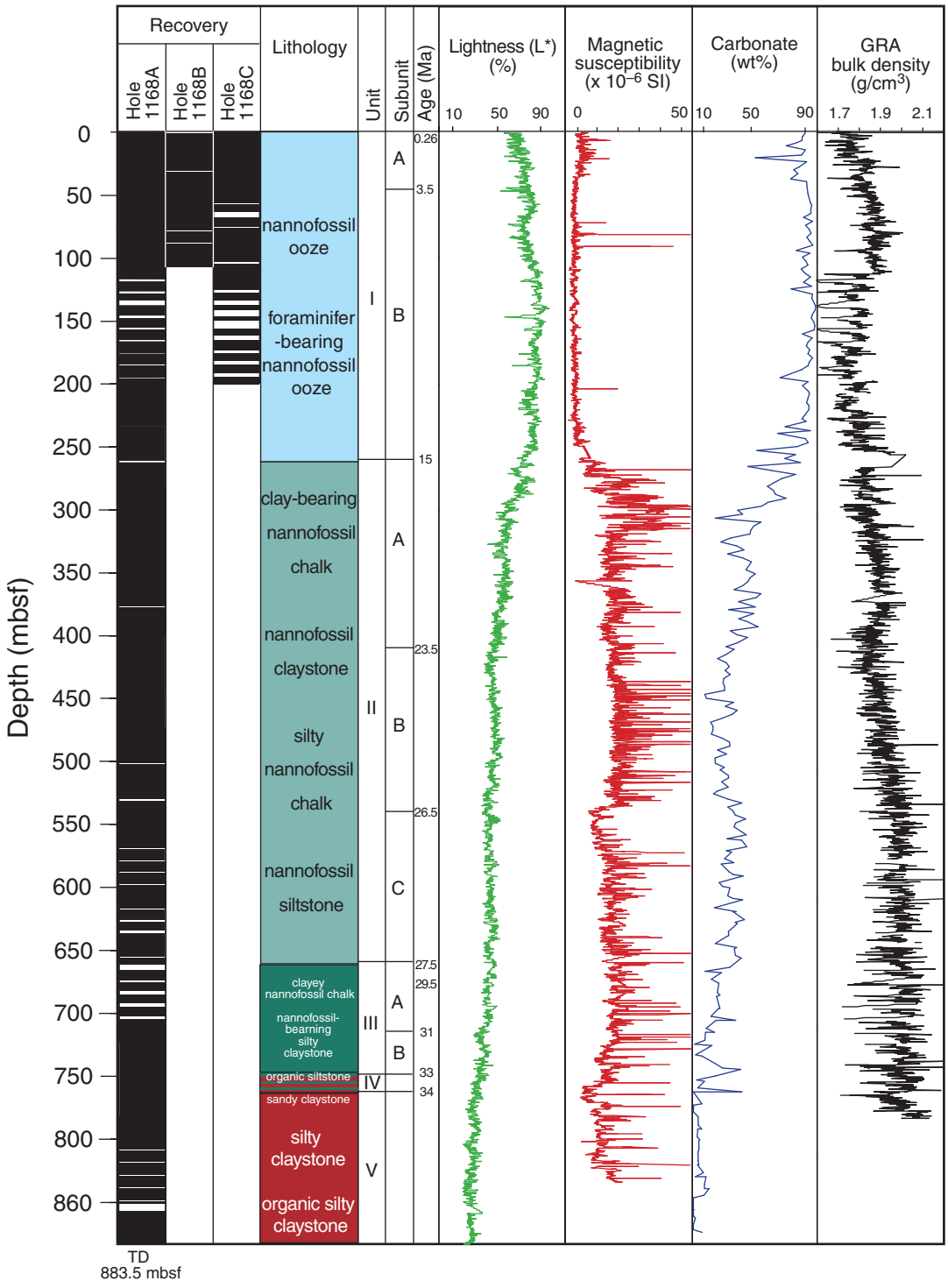

Figure F5. Lithostratigraphic summary of Site 1168, western Tasmania margin. **A.** 0–200 mbsf. GRA = gamma-ray attenuation. TD = total depth (Continued on next four pages).

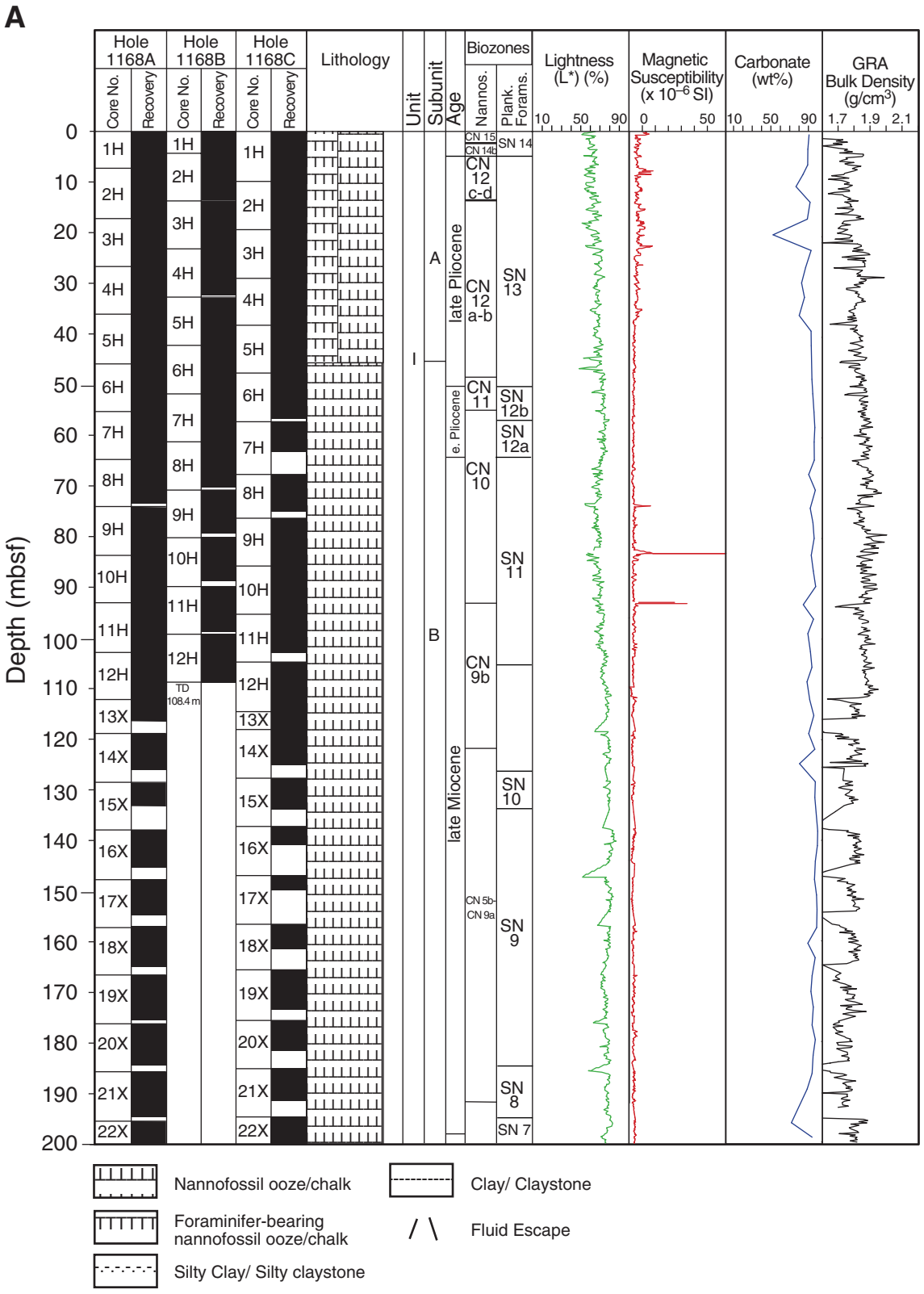

Figure F5 (continued). **B.** 200–400 mbsf.

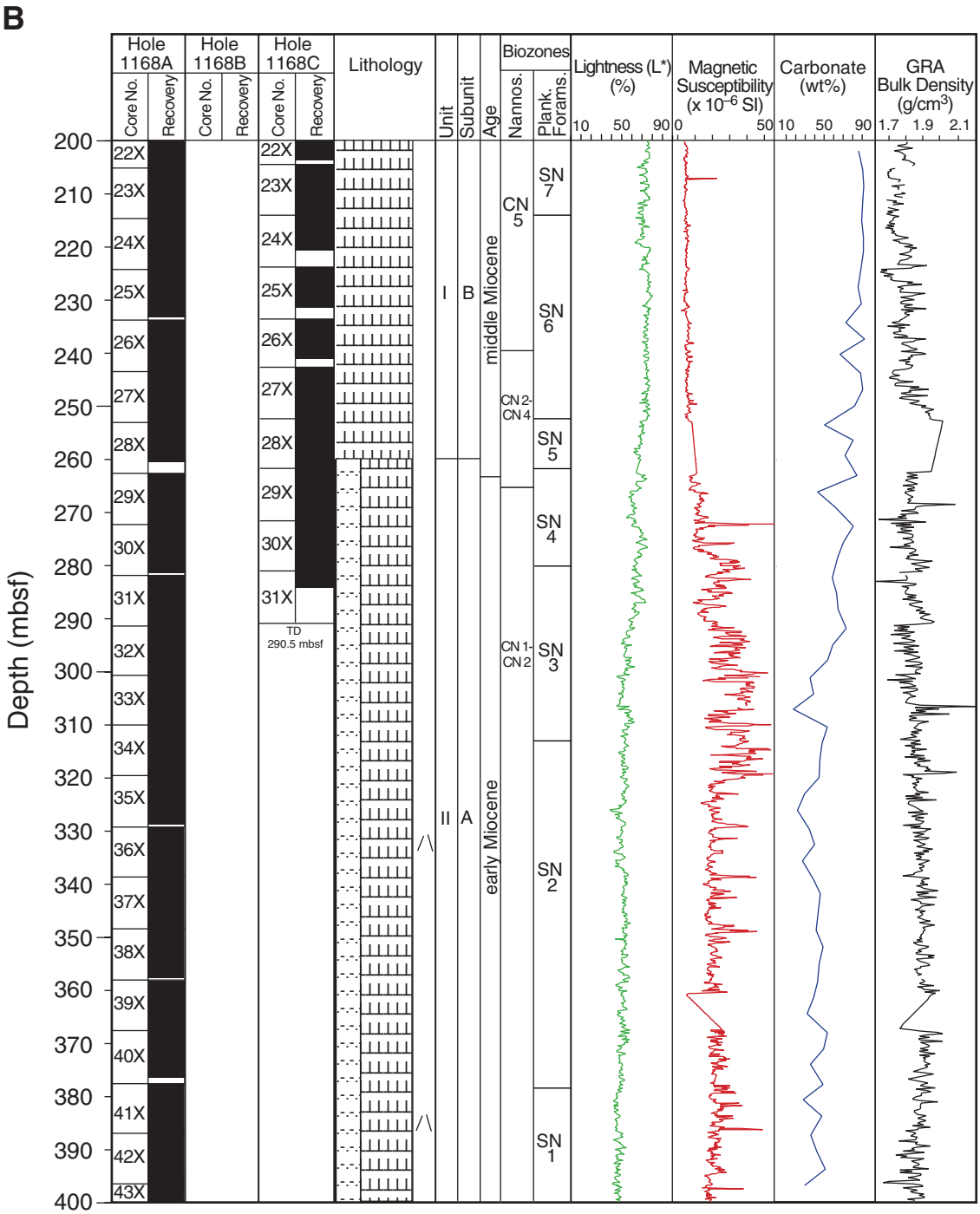

Figure F5 (continued). C. 400–600 mbsf.

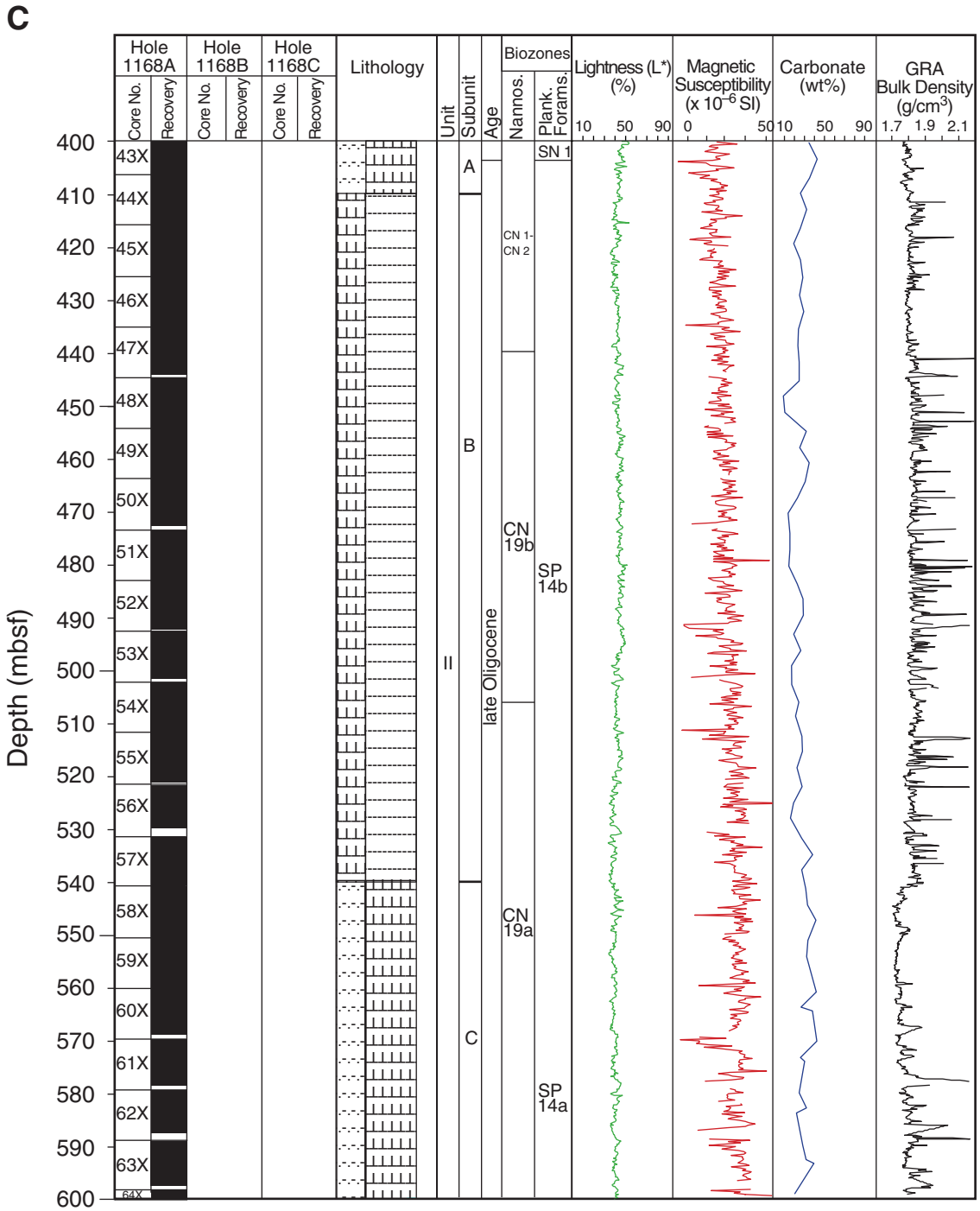

Figure F5 (continued). D. 600–800 mbsf.

D

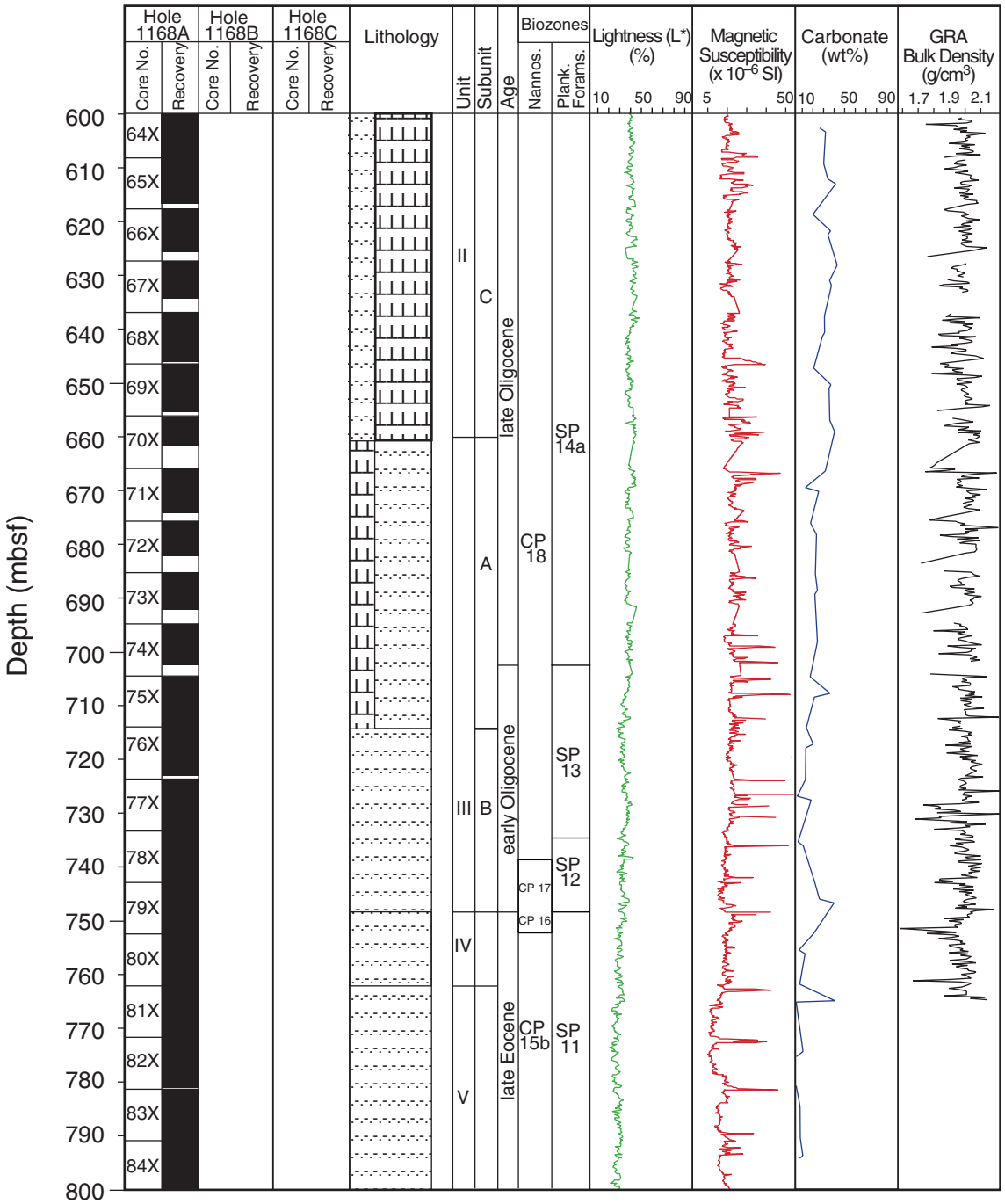

Figure F5 (continued). E. 800–883.5 mbsf.

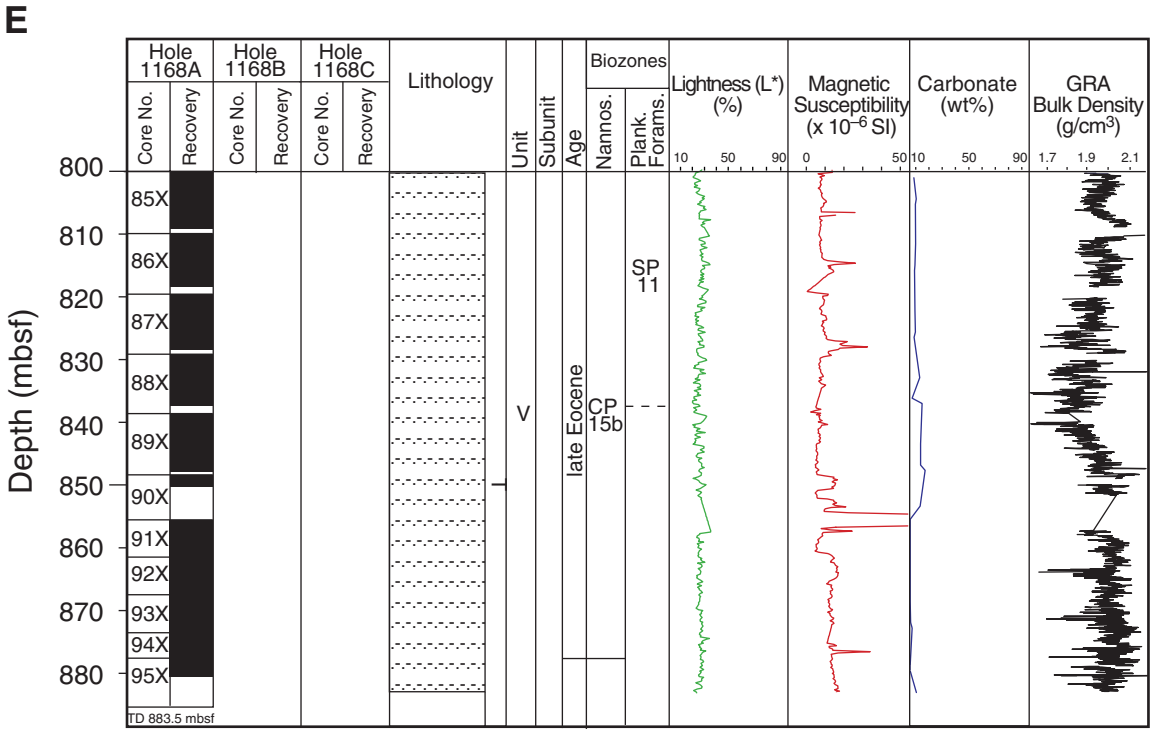

Figure F6. Correlation between lightness (L*) and coulometric carbonate data for Hole 1168A in the western Tasmania margin.

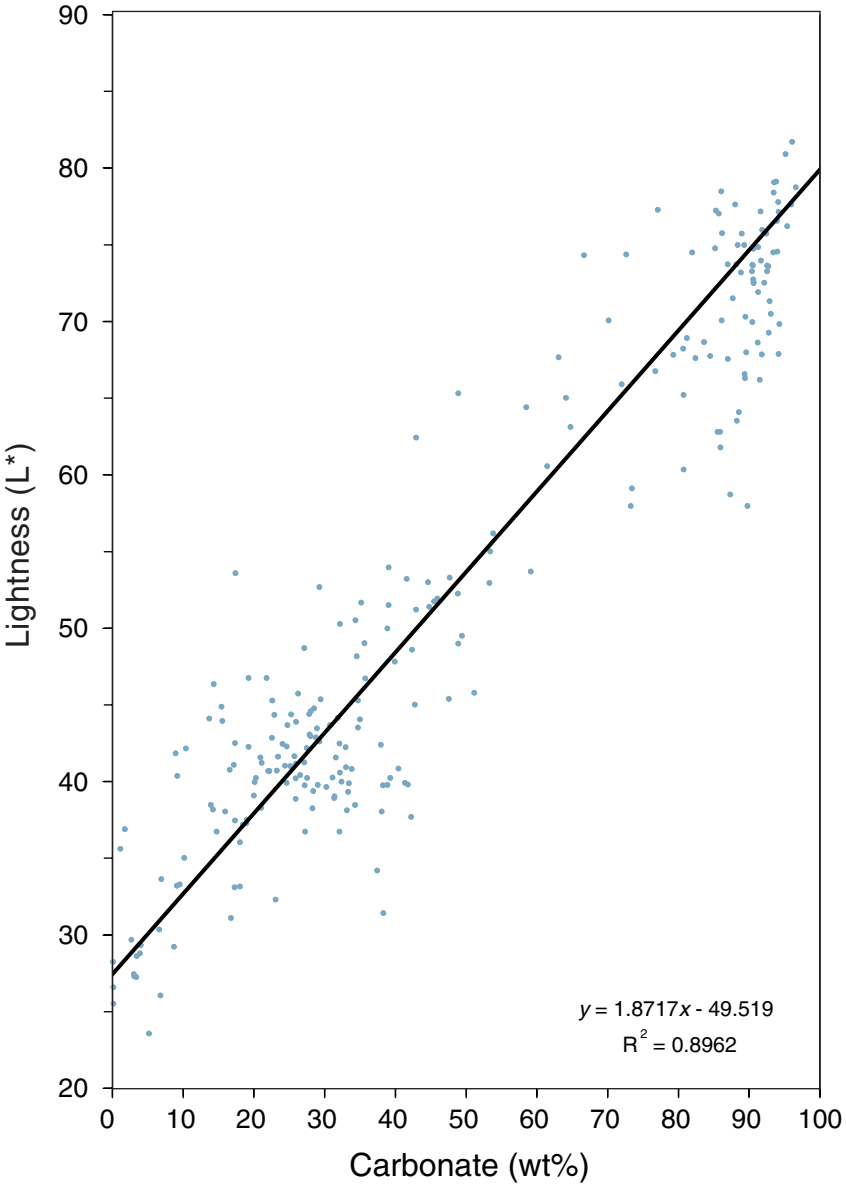

Figure F7. Sediment composition for Hole 1168A, western Tasmania margin, from shipboard smear-slide data.

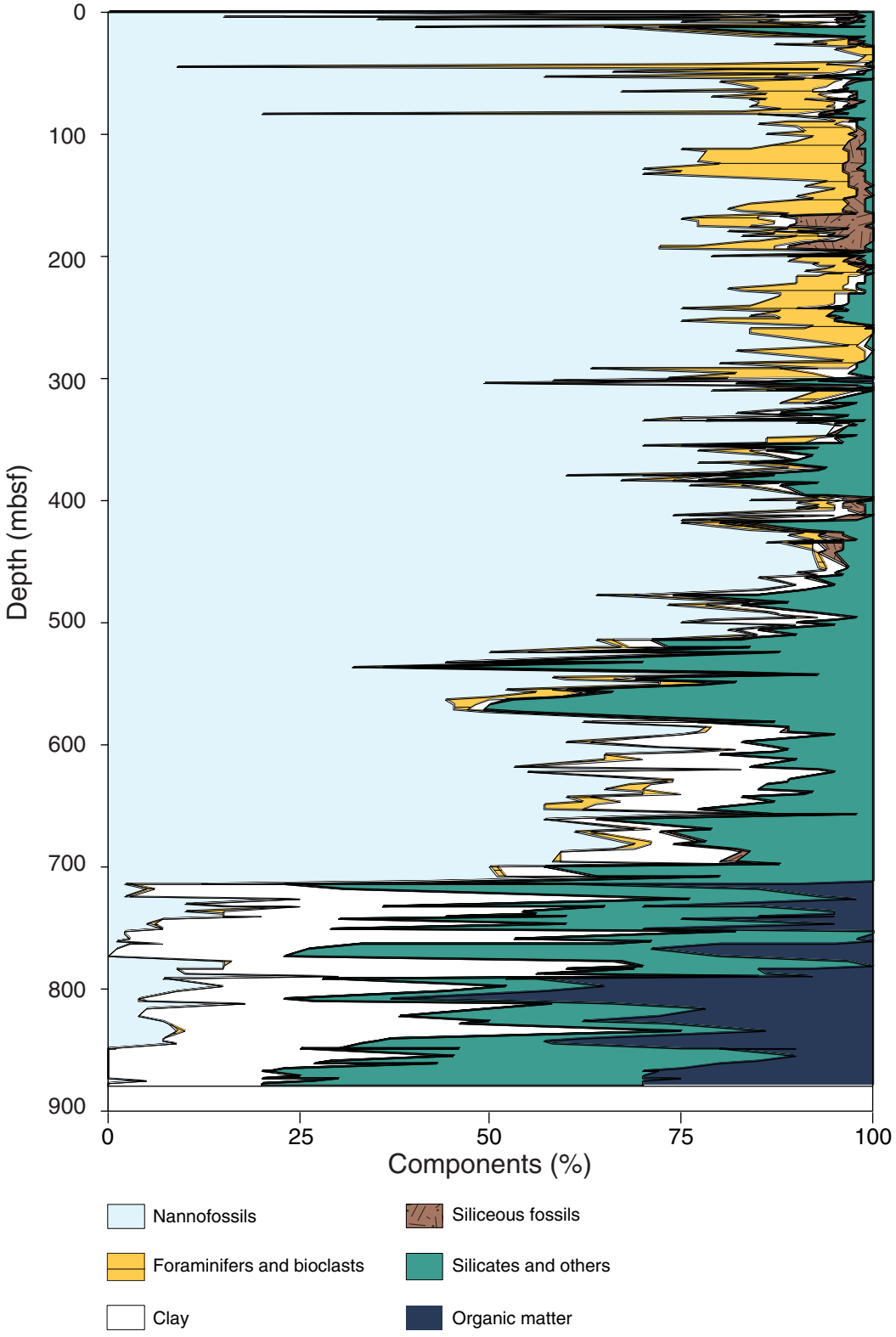

Figure F8. Close-up photograph of greenish gray (5GY 6/1) sandy layers in the light greenish gray (10GY 8/1) nannofossil ooze of Subunit IA (interval 189-1168B-3H-5, 16–30 cm).

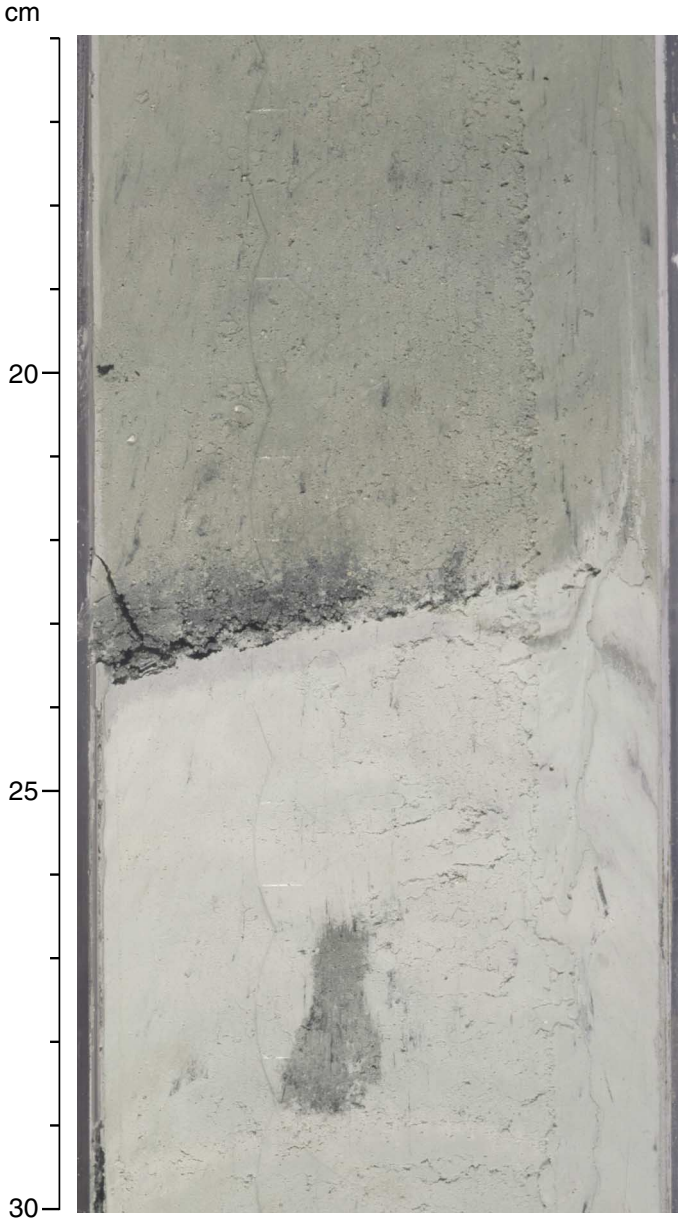

Figure F9. High-resolution lightness data presumably of Pliocene–Pleistocene age of Hole 1168A (3–23 mbsf; Subunit IA). In order to indicate the strong cyclicity of gray level variability, the 2-cm resolution data set is transformed using a 10-point moving average (blue line) and 50-point moving average (red line). [N1]

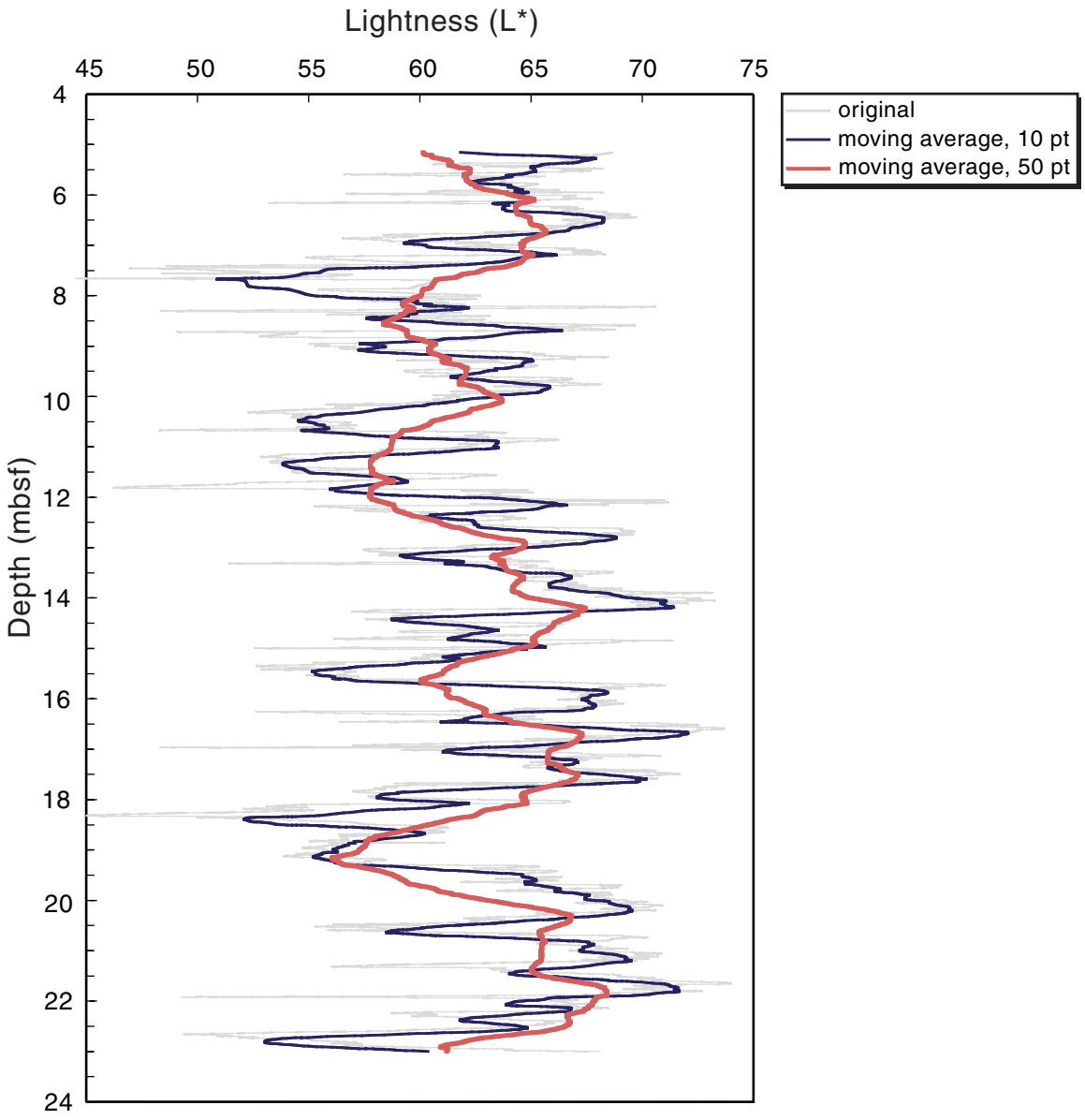

Figure F10. Power spectra of lightness (L*) for the interval from 2 to 23 mbsf in Hole 1168A. The spectral analysis of lightness (L*) and magnetic susceptibility time series is based on the Blackman-Tukey method using a Fourier transformation. Both spectra show cycles in comparable lengths of 3.71 and 3.58 m for the most dominant and 1.85 and 1.79 m for the secondary cycle. [N1]

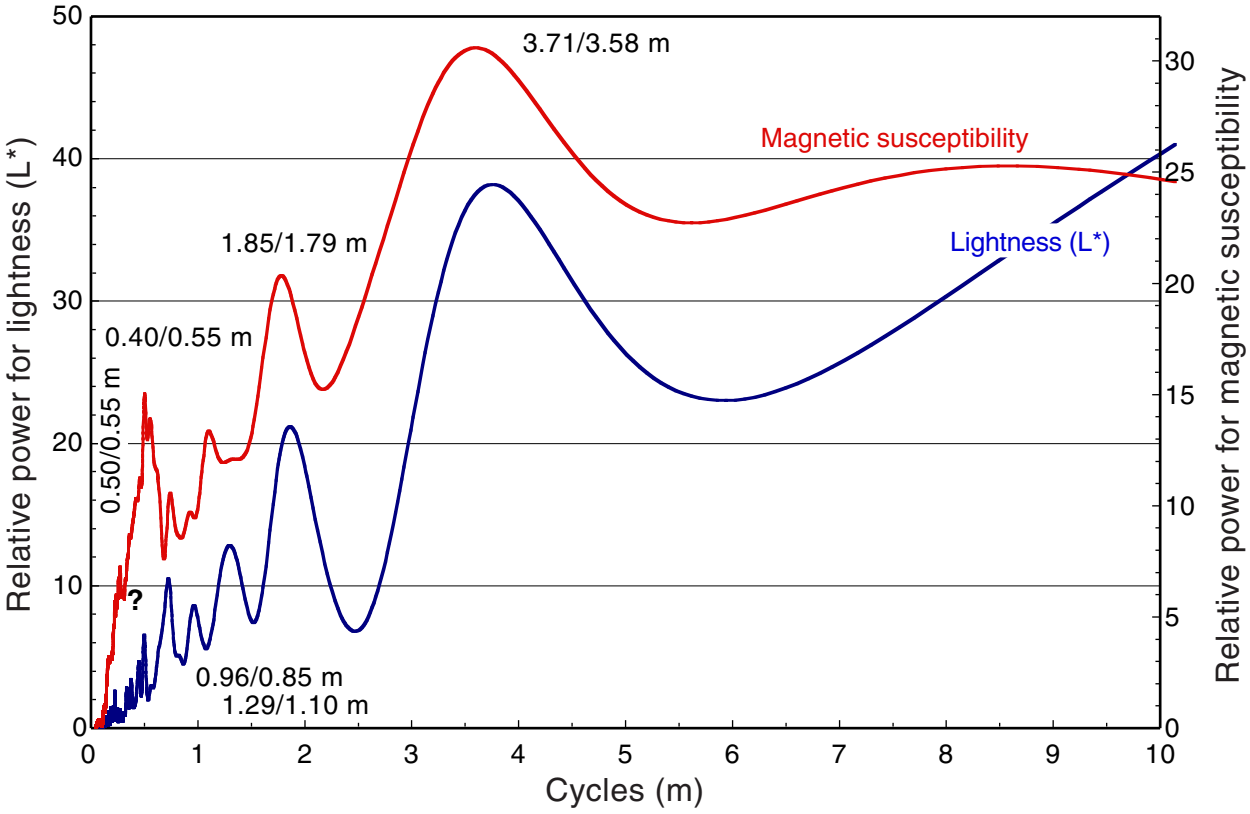

Figure F11. Comparison of the B chromaticity coordinate (trending to yellow with positive numbers; dark gray line) and magnetic susceptibility (red) between 265 and 290 mbsf in Hole 1168A. Note that B and magnetic susceptibility are proportional to each other.

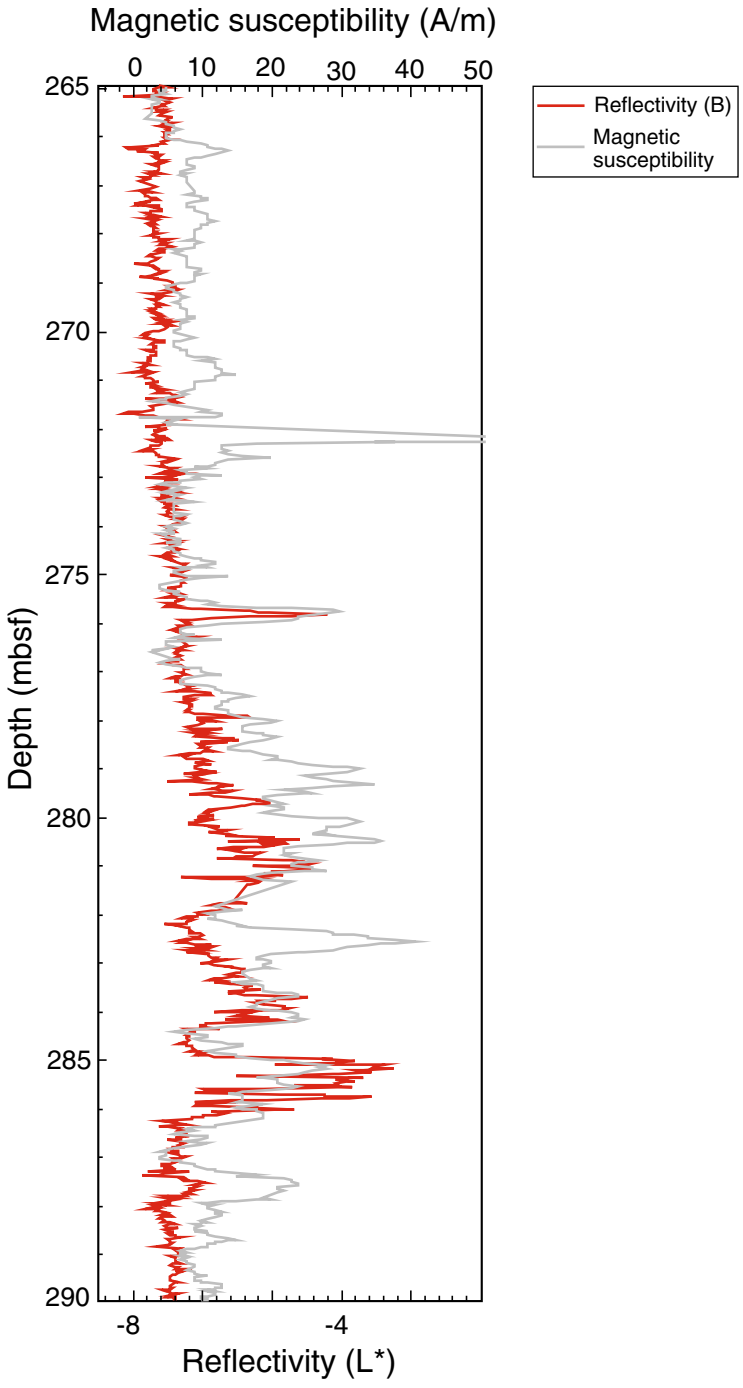

Figure F12. High-resolution record (2-cm sampling intervals) of lightness from 265 to 290 mbsf in Hole 1168A.

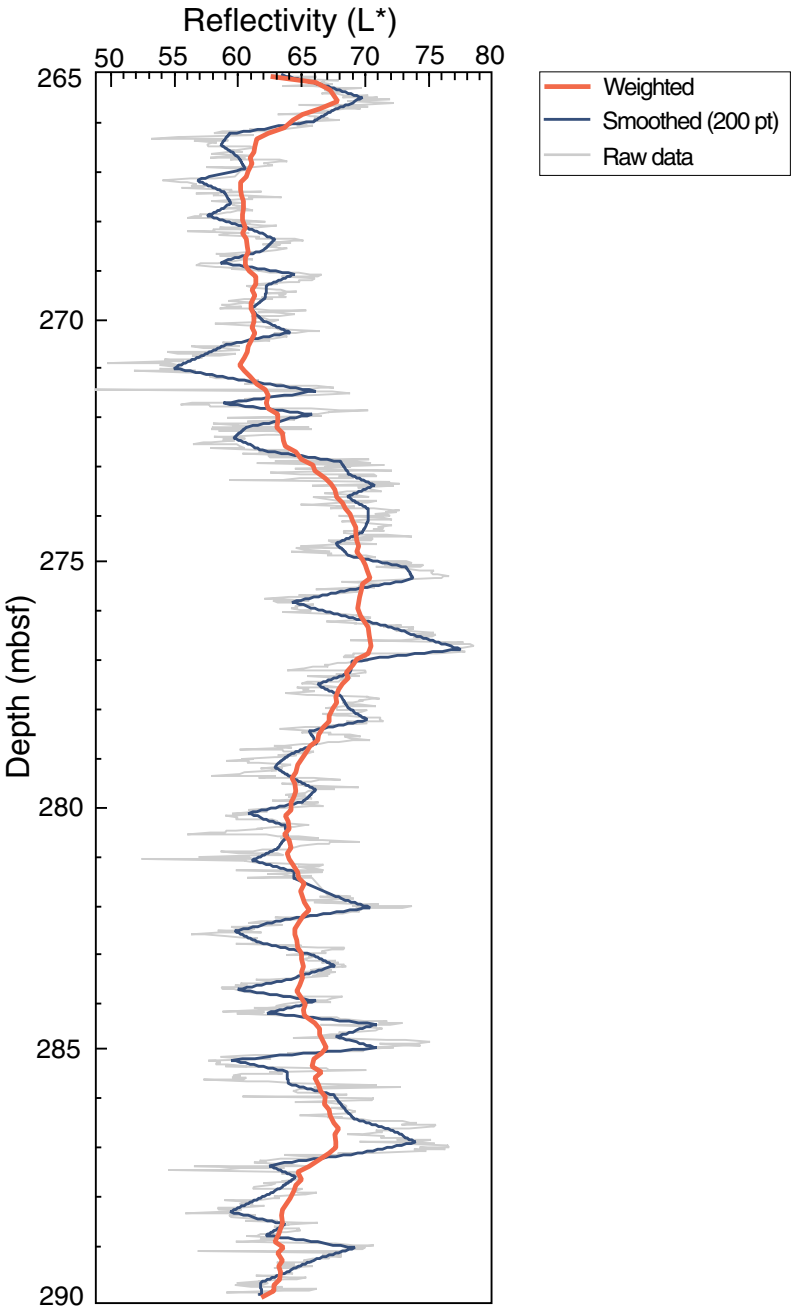

Figure F13. Comparison of lightness (L*) (dark gray line) and magnetic susceptibility (red line) between 265 and 290 mbsf in Hole 1168A showing good correlation between gray level and magnetic susceptibility.

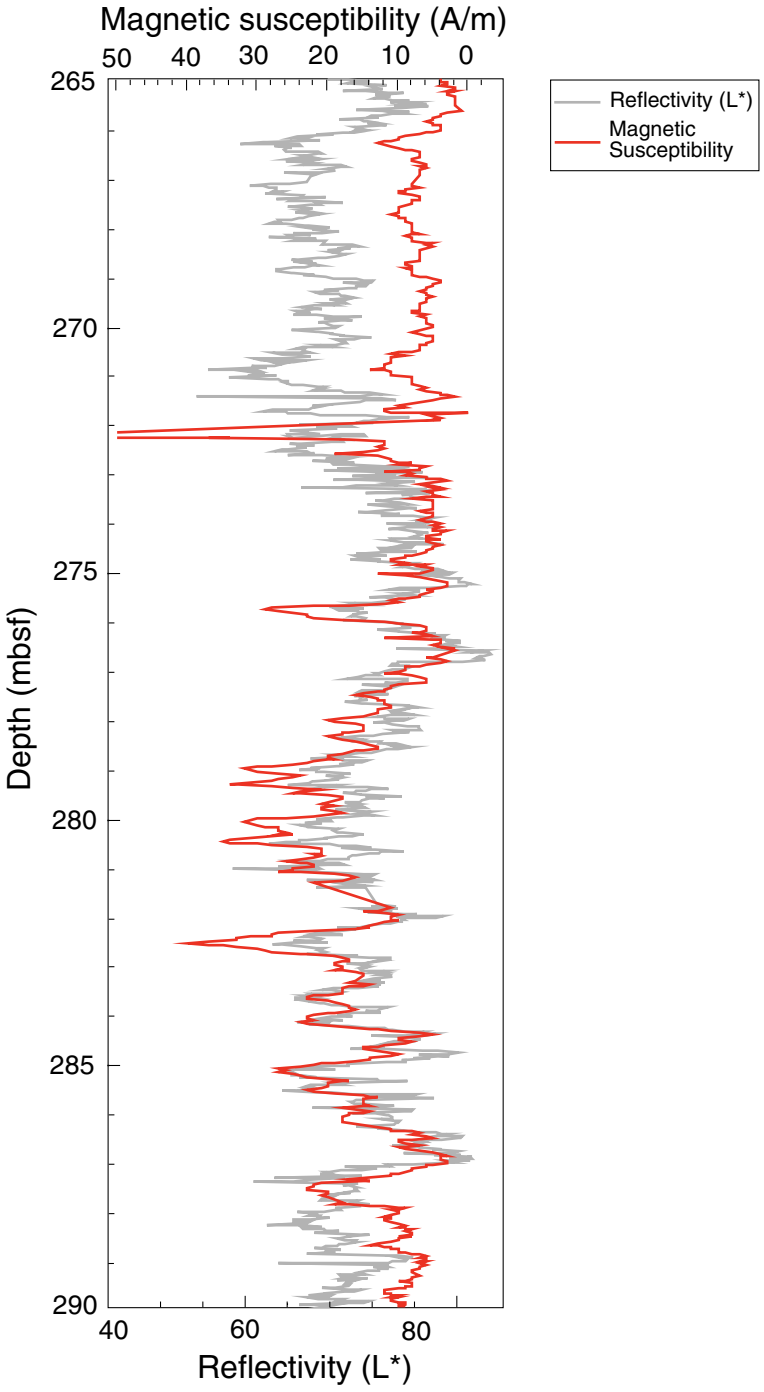

Figure F14. Power spectra of the intervals from 265 to 290 mbsf in Hole 1168A. Spectral analysis of lightness times series is based on the Blackman-Tukey method using a Fourier transformation. [N1]

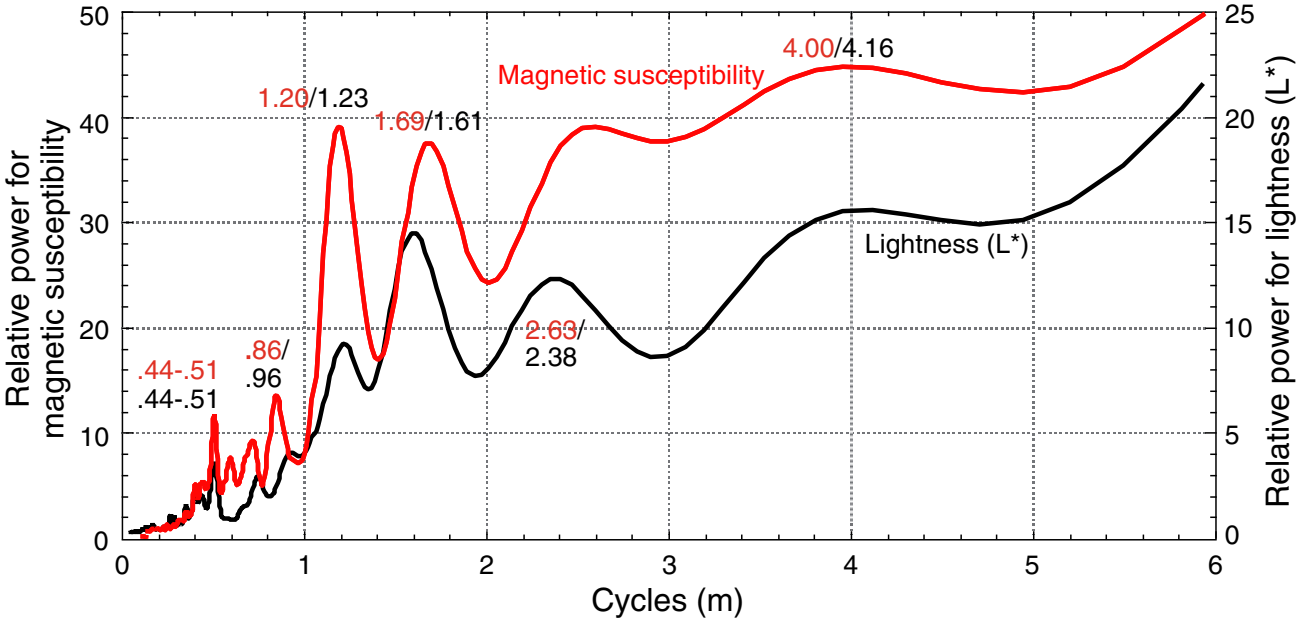

Figure F15. Close-up photograph showing a fluid escape structure and associated brecciated sediments in the nannofossil claystone of Subunit IIA (interval 189-1168A-36X-3, 35–75 cm).

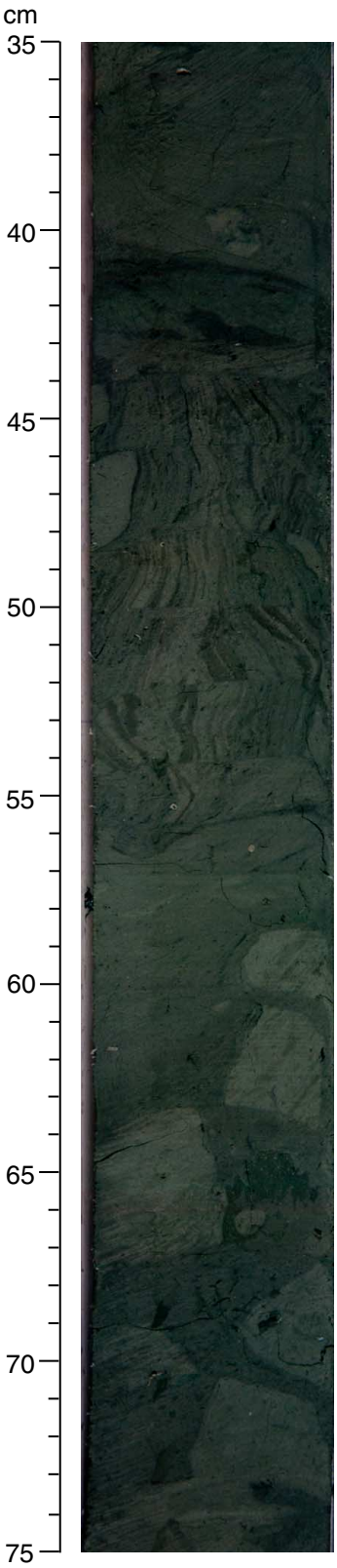

Figure F16. Close-up photograph showing layers of glauconitic clayey siltstone in Unit IV (interval 189-1168A-79X-6, 25–50 cm).

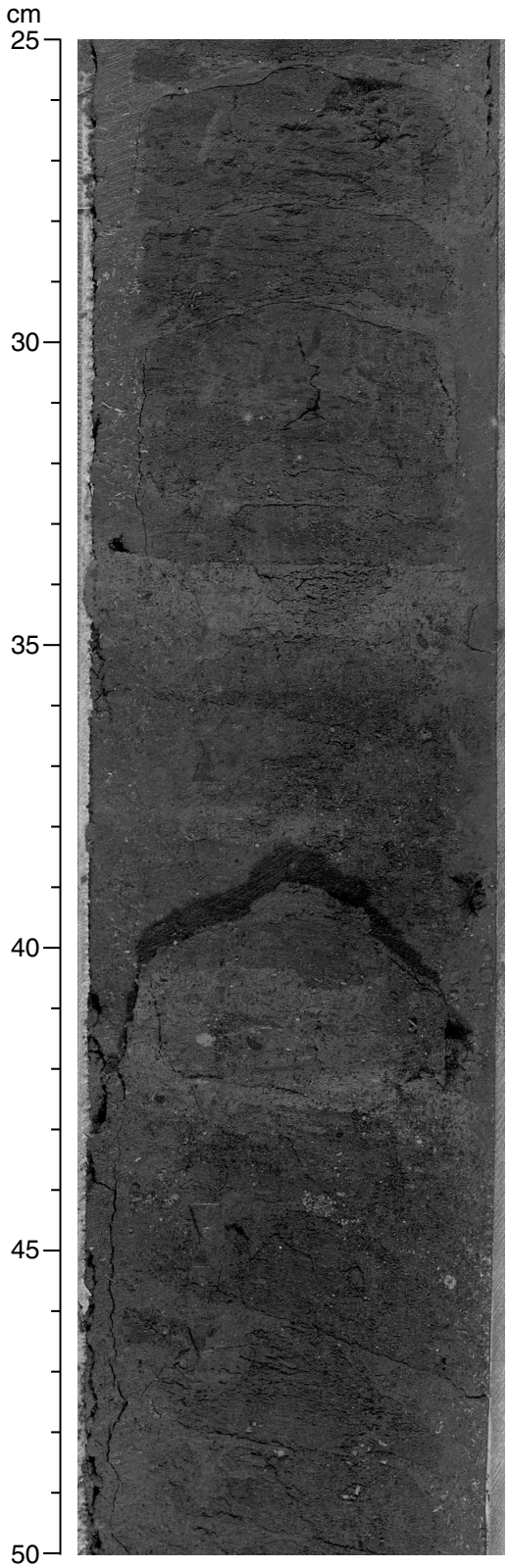

Figure F17. Clay mineral units of Site 1168, western Tasmania margin.

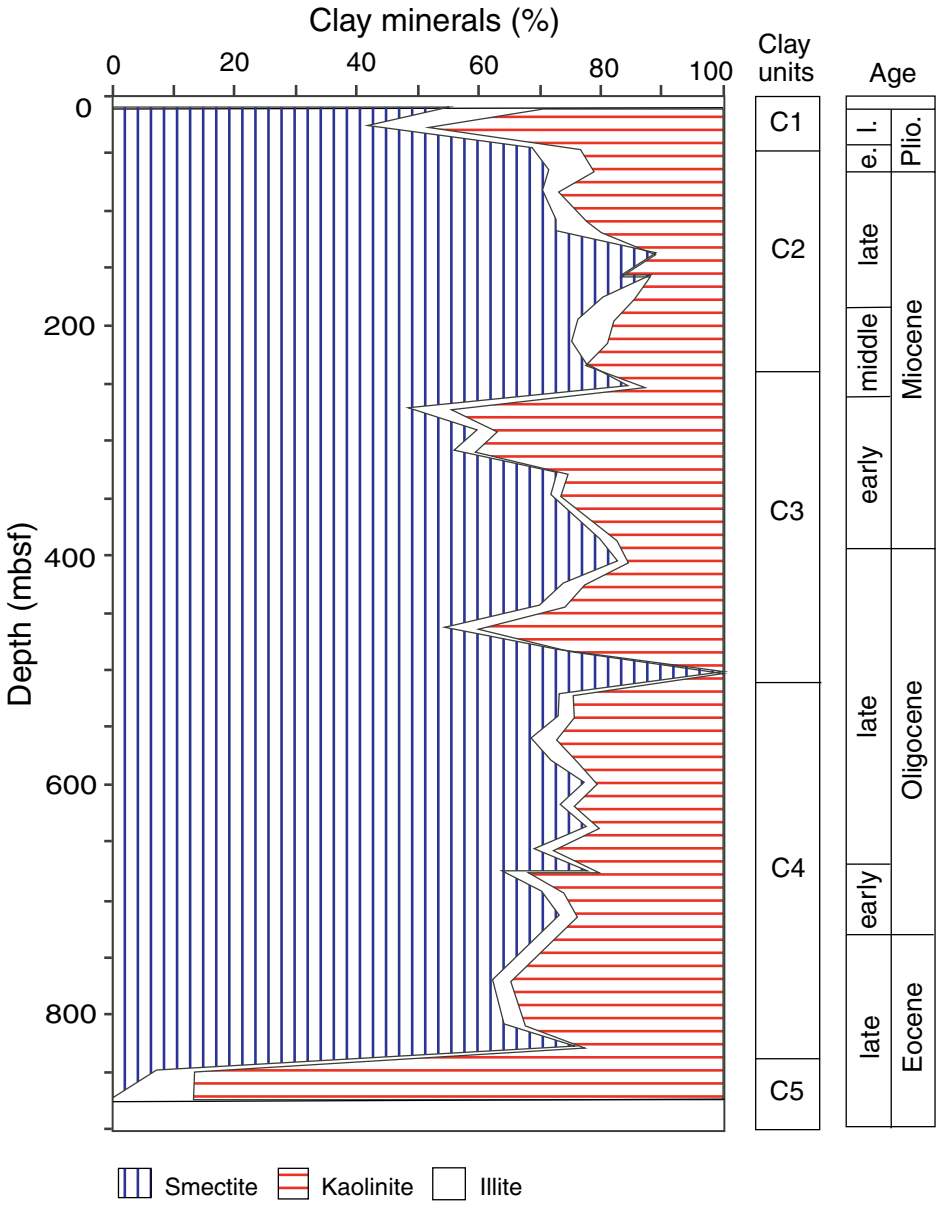

Figure F18. Late Eocene paleogeography and paleoenvironment of the western Tasmania margin based on seismic data (Hill et al., 1997) and results from Sites 1168 and from DSDP Site 282 (Kennett, Houtz, et al., 1975).

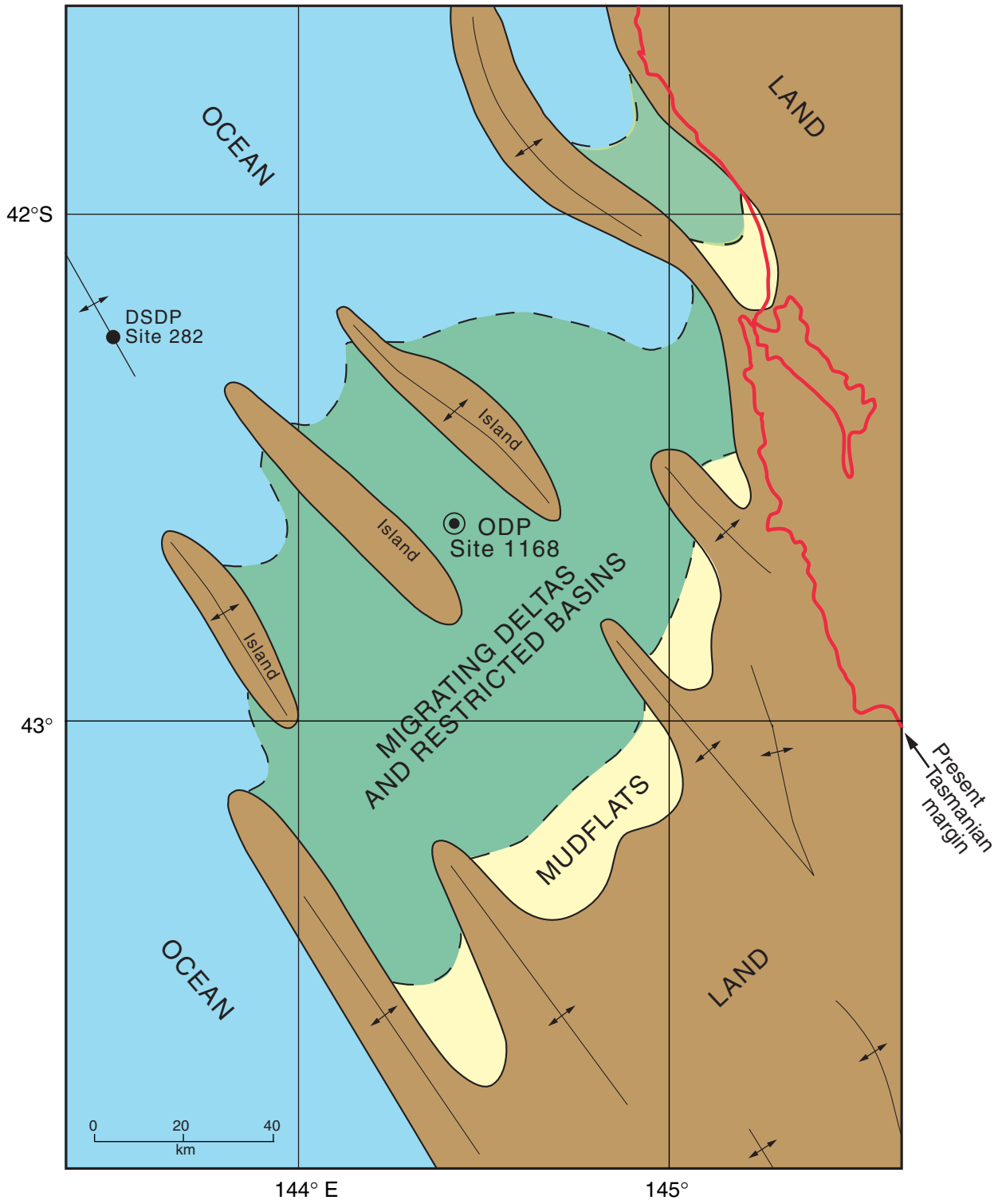

Figure F19. Site 1168 age-depth plot and linear sedimentation rates. Age-depth curve using multiple microfossil and paleomagnetic datums for Site 1168. Bioevents used are listed in Table T12, p. 150. The breaks in sedimentation at ~400 and 700 mbsf are consistent with changes in lithology at these depths.

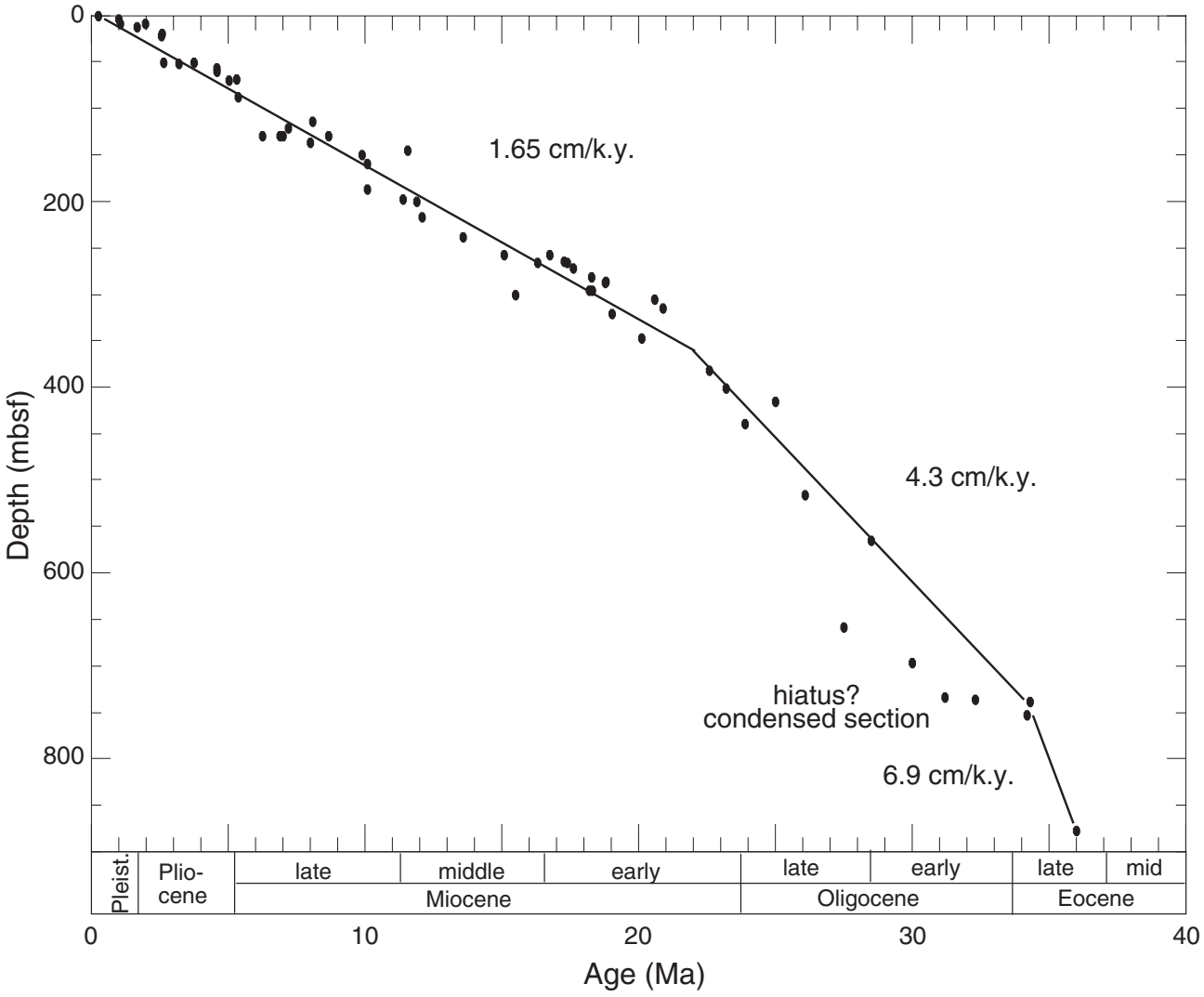

Figure F20. Site 1168 paleodepth and bottom-water conditions, based largely on benthic foraminifers and solely on Hole 1168A.

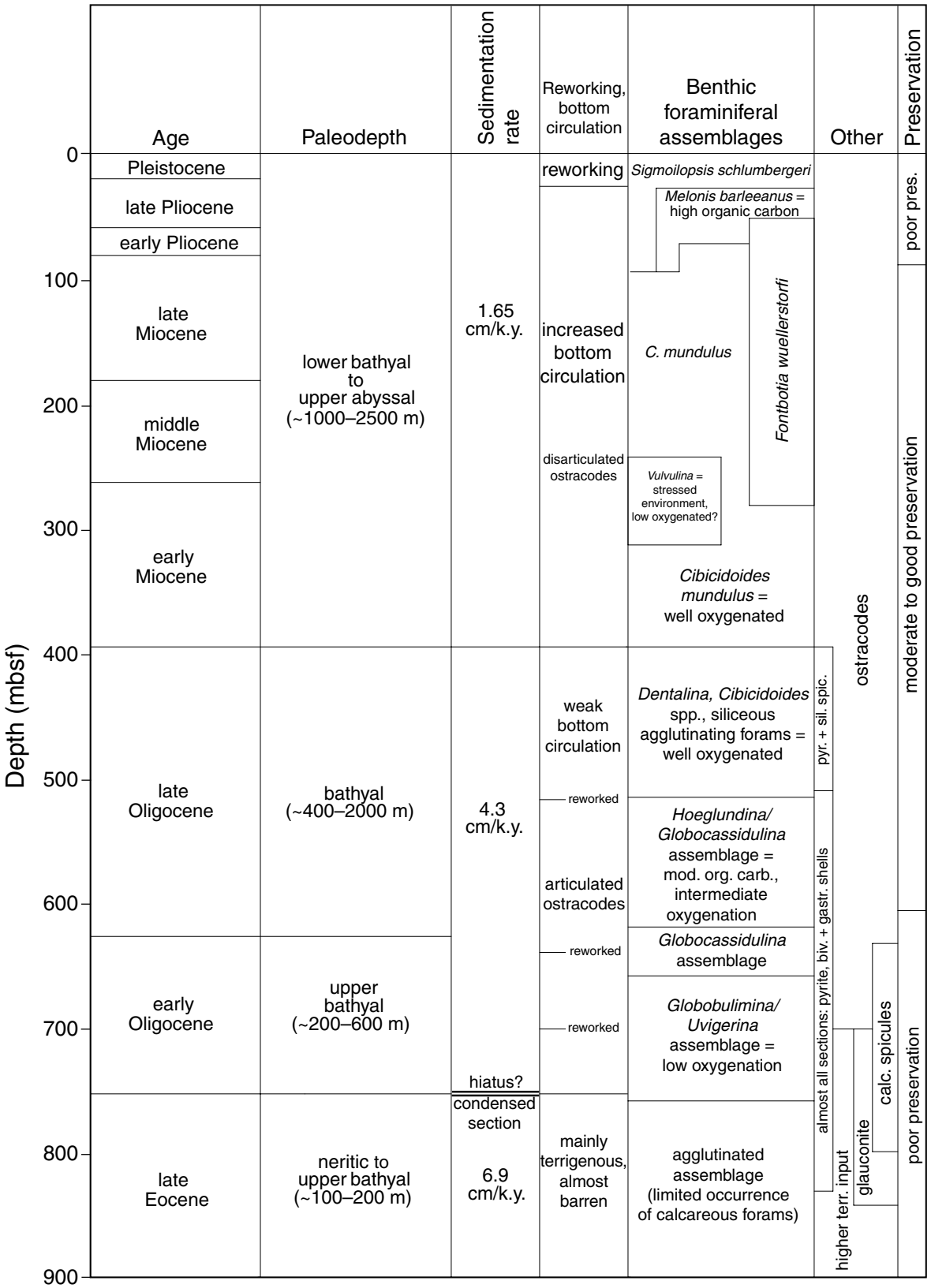

Figure F21. Siliceous microfossil abundance and preservation vs. $H_4SiO_4^0$ in pore water for Hole 1168A.

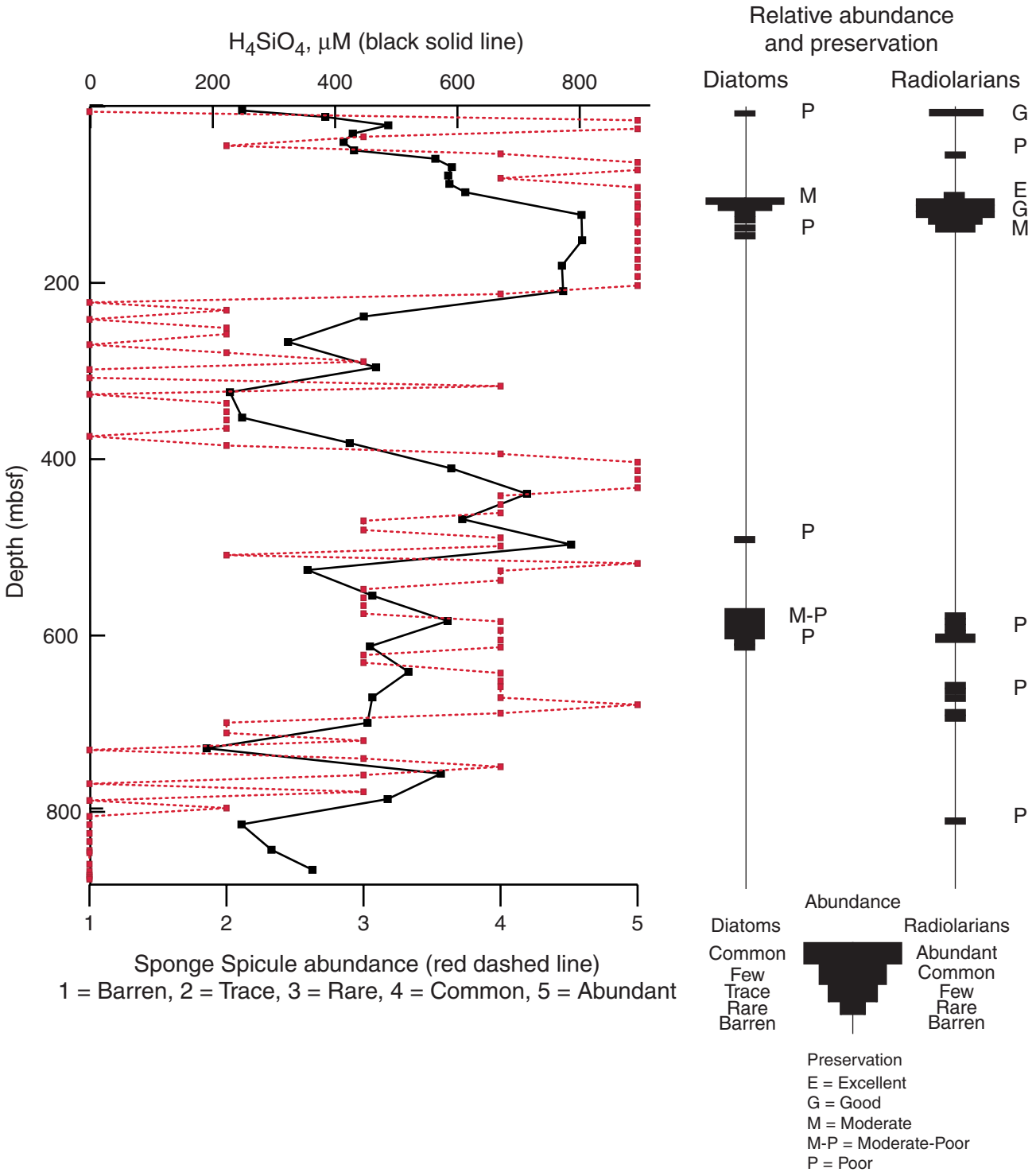

Figure F22. Long-core magnetic inclination and intensity for the uppermost 50 mbsf for Holes 1168A, 1168B, and 1168C.

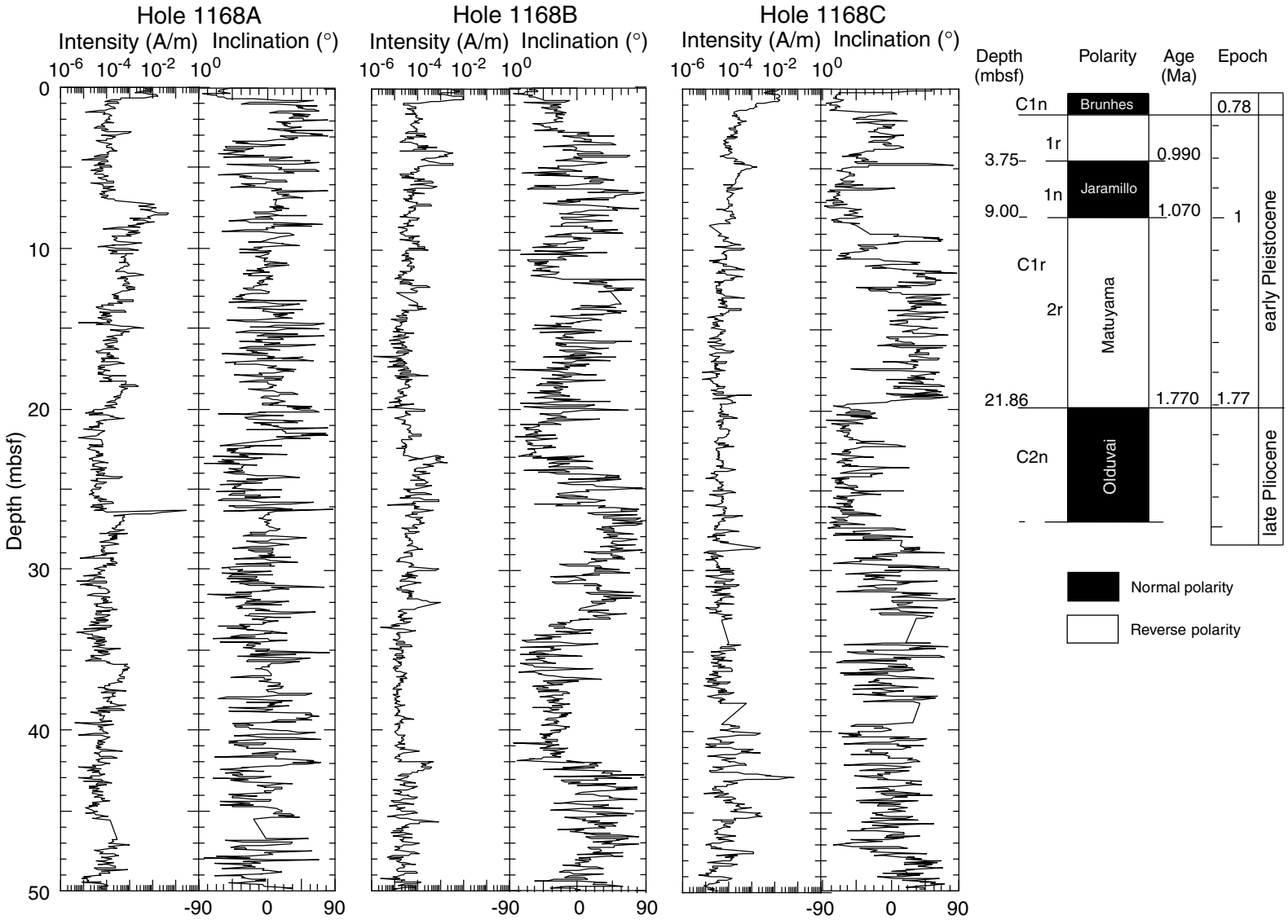

Figure F23. Long-core magnetic inclination and intensity for Hole 1168A between 250 and 350 mbsf.

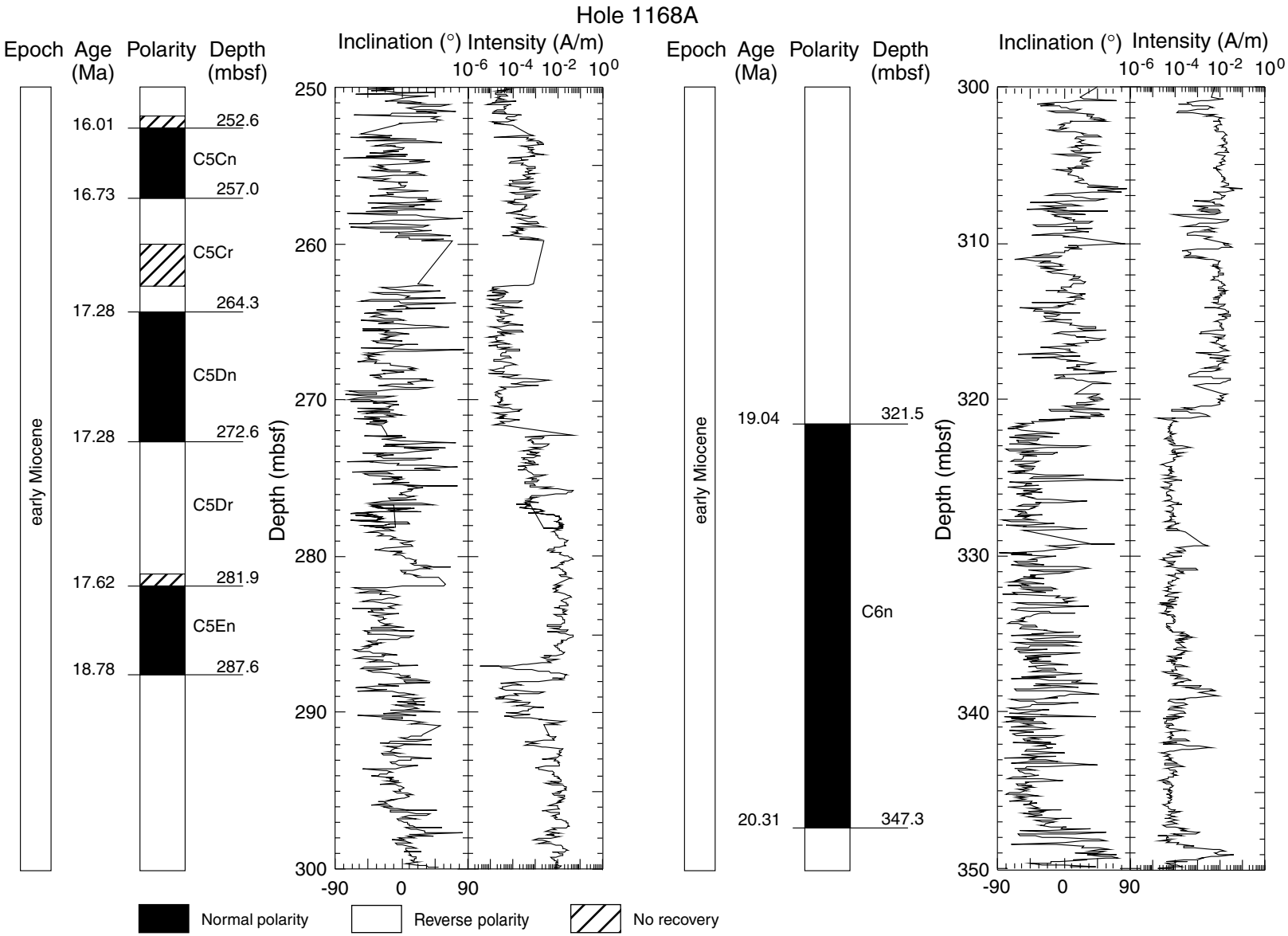

Figure F24. Principal component analysis of natural remanent magnetization of Sample 189-1168A-34X-CC, 25 cm. MAD = maximum angular deviation.

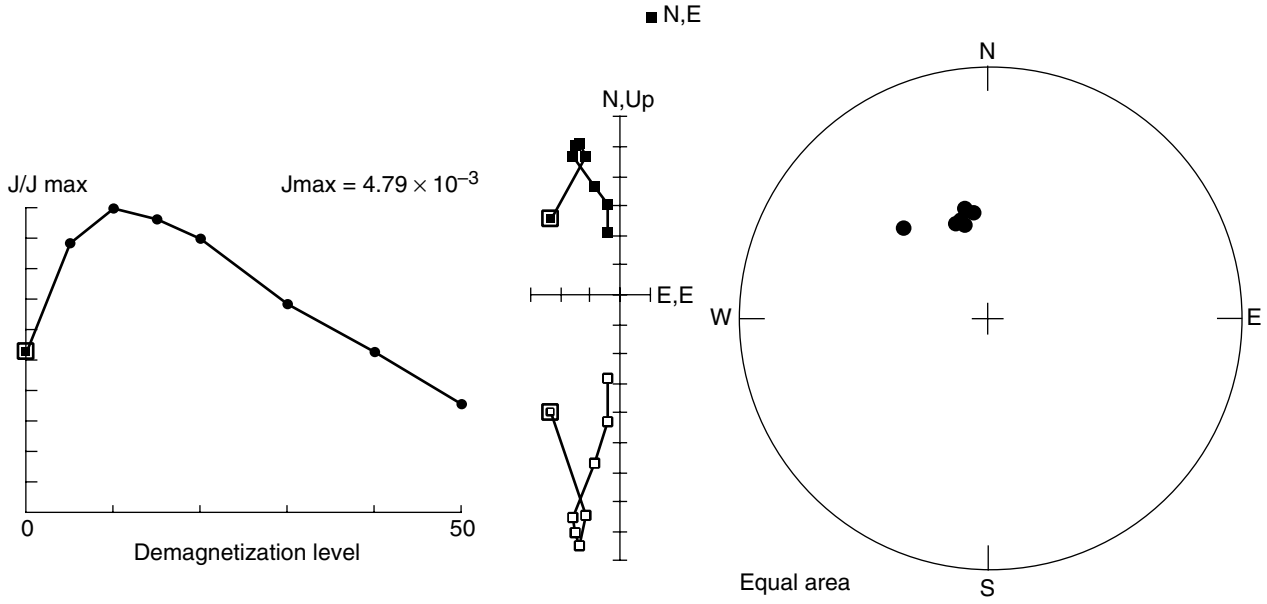

Principal component analysis (15,20,30,40,50)
Declination: 336.5
Inclination: 58.7
MAD = 3.8

- Initial point
- Initial point
- Data point
- Horizontal plane
- Vertical plane

Figure F25. Magnetic characterization of Samples 189-1168A-30X-4, 104 cm, and 36X-6, 145 cm.

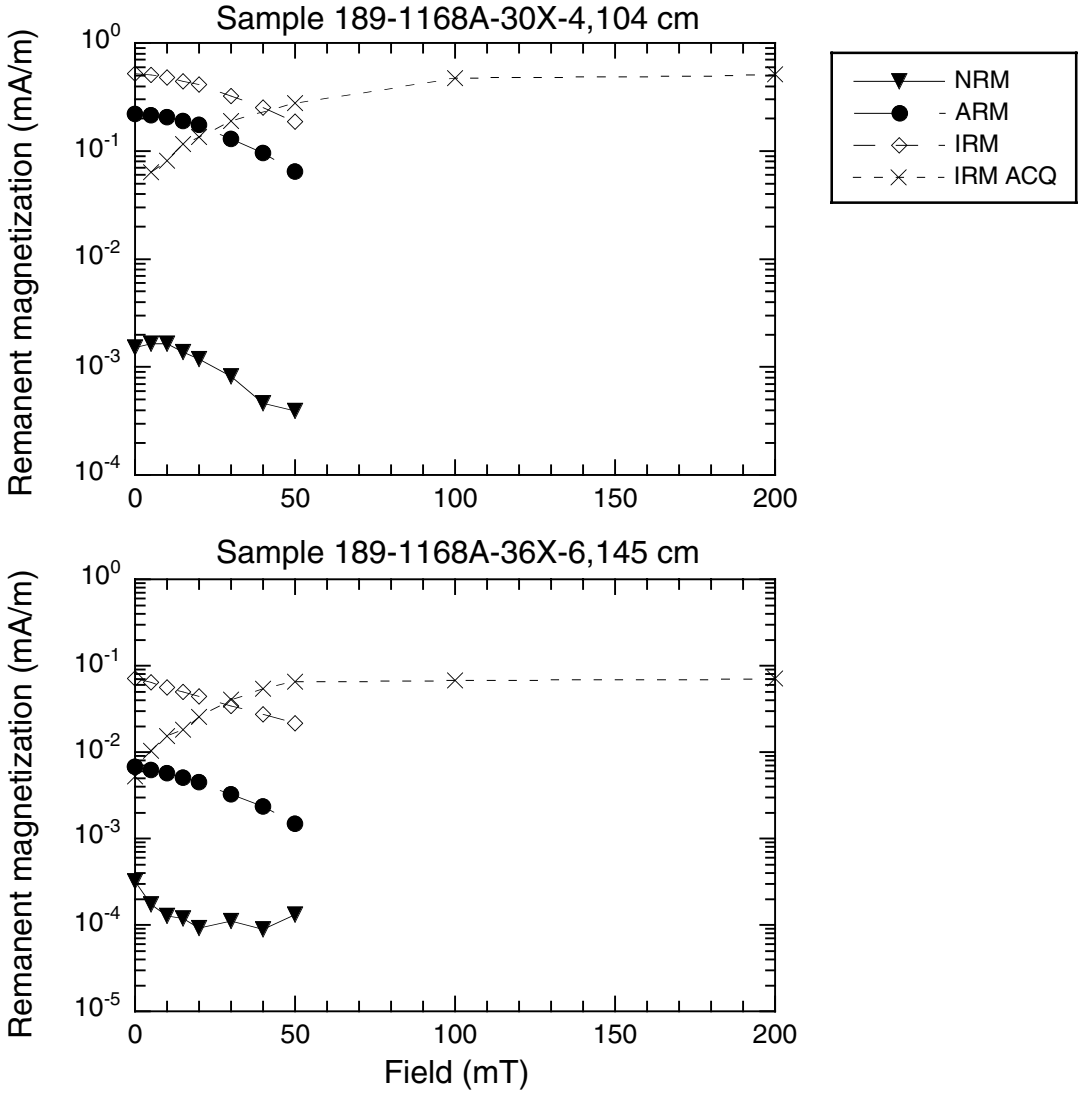

Figure F26. A. Smoothed (21-cm Gaussian) spectral reflectance (L*) data for the upper 130 mcd from Site 1168. Holes 1168B and 1168C are offset from Hole 1168A by a constant (20 and 40 L* units, respectively). **B.** Smoothed (21-cm Gaussian) magnetic susceptibility data for the upper 130 mcd from Site 1168. Holes 1168B and 1168C are offset from Hole 1168A by a constant (10×10^{-6} and 20×10^{-6}, respectively). **C.** Smoothed (21-cm Gaussian) GRA bulk-density data for the upper 130 mcd from Site 1168. Holes 1168B and 1168C are offset from Hole 1168A by a constant (0.1 g/cm^3 and 0.2 g/cm^3, respectively).

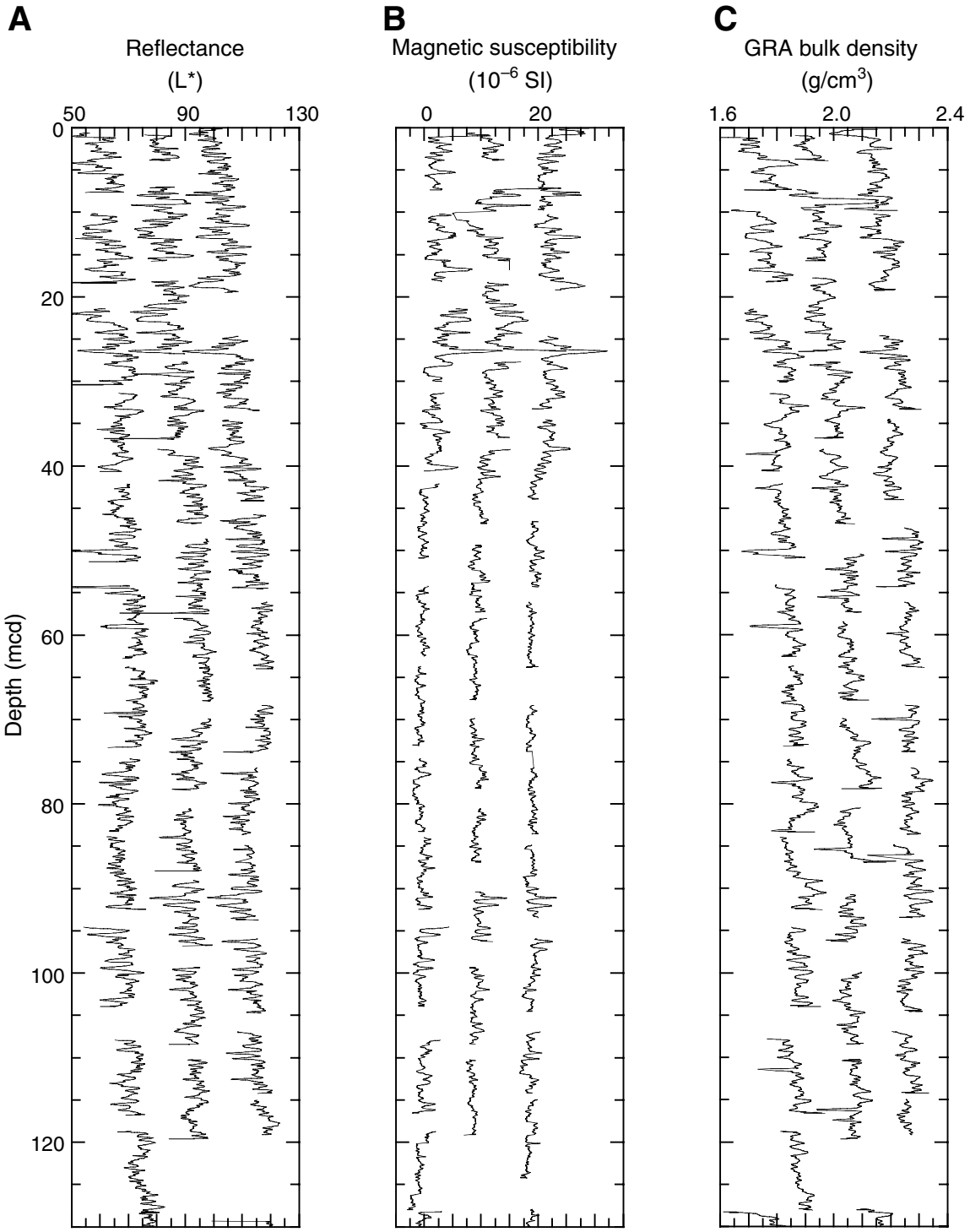

Figure F27. Plots of carbonate (thin line = raw data; solid line = smoothed data), total organic carbon (TOC) (squares = CNS analyzer data; dots = Rock-Eval pyrolysis values), and total nitrogen, C/N ratios, and hydrogen index values for Hole 1168A. Shaded areas on the C/N ratio plot delineate typical marine and terrestrial organic matter fields. Lithostratigraphic units are indicated on the far right side of the figure.

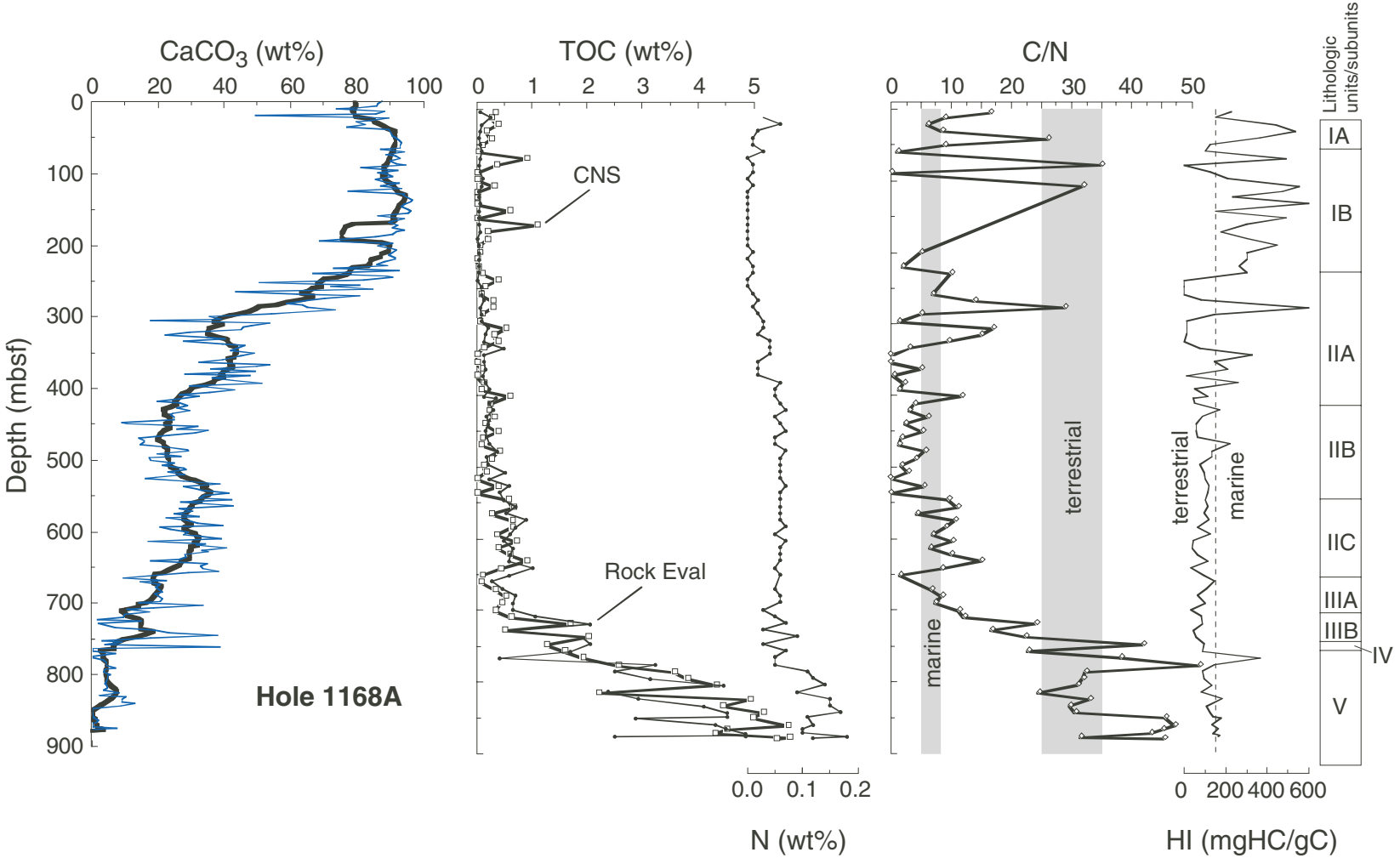

Figure F28. Total sulfur contents (squares) compared to C/S ratios (circles) for Hole 1168A. Dashed lines indicate transitions between marine, brackish, and fresh environments of formation. Lithostratigraphic units are indicated on the far right side of the diagram.

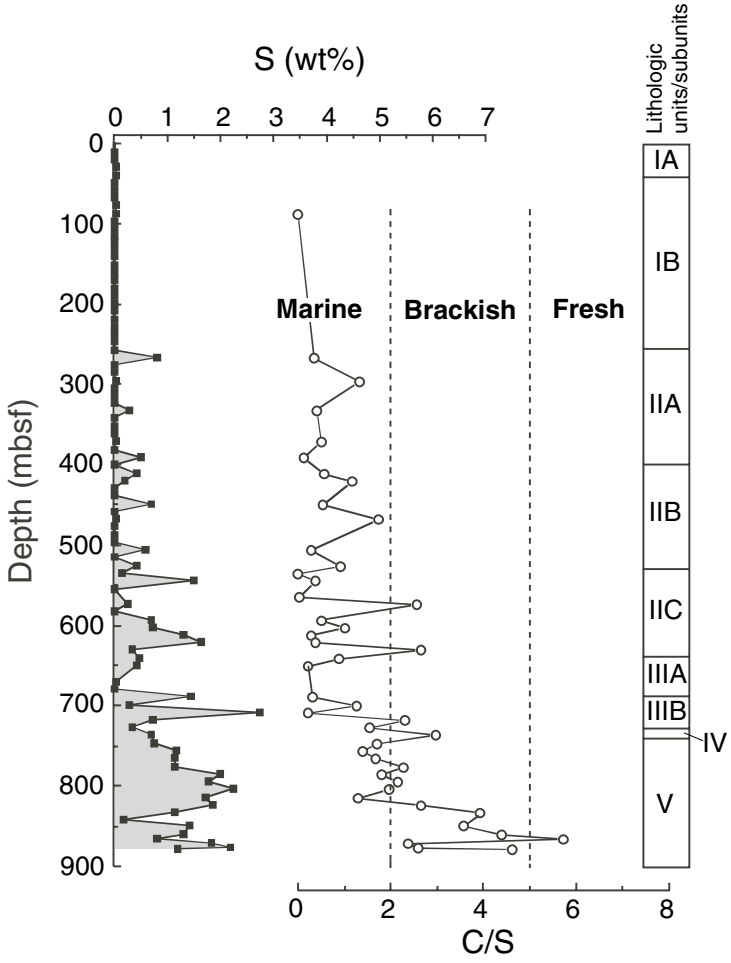

Figure F29. T_{max} values generated from Rock-Eval pyrolysis analyses of organic matter for Hole 1168A. The high variability of values above ~400 mbsf (open squares) is likely caused by very low TOC values in these samples. Below 400 mbsf (solid squares), T_{max} values are indicative of immature organic matter relative to oil generation, although values approach the "oil window" at the base of the core.

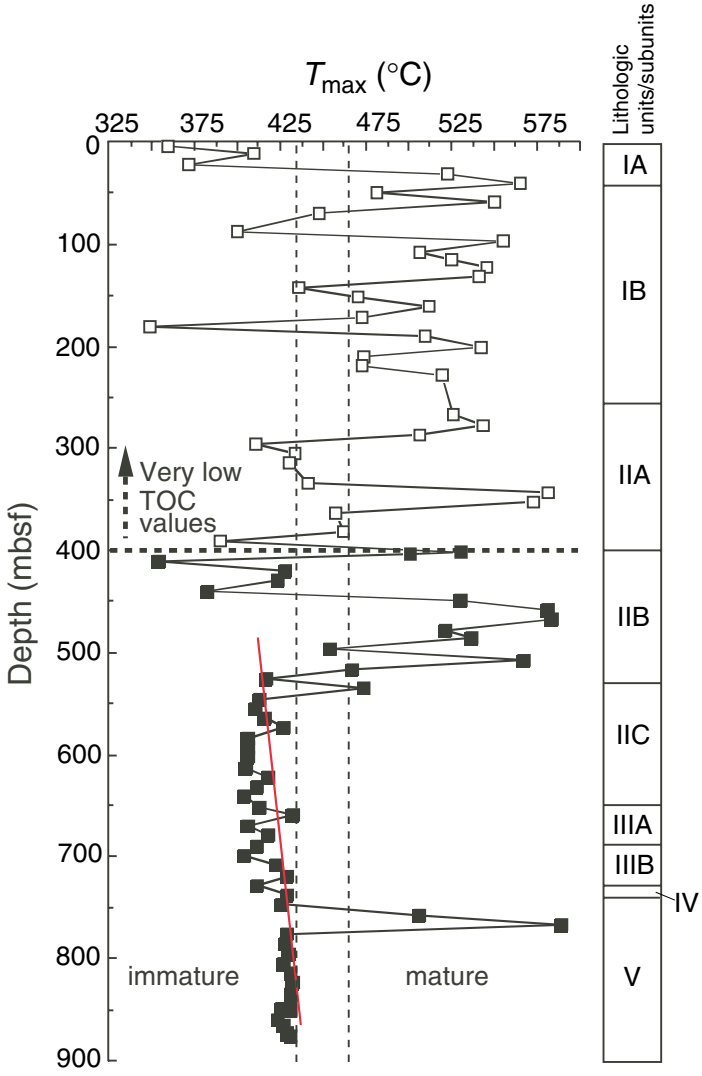

Figure F30. Total organic carbon vs. calcium carbonate content for sediments in Hole 1168A.

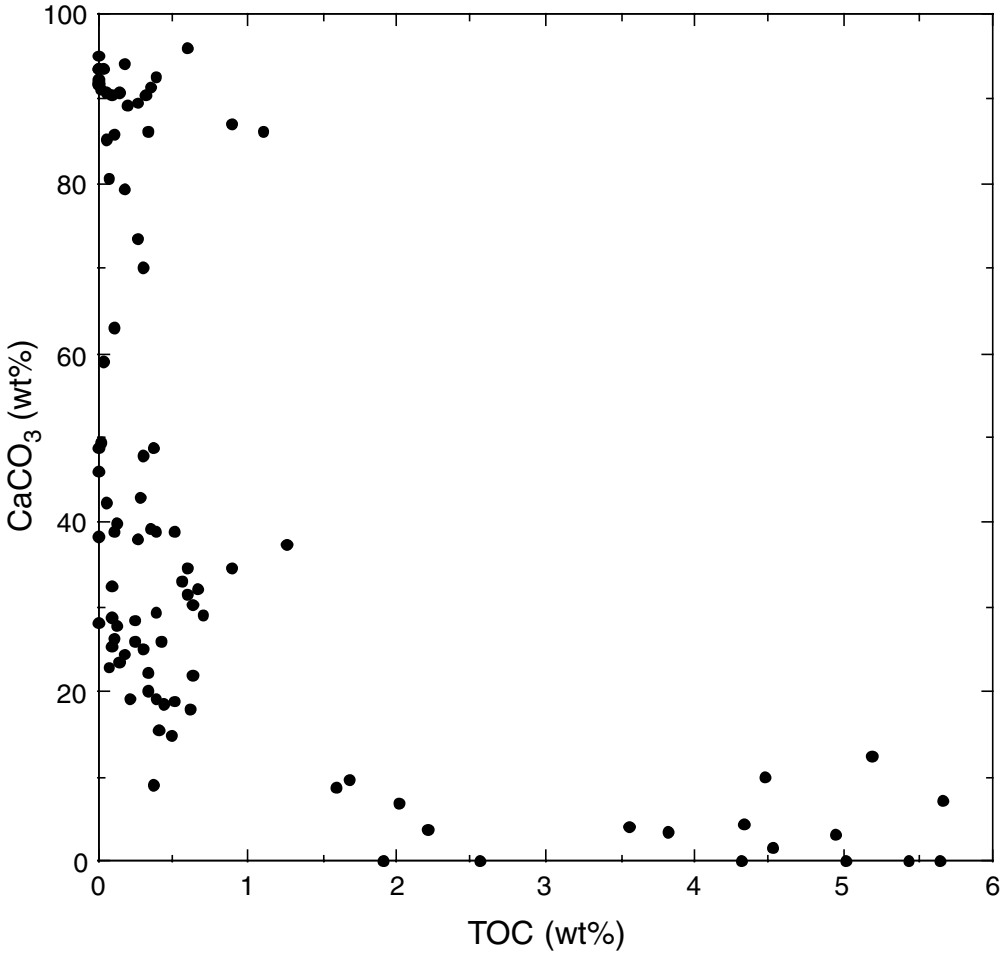

Figure F31. Methane (C_1) concentrations, methane vs. ethane plus propane ratios (C_1/C_2+C_3), and the percent wetness ($[C_2+C_3/C_1+C_2+C_3]100$) from headspace gas analysis. Dashed lines delineate biogenic and thermogenic fields on the C_1/C_2+C_3 plot (Hinz et al., 1986), whereas the shaded area on the percent wetness plot marks values typical for economically viable gas reservoirs.

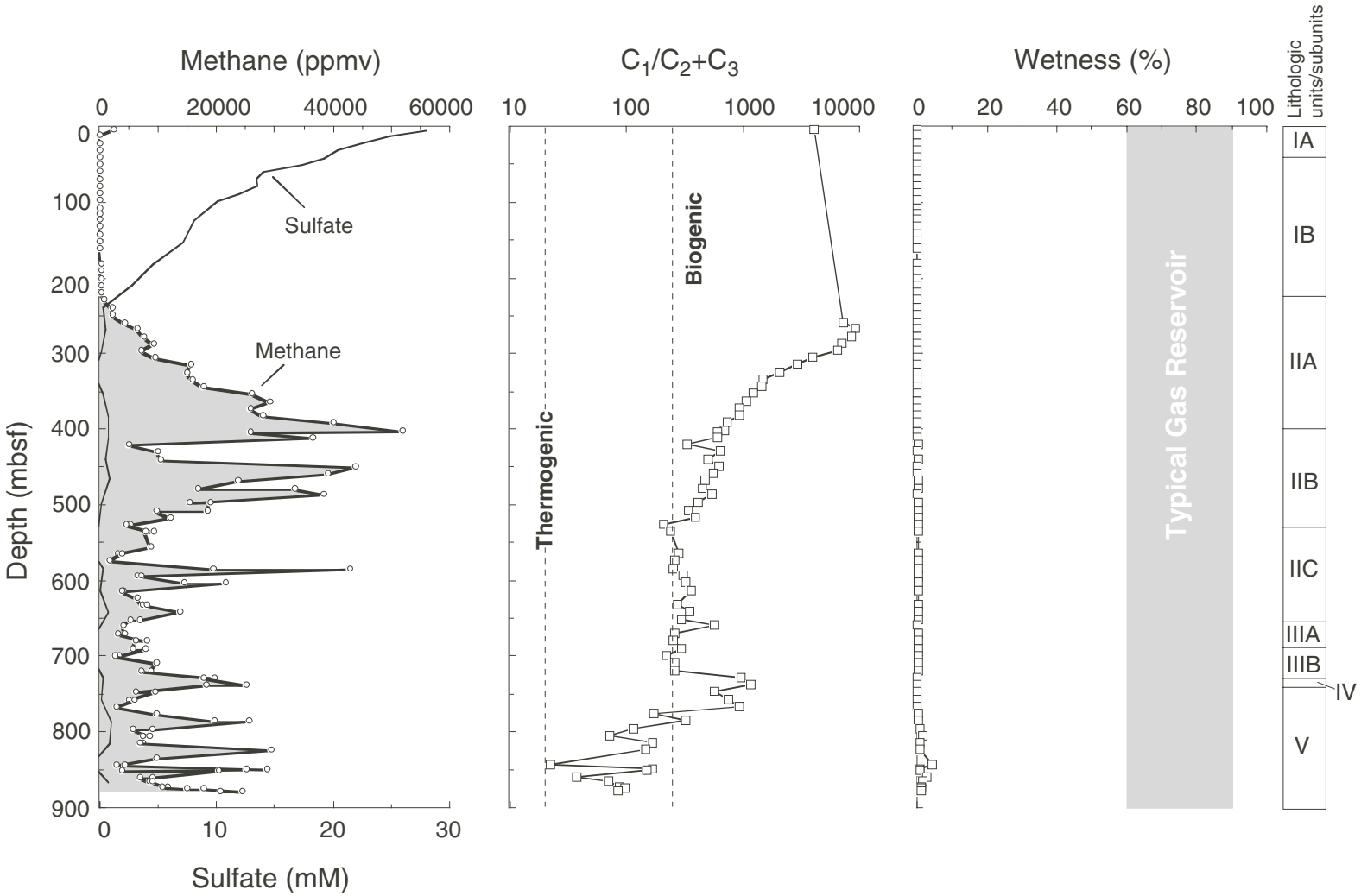

Figure F32. Concentration-depth profiles of interstitial water chemistry at Site 1168 with the approximate location of lithostratigraphic boundaries (see **"Lithostratigraphy,"** p. 8). Where appropriate, standard seawater concentrations are indicated. (Continued on next two pages.)

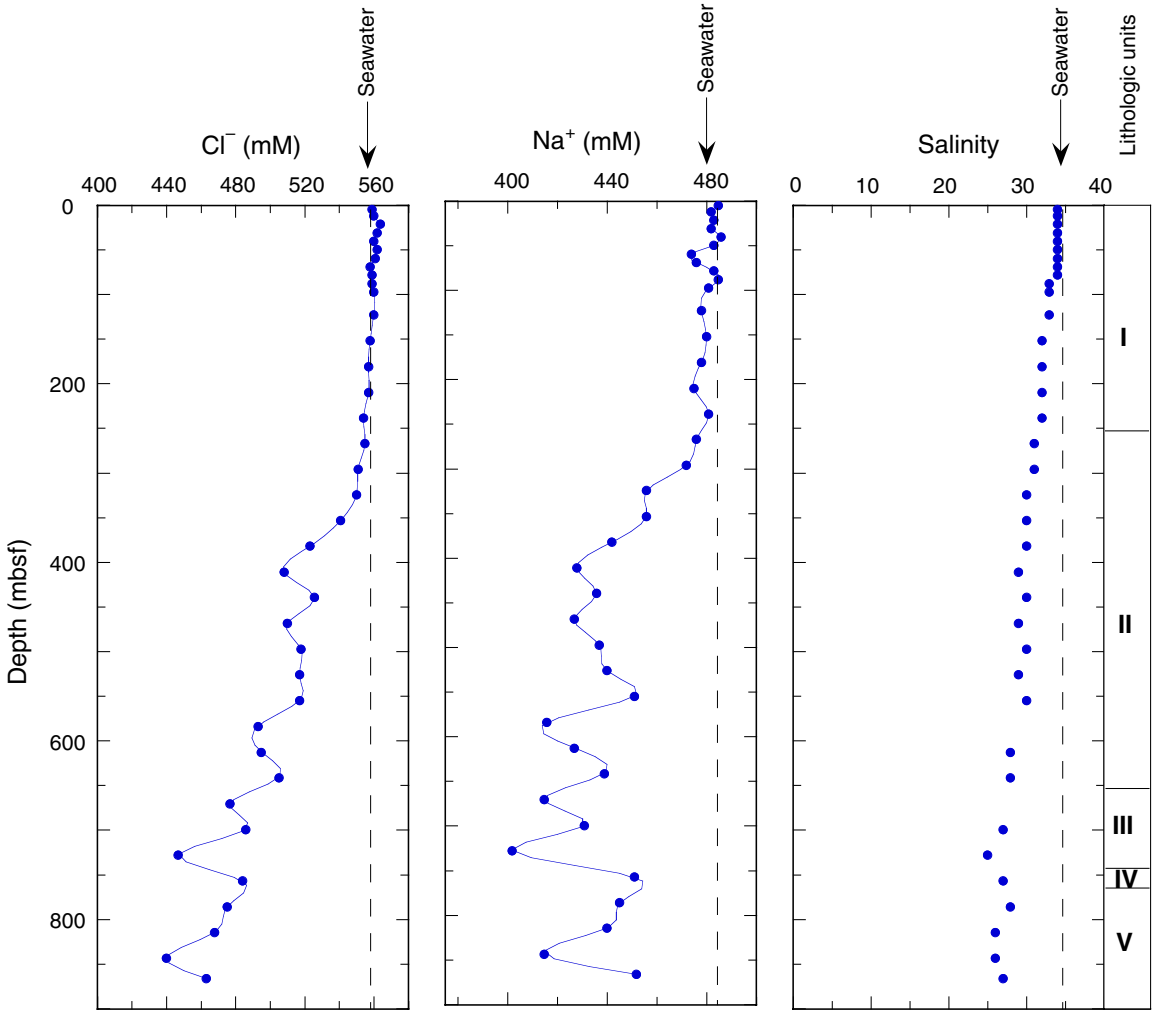

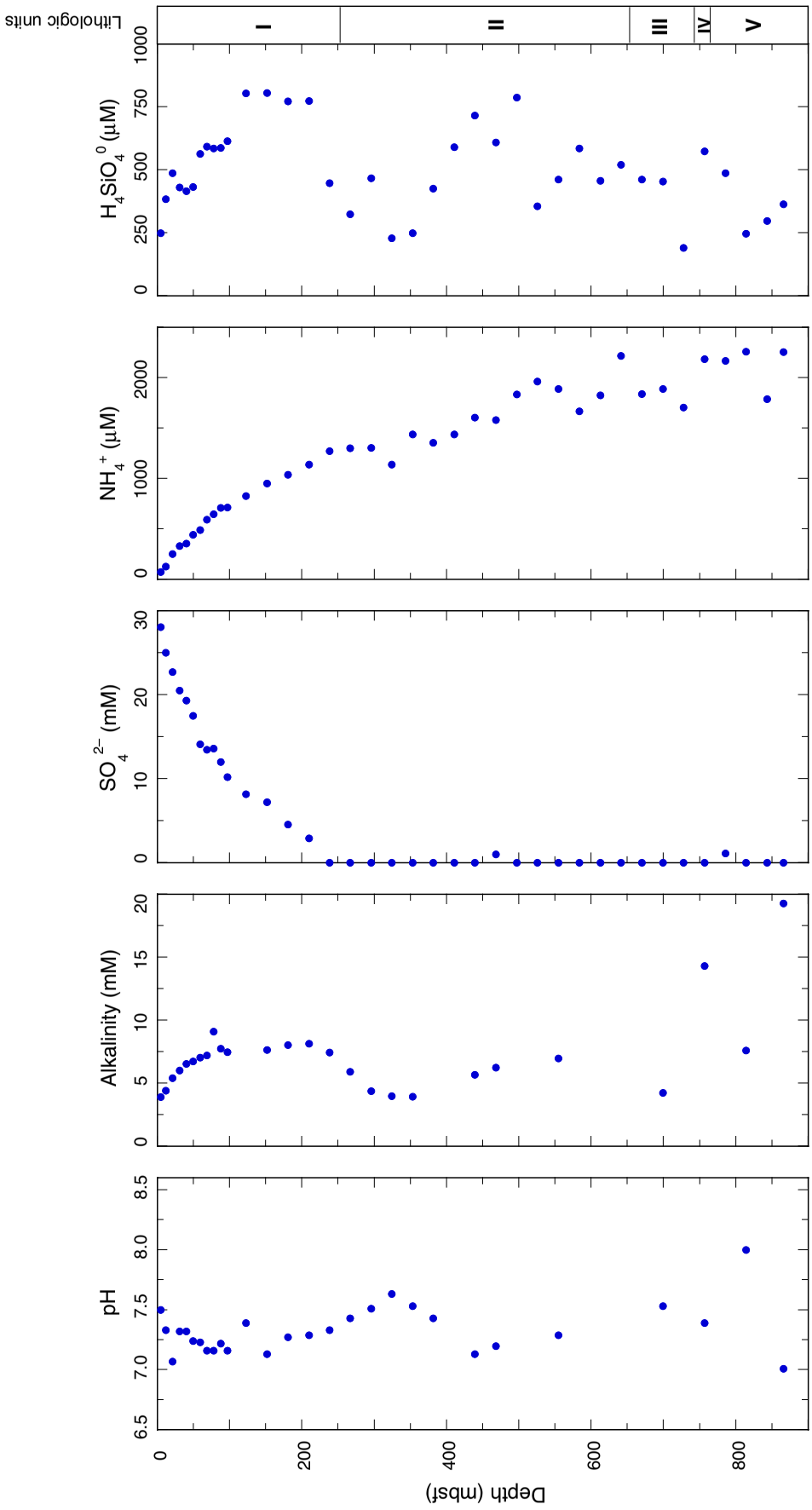

Figure F32 (continued).

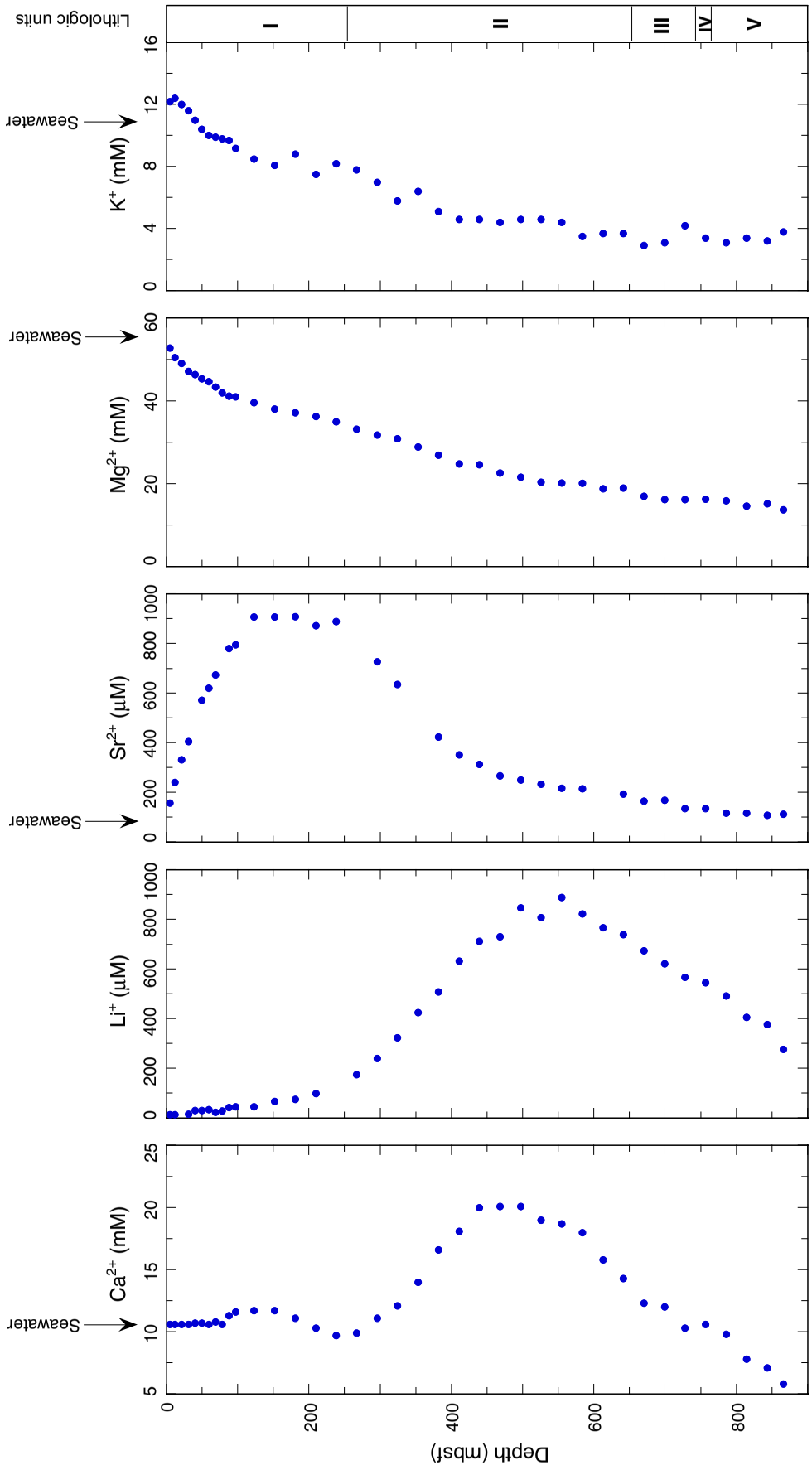

Figure F32 (continued).

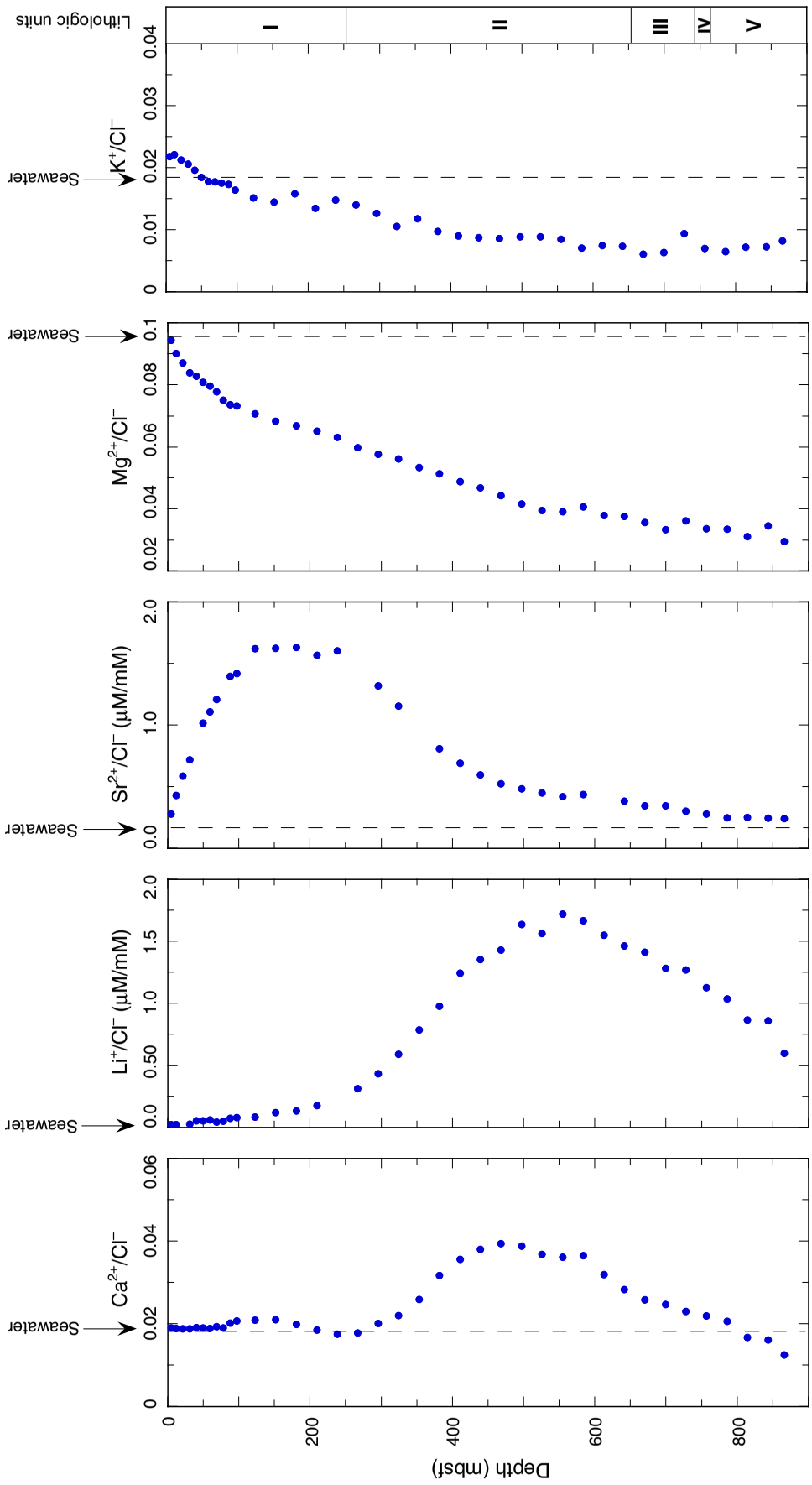

Figure F33. Concentration-depth profiles of Ca^{2+}, Sr^{2+}, Mg^{2+}, Li^+, and K^+ normalized to Cl^- with the approximate location of lithostratigraphic boundaries (see "Lithostratigraphy," p. 8). Standard seawater ratios are indicated.

Figure F34. Concentration of Ca^{2+} (green line) compared to the weight percent $CaCO_3$ with the approximate location of lithostratigraphic boundaries (see **"Lithostratigraphy,"** p. 8). Shaded interval highlights the lithostratigraphic Subunit IIB, where maximum interstitial Ca^{2+} values coincide with low weight percent $CaCO_3$.

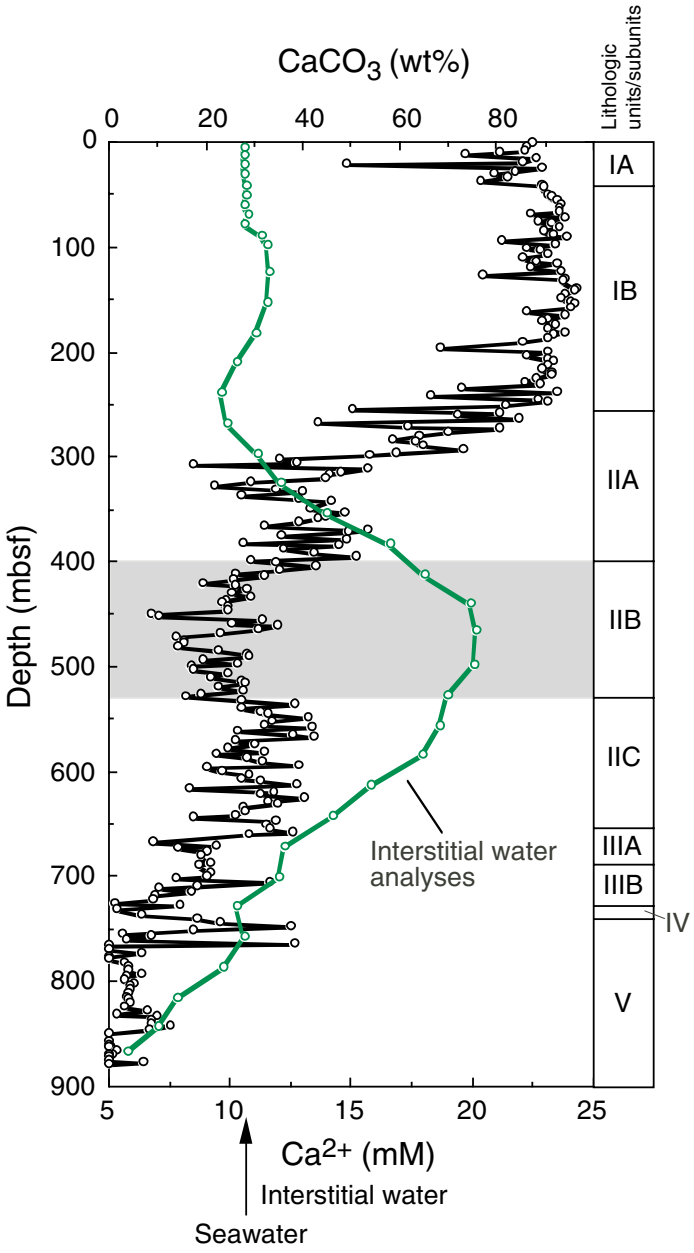

Figure F35. Concentration of dissolved silica within interstitial waters of Hole 1168A (thick line) compared to siliceous sponge spicule abundance (thin line).

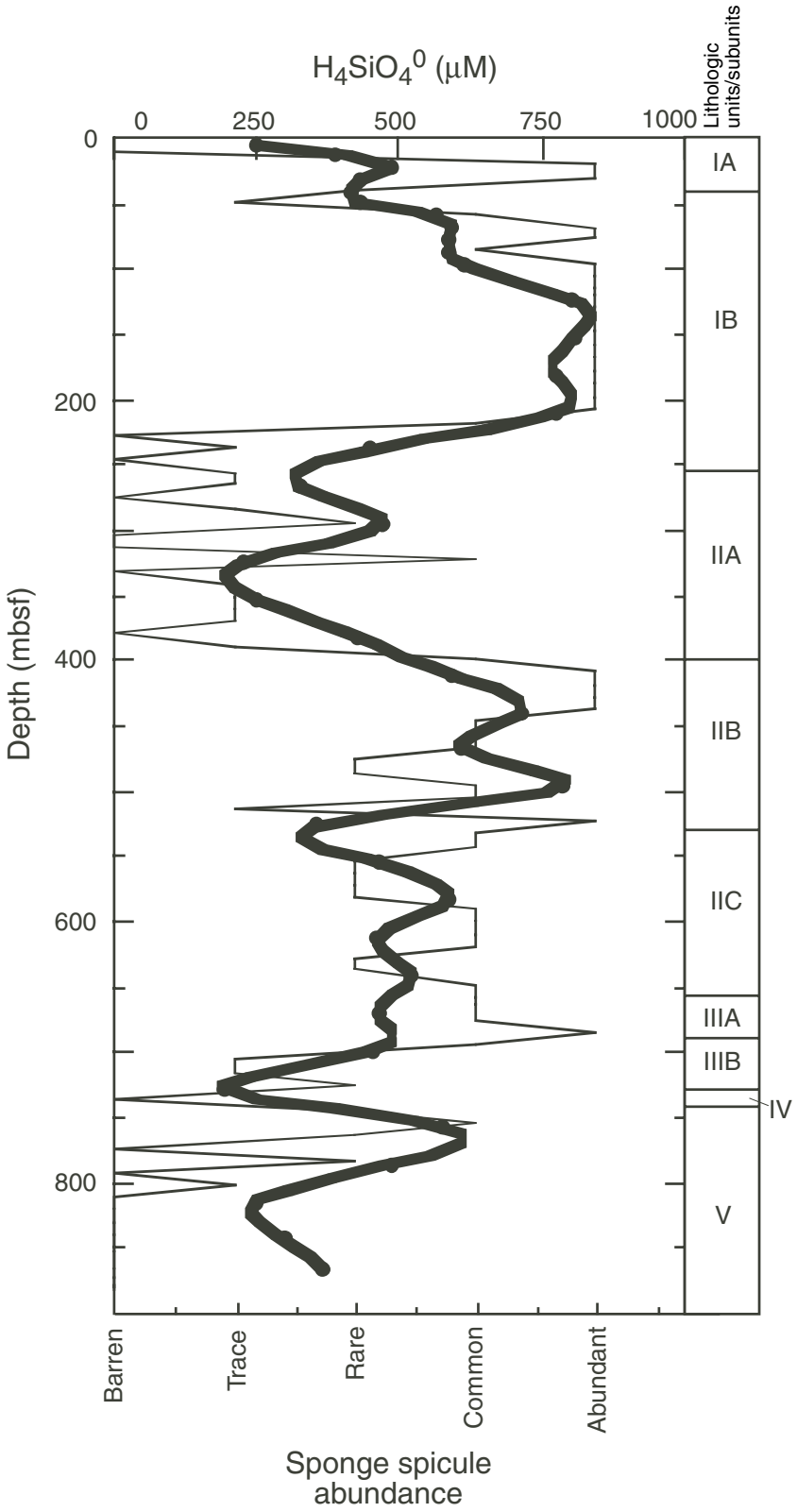

Figure F36. A. GRA density (dots) and wet bulk density determined for discrete samples (open circles) vs. depth for Hole 1168A. (Continued on next page.)

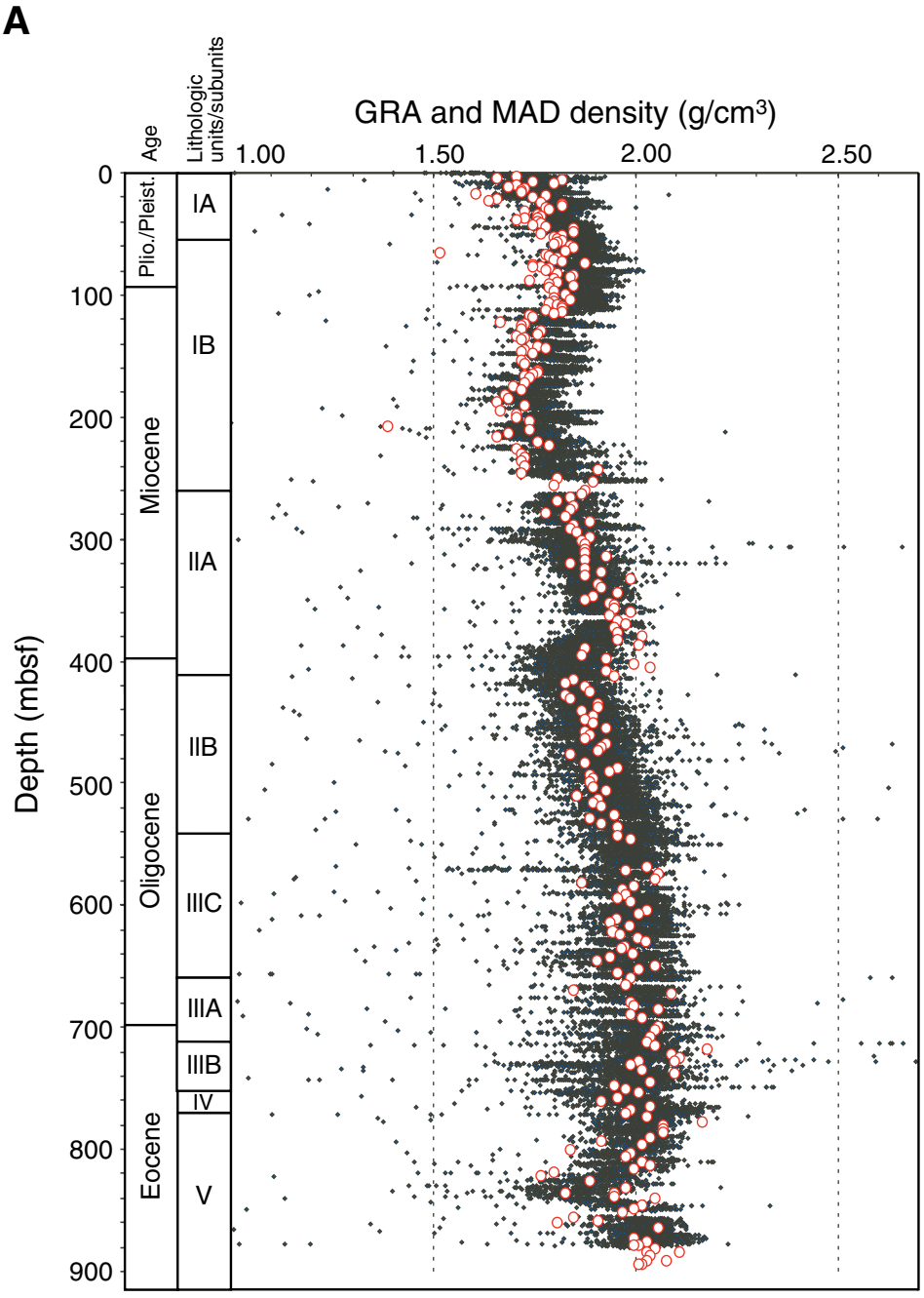

Figure F36 (continued). B. Whole-core magnetic susceptibility vs. depth measured on whole cores by the MST for Hole 1168A.

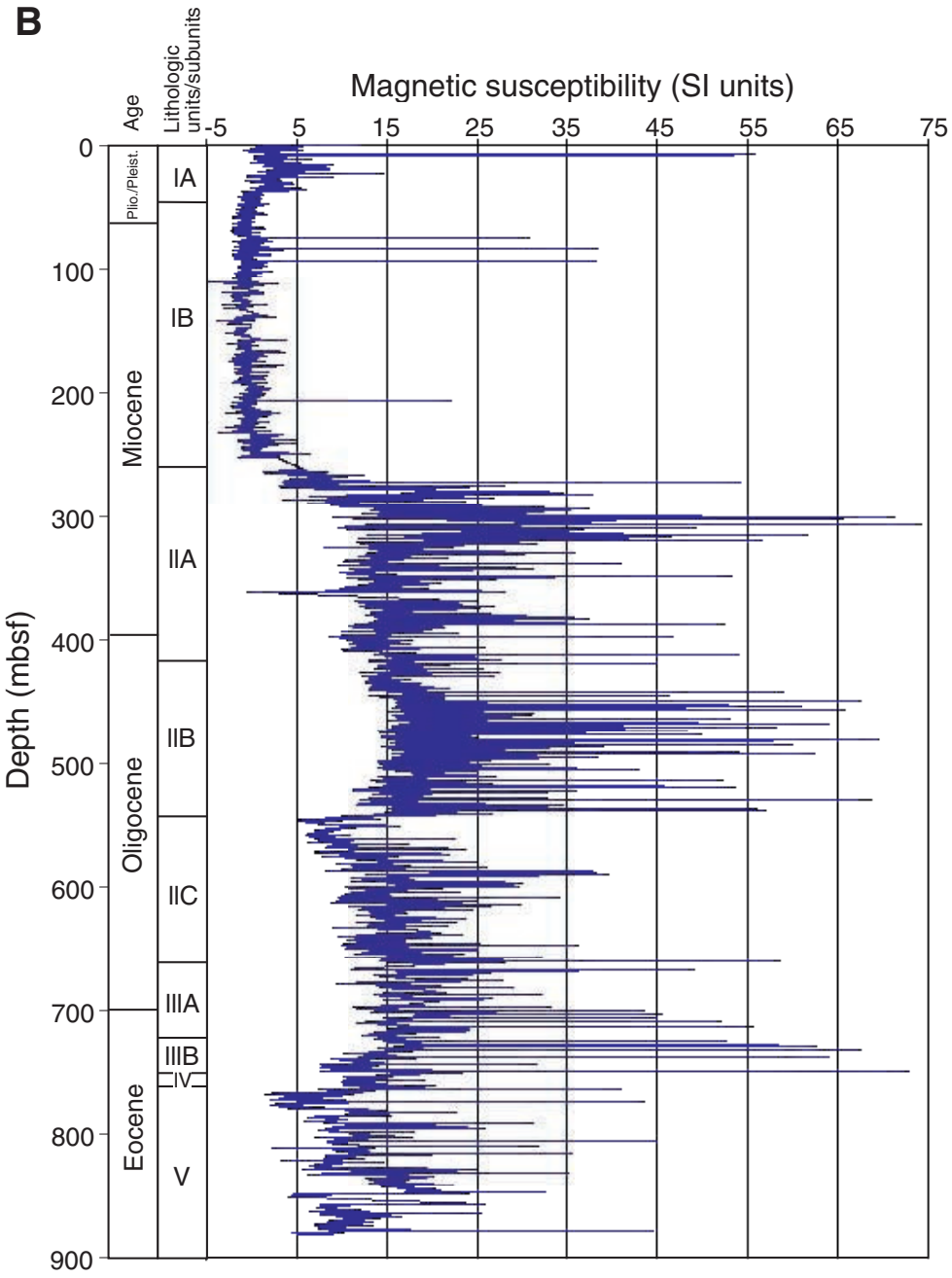

Figure F37. *P*-wave velocities (PWS1, PWS2, and PWS3) measured for discrete samples and *P*-wave velocities measured in whole cores (MST) vs. depth in Hole 1168A.

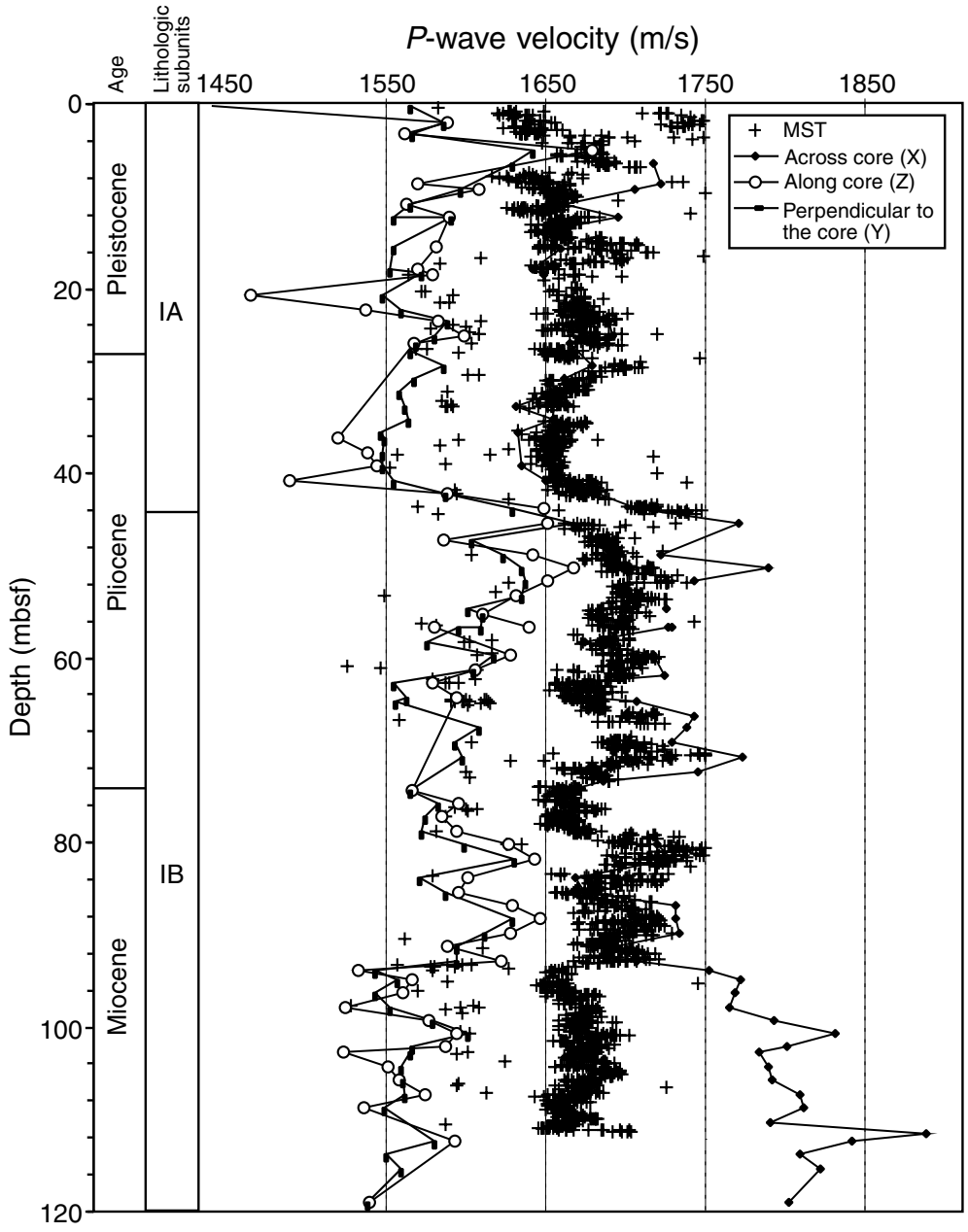

Figure F38. A. *P*-wave velocities (PWS1, PWS2, and PWS3) measured for discrete samples vs. depth. (Continued on next page.)

A

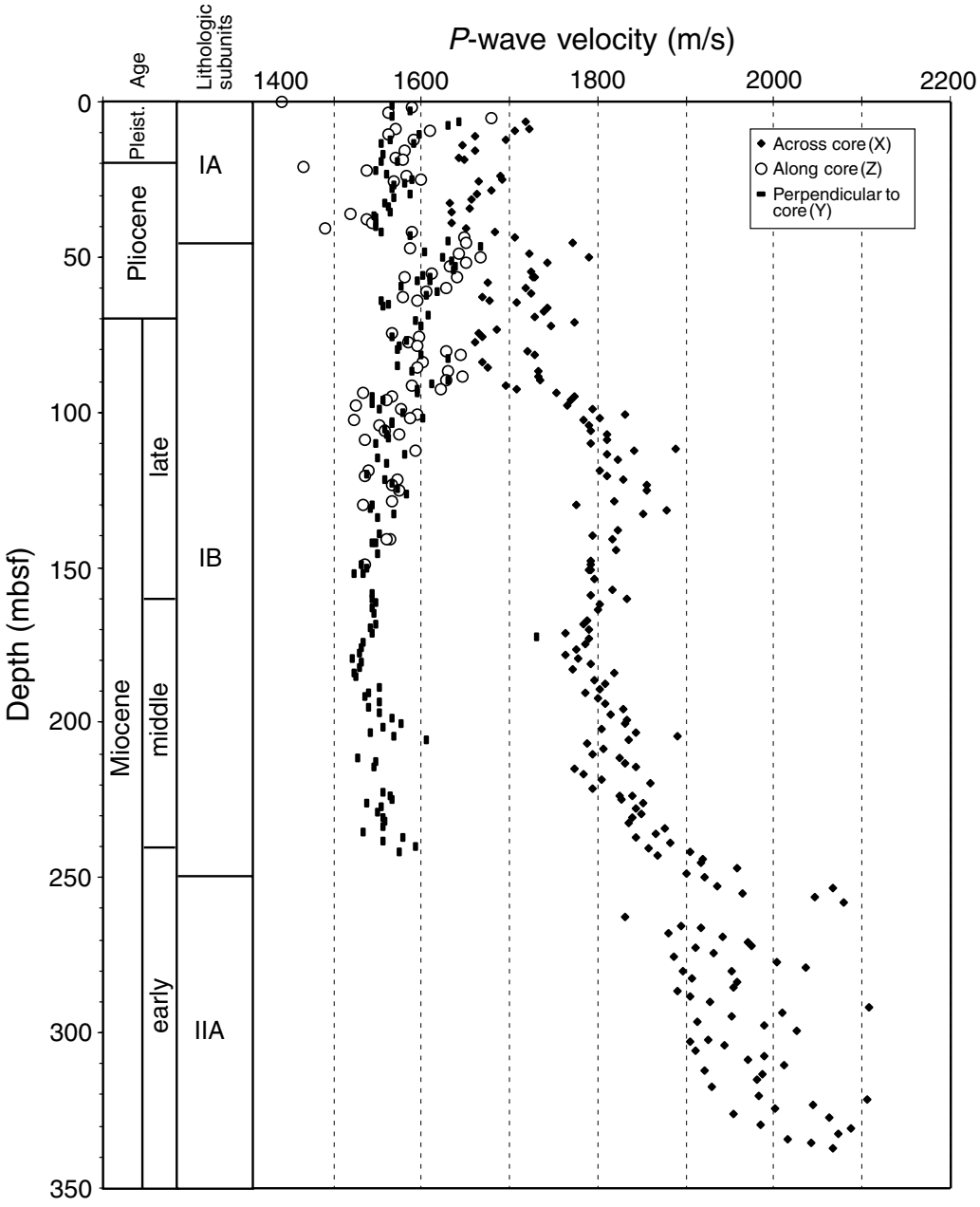

Figure F38 (continued). B. Three-dimensional *P*-wave velocities (Hamilton frame, PWS3) measurements for cemented sandstone sample cubes from Cores 189-1168A-72X and 86X vs. depth exhibit inhomogeneities because of the intensive cementation. Directions x and y were both measured along the bedding, y velocities are relatively faster. Direction z (perpendicular to the bedding) exhibits the slowest velocities. The top figure illustrates the three directions of measurement.

B

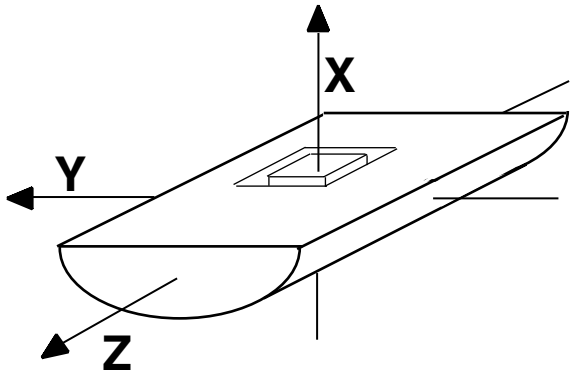

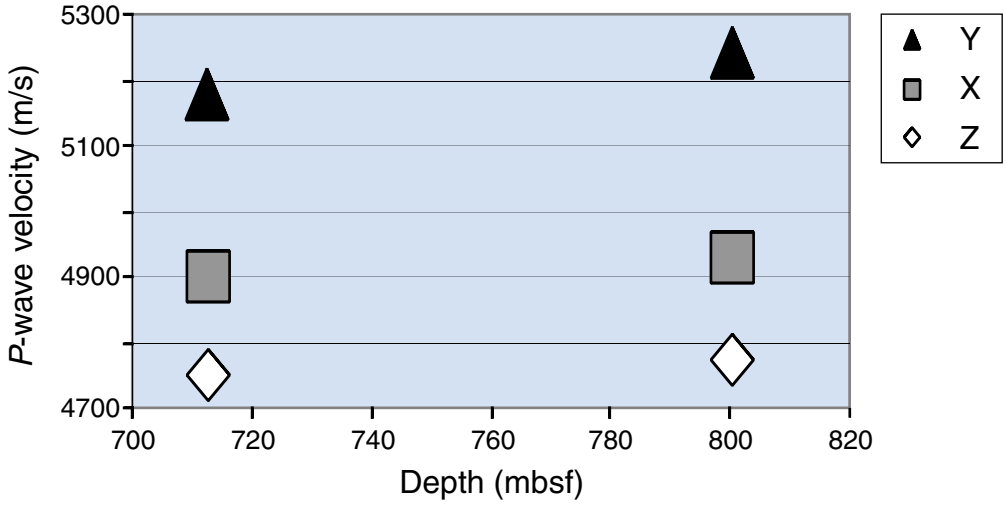

Figure F39. Thermal conductivity measured on whole cores vs. depth.

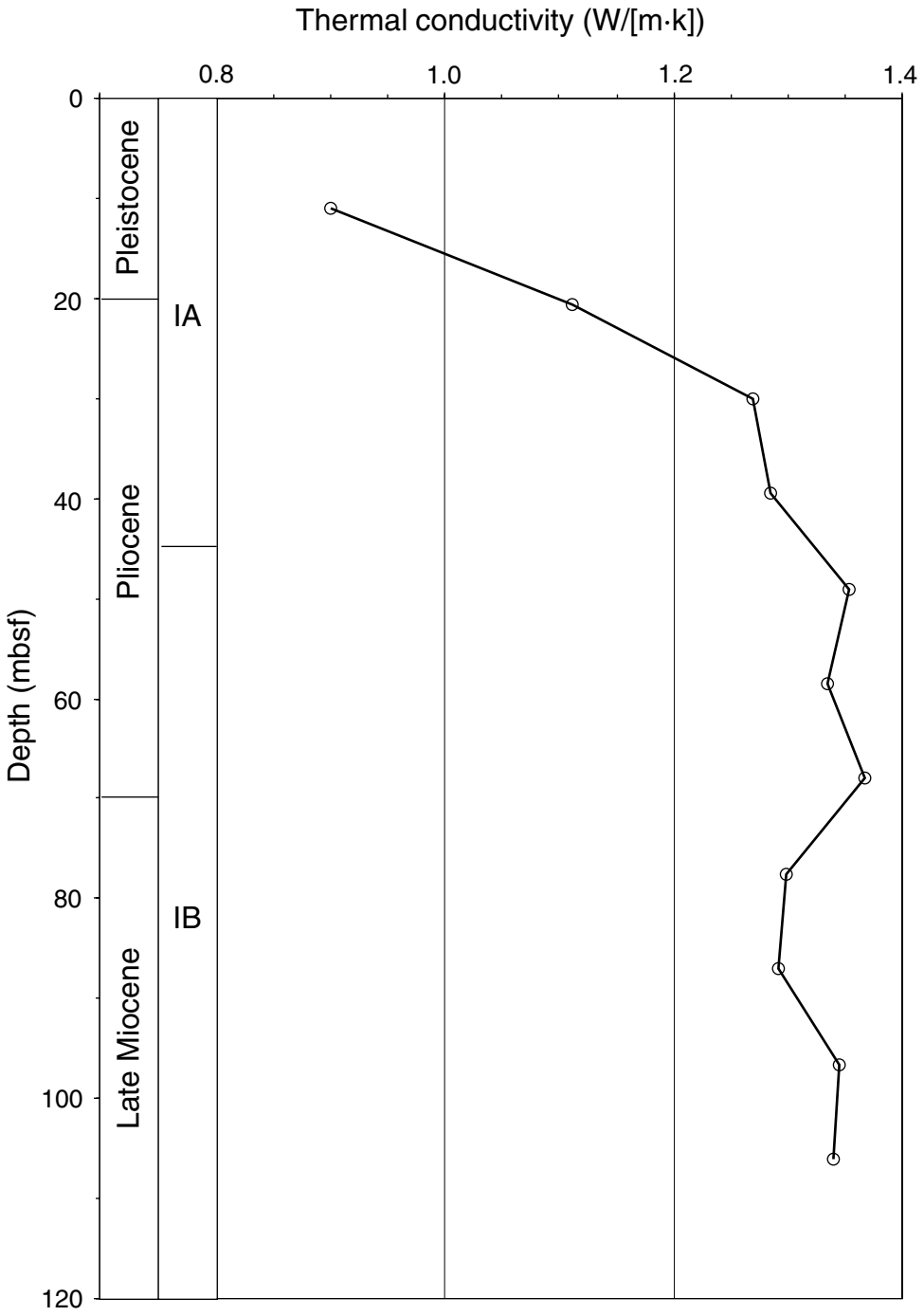

Figure F40. Wet bulk density, water content, and porosity measured at discrete intervals vs. depth for Hole 1168A. A cemented sandstone (Core 189-1168A-72X) is indicated by the "s" in each panel.

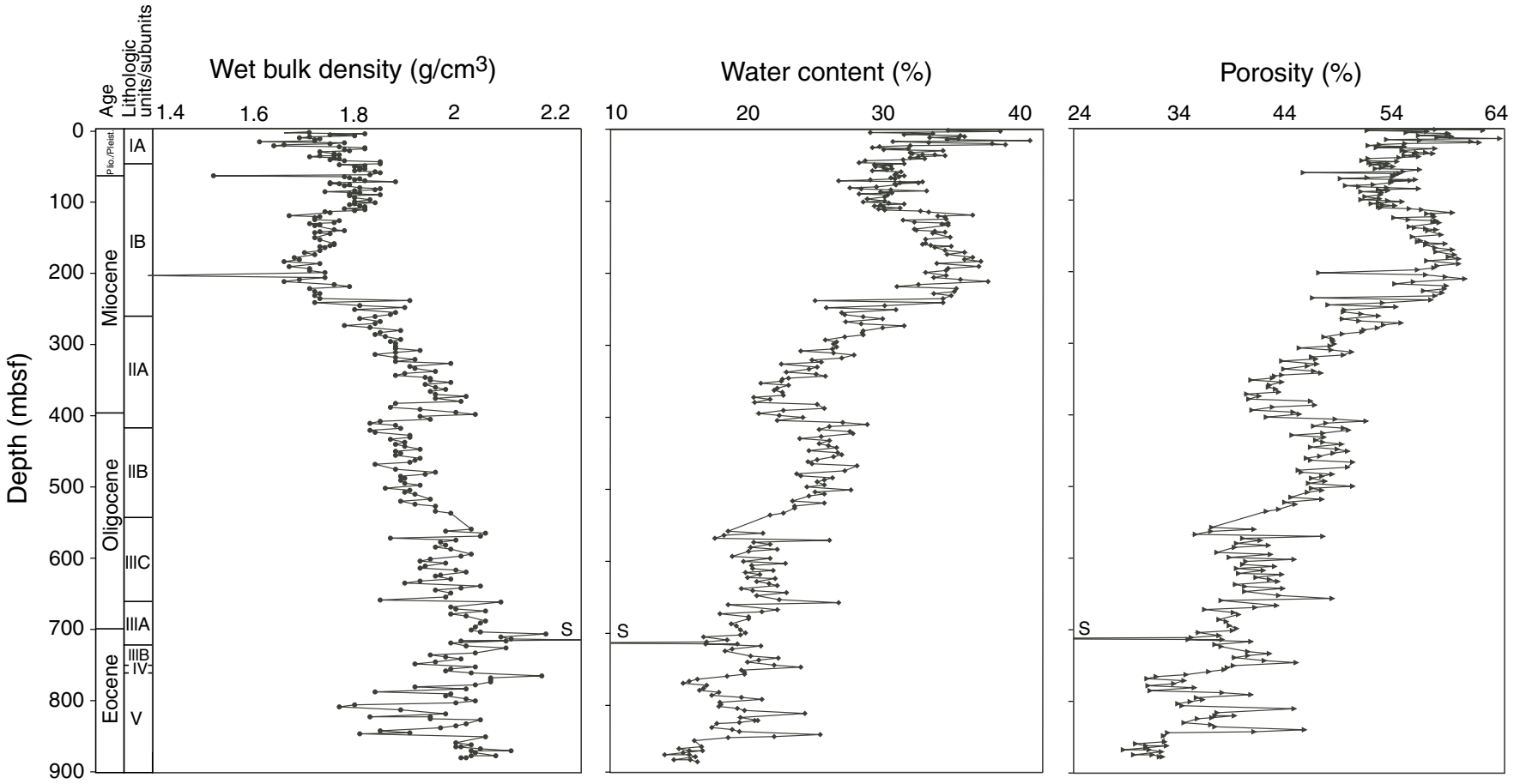

Figure F41. Penetration temperature record from the Adara tool deployment in Core 189-1168A-12H at 111.71 mbsf. The equilibrium temperature calculated from the penetration decay is shown by the horizontal solid line.

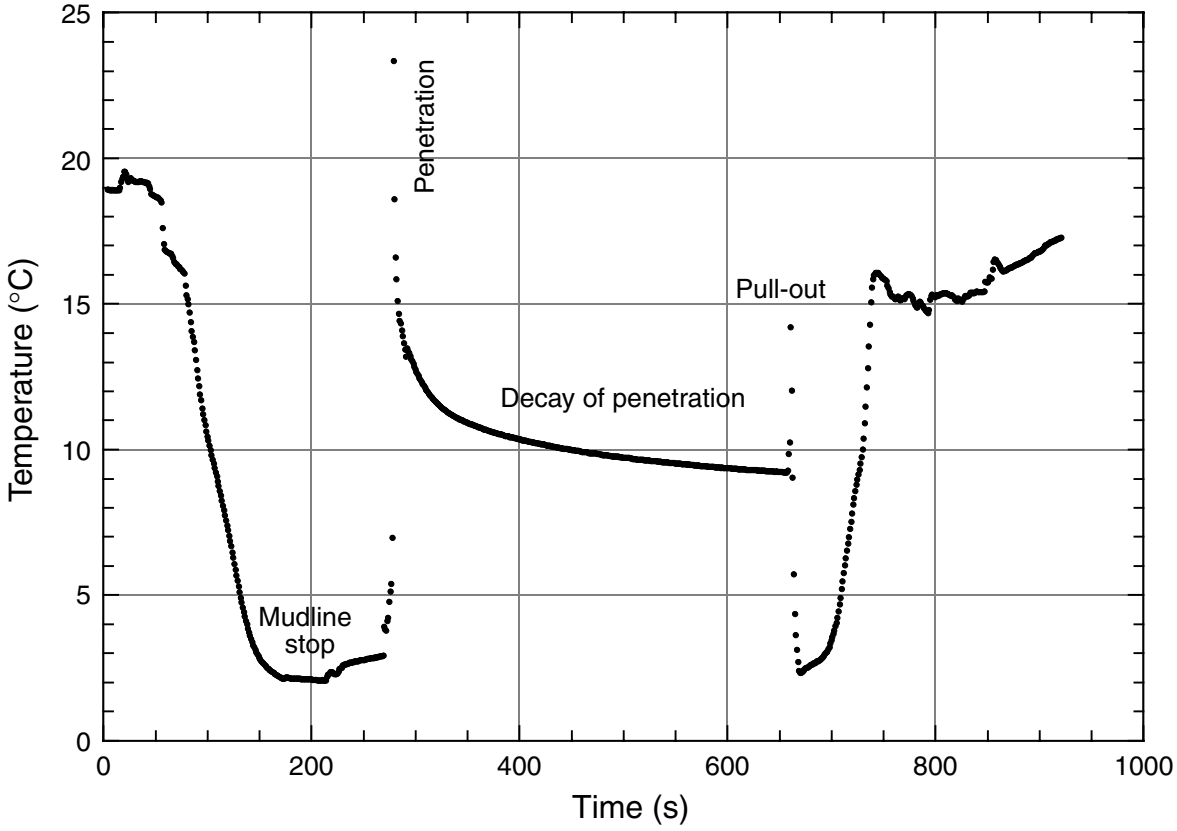

Figure F42. Temperature vs. depth plot for Site 1168.

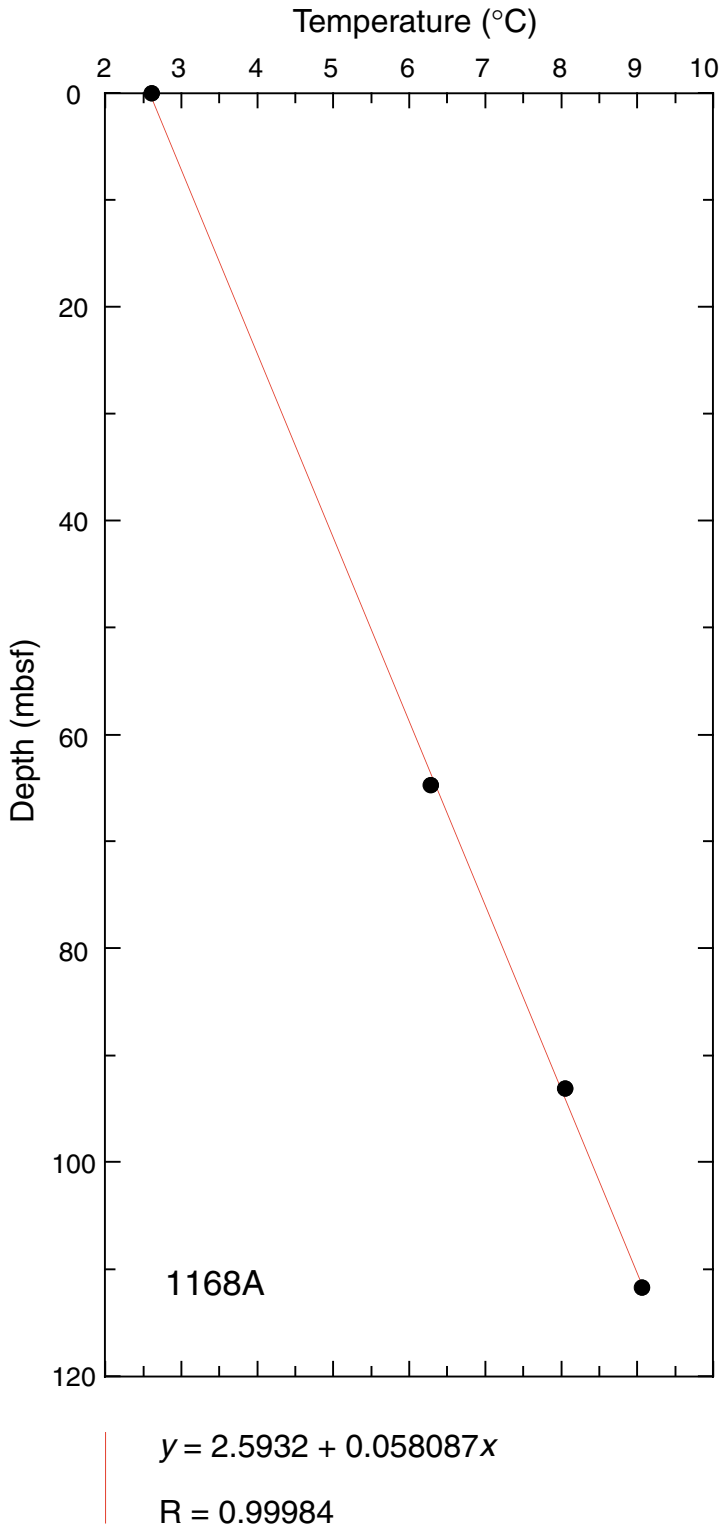

Figure F43. Undrained shear strength from miniature vane-shear measurements (line) and GRA density (dots) vs. depth for Hole 1168A.

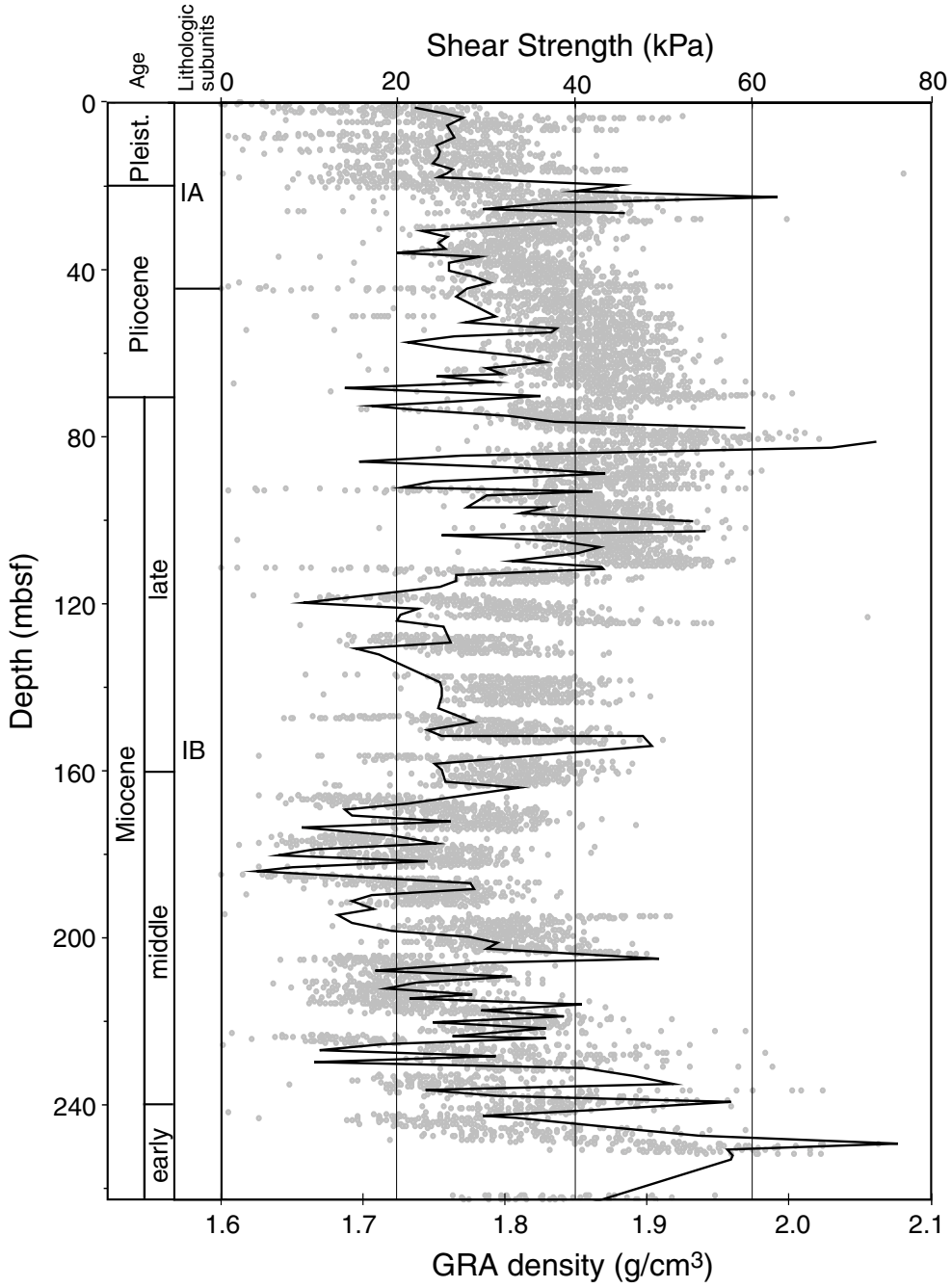

Figure F44. Details of the logging operations in Hole 1168B. Depths are shown in either meters below rig floor (mbrf) or meters below seafloor (mbsf).

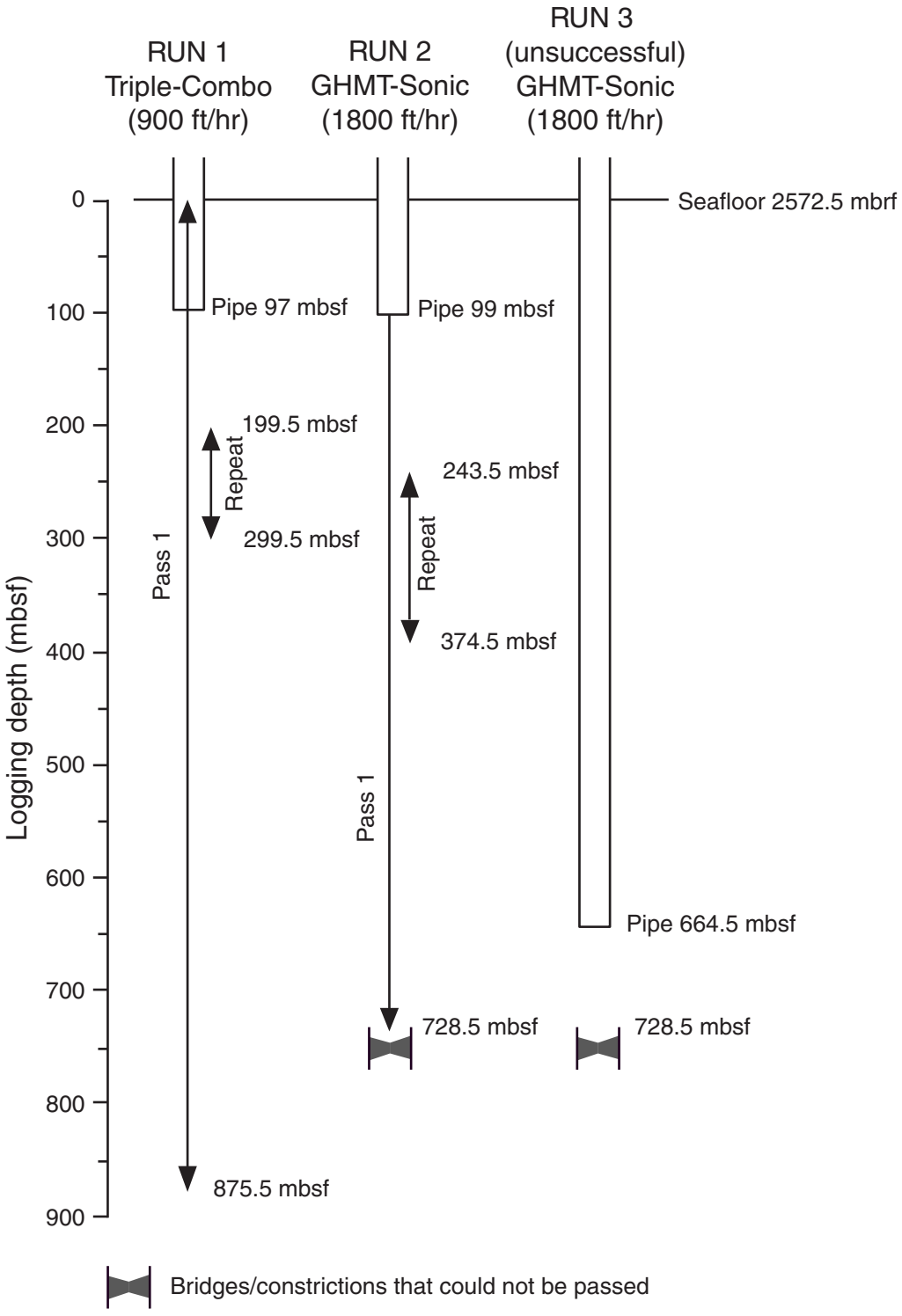

Figure F45. Caliper, gamma-ray, resistivity, and magnetic susceptibility (log and core) values from Hole 1168A.

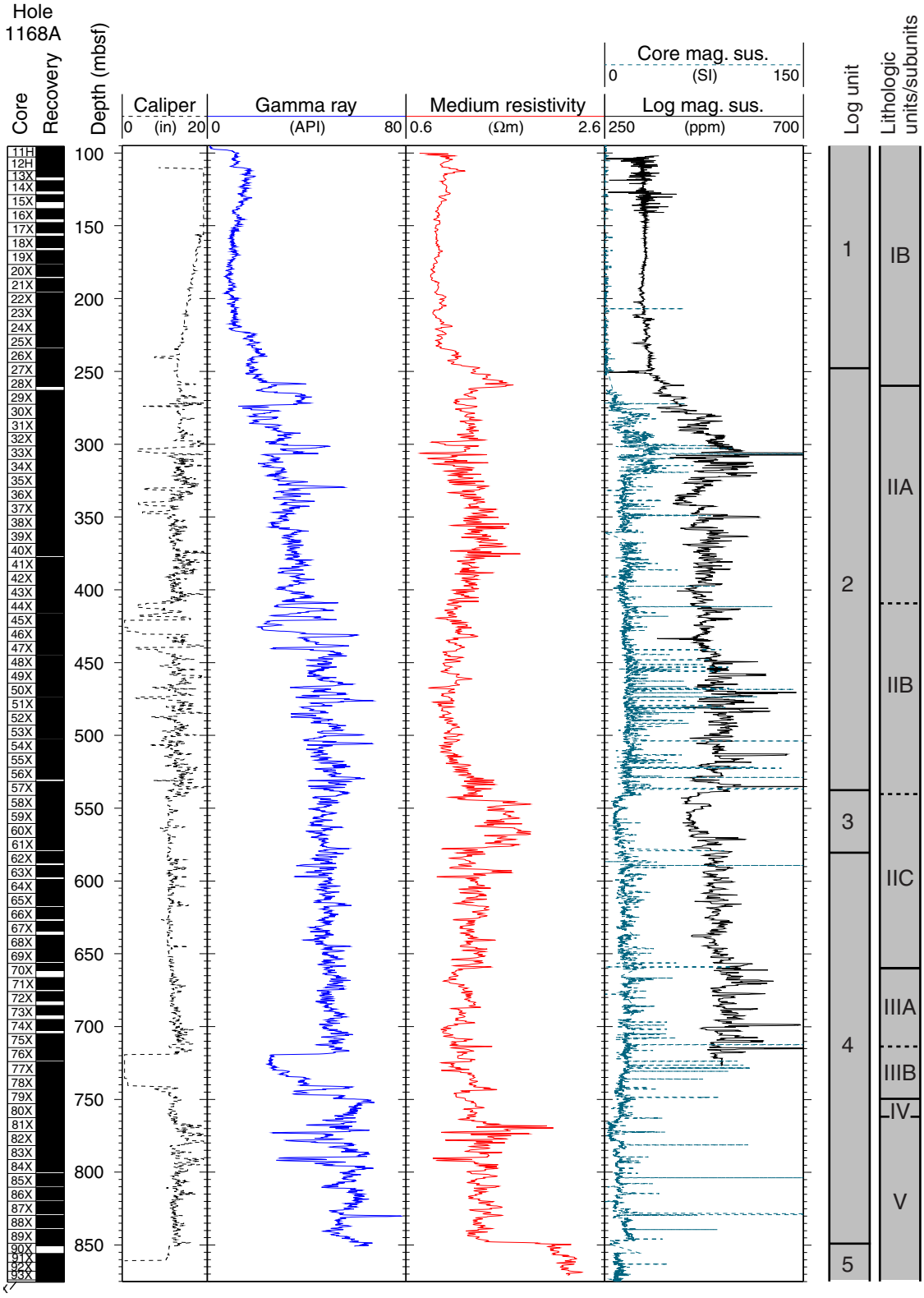

Figure F46. Velocity, density, porosity, and photoelectric effect (PEFL) values from Hole 1168A.

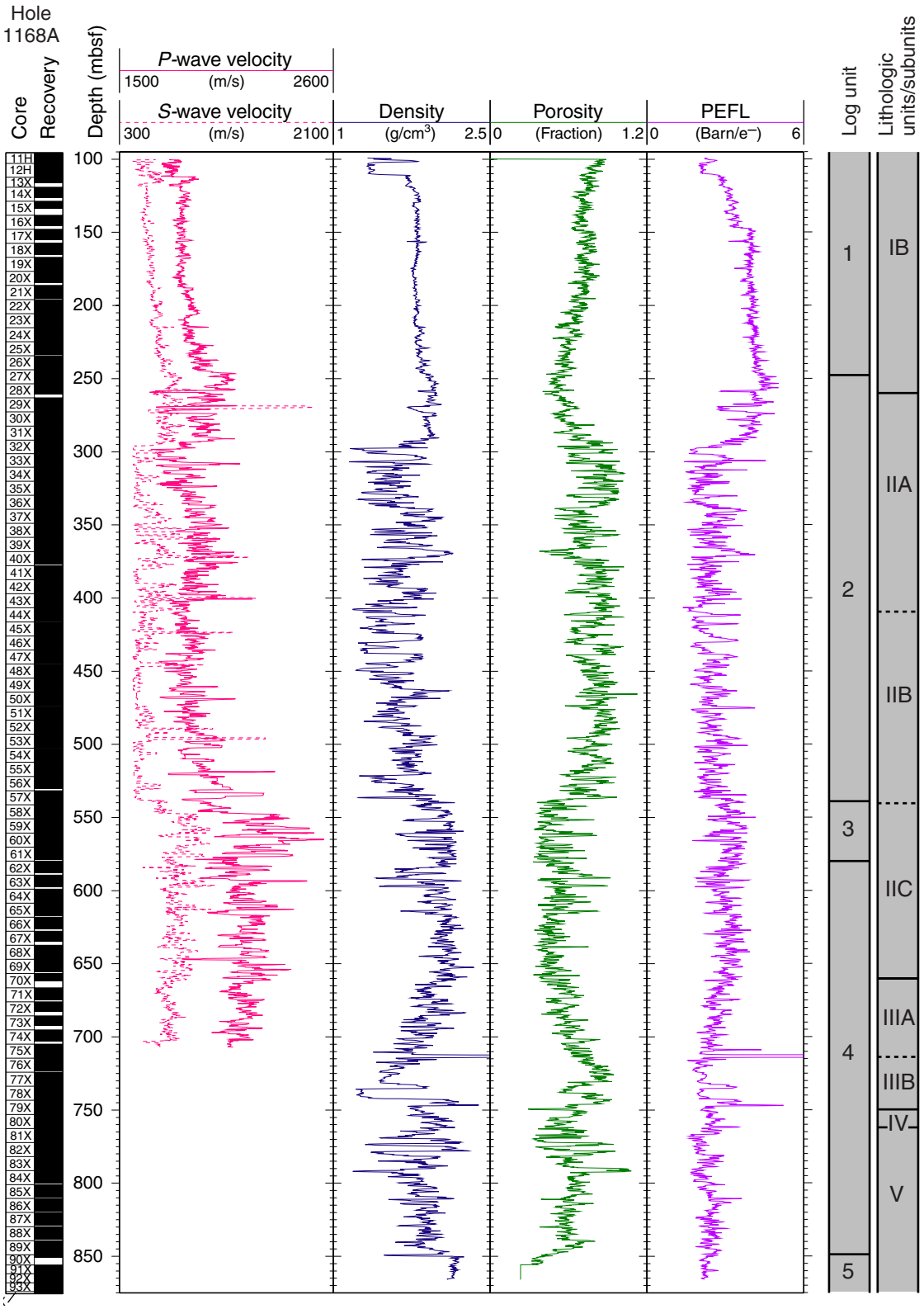

Figure F47. Total gamma-ray and spectral gamma-ray values from Hole 1168A. HSGR = total gamma radiation (from Th, K, and U), HCGR = gamma radiation from Th and K only.

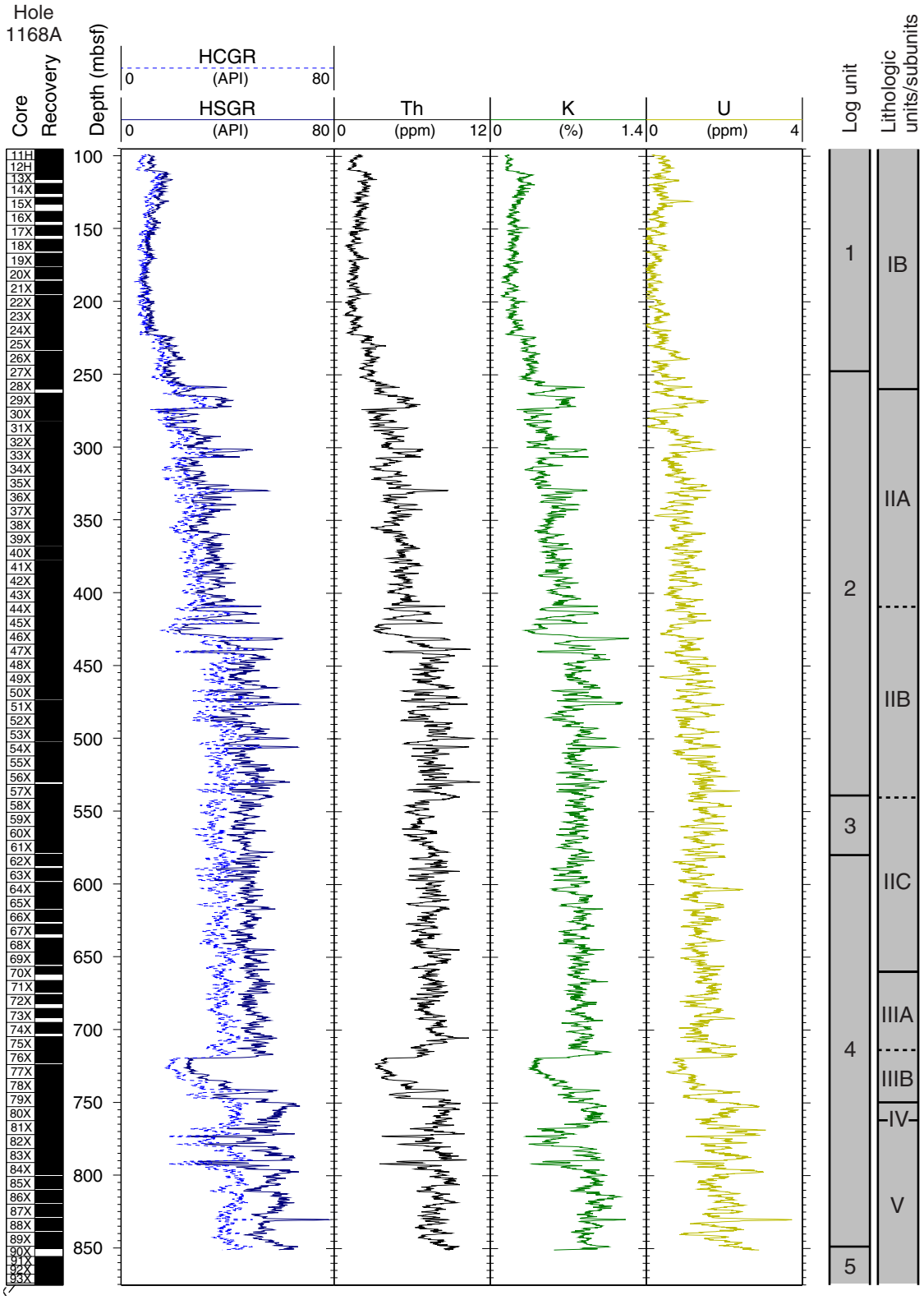

Figure F48. Intervals from the logs where hole conditions were particularly poor. Notice that where the borehole is particularly wide (calipers readings = >18 in) density readings are low and porosity readings are high.

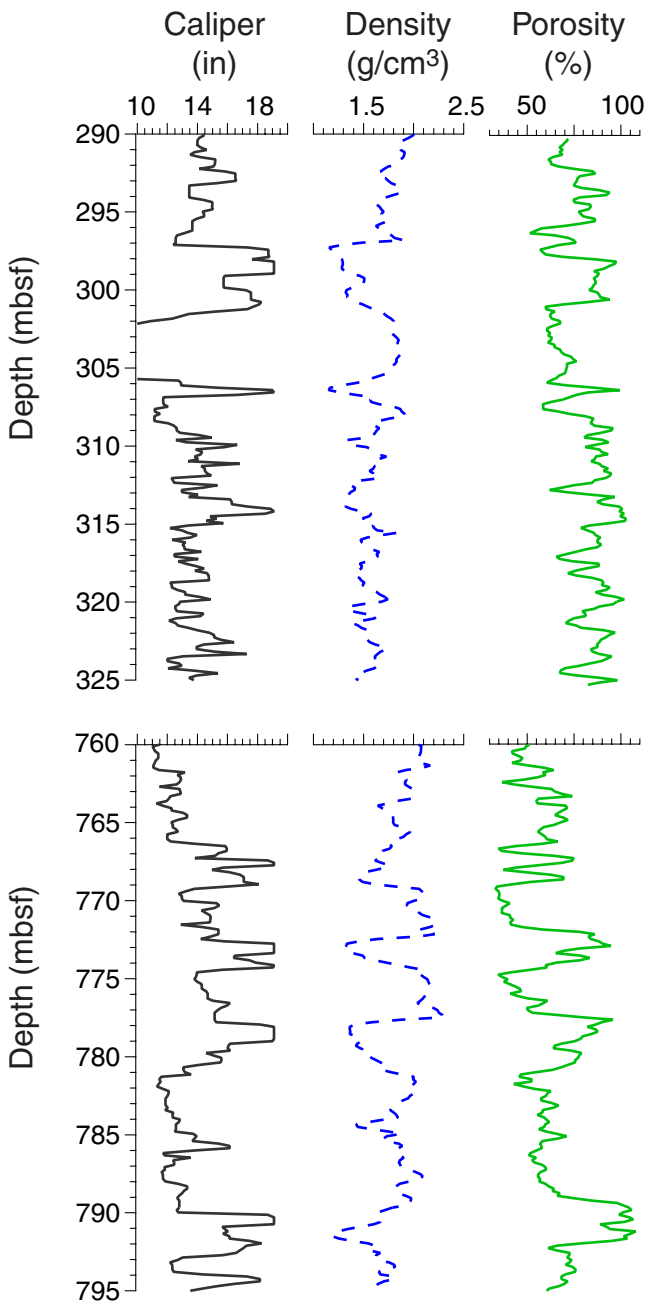

Figure F49. Downhole log bulk density plotted with core bulk density.

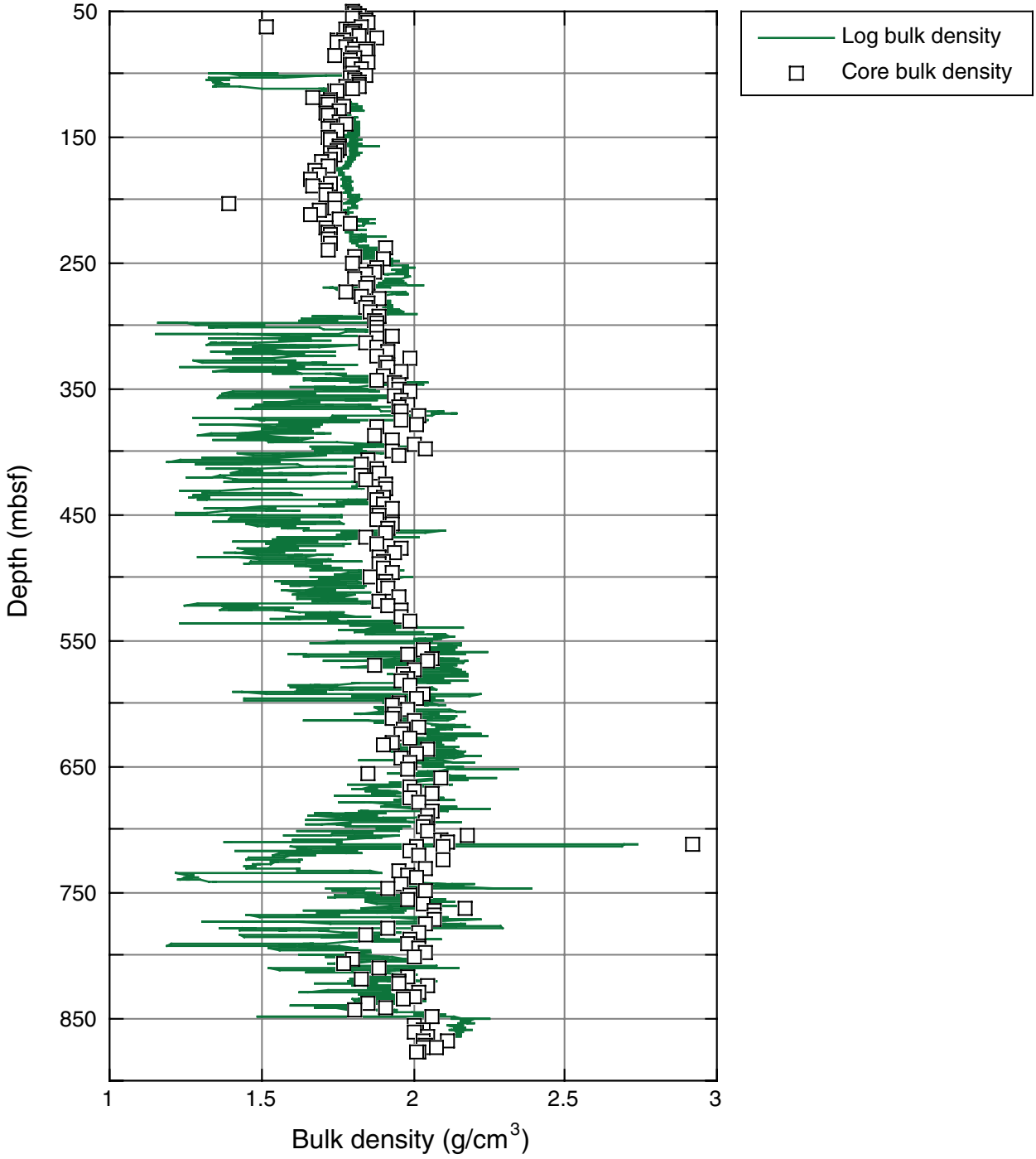

Figure F50. Downhole density porosity and neutron porosity plotted with core porosity.

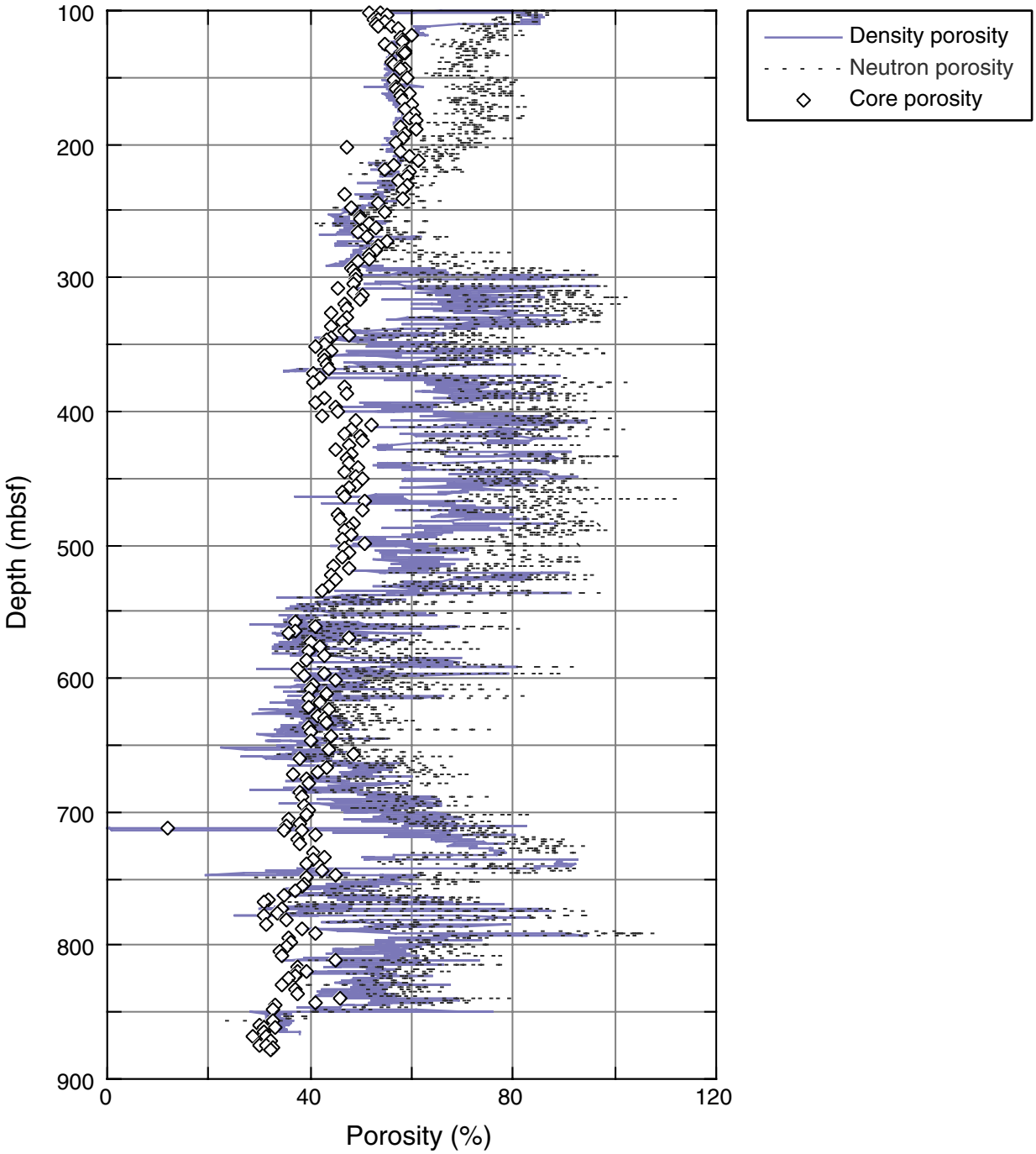

Figure F51. Downhole *P*-wave velocities (V_p) from the DSI logs plotted with the *P*-wave velocities measured vertically on half cores.

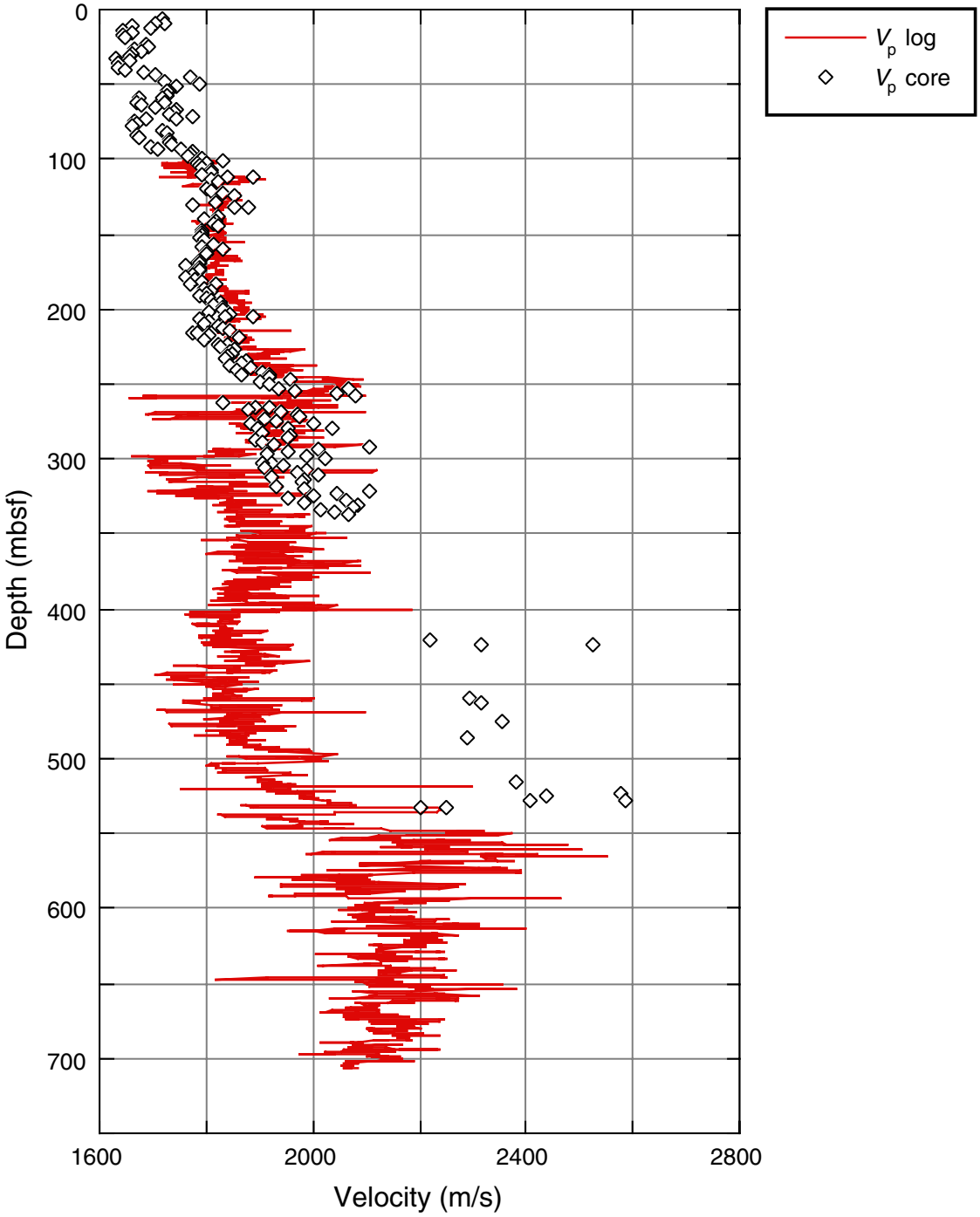

Figure F52. Core magnetic susceptibility data from Holes 1168A and 1168C are shown with log magnetic susceptibility before (top) and after (bottom) core-log integration. The record from Hole 1168C was offset by +30 SI for visual clarity. Mapping the core data to downhole logs gives more precise estimates for the size and position of the core depths.

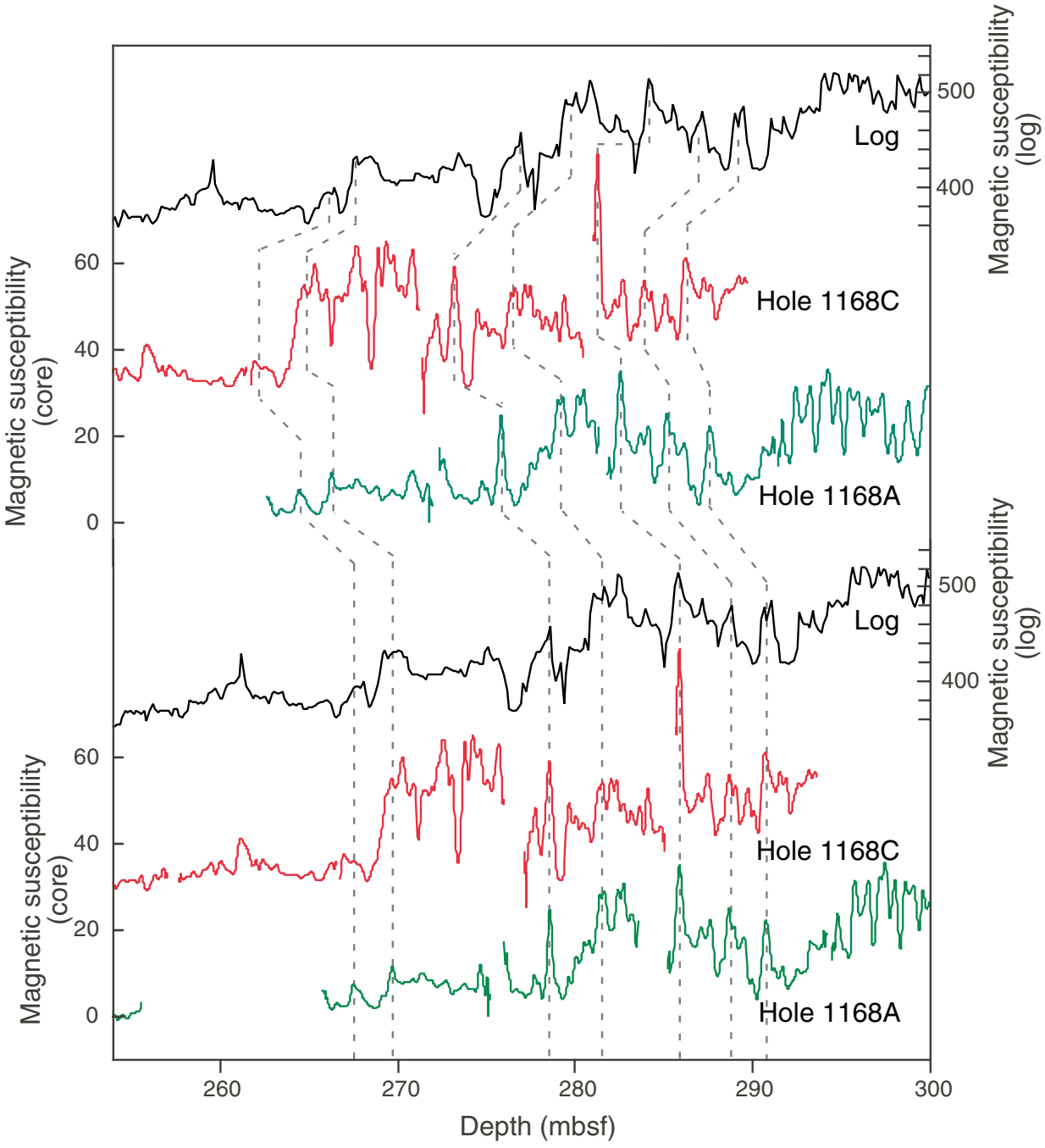

Figure F53. Sonic two-way traveltime curve for Site 1168.

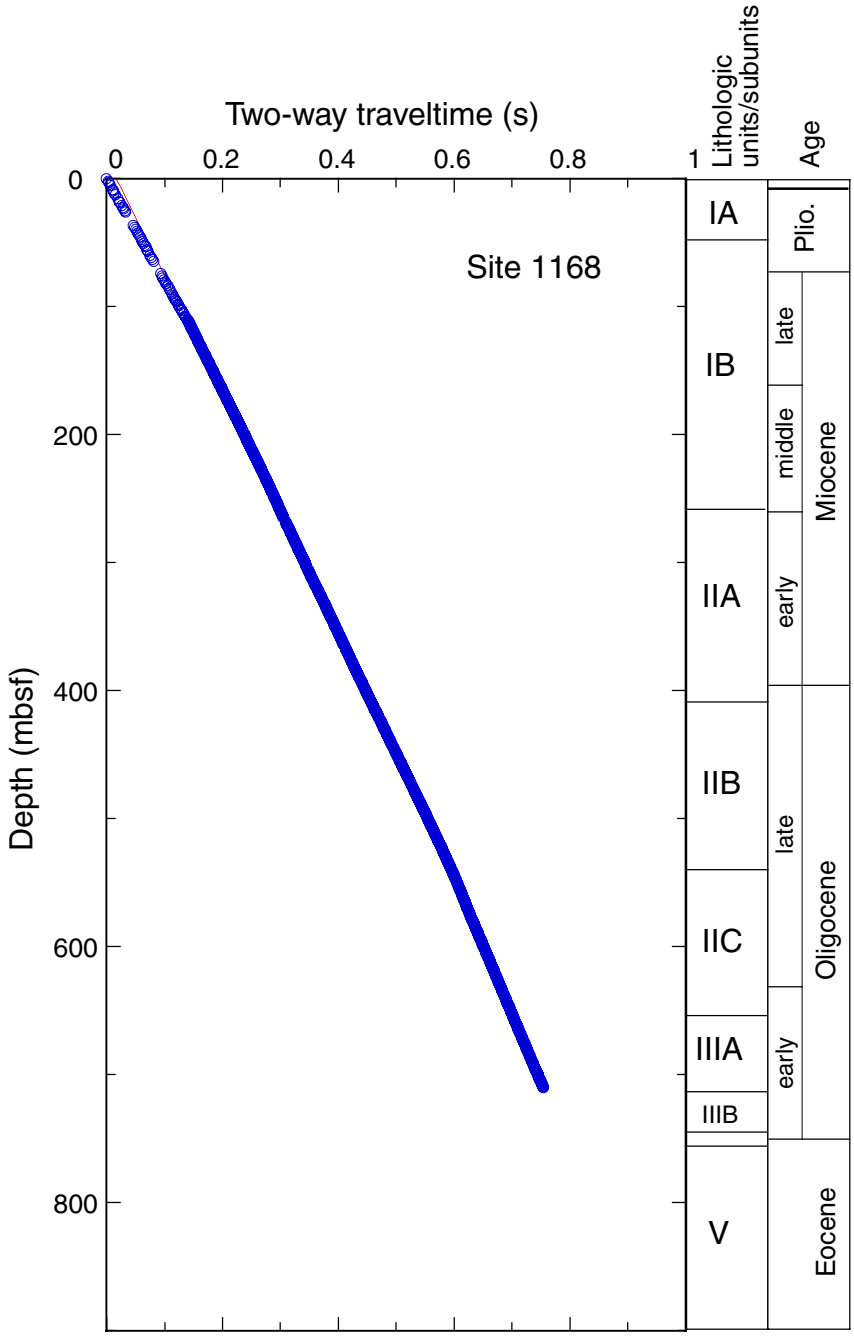

$$Y = 1.668 \times 10^{-2} + 1.105 \times 10^{-3} (X) + 8.3005 \times 10^{-10} (X^2) - 1.3027 \times 10^{-10} (X^3)$$

Figure F54. Downhole Th/U ratios from Hole 1168A. Th/U values <2 are indicative of reducing conditions, and Th/U values >7 are indicative of oxidizing conditions (Adams and Weaver, 1958; Doveton, 1991).

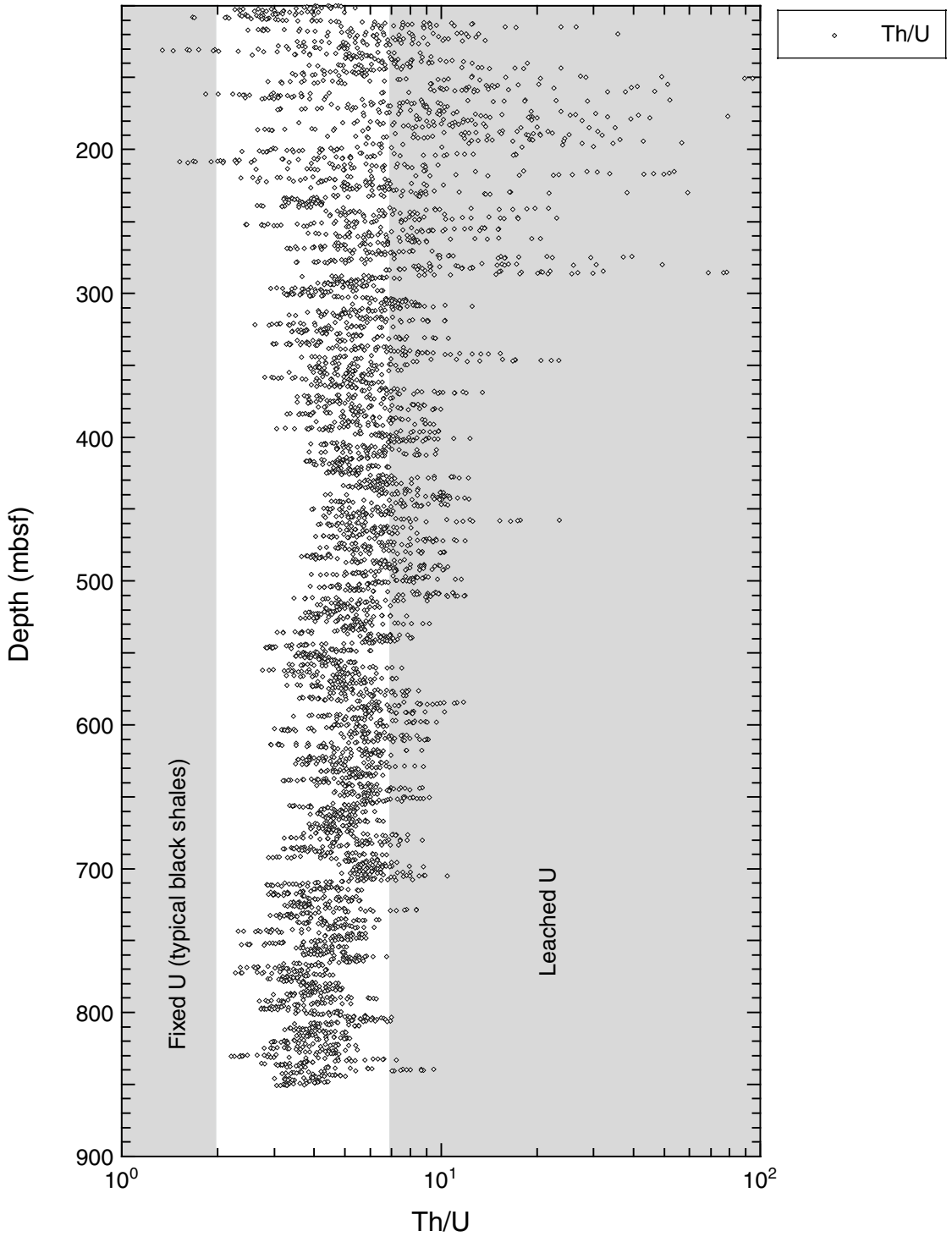

Table T1. Coring summary, Site 1168. (Continued on next two pages.)

Hole 1168A
Latitude: 42°36.5809′S
Longitude: 144°24.7620′E
Time on site: 9 days, 13 hr; 229.00 hr (0800 hr, 17 March–2215 hr, 26 March 2000)
Time on hole: 182.25 hr (0800 hr, 17 March–2215 hr, 24 March 2000)
Seafloor (drill pipe measurement from rig floor, mbrf): 2474.2
Distance between rig floor and sea level (m): 10.9
Water depth (drill pipe measurement from sea level, m): 2463.3
Total depth (from rig floor, mbrf): 3357.7
Total penetration (mbsf): 883.5
Total length of cored section (m): 883.5
Total core recovered (m): 836.85
Core recovery (%): 94.7
Total number of cores: 95

Hole 1168B
Latitude: 42°36.5692′S
Longitude: 144°24.7594′E
Time on hole: 14.00 hr (2215 hr, 24 March–1215 hr, 25 March 2000)
Seafloor (drill pipe measurement from rig floor, mbrf): 2474.6
Distance between rig floor and sea level (m): 11.0
Water depth (drill pipe measurement from sea level, m): 2463.6
Total depth (from rig floor, mbrf): 2583.0
Total penetration (mbsf): 108.4
Total length of cored section (m): 108.4
Total core recovered (m): 106.52
Core recovery (%): 98.3
Total number of cores: 12

Hole 1168C
Latitude: 42°36.5533′S
Longitude: 144°24.7614′E
Time on hole: 32.75 hr (1215 hr, 25 March–2100 hr, 26 March 2000)
Seafloor (drill pipe measurement from rig floor, mbrf): 2475.0
Distance between rig floor and sea level (m): 11.0
Water depth (drill pipe measurement from sea level, m): 2464.0
Total depth (from rig floor, mbrf): 2765.5
Total penetration (mbsf): 290.5
Total length of cored section (m): 290.5
Total core recovered (m): 248.15
Core recovery (%): 85.4
Total number of cores: 31

Core	Date (March 2000)	Local Time	Depth (mbsf) Top	Depth (mbsf) Bottom	Length (m) Cored	Length (m) Recovered	Recovery (%)
189-1168A-							
1H	17	1745	0.0	7.3	7.3	7.26	99.5
2H	17	1830	7.3	16.8	9.5	9.72	102.3
3H	17	1915	16.8	26.3	9.5	9.94	104.6
4H	17	1955	26.3	35.8	9.5	9.50	100.0
5H	17	2145	35.8	45.3	9.5	10.19	107.3
6H	17	2235	45.3	54.8	9.5	9.97	105.0
7H	17	2350	54.8	64.3	9.5	10.18	107.2
8H	18	0100	64.3	73.8	9.5	9.33	98.2
9H	18	0145	73.8	83.3	9.5	9.23	97.2
10H	18	0500	83.3	92.8	9.5	10.16	107.0
11H	18	0600	92.8	102.3	9.5	9.84	103.6
12H	18	0845	102.3	111.8	9.5	9.81	103.3
13X	18	0945	111.8	118.5	6.7	4.20	62.7
14X	18	1025	118.5	128.1	9.6	7.36	76.7
15X	18	1110	128.1	137.7	9.6	4.84	50.4
16X	18	1205	137.7	147.3	9.6	7.21	75.1
17X	18	1255	147.3	156.9	9.6	7.06	73.5
18X	18	1340	156.9	166.5	9.6	8.03	83.7
19X	18	1425	166.5	176.1	9.6	8.78	91.5
20X	18	1510	176.1	185.7	9.6	8.15	84.9
21X	18	1600	185.7	195.4	9.7	8.97	92.5
22X	18	1645	195.4	205.0	9.6	9.76	101.7
23X	18	1740	205.0	214.6	9.6	9.74	101.5

Table T1 (continued).

Core	Date (March 2000)	Local Time	Depth (mbsf) Top	Depth (mbsf) Bottom	Length (m) Cored	Length (m) Recovered	Recovery (%)
24X	18	1820	214.6	224.2	9.6	9.71	101.2
25X	18	1915	224.2	233.8	9.6	8.97	93.4
26X	18	2005	233.8	243.4	9.6	9.77	101.8
27X	18	2100	243.4	253.0	9.6	9.92	103.3
28X	18	2200	253.0	262.6	9.6	7.33	76.4
29X	18	2245	262.6	272.2	9.6	9.78	101.9
30X	18	2335	272.2	281.8	9.6	9.33	97.2
31X	19	0030	281.8	291.4	9.6	9.84	102.5
32X	19	0125	291.4	300.7	9.3	9.63	103.6
33X	19	0220	300.7	310.0	9.3	9.32	100.2
34X	19	0315	310.0	319.6	9.6	9.90	103.1
35X	19	0355	319.6	329.2	9.6	9.27	96.6
36X	19	0500	329.2	338.8	9.6	9.87	102.8
37X	19	0545	338.8	348.4	9.6	9.84	102.5
38X	19	0630	348.4	358.0	9.6	9.52	99.2
39X	19	0720	358.0	367.6	9.6	9.53	99.3
40X	19	0810	367.6	377.3	9.7	8.99	92.7
41X	19	0915	377.3	386.9	9.6	9.82	102.3
42X	19	1005	386.9	396.5	9.6	9.76	101.7
43X	19	1050	396.5	406.1	9.6	9.56	99.6
44X	19	1200	406.1	415.7	9.6	9.42	98.1
45X	19	1250	415.7	425.3	9.6	9.85	102.6
46X	19	1350	425.3	434.9	9.6	9.85	102.6
47X	19	1530	434.9	444.5	9.6	9.37	97.6
48X	19	1700	444.5	454.1	9.6	9.74	101.5
49X	19	1815	454.1	463.7	9.6	9.64	100.4
50X	19	1935	463.7	473.3	9.6	9.05	94.3
51X	19	2100	473.3	482.9	9.6	9.91	103.2
52X	19	2305	482.9	492.5	9.6	9.21	95.9
53X	20	0045	492.5	502.1	9.6	9.01	93.9
54X	20	0205	502.1	511.7	9.6	9.69	100.9
55X	20	0325	511.7	521.4	9.7	9.50	97.9
56X	20	0455	521.4	531.1	9.7	8.20	84.5
57X	20	0625	531.1	540.7	9.6	9.46	98.5
58X	20	0805	540.7	550.4	9.7	9.94	102.5
59X	20	0940	550.4	560.0	9.6	9.97	103.9
60X	20	1145	560.0	569.6	9.6	9.19	95.7
61X	20	1310	569.6	579.2	9.6	8.76	91.3
62X	20	1445	579.2	588.8	9.6	8.07	84.1
63X	20	1615	588.8	598.4	9.6	8.55	89.1
64X	20	1755	598.4	608.0	9.6	10.02	104.4
65X	20	1920	608.0	617.6	9.6	8.58	89.4
66X	20	2100	617.6	627.2	9.6	7.94	82.7
67X	20	2230	627.2	636.8	9.6	6.96	72.5
68X	21	0005	636.8	646.4	9.6	9.19	95.7
69X	21	0135	646.4	656.1	9.7	8.59	88.6
70X	21	0305	656.1	665.8	9.7	5.45	56.2
71X	21	0425	665.8	675.4	9.6	8.18	85.2
72X	21	0600	675.4	685.0	9.6	6.61	68.9
73X	21	0730	685.0	694.7	9.7	6.67	68.8
74X	21	0850	694.7	704.3	9.6	7.69	80.1
75X	21	1020	704.3	713.9	9.6	9.74	102.5
76X	21	1210	713.9	723.6	9.7	8.99	92.7
77X	21	1345	723.6	733.2	9.6	9.86	102.7
78X	21	1505	733.2	742.8	9.6	10.03	104.5
79X	21	1645	742.8	752.4	9.6	9.78	101.9
80X	21	1835	752.4	762.0	9.6	9.64	100.4
81X	21	2000	762.0	771.6	9.6	9.87	102.8
82X	21	2135	771.6	781.2	9.6	9.45	98.4
83X	21	2300	781.2	790.8	9.6	9.73	101.4
84X	22	0035	790.8	800.4	9.6	8.77	91.4
85X	22	0215	800.4	809.9	9.5	8.71	91.7
86X	22	0355	809.9	819.5	9.6	8.48	88.3
87X	22	0530	819.5	829.1	9.6	8.91	92.8
88X	22	0715	829.1	838.7	9.6	8.65	90.1
89X	22	0850	838.7	848.3	9.6	9.11	94.9
90X	22	1105	848.3	855.4	7.1	2.03	28.6
91X	22	1340	855.4	861.4	6.0	8.02	133.7

Table T1 (continued).

Core	Date (March 2000)	Local Time	Depth (mbsf) Top	Depth (mbsf) Bottom	Length (m) Cored	Length (m) Recovered	Recovery (%)
92X	22	1615	861.4	867.5	6.1	9.73	162.0
93X	22	2000	867.5	873.5	6.0	8.55	142.5
94X	22	2235	873.5	877.5	4.0	4.70	117.5
95X	23	0210	877.5	883.5	6.0	2.95	49.2
				Totals:	883.5	836.85	94.7
189-1168B-							
1H	25	0125	0.0	3.9	3.9	3.94	101.0
2H	25	0225	3.9	13.4	9.5	9.00	94.7
3H	25	0315	13.4	22.9	9.5	10.09	106.2
4H	25	0405	22.9	32.4	9.5	9.36	98.5
5H	25	0455	32.4	41.9	9.5	9.78	103.0
6H	25	0540	41.9	51.4	9.5	9.71	102.2
7H	25	0635	51.4	60.9	9.5	9.97	105.0
8H	25	0725	60.9	70.4	9.5	9.06	95.4
9H	25	0830	70.4	79.9	9.5	8.55	90.0
10H	25	0920	79.9	89.4	9.5	8.14	85.7
11H	25	1030	89.4	98.9	9.5	9.36	98.5
12H	25	1125	98.9	108.4	9.5	9.56	100.6
				Totals:	108.4	106.52	98.3
189-1168C-							
1H	25	1400	0.0	9.5	9.5	9.99	105.2
2H	25	1445	9.5	19.0	9.5	9.85	103.7
3H	25	1535	19.0	28.5	9.5	9.45	99.5
4H	25	1630	28.5	38.0	9.5	10.00	105.3
5H	25	1710	38.0	47.5	9.5	9.62	101.3
6H	25	1805	47.5	57.0	9.5	8.79	92.5
7H	25	1850	57.0	66.5	9.5	6.07	63.9
8H	25	1935	66.5	76.0	9.5	8.25	86.8
9H	25	2025	76.0	85.5	9.5	9.96	104.8
10H	25	2120	85.5	95.0	9.5	9.20	96.8
11H	25	2205	95.0	104.5	9.5	7.75	81.6
12H	25	2255	104.5	114.0	9.5	9.96	104.8
13X	26	0005	114.0	117.7	3.7	3.49	94.3
14X	26	0040	117.7	127.3	9.6	7.22	75.2
15X	26	0115	127.3	136.9	9.6	6.29	65.5
16X	26	0150	136.9	146.5	9.6	3.67	38.2
17X	26	0300	146.5	156.1	9.6	2.74	28.5
18X	26	0415	156.1	165.7	9.6	6.12	63.8
19X	26	0530	165.7	175.3	9.6	7.72	80.4
20X	26	0615	175.3	185.0	9.7	6.22	64.1
21X	26	0720	185.0	194.7	9.7	6.48	66.8
22X	26	0800	194.7	204.3	9.6	9.02	94.0
23X	26	0840	204.3	213.9	9.6	9.65	100.5
24X	26	0920	213.9	223.5	9.6	6.81	70.9
25X	26	1000	223.5	233.2	9.7	7.97	82.2
26X	26	1045	233.2	242.5	9.3	7.69	82.7
27X	26	1135	242.5	252.1	9.6	9.72	101.3
28X	26	1230	252.1	261.7	9.6	9.85	102.6
29X	26	1325	261.7	271.3	9.6	9.98	104.0
30X	26	1410	271.3	280.9	9.6	9.56	99.6
31X	26	1510	280.9	290.5	9.6	9.06	94.4
				Totals:	290.5	248.15	85.4

Table T2. Identification and abundances of nannofossils, Site 1168. (**See table notes.** Continued on next seven pages.)

Core, section, interval (cm)	Depth (mbsf)	Preservation	Group abundance	*Amaurolithus delicatus*	*Amaurolithus minae*	*Amaurolithus primus*	*Blackites spinosus*	*Braarudosphaera bigelowii*	*Calcidiscus leptoporus*	*Calcidiscus macintyrei*	*Calcidiscus premacintyrei*	*Catinaster coalitus*	*Ceratolithus acutus*	*Chiasmolithus altus*	*Chiasmolithus medius*	*Chiasmolithus oamaruensis*	*Chiasmolithus* spp.	*Clausicoccus subdistichus*	*Coccolithus formosus*	*Coccolithus miopelagicus*	*Coccolithus pelagicus*	*Coronocyclus nitescens*	*Cyclicargolithus abisectus*	*Cyclicargolithus floridanus*	*Discoaster asymmetricus*	*Discoaster bellus*	*Discoaster blackstockae*	*Discoaster brouweri*	*Discoaster calcaris*	*Discoaster challengeri*	*Discoaster deflandrei*	*Discoaster druggii*	*Discoaster formosus*	*Discoaster germanicus*	*Discoaster intercalaris*	*Discoaster loeblichii*	*Discoaster menardiformis*	*Discoaster pentaradiatus*	*Discoaster saipanensis*	*Discoaster* spp.	*Discoaster subsurculus*	*Discoaster surculus*	*Discoaster tamalis*	*Discoaster tanii*	*Discoaster tridiatus*	*Discoaster variabilis*	*Gephyrocapsa caribbeanica*	*Gephyrocapsa* spp. (small)
189-1168A-																																														
1H-CC, 22-24	7.24	G	A																																											C
2H-CC, 9-11	17.00	G	A							F																																				
3H-CC, 29-32	26.71	G	A																																							R				
4H-CC, 0-5	35.75	G	A																																							R				
5H-CC, 38-41	45.96	G	A																						R																					
6H-CC, 26-29	55.24	G	A																																											
7H-CC, 24-29	64.93	G	A	F						A																																				
8H-CC, 8-13	73.58	G	A							A			R												F																		R				
9H-CC, 27-32	82.98	G	A	R						A			C																																C		
10H-CC, 30-35	93.41	G	A	F						A																										C								A		
11H-CC, 18-23	102.59	G	A	C																							F								C								A		
12H-CC, 35-40	112.06	G	A			F				C																			F							C		C					C		
13X-CC, 15-20	115.95	G	A			F																												C	C	F						F			
14X-CC, 25-30	125.81	G	A							A											A															C								A		
15X-CC, 12-17	132.89	G	A																																											
16X-CC, 15-20	144.86	G	A																																											
17X-CC, 17-22	154.31	G	A								C																																			
18X-CC, 29-34	164.88	G	A								C																																			
19X-CC, 16-21	175.23	G	A							C																																				
20X-CC, 25-30	184.20	G	A																																											
21X-CC, 17-22	194.62	G	A																																											
22X-CC, 29-34	205.11	G	A																						F																					
23X-CC, 22-27	214.69	G	A																						F																					
24X-CC, 21-25	224.27	G	A								R														F																					
25X-CC, 21-26	233.12	G	A								R														F																					
26X-CC, 26-30	243.53	G	A								F														C																					
27X-CC, 39-43	253.28	G	A								F														C																					
28X-CC, 44-48	260.29	G	A								R														C																					
29X-CC, 32-36	272.34	G	A								F														C																				A		
30X-CC, 6-11	281.48	G	A																						A						A													A		
31X-CC, 30-35	291.59	G	A																						A						A													A		
32X-CC, 0-5	300.58	G	A																				F		C					F	C															
33X-CC, 32-37	309.97	G	A																						C					R	C															
34X-CC, 0-5	319.45	G	A																						A								F													
35X-CC, 39-44	328.82	G	A																						A						A															
36X-CC, 35-40	339.02	G	A																						A						C															
37X-CC, 29-34	348.59	G	A																		F				A																					
38X-CC, 50-55	357.87	G	A																		A				C						F															
39X-CC, 29-34	367.48	G	A																		C				A					R	A															

Table T2 (continued).

Core, section, interval (cm)	Depth (mbsf)	Preservation	Group abundance	*Helicosphaera ampliaperta*	*Helicosphaera bramlettei*	*Helicosphaera intermedia*	*Helicosphaera neogranulata*	*Helicosphaera pavimentum*	*Helicosphaera recta*	*Helicosphaera sellii*	*Helicosphaera wallichii*	*Isthmolithus recurvus*	*Lanternithus minutus*	*Micrantholithus flos*	*Pontosphaera* spp.	*Pseudoemiliania lacunosa*	*Reticulofenestra bisecta*	*Reticulofenestra coenura*	*Reticulofenestra daviesii*	*Reticulofenestra haqii*	*Reticulofenestra pseudoumbilica*	*Reticulofenestra reticulata*	*Reticulofenestra samodurovii*	*Reticulofenestra* spp.	*Reticulofenestra umbilicus*	*Rhabdosphaera tenuis*	*Sphenolithus belemnos*	*Sphenolithus calyculus*	*Sphenolithus capricornutus*	*Sphenolithus conicus*	*Sphenolithus dissimilis*	*Sphenolithus distentus*	*Sphenolithus heteromorphus*	*Sphenolithus moriformis*	*Sphenolithus predistentus*	*Triquetrorhabdulus carinatus*	*Triquetrorhabdulus rugosus*	*Triquetrorhabdulus serratus*	*Zygrhablithus bijugatus*
189-1168A-																																							
1H-CC, 22-24	7.24	G	A													F																							
2H-CC, 9-11	17.00	G	A							F																													
3H-CC, 29-32	26.71	G	A																																				
4H-CC, 0-5	35.75	G	A																																				
5H-CC, 38-41	45.96	G	A													R																							
6H-CC, 26-29	55.24	G	A																		A																		
7H-CC, 24-29	64.93	G	A							F						A																							
8H-CC, 8-13	73.58	G	A							C											C																		
9H-CC, 27-32	82.98	G	A							F											A																		
10H-CC, 30-35	93.41	G	A							C											A																		
11H-CC, 18-23	102.59	G	A							C											A																		
12H-CC, 35-40	112.06	G	A																		A																		
13X-CC, 15-20	115.95	G	A																		A																		
14X-CC, 25-30	125.81	G	A							F											A																		
15X-CC, 12-17	132.89	G	A																																		F		
16X-CC, 15-20	144.86	G	A																																		F		
17X-CC, 17-22	154.31	G	A																		A																R		
18X-CC, 29-34	164.88	G	A																		A																R		
19X-CC, 16-21	175.23	G	A																		A																R		
20X-CC, 25-30	184.20	G	A																		A																R		
21X-CC, 17-22	194.62	G	A																		A																		
22X-CC, 29-34	205.11	G	A																																				
23X-CC, 22-27	214.69	G	A																																				
24X-CC, 21-25	224.27	G	A																		A																		
25X-CC, 21-26	233.12	G	A																		A																		
26X-CC, 26-30	243.53	G	A																														R						
27X-CC, 39-43	253.28	G	A																														R						
28X-CC, 44-48	260.29	G	A																														R						
29X-CC, 32-36	272.34	G	A																														R	C					
30X-CC, 6-11	281.48	G	A																														C	C					
31X-CC, 30-35	291.59	G	A																														C	C					
32X-CC, 0-5	300.58	G	A	F																							R							C					
33X-CC, 32-37	309.97	G	A			R									R												F							C					
34X-CC, 0-5	319.45	G	A																																				
35X-CC, 39-44	328.82	G	A	R																														R					
36X-CC, 35-40	339.02	G	A			R																												C					
37X-CC, 29-34	348.59	G	A												R															R				R					
38X-CC, 50-55	357.87	G	A																															A					
39X-CC, 29-34	367.48	G	A	R											R																			C					

Table T2 (continued).

Core, section, interval (cm)	Depth (mbsf)	Preservation	Group abundance	*Amaurolithus delicatus*	*Amaurolithus ninae*	*Amaurolithus primus*	*Blackites spinosus*	*Braarudosphaera bigelowii*	*Calcidiscus leptoporus*	*Calcidiscus macintyrei*	*Calcidiscus premacintyrei*	*Catinaster altus*	*Ceratolithus acutus*	*Chiasmolithus altus*	*Chiasmolithus modestus*	*Chiasmolithus oamaruensis*	*Chiasmolithus* spp.	*Clausicoccus subdistichus*	*Coccolithus formosus*	*Coccolithus miopelagicus*	*Coccolithus pelagicus*	*Coronocyclus nitescens*	*Cyclicargolithus abisectus*	*Cyclicargolithus floridanus*	*Discoaster asymmetricus*	*Discoaster bellus*	*Discoaster blackstockae*	*Discoaster brouweri*	*Discoaster calculosus*	*Discoaster challengeri*	*Discoaster deflandrei*	*Discoaster druggii*	*Discoaster formosus*	*Discoaster germanicus*	*Discoaster intercalaris*	*Discoaster loeblichii*	*Discoaster mendomobensis*	*Discoaster pentaradiatus*	*Discoaster saipanensis*	*Discoaster* spp.	*Discoaster subsurculus*	*Discoaster surculus*	*Discoaster tamalis*	*Discoaster tanii*	*Discoaster triradiatus*	*Discoaster variabilis*	*Gephyrocapsa caribbeanica*	*Gephyrocapsa* spp. (small)
40X-CC, 46-51	376.54	G	A																	A		F	C	A					R		F														
41X-CC, 50-55	387.07	G	A																				A	A							C														
42X-CC, 32-37	396.61	G	A																	F			F	A							C														
43X-CC, 34-39	406.01	G	A																	F			C								C														
44X-CC, 32-37	415.47	G	A																				C	A																						
45X-CC, 37-42	425.50	G	A					R														A	C	A																						
46X-CC, 37-42	435.10	G	A																				C	A																						
47X-CC, 38-43	444.22	G	A					R															C	A																						
48X-CC, 35-40	454.19	M	A																																											
49X-CC, 41-46	463.69	M	A																				R	A																						
50X-CC, 43-48	472.70	M	A																					A																						
51X-CC, 35-40	483.16	M	A																					A																						
52X-CC, 33-38	492.06	M	A																					A																						
53X-CC, 34-39	501.46	G	A																					C																						
54X-CC, 30-35	511.74	G	A																			F	C	C																						
55X-CC, 31-36	521.15	G	A					C						A								C		A																						
56X-CC, 31-36	529.55	G	A					C						C								C	C	A							C														
57X-CC, 28-33	540.51	G	A											C								F		A							F														
58X-CC, 45-50	550.59	G	A					F						F								C		C							F														
59X-CC, 39-44	560.32	G	A					C						A								C	A								F														
60X-CC, 41-46	569.14	G	A					F						F									C	A																						
61X-CC, 33-38	578.31	M	A											C									C	A																						
62X-CC, 32-37	587.22	M	A											C									C	A																						
63X-CC, 30-35	597.30	M	A											A									C	A																						
64X-CC, 45-50	608.37	M	A											A									C	A																						
65X-CC, 27-32	616.53	G	A											A									F	C																						
66X-CC, 34-39	625.49	G	A											A									A	C																						
67X-CC, 25-30	634.11	M	A											A									C	F																						
68X-CC, 40-45	645.94	G	A											F								C	A	A																						
69X-CC, 32-37	654.94	G	A			F								A								C	C	A	A																						
70X-CC, 36-41	661.50	G	A											A								C	A	A							R														
71X-CC, 36-41	673.93	G	C											A								C	A																						
72X-CC, 35-40	681.96	G	A											A								C	F	A	A						F														
73X-CC, 34-39	691.62	G	A					R						A								C	F	A	A																						
74X-CC, 32-37	702.34	G	A											A								A		A																						
75X-CC, 27-32	714.09	G	C											C								C		A																						
76X-CC, 48-53	722.84	G	A											A										A																						
77X-CC, 34-39	733.41	M	A											A										A																						
78X-CC, 43-48	743.28	M	A											A						C																										
79X-CC, 34-39	752.53	M	A											C			R																													

Table T2 (continued).

Core, section, interval (cm)	Depth (mbsf)	Preservation	Group abundance	*Helicosphaera ampliaperta*	*Helicosphaera bramlettei*	*Helicosphaera intermedia*	*Helicosphaera neogranulata*	*Helicosphaera pavimentum*	*Helicosphaera recta*	*Helicosphaera sellii*	*Helicosphaera wallichii*	*Isthmolithus recurvus*	*Lanternithus minutus*	*Micrantholithus flos*	*Pontosphaera* spp.	*Pseudoemiliania lacunosa*	*Reticulofenestra bisecta*	*Reticulofenestra coenura*	*Reticulofenestra daviesii*	*Reticulofenestra haqii*	*Reticulofenestra psuedoumbilica*	*Reticulofenestra reticulata*	*Reticulofenestra samodurovii*	*Reticulofenestra* spp.	*Reticulofenestra umbilicus*	*Rhabdosphaera tenuis*	*Sphenolithus belemnos*	*Sphenolithus calyculus*	*Sphenolithus capricornutus*	*Sphenolithus conicus*	*Sphenolithus dissimilis*	*Sphenolithus distentus*	*Sphenolithus heteromorphus*	*Sphenolithus moriformis*	*Sphenolithus predistentus*	*Triquetrorhabdulus carinatus*	*Triquetrorhabdulus rugosus*	*Triquetrorhabdulus serratus*	*Zygrhablithus bijugatus*
40X-CC, 46-51	376.54	G	A																														C					R
41X-CC, 50-55	387.07	G	A			F									F													R					C					
42X-CC, 32-37	396.61	G	A			R									F																		C					
43X-CC, 34-39	406.01	G	A			F									F																		C					
44X-CC, 32-37	415.47	G	A																																			
45X-CC, 37-42	425.50	G	A																														R					R
46X-CC, 37-42	435.10	G	A																																			
47X-CC, 38-43	444.22	G	A														R		R																			
48X-CC, 35-40	454.19	M	A														F		R				F															
49X-CC, 41-46	463.69	M	A														F																					
50X-CC, 43-48	472.70	M	A														F																					R
51X-CC, 35-40	483.16	M	A														F																					F
52X-CC, 33-38	492.06	M	A														C		C																			
53X-CC, 34-39	501.46	G	A			F									R		C		F												R			F				C
54X-CC, 30-35	511.74	G	A		F	C											A												R		C			C				R
55X-CC, 31-36	521.15	G	A														C																	C				A
56X-CC, 31-36	529.55	G	A														A																	C				C
57X-CC, 28-33	540.51	G	A		C												A		C																			A
58X-CC, 45-50	550.59	G	A														A		C															F				
59X-CC, 39-44	560.32	G	A												F		C																	F				A
60X-CC, 41-46	569.14	G	A														C																					
61X-CC, 33-38	578.31	M	A														C		C																			
62X-CC, 32-37	587.22	M	A														C		C																			
63X-CC, 30-35	597.30	M	A														A																					
64X-CC, 45-50	608.37	M	A														A		A																			
65X-CC, 27-32	616.53	G	A														A		C																			C
66X-CC, 34-39	625.49	G	A														A																					
67X-CC, 25-30	634.11	M	A														A																					F
68X-CC, 40-45	645.94	G	A		F	C											C																	F				
69X-CC, 32-37	654.94	G	A		F	C											C																	C				C
70X-CC, 36-41	661.50	G	A														A							F								R		F				
71X-CC, 36-41	673.93	G	C												F		A							F								R		C	R			A
72X-CC, 35-40	681.96	G	A												F									C								C		C		F		A
73X-CC, 34-39	691.62	G	A						F						F		A							C										F				F
74X-CC, 32-37	702.34	G	A						R						F		A							C														
75X-CC, 27-32	714.09	G	C											C	F		C							F		F								C				C
76X-CC, 48-53	722.84	G	A														A		A																			C
77X-CC, 34-39	733.41	M	A														C		A																			
78X-CC, 43-48	743.28	M	A									R					C								C													
79X-CC, 34-39	752.53	M	A									C					C								C													

Table T2 (continued).

Core, section, interval (cm)	Depth (mbsf)	Preservation	Group abundance	*Amaurolithus delicatus*	*Amaurolithus ninae*	*Amaurolithus primus*	*Blackites spinosus*	*Braarudosphaera bigelowii*	*Calcidiscus leptoporus*	*Calcidiscus macintyrei*	*Calcidiscus premacintyrei*	*Catinaster altus*	*Ceratolithus acutus*	*Chiasmolithus altus*	*Chiasmolithus modestus*	*Chiasmolithus oamaruensis*	*Chiasmolithus* spp.	*Clausicoccus subdistichus*	*Coccolithus formosus*	*Coccolithus miopelagicus*	*Coccolithus pelagicus*	*Coronocyclus nitescens*	*Cyclicargolithus abisectus*	*Cyclicargolithus floridanus*	*Discoaster asymmetricus*	*Discoaster bellus*	*Discoaster blackstockae*	*Discoaster brouweri*	*Discoaster calculosus*	*Discoaster challengeri*	*Discoaster deflandrei*	*Discoaster druggii*	*Discoaster formosus*	*Discoaster germanicus*	*Discoaster intercalaris*	*Discoaster loeblichii*	*Discoaster mendomobensis*	*Discoaster pentaradiatus*	*Discoaster saipanensis*	*Discoaster* spp.	*Discoaster subsurculus*	*Discoaster surculus*	*Discoaster tamalis*	*Discoaster tanii*	*Discoaster triradiatus*	*Discoaster variabilis*	*Gephyrocapsa caribbeanica*	*Gephyrocapsa* spp. (small)
80X-CC, 34-39	761.99	M	A											C																																
81X-CC, 24-29	771.82	P	R																																												
82X-CC, 33-38	781.00	M	A					R						C		R																															
83X-CC, 35-41	790.87	P	C				F	R						C							F																									
84X-CC, 31-36	799.52	M	C																C		C																	R								
85X-CC, 25-31	808.97	M	C					F													C																									
86X-CC, 37-42	818.33	G	C				R	F								R	F		F		C																	R								
87X-CC, 22-27	828.36	M	F														R		F		F																									
88X-CC, 33-40	837.68	M	C					R							R	R		C	F		C			F										R				F			R				
89X-CC, 37-42	847.76	M	F														F				F			F																					
90X-CC, 28-33	850.28		B																																											
91X-CC, 30-35	863.37		B																																											
92X-CC, 33-38	871.38		B																																											
93X-CC, 28-35	875.98		B																																											
94X-CC, 33-39	878.14		B																																											
95X-CC, 24-29	880.40		B																																											
189-1168B-																																															
1H-CC, 21-26	3.89	G	A							C											A																								F	A
2H-CC, 11-16	12.85	G	A							A											A																									
3H-CC, 28-33	23.44	G	A							A											A							C														R				
4H-CC, 15-20	32.21	G	A							A											A							F																	
5H-CC, 11-16	42.13	M	A							A											A							C														R				
6H-CC, 8-13	51.51	M	A							A											A							F													F				
7H-CC, 8-13	61.32	G	A	R						A											A							F										F							
8H-CC, 15-20	69.91	G	A							A											A																	C				R			
9H-CC, 0-5	78.9	M	A							A											A				F															A		R			
10H-CC, 12-17	87.99	M	A							A											A																									
11H-CC, 12-17	98.71	G	A																																											
12H-CC, 7-12	108.41	G	A			R				F			F																											F					
189-1168C-																																														
1H-CC, 12-17	9.94	G	A																																											
2H-CC, 25-30	19.3	G	A								C																																			
3H-CC, 19-24	28.4	G	A																																									R			
4H-CC, 16-21	38.45	G	A																																									R			
5H-CC, 20-25	47.57	G	A							A	C																																	R			
6H-CC, 22-25	56.26	G	A		R					A	C																																	R			
7H-CC, 13-17	63.03	G	A							A	C																																	R			
8H-CC, 0-5	74.7	M	A							A	C																																				
9H-CC, 25-30	85.91	M	A							A	C																																				

Table T2 (continued).

Core, section, interval (cm)	Depth (mbsf)	Preservation	Group abundance	*Helicosphaera ampliaperta*	*Helicosphaera bramlettei*	*Helicosphaera intermedia*	*Helicosphaera neogranulata*	*Helicosphaera pavimentum*	*Helicosphaera recta*	*Helicosphaera sellii*	*Helicosphaera wallichii*	*Isthmolithus recurvus*	*Lanternithus minutus*	*Micrantholithus flos*	*Pontosphaera* spp.	*Pseudoemiliania lacunosa*	*Reticulofenestra bisecta*	*Reticulofenestra coenura*	*Reticulofenestra daviesii*	*Reticulofenestra haqii*	*Reticulofenestra psuedoumbilica*	*Reticulofenestra reticulata*	*Reticulofenestra samodurovii*	*Reticulofenestra* spp.	*Reticulofenestra umbilicus*	*Rhabdosphaera tenuis*	*Sphenolithus belemnos*	*Sphenolithus calyculus*	*Sphenolithus capricornutus*	*Sphenolithus conicus*	*Sphenolithus dissimilis*	*Sphenolithus distentus*	*Sphenolithus heteromorphus*	*Sphenolithus moriformis*	*Sphenolithus predistentus*	*Triquetrorhabdulus carinatus*	*Triquetrorhabdulus rugosus*	*Triquetrorhabdulus serratus*	*Zygrhablithus bijugatus*
80X-CC, 34-39	761.99	M	A									R					C		C																		F
81X-CC, 24-29	771.82	P	R																	R																	
82X-CC, 33-38	781.00	M	A									F					C								C											F
83X-CC, 35-41	790.87	P	C														C					R			F											F
84X-CC, 31-36	799.52	M	C									F			F		C																			
85X-CC, 25-31	808.97	M	C									F	F				C	F							F											
86X-CC, 37-42	818.33	G	C										F											F	F											F
87X-CC, 22-27	828.36	M	F														F	F					F													R
88X-CC, 33-40	837.68	M	C										F				A					C			C	R										F
89X-CC, 37-42	847.76	M	F			F									F		F	F															F			
90X-CC, 28-33	850.28		B																																	
91X-CC, 30-35	863.37		B																																	
92X-CC, 33-38	871.38		B																																	
93X-CC, 28-35	875.98		B																																	
94X-CC, 33-39	878.14		B																																	
95X-CC, 24-29	880.40		B																																	
189-1168B-																																				
1H-CC, 21-26	3.89	G	A				F			C																										
2H-CC, 11-16	12.85	G	A							F						C																				
3H-CC, 28-33	23.44	G	A							C																										
4H-CC, 15-20	32.21	G	A																																	
5H-CC, 11-16	42.13	M	A							F																										
6H-CC, 8-13	51.51	M	A							F																										
7H-CC, 8-13	61.32	G	A																																	
8H-CC, 15-20	69.91	G	A							F											C															
9H-CC, 0-5	78.9	M	A							C						C					A															
10H-CC, 12-17	87.99	M	A							F																										
11H-CC, 12-17	98.71	G	A																																	
12H-CC, 7-12	108.41	G	A																																	
189-1168C-																																				
1H-CC, 12-17	9.94	G	A																																	
2H-CC, 25-30	19.3	G	A								R																									
3H-CC, 19-24	28.4	G	A																																	
4H-CC, 16-21	38.45	G	A																																	
5H-CC, 20-25	47.57	G	A																			C														
6H-CC, 22-25	56.26	G	A																			C														
7H-CC, 13-17	63.03	G	A																			C														
8H-CC, 0-5	74.7	M	A								F											C														
9H-CC, 25-30	85.91	M	A								F											C														

Table T2 (continued).

Core, section, interval (cm)	Depth (mbsf)	Preservation	Group abundance	*Amaurolithus delicatus*	*Amaurolithus ninae*	*Amaurolithus primus*	*Blackites spinosus*	*Braarudosphaera bigelowii*	*Calcidiscus leptoporus*	*Calcidiscus macintyrei*	*Calcidiscus premacintyrei*	*Catinaster altus*	*Ceratolithus acutus*	*Chiasmolithus altus*	*Chiasmolithus modestus*	*Chiasmolithus oamaruensis*	*Chiasmolithus* spp.	*Clausicoccus subdistichus*	*Coccolithus formosus*	*Coccolithus miopelagicus*	*Coccolithus pelagicus*	*Coronocyclus nitescens*	*Cyclicargolithus abisectus*	*Cyclicargolithus floridanus*	*Discoaster asymmetricus*	*Discoaster bellus*	*Discoaster blackstockae*	*Discoaster brouweri*	*Discoaster calculosus*	*Discoaster challengeri*	*Discoaster deflandrei*	*Discoaster druggii*	*Discoaster formosus*	*Discoaster germanicus*	*Discoaster intercalaris*	*Discoaster loeblichii*	*Discoaster mendomobensis*	*Discoaster pentaradiatus*	*Discoaster saipanensis*	*Discoaster* spp.	*Discoaster subsurculus*	*Discoaster surculus*	*Discoaster tamalis*	*Discoaster tanii*	*Discoaster triradiatus*	*Discoaster variabilis*	*Gephyrocapsa caribbeanica*	*Gephyrocapsa* spp. (small)
10H-CC, 47-52		G	A																																			F	R					
11H-CC, 0-5	102.7	G	A		R																																	F	F					
12H-CC, 24-29	114.41	G	A																																	F		C						
13X-CC, 13-18	117.44	G	A																			A								F						F				R			
14X-CC, 15-21	124.86	M	A								A											A						R								F							
15X-CC, 13-18	133.54	M	A																			A														R							
16X-CC, 21-26	140.52	M	A								C											A						R															
17X-CC, 13-18	149.19	M	A								C											A						R															
18X-CC, 12-17	162.17	M	A								C											A								F													
19X-CC, 13-18	173.37	M	A								C										C																						
20X-CC, 15-20	181.47	M	A								F										C	F																					
21X-CC, 21-26	191.43	M	A								F										A	F	R																				
22X-CC, 13-18	203.67	M	A								F											C				R																	
23X-CC, 21-27	213.89	M	A																			A				F																	
24X-CC, 21-26	220.66	M	A								C											C																					
25X-CC, 25-30	231.42	M	A																		C	A				F																	
26X-CC, 13-18	240.84	M	A																			C																					
27X-CC, 17-22	252.17	M	A										F																														
28X-CC, 32-37	261.9	M	A										F																														
29X-CC, 40-45	271.63	M	A										C																														
30X-CC, 32-37	280.81	M	A								C																													C				
31X-CC, 0-5	289.91	M	A																			C									A												

Notes: Preservation: G = good, M = moderate, P = poor. Abundance: A = abundant, C = common, F = few, R = rare.

Table T2 (continued).

Core, section, interval (cm)	Depth (mbsf)	Preservation	Group abundance	*Helicosphaera ampliaperta*	*Helicosphaera bramlettei*	*Helicosphaera intermedia*	*Helicosphaera neogranulata*	*Helicosphaera pavimentum*	*Helicosphaera recta*	*Helicosphaera sellii*	*Helicosphaera wallichii*	*Isthmolithus recurvus*	*Lanternithus minutus*	*Micrantholithus flos*	*Pontosphaera* spp.	*Pseudoemiliania lacunosa*	*Reticulofenestra bisecta*	*Reticulofenestra coenura*	*Reticulofenestra daviesii*	*Reticulofenestra haqii*	*Reticulofenestra psuedoumbilica*	*Reticulofenestra reticulata*	*Reticulofenestra samodurovii*	*Reticulofenestra* spp.	*Reticulofenestra umbilicus*	*Rhabdosphaera tenuis*	*Sphenolithus belemnos*	*Sphenolithus calyculus*	*Sphenolithus capricornutus*	*Sphenolithus conicus*	*Sphenolithus dissimilis*	*Sphenolithus distentus*	*Sphenolithus heteromorphus*	*Sphenolithus moriformis*	*Sphenolithus predistentus*	*Triquetrorhabdulus carinatus*	*Triquetrorhabdulus rugosus*	*Triquetrorhabdulus serratus*	*Zygrhablithus bijugatus*
10H-CC, 47-52		G	A																																			
11H-CC, 0-5	102.7	G	A																																			
12H-CC, 24-29	114.41	G	A																																		F	
13X-CC, 13-18	117.44	G	A																			A																
14X-CC, 15-21	124.86	M	A																																			
15X-CC, 13-18	133.54	M	A																			C													F			
16X-CC, 21-26	140.52	M	A																			C																
17X-CC, 13-18	149.19	M	A																			A																
18X-CC, 12-17	162.17	M	A																			C													F			
19X-CC, 13-18	173.37	M	A																																			
20X-CC, 15-20	181.47	M	A																																			
21X-CC, 21-26	191.43	M	A																																F			
22X-CC, 13-18	203.67	M	A																																C			
23X-CC, 21-27	213.89	M	A																																F			
24X-CC, 21-26	220.66	M	A																																			
25X-CC, 25-30	231.42	M	A							R																												
26X-CC, 13-18	240.84	M	A		R					R																									R			
27X-CC, 17-22	252.17	M	A																															F				
28X-CC, 32-37	261.9	M	A																															R				
29X-CC, 40-45	271.63	M	A																															R				
30X-CC, 32-37	280.81	M	A																															F				
31X-CC, 0-5	289.91	M	A																																F			

Table T3. Calcareous nannofossil datum levels and their assigned age estimates, Site 1168.

Depth (mbsf)		Event	Age (Ma)	Reference
0.64	FO	*Emiliania huxleyi*	0.26	Berggren et al., 1995
8.36	LO	*Pseudoemiliania lacunosa*	0.46	Lourens et al., 1996
12.12	LO	*Calcidiscus macintyrei*	1.67	Lourens et al., 1996
21.86	LO	*Discoaster surculus*	2.55	Berggren et al., 1995
50.60	LO	*Reticulofenestra pseudoumbilica*	3.75	Berggren et al., 1995
60.09	LO	*Amaurolithus delicatus*	4.60	Gartner, 1992
69.39	LO	*Ceratolithus acutus*	5.05	Lourens et al., 1996
88.20	FO	*Ceratolithus acutus*	5.37	Lourens et al., 1996
120.88	FO	*Amaurolithus primus*	7.2	Berggren et al., 1995
199.87	LO	*Cyclicargolithus floridanus*	11.9	Gartner, 1992
238.33	LO	*Sphenolithus heteromorphous*	13.6	Berggren et al., 1995
266.32	FO	*Calcidiscus premacintyrei*	17.4	Gartner, 1992
296.09	FO	*Sphenolithus heteromorphous*	18.2	Berggren et al., 1995
296.09	LO	*Sphenolithus belemnos*	18.3	Berggren et al., 1995
305.28	FO	*Sphenolithus belemnos*	20.6	Berggren et al., 1995
439.66	LO	*Reticulofenestra bisecta*	23.9	Berggren et al., 1995
516.45	LO	*Chiasmolithus altus*	26.1	Berggren et al., 1995
658.22	LO	*Sphenolithus distentus*	27.5	Berggren et al., 1995
733.60	LO	*Reticulofenestra umbilica*	31.2	Berggren et al., 1995
735.74	LO	*Isthmolithus recurvus*	32.3	Berggren et al., 1995
753.44	LO	*Discoaster saipanensis*	34.2	Berggren et al., 1995
878.07	FO	*Isthmolithus recurvus*	36.0	Berggren et al., 1995

Notes: The depth of each datum is assigned at the midpoint between depths of observed samples. FO = first occurrence, LO = last occurrence.

Table T4. Calcareous nannofossil datum levels, Site 1168.

Bioevent	Age (Ma)	Interval (cm)		Depth (mbsf)		Mean (m)	Error bar (m)
		Top	Bottom	Top	Bottom		
FO *Emiliania huxleyi**	0.26	1H-1, 55	1H-1, 72	0.55	0.72	0.64	0.09
LO *Pseudoemiliania lacunosa**	0.46	1H-CC	2H-CC	3.86	12.85	8.36	4.50
LO *Calcidiscus macintyrei*	1.67	1H-CC	2H-CC	7.24	17.00	12.12	4.88
LO *Discoaster surculus*	2.55	2H-CC	3H-CC	17.00	26.71	21.86	4.86
LO *Reticulofenestra pseudoumbilica*	3.75	5H-CC	6H-CC	45.96	55.24	50.60	4.64
LO *Amaurolithus delicatus*	4.60	6H-CC	7H-CC	55.24	64.93	60.09	4.85
LO *Ceratolithus acutus*	5.05	7H-CC	8H-CC	64.93	73.84	69.39	4.46
FO *Ceratolithus acutus*	5.37	9H-CC	10H-CC	82.98	93.41	88.20	5.22
FO *Amaurolithus primus*	7.20	13X-CC	14X-CC	115.95	125.81	120.88	4.93
LO *Cyclicargolithus floridanus*	11.90	21X-CC	22X-CC	194.62	205.11	199.87	5.25
LO *Sphenolithus heteromorphus*	13.60	25X-CC	26X-CC	233.12	243.53	238.33	5.21
FO *Calcidiscus premacintyrei*	17.40	28X-CC	29X-CC	260.29	272.34	266.32	6.02
FO *Sphenolithus heteromorphus*	18.20	31X-CC	32X-CC	291.59	300.58	296.09	4.50
LO *Sphenolithus belemnos*	18.30	31X-CC	32X-CC	291.59	300.58	296.09	4.50
FO *Sphenolithus belemnos*	20.60	32X-CC	33X-CC	300.59	309.97	305.28	4.69
LO *Reticulofenestra bisecta*	23.90	46X-CC	47X-CC	435.10	444.22	439.66	4.56
LO *Chiasmolithus altus*	26.10	54X-CC	55X-CC	511.74	521.15	516.45	4.71
LO *Sphenolithus distentus*	27.50	69X-CC	70X-CC	654.94	661.50	658.22	3.28
LO *Reticulofenestra umbilica*	31.20	77X-CC	78X-1, 38	733.41	733.79	733.60	0.19
LO *Isthmolithus recurvus*	32.30	78X-2, 10	78X-2, 144	735.01	736.47	735.74	0.73
LO *Discoaster saipanensis*	34.20	79X-CC	80-2, 21	752.53	754.34	753.44	0.91
FO *Isthmolithus recurvus*	36.00	94X-3, 137	94X-CC	878.00	878.14	878.07	0.07

Notes: * = samples are from Hole 1168B; all other samples are from Hole 1168A. FO = first occurrence, LO = last occurrence. CC = core catcher.

Table T5. Planktonic foraminifer bioevents and their ages, Site 1168.

Hole	Bioevent	Age (Ma)	Interval Top	Interval Bottom	Depth (mbsf) Top	Depth (mbsf) Bottom	Average depth (mbsf)
1168B							
	FO *G. truncatulinoides*	2.0	1H-CC	2H-CC	3.89	12.85	8.37
1168C							
	FO *G. inflata*	3.2	5H-CC	6H-CC	47.57	56.26	51.92
	LO *G. pliozea*	4.6	6H-CC	7H-CC	56.26	63.03	59.65
	FO *G. puncticulata*	5.3	7H-CC	8H-CC	63.03	74.70	68.87
	FO *G. conomiozea*	6.9	14X-CC	15X-CC	124.86	133.54	129.20
	LO *P. continuosa*	8.0	15X-CC	16X-CC	133.54	140.52	137.03
	LO *N. nympha*	10.1	20X-CC	21X-CC	181.47	191.43	186.45
	LO *P. mayeri*	11.4	21X-CC	22X-CC	191.43	203.67	197.55
	FO *P. mayeri*	12.1	23X-CC	24X-CC	213.89	220.66	217.28
1168A							
	FO *O. suturalis*	15.1	27X-CC	28X-CC	253.28	260.29	256.79
	FO *P. curva*	16.3	28X-CC	29X-CC	260.29	272.34	266.32
	FO *G. trilobus*	18.8	30X-CC	31X-CC	281.48	291.59	286.54
	FO *G. connecta*	20.9	33X-CC	34X-CC	309.97	319.45	314.71
	FO *G. woodi*	22.6	40X-CC	41X-CC	376.54	387.07	381.81
	FO *G. dehiscens*	23.2	42X-CC	43X-CC	396.61	406.01	401.31
	LO *C. cubensis*	28.5	59X-CC	60X-CC	560.32	569.14	564.73
	LO *S. angiporoides*	30.0	74X-CC	75X-CC	691.62	702.34	696.98
	LO *S. brevis*	33.0	76X-CC	77X-CC	722.84	733.41	728.13
	LO *G. index*	34.3	77X-CC	78X-CC	733.41	743.18	738.30
	FO *S. brevis*	34.8	78X-CC	79X-CC	743.28	752.53	747.91

Notes: FO = first occurrence, LO = last occurrence. CC = core catcher.

Table T6. Range chart of planktonic foraminifers, Site 1168. (See table note. Continued on next seven pages.)

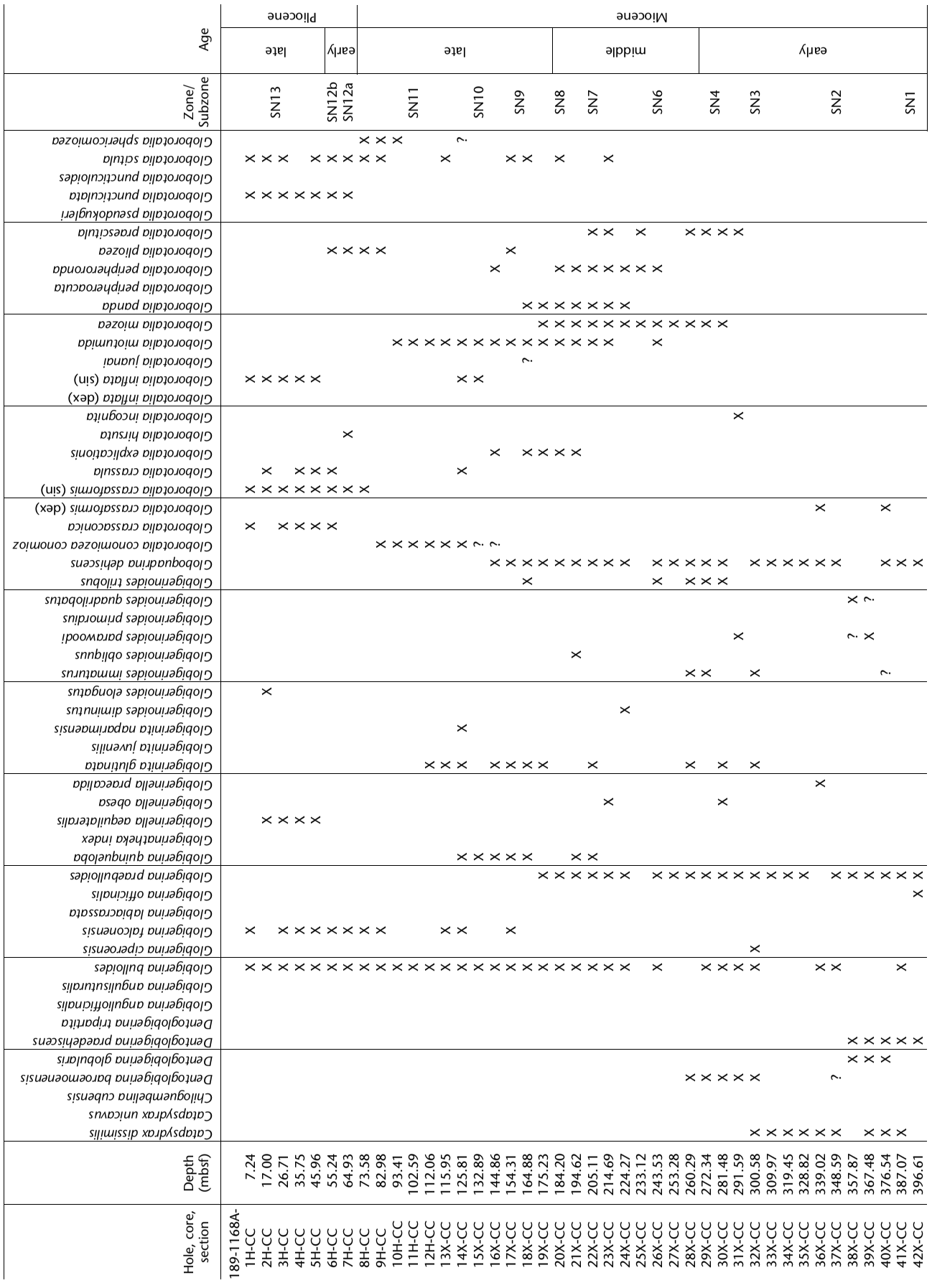

Table T6 (continued).

Hole, core, section	Depth (mbsf)	*Globorotalia tosaensis*	*Globorotalia triangula*	*Globorotalia truncatulinoides*	*Globorotalia ungulata*	*Globorotalia zealandica*	*Globoturborotalita suteri*	*Globoturborotalita testarugosa*	*Globoturborotalita apertura*	*Globoturborotalita brazieri*	*Globoturborotalita connecta*	*Globoturborotalita decoraperta*	*Globoturborotalita druryi*	*Globoturborotalita nepenthes*	*Globoturborotalita woodi*	*Guembelitria triseriata*	*Morozovella formosa formosa*	*Morozovella subbotinae = G. re*	*Neogloboquadrina dutertrei*	*Neogloboquadrina humerosa*	*Neogloboquadrina pachyderma* (sin)	*Orbulina suturalis*	*Orbulina universa*	*Paragloborotalia acrostoma*	*Paragloborotalia continuosa*	*Paragloborotalia mayeri*	*Paragloborotalia nana*	*Paragloborotalia nympha*	*Paragloborotalia opima*	*Paragloborotalia semivera*	*Paragloborotalia siakensis*	*Praeorbulina bispherica*	*Praeorbulina circularis*	*Praeorbulina sicana*	*Praeorbulina transitoria*	*Sphaeroidinellop paenedehiscens*	*Sphaeroidinellopsis seminulina*	*Subbotina angiporoides*	*Subbotina brevis*	*Subbotina eocaena*	*Subbotina linaperta*	*Tenuitella gemma*	*Tenuitella insolita*	*Tenuitella minutissima*	*Tenuitella munda*	*Tenuitellinata angustiumbilicata*	*Turborotalia euapertura*	*Turborotalita humilis*	Zone/ Subzone	Age		
189-1168A-																																																	
1H-CC	7.24																				X		X																											
2H-CC	17.00				X																X		X																											
3H-CC	26.71																						X																											
4H-CC	35.75																				X		X																											
5H-CC	45.96																				X		X																											
6H-CC	55.24																				X		X																											
7H-CC	64.93																						X																											
8H-CC	73.58																				X		X																											
9H-CC	82.98																				X		X																											
10H-CC	93.41																				X		X																											
11H-CC	102.59																				X		X																											
12H-CC	112.06								X												X		X																											
13X-CC	115.95								X												X		X																											
14X-CC	125.81								X												X		X																											
15X-CC	132.89								X												X		X										X														X	SN10			
16X-CC	144.86								X						X						X		X		X																									
17X-CC	154.31								X						X								X		X																										
18X-CC	164.88											X										X	X																									SN9			
19X-CC	175.23													X								X	X		X			X																					
20X-CC	184.20														X							X	X		X			X																			SN8			
21X-CC	194.62												X	?	X							X			X			X																					
22X-CC	205.11														X							X				X																			SN7			
23X-CC	214.69														X							X				X																					
24X-CC	224.27				X																	X																											
25X-CC	233.12																					X																											
26X-CC	243.53														X							X														X										SN6			
27X-CC	253.28														X							X																											
28X-CC	260.29														X							X												X														
29X-CC	272.34				X										X																		X		X		X											
30X-CC	281.48				X					X					X																															SN4			
31X-CC	291.59									X	X				X														X																				
32X-CC	300.58														X												X		X																SN3			
33X-CC	309.97									X	X				X												X		X																			
34X-CC	319.45														X																																	
35X-CC	328.82														X		X												X																			
36X-CC	339.02														X												X		X																			
37X-CC	348.59														X										X				X																SN2			
38X-CC	357.87														X					X				X	X				X																			
39X-CC	367.48																										X																					
40X-CC	376.54														X														X																			
41X-CC	387.07																																																
42X-CC	396.61																																														SN1			

Age		
late		Pliocene
early		
late		Miocene
middle		
early		

Table T6 (continued).

Hole, core, section	Depth (mbsf)	*Catapsydrax dissimilis*	*Catapsydrax unicavus*	*Chiloguembelina cubensis*	*Dentoglobigerina baroemoenensis*	*Dentoglobigerina globularis*	*Dentoglobigerina praedehiscens*	*Dentoglobigerina tripartita*	*Globigerina angulioffcinalis*	*Globigerina angulisuturalis*	*Globigerina bulloides*	*Globigerina ciperoensis*	*Globigerina falconensis*	*Globigerina labiacrassata*	*Globigerina officinalis*	*Globigerina praebulloides*	*Globigerina quinqueloba*	*Globigerinatheka index*	*Globigerinella aequilateralis*	*Globigerinella obesa*	*Globigerinella praecalida*	*Globigerinita glutinata*	*Globigerinita juvenilis*	*Globigerinita naparimaensis*	*Globigerinoides diminutus*	*Globigerinoides elongatus*	*Globigerinoides immaturus*	*Globigerinoides obliquus*	*Globigerinoides parawoodi*	*Globigerinoides primordius*	*Globigerinoides quadrilobatus*	*Globigerinoides trilobus*	*Globoquadrina dehiscens*	*Globorotalia conomiozea conomioz*	*Globorotalia crassaconica*	*Globorotalia crassaformis* (dex)	*Globorotalia crassaformis* (sin)	*Globorotalia crassula*	*Globorotalia explicationis*	*Globorotalia hirsuta*	*Globorotalia incognita*	*Globorotalia inflata* (dex)	*Globorotalia inflata* (sin)	*Globorotalia juanai*	*Globorotalia miotumida*	*Globorotalia miozea*	*Globorotalia panda*	*Globorotalia peripheroacuta*	*Globorotalia peripheroronda*	*Globorotalia pliozea*	*Globorotalia praescitula*	*Globorotalia pseudokugleri*	*Globorotalia puncticulata*	*Globorotalia puncticuloides*	*Globorotalia scitula*	*Globorotalia sphericomiozea*	Zone/ Subzone	Age	
43X-CC	406.01					X		X				X			X	X	?					X																																				late	Oligocene
44X-CC	415.47					X		X	X							X																																											
45X-CC	425.50					X			X	?					X	X						X																																					
46X-CC	435.10					X									X	X						X																																					
47X-CC	444.22											X			X	X						X																																					
48X-CC	454.19					X									X	X						X																																					
49X-CC	463.69					X	X	X							X	X																																											
50X-CC	472.70	X				X									X	X														X																													
51X-CC	483.16	X				X								X	X						X		X																									X									SP14b		
52X-CC	492.06	X				X									X	X				X			X																																				
53X-CC	501.46	X				?									X	X																																											
54X-CC	511.74	X				X		X	?						X	a																																											
55X-CC	521.15					X						X			X	X				X		X																																					
56X-CC	529.55	X				X									X	X				X		X																																					
57X-CC	540.51							X							X	X				X		X																																					
58X-CC	550.59					X									X	X						X																																					
59X-CC	560.32					?									X	X						X																																					
60X-CC	569.14	X		X		X			?					X	X	X																																										early	
61X-CC	578.31	X	X			X								X	X	X																																											
62X-CC	587.22	X		X		X								X		X																																											
63X-CC	597.30	X		X										X	X																																												
64X-CC	608.37	X												X																																													
65X-CC	616.53	X	X																																																								
66X-CC	625.49	X	X											X		X																																									SP14a		
67X-CC	634.11	X	X	X										?	X	X																																											
68X-CC	645.94	X		X											X	X																																											
69X-CC	654.94	X		X		X								X	X	X						X																																					
70X-CC	661.50	X		X										X	X																																												
71X-CC	673.93			X										X		X																																											
72X-CC	681.96			X										X		X																																											
73X-CC	691.62	X		X										X	X																																												
74X-CC	702.34	X														X																																											
75X-CC	714.09			X		X								X	X	X																																									SP12-13		
76X-CC	722.84		X	X		X									X																																												
77X-CC	733.41		X	X		X									X																																												

Table T6 (continued).

Hole, core, section	Depth (mbsf)	*Globorotalia tosaensis*	*Globorotalia triangula*	*Globorotalia truncatulinoides*	*Globorotalia ungulata*	*Globorotalia zealandica*	*Globorotaloides suteri*	*Globorotaloides testarugosa*	*Globoturborotalita apertura*	*Globoturborotalita brazieri*	*Globoturborotalita connecta*	*Globoturborotalita decoraperta*	*Globoturborotalita druryi*	*Globoturborotalita nepenthes*	*Globoturborotalita woodi*	*Guembelitria triseriata*	*Morozovella formosa formosa*	*Morozovella subbotinae = G. re*	*Neogloboquadrina dutertrei*	*Neogloboquadrina humerosa*	*Neogloboquadrina pachyderma s*	*Orbulina suturalis*	*Orbulina universa*	*Paragloborotalia acrostoma*	*Paragloborotalia continuosa*	*Paragloborotalia mayeri*	*Paragloborotalia nana*	*Paragloborotalia nympha*	*Paragloborotalia opima*	*Paragloborotalia semivera*	*Paragloborotalia siakensis*	*Praeorbulina bisphericus*	*Praeorbulina circularis*	*Praeorbulina sicana*	*Praeorbulina transitoria*	*Sphaeroidinellop paenedehiscens*	*Sphaeroidinellopsis seminulina*	*Subbotina angiporoides*	*Subbotina brevis*	*Subbotina eocaena*	*Subbotina linaperta*	*Tenuitella gemma*	*Tenuitella insolita*	*Tenuitella minutissima*	*Tenuitella munda*	*Tenuitellinata angustiumbilicata*	*Turborotalia euapertura*	*Turborotalita humilis*	Zone/ Subzone	Age	
43X-CC	406.01																																						X			X	X				
44X-CC	415.47																																										X	X				
45X-CC	425.50																																							X				X				
46X-CC	435.10																												X										X				X				
47X-CC	444.22							?																																			X	X				
48X-CC	454.19																																							X				X	X				
49X-CC	463.69						X																																					X				
50X-CC	472.70																			X								X				X					X				X		X	X	X				
51X-CC	483.16																																											X		X		SP14b	late	
52X-CC	492.06																											X	X											X				X	X				
53X-CC	501.46						?																																						X				
54X-CC	511.74						X																					X												X				X				
55X-CC	521.15						X																																	X				X				
56X-CC	529.55						X											X																										X				
57X-CC	540.51						X									X																												X	X				
58X-CC	550.59						X																					X																X				
59X-CC	560.32																																										?	X	X				
60X-CC	569.14																											X																X	X				
61X-CC	578.31																											X															?		X	X				
62X-CC	587.22		X																									X																X	X				
63X-CC	597.30						?																																					X		X	X				
64X-CC	608.37						?									X												X		X									X				X		X	X				
65X-CC	616.53																											X																X		X	X				
66X-CC	625.49															X												X																		X	X				
67X-CC	634.11															X												X												?						X	X	SP14a			
68X-CC	645.94						X									X												X																X		X	X				
69X-CC	654.94																											X																X		X	X		early		
70X-CC	661.50						X																					X																X		X	X				
71X-CC	673.93															X												X																							
72X-CC	681.96						X									X												X																X							
73X-CC	691.62						X									X												X																							
74X-CC	702.34																																						X											
75X-CC	714.09																											X											X				X				SP12-13			
76X-CC	722.84						X																																X		X	X	X							
77X-CC	733.41						X																																X			X	X							

Oligocene

Table T6 (continued).

Hole, core, section	Depth (mbsf)	*Catapsydrax dissimilis*	*Catapsydrax unicavus*	*Chiloguembelina cubensis*	*Dentoglobigerina baroemoenensis*	*Dentoglobigerina globularis*	*Dentoglobigerina praedehiscens*	*Dentoglobigerina tripartita*	*Globigerina angulioffinicinalis*	*Globigerina angulisuturalis*	*Globigerina bulloides*	*Globigerina ciperoensis*	*Globigerina falconensis*	*Globigerina labiacrassata*	*Globigerina officinalis*	*Globigerina praebulloides*	*Globigerina quinqueloba*	*Globigerinatheka index*	*Globigerinella aequilateralis*	*Globigerinella obesa*	*Globigerinella praecalida*	*Globigerinita glutinata*	*Globigerinita juvenilis*	*Globigerinita naparimaensis*	*Globigerinoides diminutus*	*Globigerinoides elongatus*	*Globigerinoides immaturus*	*Globigerinoides obliquus*	*Globigerinoides parawoodi*	*Globigerinoides primordius*	*Globigerinoides quadrilobatus*	*Globigerinoides trilobus*	*Globoquadrina dehiscens*	*Globorotalia conomiozea conomioz*	*Globorotalia crassaconica*	*Globorotalia crassaformis* (dex)	*Globorotalia crassaformis* (sin)	*Globorotalia crassula*	*Globorotalia explicationis*	*Globorotalia hirsuta*	*Globorotalia incognita*	*Globorotalia inflata* (dex)	*Globorotalia inflata* (sin)	*Globorotalia juanai*	*Globorotalia miotumida*	*Globorotalia miozea*	*Globorotalia panda*	*Globorotalia peripheroacuta*	*Globorotalia peripheroronda*	*Globorotalia pliozea*	*Globorotalia praescitula*	*Globorotalia pseudokugleri*	*Globorotalia puncticulata*	*Globorotalia puncticuloides*	*Globorotalia scitula*	*Globorotalia sphericomiozea*	Zone/ Subzone	Age	
78X-CC	743.28																																																								SP11	late	Eocene
79X-CC	752.53																	X																																									
80X-CC	761.99																	X																																									
81X-CC	771.82																																																										
82X-CC	781.00																	X																																									
83X-CC	798.87																	X																																									
84X-CC	799.52																	X																																									
85X-CC	808.97																	X																																									
86X-CC	818.33																	X																																									
87X-CC	828.36																																																										
88X-CC	837.68														X			X																																									
89X-CC	847.76																																																										
90X-CC	850.28									X																																																	
91X-CC	863.37																																																								Barren		
92X-CC	871.38																																																										
93X-CC	875.98																																																										
94X-CC	878.14																																																										
95X-CC	880.40																																																										
189-1168B-																																																											
1H-CC	3.89										X		X				X			X	X	X													X		X	X					X												X		SN14	Pleist.	
2H-CC	12.85										X						X				X	X													X		X	X					X												X		SN13	late	Pliocene
3H-CC	23.44										X						X		X	X		X															X	X					X										X		X				
4H-CC	32.21										X		X				X					X															X	X					X										X		X				
5H-CC	42.13										X		X						X	X		X															X	X				X	X									X	X	X	X				
6H-CC	51.51										X		X				X		X			X				X									X		X	X					X										X	X	X				
7H-CC	61.32										X						X					X															X													X			X				SN12a	e.	
8H-CC	69.91										X						X					X												X																X						X	SN11	late	Miocene
9H-CC	78.90										X						X					X												X										X															
10H-CC	87.99										X		X				X					X												X										X	X														
11H-CC	98.53										X						X					X												X	X										X										X	X			
12H-CC	100.63										X						X				X	X												X											X														
189-1168C-																																																											
1H-CC	9.94										X		X				X		X			X													X		X						X												X		SN13	late	Pliocene
2H-CC	19.30										X		X				X		X			X													X		X						X												X				
3H-CC	28.40										X		X				X		X			X													X		X						X												X				
4H-CC	38.45										X		X				X		X			X													X		X						X										X		X				
5H-CC	47.57										X		X				X		X			X															X						X										X		X				
6H-CC	56.26										X		X				X		X			X															X																X		X		SN12b	e.	
7H-CC	63.03										X						X		X			X												X																X			X		X		SN12a		

Table T6 (continued).

Hole, core, section	Depth (mbsf)	*Globorotalia tosaensis*	*Globorotalia triangula*	*Globorotalia truncatulinoides*	*Globorotalia ungulata*	*Globorotalia zealandica*	*Globorotaloides suteri*	*Globorotaloides testarugosa*	*Globoturborotalita apertura*	*Globoturborotalita brazieri*	*Globoturborotalita connecta*	*Globoturborotalita decoraperta*	*Globoturborotalita druryi*	*Globoturborotalita nepenthes*	*Globoturborotalita woodi*	*Guembelitria triseriata*	*Morozovella formosa formosa*	*Morozovella subbotinae = G. re*	*Neogloboquadrina dutertrei*	*Neogloboquadrina humerosa*	*Neogloboquadrina pachyderma s*	*Orbulina suturalis*	*Orbulina universa*	*Paragloborotalia acrostoma*	*Paragloborotalia continuosa*	*Paragloborotalia mayeri*	*Paragloborotalia nana*	*Paragloborotalia nympha*	*Paragloborotalia opima*	*Paragloborotalia semivera*	*Paragloborotalia siakensis*	*Praeorbulina bisphericus*	*Praeorbulina circularis*	*Praeorbulina sicana*	*Praeorbulina transitoria*	*Sphaeroidinellop paenedehiscens*	*Sphaeroidinellopsis seminulina*	*Subbotina angiporoides*	*Subbotina brevis*	*Subbotina eocaena*	*Subbotina linaperta*	*Tenuitella gemma*	*Tenuitella insolita*	*Tenuitella minutissima*	*Tenuitella munda*	*Tenuitellinata angustiumbilicata*	*Turborotalia euapertura*	*Turborotalita humilis*	Zone/ Subzone	Age		
78X-CC	743.28						X																													X	?	X		?											
79X-CC	752.53						X																													X		X													
80X-CC	761.99																																			X		X													
81X-CC	771.82																																																		
82X-CC	781.00																																			X															
83X-CC	798.87																																			X															
84X-CC	799.52																																			X		X													
85X-CC	808.97						?																													X		X		X											
86X-CC	818.33																																			X		X													
87X-CC	828.36																																																		
88X-CC	837.68						?																					X								X		X													
89X-CC	847.76																																																		
90X-CC	850.28																																																		
91X-CC	863.37																																																		
92X-CC	871.38																																																		
93X-CC	875.98																																																		
94X-CC	878.14																																																		
95X-CC	880.40																																																		
189-1168B-																																																			
1H-CC	3.89			X																	X		X																												
2H-CC	12.85		X																				X																												
3H-CC	23.44																				X		X																												
4H-CC	32.21																				X																														
5H-CC	42.13																						X																												
6H-CC	51.51	X																		?	X		X																												
7H-CC	61.32																				X		X																												
8H-CC	69.91																				X		X																												
9H-CC	78.90								X												X		X																												
10H-CC	87.99								X											?	X		X																												
11H-CC	98.53								X							X					X		X																												
12H-CC	100.63								X							X																																			
189-1168C-																																																			
1H-CC	9.94	X																			X		X																												
2H-CC	19.30																				X		X																												
3H-CC	28.40																				X		X																												
4H-CC	38.45																				X		X																												
5H-CC	47.57																				X		X																												
6H-CC	56.26																				X		X																												
7H-CC	63.03																				X		X																												

Table T6 (continued).

Hole, core, section	Depth (mbsf)	*Catapsydrax dissimilis*	*Catapsydrax unicavus*	*Chiloguembelina cubensis*	*Dentoglobigerina baroemoenensis*	*Dentoglobigerina globularis*	*Dentoglobigerina praedehiscens*	*Dentoglobigerina tripartita*	*Globigerina angulofficinalis*	*Globigerina angulisuturalis*	*Globigerina bulloides*	*Globigerina ciperoensis*	*Globigerina falconensis*	*Globigerina labiacrassata*	*Globigerina officinalis*	*Globigerina praebulloides*	*Globigerina quinqueloba*	*Globigerinatheka index*	*Globigerinella aequilateralis*	*Globigerinella obesa*	*Globigerinella praecalida*	*Globigerinita glutinata*	*Globigerinita juvenilis*	*Globigerinita naparimaensis*	*Globigerinoides diminutus*	*Globigerinoides elongatus*	*Globigerinoides immaturus*	*Globigerinoides obliquus*	*Globigerinoides parawoodi*	*Globigerinoides primordius*	*Globigerinoides quadrilobatus*	*Globigerinoides trilobus*	*Globoquadrina dehiscens*	*Globorotalia conomiozea conomioz*	*Globorotalia crassaconica*	*Globorotalia crassaformis* (dex)	*Globorotalia crassaformis* (sin)	*Globorotalia crassula*	*Globorotalia explicationis*	*Globorotalia hirsuta*	*Globorotalia incognita*	*Globorotalia inflata* (dex)	*Globorotalia inflata* (sin)	*Globorotalia juanai*	*Globorotalia miotumida*	*Globorotalia miozea*	*Globorotalia panda*	*Globorotalia peripheroacuta*	*Globorotalia peripheroronda*	*Globorotalia pliozea*	*Globorotalia praescitula*	*Globorotalia pseudokugleri*	*Globorotalia puncticulata*	*Globorotalia puncticuloides*	*Globorotalia scitula*	*Globorotalia sphericomiozea*	Zone Subzone	Age	
8H-CC	74.70										X						X		X			X												X											X										X		SN11	late	Miocene
9H-CC	85.91										X		X				X					X												X											X														
10H-CC	94.47										X		X				X			X		X												X											X														
11H-CC	102.70										X						X					X												X											X														
12H-CC	114.41										X						X			X		X												X											X														
13X-CC	117.44										X						X					X												X					X						X		?												
14X-CC	124.86										X						X					X												X					X						X		X												
15X-CC	133.54										X						X			X		X																	X						X		X								X		SN10		
16X-CC	140.52										X						X					X											X						X						X		X										SN9		
17X-CC	149.19										X						X			X		X						X					X						X						X		X												
18X-CC	162.17										X		X									X											X						X						X		X								X				
19X-CC	173.37										X		X									X											X						X						X		X								X				
20X-CC	181.47										X		X				X			X		X											X						X						X		X										SN8		
21X-CC	191.43										X						X					X											X						X						X		X											mid	
22X-CC	203.67										X		X				X			X		X												X					X						X	X	X										SN7		
23X-CC	213.89										X						X					X											X	X					X							X	X		X						X				

Note: X = present, ? = questionable identification.

Table T6 (continued).

Hole, core, section	Depth (mbsf)	*Globorotalia tosaensis*	*Globorotalia triangula*	*Globorotalia truncatulinoides*	*Globorotalia ungulata*	*Globorotalia zealandica*	*Globorotaloides suteri*	*Globorotaloides testarugosa*	*Globoturborotalita apertura*	*Globoturborotalita brazieri*	*Globoturborotalita connecta*	*Globoturborotalita decoraperta*	*Globoturborotalita druryi*	*Globoturborotalita nepenthes*	*Globoturborotalita woodi*	*Guembelitria triseriata*	*Morozovella formosa formosa*	*Morozovella subbotinae = G. re*	*Neogloboquadrina dutertrei*	*Neogloboquadrina humerosa*	*Neogloboquadrina pachyderma s*	*Orbulina suturalis*	*Orbulina universa*	*Paragloborotalia acrostoma*	*Paragloborotalia continuosa*	*Paragloborotalia mayeri*	*Paragloborotalia nana*	*Paragloborotalia nympha*	*Paragloborotalia opima*	*Paragloborotalia semivera*	*Paragloborotalia siakensis*	*Praeorbulina bisphericus*	*Praeorbulina circularis*	*Praeorbulina sicana*	*Praeorbulina transitoria*	*Sphaeroidinellop paenedehiscens*	*Sphaeroidinellopsis seminulina*	*Subbotina angiporoides*	*Subbotina brevis*	*Subbotina eocaena*	*Subbotina linaperta*	*Tenuitella gemma*	*Tenuitella insolita*	*Tenuitella minutissima*	*Tenuitella munda*	*Tenuitellinata angustiumbilicata*	*Turborotalia euapertura*	*Turborotalita humilis*	Zone/ Subzone	Age	
8H-CC	74.70																				X		X																								
9H-CC	85.91																				X		X																								
10H-CC	94.47																				X		X																								
11H-CC	102.70																				X		X																							SN11	late	
12H-CC	114.41							X													X		X																									
13X-CC	117.44							X												X	X		X																									
14X-CC	124.86							X													X		X																									
15X-CC	133.54																				X		X																						?	SN10		
16X-CC	140.52							X													X				X																							
17X-CC	149.19											X									X				X																							
18X-CC	162.17							X															X					X																	SN9		
19X-CC	173.37							X				X											X		X																							
20X-CC	181.47							X				X											X		X			X																	SN8		
21X-CC	191.43							X															X		X	?		X																			
22X-CC	203.67							X							X								X		X	X		X																	SN7	mid	
23X-CC	213.89														X								X		?	X																					

Table T7. Radiolarian datums recognized, Hole 1168A.

Datum	Age (Ma)	Interval		Depth (mbsf)		Mean (mbsf)	Error (m)
		Top	Bottom	Top	Bottom		
FO *Stylacontarium aquilonarium*	7.0	14X-CC	15X-CC	125.8	132.9	129.4	7.1
LO *Cyrtocapsella japonica*	9.9	16X-CC	17X-CC	144.9	154.3	149.6	9.4
LAO *Cyrtocapsella japonica*	10.1	17X-CC	18X-CC	154.3	164.9	159.6	10.6

Note: FO = first occurrence, LO = last occurrence, LAO = last abundant occurrence.

Table T8. Radiolarian datum recognized, Hole 1168C.

Datum	Age (Ma)	Interval		Depth (mbsf)		Mean (mbsf)	Error (m)
		Top	Bottom	Top	Bottom		
LO *Stichocorys delmontensis*	5.18-6.9	12H-CC	13X-CC	114	117	115.5	3

Note: LO = last occurrence.

Table T9. Distribution and abundance of diatoms and silicoflagellates, Site 1168. (**See table notes.** Continued on next page.)

Hole, core, section	Depth (mbsf)	Group Preservation	Group abundance	*Actinocyclus ingens*	*Actinocyclus ingens* var. *ovalis*	*Arachnodiscus* spp.	*Azpeitia tabularis* group	*Chaetoceros* resting spores	*Coscinodiscus marginatus*	*Coscinodiscus* spp.	*Eucampia antarctica*	*Fragilariopsis* spp.	*Fragilariopsis reinholdii*	*Proboscia barboi*	*Rhizosolenia* spp.	*Thalassionema nitzschioides*	*Thalassionema nitzschioides* var. *parva*	*Thalassiosira convexa* var. *aspinosa*	*Thalassiosira leptopus*	*Thalassiothrix antarctica-longissima* group	Silicoflagellate tests	Sponge spicules
189-1168A-																						
1H-CC	7.24	P	T							T											B	B
2H-CC	17.00	P	T							R											B	A
3H-CC	26.71		B																		B	A
4H-CC	35.75		B																		B	B
5H-CC	45.96		B																		B	T
6H-CC	55.24		B																		B	A
7H-CC	64.93		B																		B	A
8H-CC	73.58		B																		B	A
9H-CC	82.98		B																		B	F
10H-CC	93.41		B																		B	F
11H-CC	102.59		B																		B	A
12H-CC	112.06	M	C	C				C	F		R		F	R	R	F	R			A	B	A
13X-CC	115.95	M	C	F	F		R						R		R					A	R	A
14X-CC	125.81	M	F	R	F			R										F	R	F	R	A
15X-CC	132.89	P	T							T											B	C
16X-CC	144.86		T							T											B	C
17X-CC	154.31		B																		B	C
18X-CC	164.88	P	T							T											B	C
19X-CC	175.23		B																		B	C
20X-CC	184.20	P	T							T											B	C
21X-CC	194.62		B																		B	C
22X-CC	205.11		B																		B	C
23X-CC	214.69		B																		B	R
24X-CC	224.27		B																		B	B
25X-CC	233.12		B																		B	R
26X-CC	243.53		B																		B	R
27X-CC	253.28		B																		B	B
28X-CC	260.29		B																		B	B
29X-CC	272.34		B																		B	B
30X-CC	281.48		B																		B	R
31X-CC	291.59		B																		B	B
32X-CC	300.58		B																		B	B
33X-CC	309.97		B																		B	B
34X-CC	319.45		B																		B	B
35X-CC	328.82		B																		B	B
36X-CC	339.02		B																		B	B
37X-CC	348.59		B																		B	B
38X-CC	357.87		B																		B	B
39X-CC	367.48		B																		B	B
40X-CC	376.54		B																		B	B
41X-CC	387.07		B																		B	B
42X-CC	396.61		B																		B	A
43X-CC	406.01		B																		B	A
44X-CC	415.47		B																		B	A
45X-CC	425.50		B																		B	A
46X-CC	435.10		B																		B	A
47X-CC	444.22		B																		B	A
48X-CC	454.19		B																		B	B
49X-CC	463.69		B																		B	R
50X-CC	472.70		B																		B	R
51X-CC	483.16		B																		B	B
52X-CC	492.06		B																		B	B
53X-CC	501.46		B																		B	B
54X-CC	511.74		B																		B	B

Table T9 (continued).

Hole, core, section	Depth (mbsf)	Group Preservation	Group abundance	*Actinocyclus ingens*	*Actinocyclus ingens* var. *ovalis*	*Arachnodiscus* spp.	*Azpeitia tabularis* group	*Chaetoceros* resting spores	*Coscinodiscus marginatus*	*Coscinodiscus* spp.	*Eucampia antarctica*	*Fragilariopsis* spp.	*Fragilariopsis reinholdii*	*Proboscia barboi*	*Rhizosolenia* spp.	*Thalassionema nitzschioides*	*Thalassionema nitzschioides* var. *parva*	*Thalassiosira convexa* var. *aspinosa*	*Thalassiosira leptopus*	*Thalassiothrix antarctica-longissima* group	Silicoflagellate tests	Sponge spicules
55X-CC	521.15		B																		B	F
56X-CC	529.55		B																		B	R
57X-CC	540.51		B																		B	F
58X-CC	550.59		T									T									B	B
59X-CC	560.32		B																		B	B
60X-CC	569.14		B																		B	B
61X-CC	578.31	M-P	R			R															B	C
62X-CC	587.22	M-P	R			R															B	C
63X-CC	597.30	P	R			R															B	F
64X-CC	608.37	P	R			R															B	F
65X-CC	616.53	P	T									T									B	F
66X-CC	625.49	P	T							T											B	F
67X-CC	634.11		B																		B	B
68X-CC	645.94		B																		B	T
69X-CC	654.94		B																		B	B
70X-CC	661.50		B																		B	B
71X-CC	673.93		B																		B	B
72X-CC	681.96		B																		B	B
73X-CC	691.62		B																		B	B
74X-CC	702.34		B																		B	B
75X-CC	714.09		B																		B	B
76X-CC	722.84		B																		B	B
77X-CC	733.41		B																		B	B
78X-CC	743.18		B																		B	B
79X-CC	752.53		B																		B	B
80X-CC	761.99		B																		B	B
81X-CC	771.82		B																		B	B
82X-CC	781.00		B																		B	B
83X-CC	790.87		B																		B	B
84X-CC	799.52		B																		B	B
85X-CC	808.97		B																		B	B
86X-CC	818.33		B																		B	B
87X-CC	828.36		B																		B	B
88X-CC	837.68		B																		B	B
89X-CC	847.76		B																		B	B
90X-CC	850.28		B																		B	B
91X-CC	863.37		B																		B	B
92X-CC	871.23		B																		B	B
93X-CC	875.98		B																		B	B
94X-CC	878.14		B																		B	B
95X-CC	880.40		B																		B	B

Notes: Preservation: G = good, M = moderate, P = poor. Abundance: A = abundant, C = common, F = few, R = rare, T = trace, B = barren.

Table T10. Distribution of terrestrial palynomorphs and organic-walled dinoflagellate cysts (dinocysts) specimens in selected samples, Hole 1168A. (**See table notes.** Continued on next three pages.)

Core, section, interval (cm)	Depth (mbsf)	Preservation	Terrestrial palynomorphs (%)	Dinocyst abundance	*Achomosphaera andalousiensis*	*Achomosphaera* spp. (pars.)	*Amiculosphaera umbraculа*	*Apteodinium australiense*	*Apteodinium spiridoides*	*Ataxodinium* spp.	*Bitectatodinium tepikiense*	*Brigantedinium* spp.	*Cannosphaeropsis* sp.	*Cerebrocysta* sp.	*Circulodinium distinctum*	*Cordosphaeridium fibrospinosum*	*Corrudinium haitanai*	*Cribroperidinium giuseppei*	*Dapsilidinium pseudocolligerum*	*Dellandrea phosphoritica group*	*Diphyes ficusoides*	*Distatodinium ellipticum*	*Echinidinium* spp.	*Eocladopyxis* sp.	*Glaphyrocysta intricata*	*Hystrichokolpoma rigaudiae*	*Hystrichostrogylon* spp.	*Impagidinium pallidum*	*Impagidinium paradoxum*	*Impagidinium* cf. *acuiealum*	*Impagidinium aspertitum*	*Impagidinium paradoxum*	*Impagidinium patulum*	*Impagidinium sphaericum*	*Impagidinium striatiatum*	*Impagidinium velorum*	*Invertocysta tabulata*	*Lejeunecysta* spp.	*Lingulodinium machaerophorum*
189-1168A-																																					
1H-CC, 22-24	7.24	G	5	A						1	1	7																1	65			29	7		2			3
2H-CC, 9-11	17.00	G	13	A							2	12																1	32			39	4	1			3	37
3H-CC, 29-32	26.71	G	4	C						1		6					6												14			41	2					2
4H-CC, 0-5	35.75	G	12	C								3											1						35			1					1	
5H-CC, 38-41	45.96	G	9	R																									6			2	2				1	
6H-CC, 26-29	55.24	G	12	C				1				1																	2				1			1		1
7H-CC, 24-29	64.93	G	0	R																									1									
8H-CC, 8-13	73.58	G	0	A																									1				5	14	1		1	
9H-CC, 27-32	82.98	G	3	F																									3				1	2	1		1	
10H-CC, 30-35	93.41	G	1	C	1																								1			1	5	2				2
14X-CC, 25-30	125.81	G	10	F	1	3																										1						
18X-CC, 29-34	164.88		0	B																																		
22X-CC, 29-34	205.11		0	B																																		
26X-CC, 26-30	243.53		0	B																																		
30X-CC, 6-11	281.48		0	B																																		
34X-CC, 0-5	319.45	G	6	A		3								7					2															7				
38X-CC, 50-55	357.87	M	1	T										1																								
42X-CC, 32-37	396.61	G	10	F					1										1															1				2
46X-CC, 37-42	435.10	G	6	C				2	1																12					1	1		1	1		1		
50X-CC, 43-48	472.70	G	10	C																								1		1								
54X-CC, 30-35	511.74	G	13	C															2						1	2												
58X-CC, 45-50	550.59	M	0	T																																		
62X-CC, 32-37	587.22	G	43	F															1							1					1							
66X-CC, 34-39	625.49	M	15	F																						1												
70X-CC, 36-41	661.50	G	5	A				2					5						17					3	23	2	8											
74X-CC, 32-37	702.34	G	10	C				5														1		17	1	30	3				1							
75X-CC, 27-32	714.09	P	70	T																																	2	
78X-CC, 43-48	743.18	P	80	T																																		
79X-CC, 34-39	752.53	M	40	F																1		1				2					1							
80X-CC, 34-39	761.99	P	75	T																																		
81X-CC, 24-29	771.82	P	90	T																																		
82X-CC, 33-38	781.00	M	60	F														1			1																1	
83X-CC, 35-41	790.87	P	99	T																																		
84X-CC, 31-36	799.52	P	99	B																																		
85X-CC, 25-31	808.97	P	90	T														2		1																		
86X-CC, 37-42	818.33	P	88	T																3																		
87X-CC, 22-27	828.36	P	87	T																5																		
92X-CC, 33-38	871.23	P	90	T																																		

Table T10 (continued).

Core, section, interval (cm)	Depth (mbsf)	Preservation	Terrestrial palynomorphs (%)	Dinocyst abundance	*Nematosphaeropsis labyrinthea*	*Operculodinium centrocarpum*	*Operculodinium echigoense*	*Operculodinium israelianum*	*Operculodinium longispinigerum*	*Operculodinium psilatum*	*Pentadinium laticinctum*	*Polysphaeridium zoharyi*	*Pyxidinopsis fairhavenensis*	*Pyxidinopsis waipawaensis*	*Reticulatosphaera actinocoronata*	*Spiniferites bentori*	*Spiniferites hyperacanthus*	*Spiniferites membranaceus*	*Spiniferites mirabilis*	*Spiniferites pachyderma*	*Spiniferites pseudofurcatus*	*Spiniferites ramosus*	*Systematophora placacantha*	*Tectatodinium pellitum*	*Thalassiphora pelagica*	*Wetzeliella articulata*	*Wetzeliella* spp. (pars.)
189-1168A-																											
1H-CC, 22-24	7.24	G	5	A	33	15		1				1				1	1		2	4		29					
2H-CC, 9-11	17.00	G	13	A	2	30										1	4		6			29					
3H-CC, 29-32	26.71	G	4	C		1		1														3					
4H-CC, 0-5	35.75	G	12	C	1	1													1			40					
5H-CC, 38-41	45.96	G	9	R														1	1			7					
6H-CC, 26-29	55.24	G	12	C	6	28													1		1	8		1	1		
7H-CC, 24-29	64.93	G	0	R																	1	1					
8H-CC, 8-13	73.58	G	0	A			110															2					
9H-CC, 27-32	82.98	G	3	F			18															4					
10H-CC, 30-35	93.41	G	1	C	7		45											2	3			50					
14X-CC, 25-30	125.81	G	10	F	4														2			20					
18X-CC, 29-34	164.88		0	B																							
22X-CC, 29-34	205.11		0	B																							
26X-CC, 26-30	243.53		0	B																							
30X-CC, 6-11	281.48		0	B																							
34X-CC, 0-5	319.45	G	6	A	2	2			46				8						1			50					
38X-CC, 50-55	357.87	M	1	T					1													1					
42X-CC, 32-37	396.61	G	10	F		1	1			3	1				5							17					
46X-CC, 37-42	435.10	G	6	C		4			2						5							43					
50X-CC, 43-48	472.70	G	10	C	2	8									1							34					
54X-CC, 30-35	511.74	G	13	C		6									2							53	40				
58X-CC, 45-50	550.59	M	0	T																		1	1				
62X-CC, 32-37	587.22	G	43	F		3									4							34					
66X-CC, 34-39	625.49	M	15	F		55																4	2				
70X-CC, 36-41	661.50	G	5	A		12																92	3		80		
74X-CC, 32-37	702.34	G	10	C		15		3														24	1				3
75X-CC, 27-32	714.09	P	70	T		6																8	1		1		
78X-CC, 43-48	743.18	P	80	T		1																1					
79X-CC, 34-39	752.53	M	40	F		2																24	33				
80X-CC, 34-39	761.99	P	75	T		1																1					
81X-CC, 24-29	771.82	P	90	T		1																1					
82X-CC, 33-38	781.00	M	60	F		15								2								4	13				
83X-CC, 35-41	790.87	P	99	T																		1					
84X-CC, 31-36	799.52	P	99	B																							
85X-CC, 25-31	808.97	P	90	T		4																1					
86X-CC, 37-42	818.33	P	88	T		1																					
87X-CC, 22-27	828.36	P	87	T																							
92X-CC, 33-38	871.23	P	90	T		1																					

Table T10 (continued).

Core, section, interval (cm)	Depth (mbsf)	Preservation	Terrestrial palynomorphs (%)	Dinocyst abundance	*Achomosphaera andalousiensis*	*Achomosphaera* spp. (pars.)	*Amiculosphaera umbracula*	*Apteodinium australiense*	*Apteodinium spiridoides*	*Ataxodinium* spp.	*Bitectatodinium tepikiense*	*Brigantedinium* spp.	*Cannosphaeropsis* sp.	*Cerebrocysta* sp.	*Circulodinium distinctum*	*Cordosphaeridium fibrospinosum*	*Corrudinium harlandii*	*Cribroperidinium giuseppei*	*Dapsilidinium pseudocolligerum*	*Deflandrea phosphoritica group*	*Diphyes ficusoides*	*Distatodinium ellipticum*	*Echinidinium* spp.	*Eocladopyxis* sp.	*Glaphyrocysta intricata*	*Hystrichokolpoma rigaudiae*	*Hystrichostrogylon* spp.	*Impagidinium pallidum*	*Impagidinium aculeatum*	*Impagidinium* cf. *aculeatum*	*Impagidinium dispertitum*	*Impagidinium paradoxum*	*Impagidinium patulum*	*Impagidinium sphaericum*	*Impagidinium strialatum*	*Impagidinium velorum*	*Invertocysta tabulata*	*Lejeunecysta* spp.	*Lingulodinium machaerophorum*
93X-CC, 28-35	875.98	P	100	B																																		
94X-CC, 33-39	878.14	P	100	T											1																								
95X-CC, 24-29	880.40	P	100	B																																			

Notes: Indications of group abundance refers to abundance of dinocysts; A = abundant, C = common, F = few, R = rare, T = trace, B = barren. Preservation: G = good, M = moderate, P = poor.

Table T10 (continued).

Core, section, interval (cm)	Depth (mbsf)	Preservation	Terrestrial palynomorphs (%)	Dinocyst abundance	*Nematosphaeropsis labyrinthea*	*Operculodinium centrocarpum*	*Operculodinium echigoense*	*Operculodinium israelianum*	*Operculodinium longispinigerum*	*Operculodinium psilatum*	*Pentadinium laticinctum*	*Polysphaeridium zoharyi*	*Pyxidinopsis fairhavenensis*	*Pyxidinopsis waipawaensis*	*Reticulatosphaera actinocoronata*	*Spiniferites bentori*	*Spiniferites hyperacanthus*	*Spiniferites membranaceus*	*Spiniferites mirabilis*	*Spiniferites pachyderma*	*Spiniferites pseudofurcatus*	*Spiniferites ramosus*	*Systematophora placacantha*	*Tectatodinium pellitum*	*Thalassiphora pelagica*	*Wetzeliella articulata*	*Wetzeliella* spp. (pars.)
93X-CC, 28-35	875.98	P	100	B																							
94X-CC, 33-39	878.14	P	100	T																							
95X-CC, 24-29	880.40	P	100	B																							

Table T11. Selected age-diagnostic dinocyst events, Hole 1168A.

Dinocyst datum	Interval		Depth (mbsf)		Mean (mbsf)	Error (m)	Age (Ma)	Source
	Top	Bottom	Top	Bottom				
LO *A. umbracula*	5H-CC	6H-CC	45.96	55.24	50.60	4.64	2.65	Williams et al., 1998a
LO *I. tabulata*	5H-CC	6H-CC	45.96	55.24	50.60	4.64	2.65	Williams et al., 1998a
FO *A. andalousiensis*	14X-CC	18X-CC	125.81	164.88	145.35	19.54	11.55	Williams et al., 1998a
LO *P. fairhavenensis*	30X-CC	34X-CC	281.48	319.45	300.47	18.99	15.50	De Verteuil and Norris, 1996
LO *Glaphyrocysta* spp.	42X-CC	46X-CC	396.61	435.10	415.86	19.25	25.00	Williams et al., 1998a

Note: LO = last occurrence, FO = first occurrence.

Table T12. Biostratigraphic events, Site 1168.

Group	Bioevent	Age (Ma)	Sample (cm)	Depth (mbsf)	Depth error (m)
N	FO *Emiliania huxleyi*	0.3	1168B-1H-1, 72	0.64	0.09
F	FO *Globorotalia truncatulinoides*	2.0	1168B-2H-CC	8.37	4.48
N	LO *Calcidiscus macintyrei*	1.7	1168A-2H-CC	12.12	4.88
N	LO *Discoaster surculus*	2.6	1168A-3H-CC	21.86	4.86
C	LO *Amiculosphaera umbracula*	2.7	1168A-6H-CC	50.60	4.64
C	LO *Invertocysts tabulata*	2.7	1168A-6H-CC	50.60	4.64
N	LO *Reticulofenestra pseudoumbilica*	3.8	1168A-6H-CC	50.60	4.64
F	FO *Globorotalia inflata*	3.2	1168C-6H-CC	51.92	4.35
F	LO *Globorotalia pliozea*	4.6	1168C-7H-CC	56.65	3.39
N	LO *Amaurolithus delicatus*	4.6	1168A-7H-CC	60.09	4.85
F	FO *Globoratalia puncticulata*	5.3	1168C-8H-CC	68.87	5.84
N	LO *Ceratolithus acutus*	5.1	1168A-8H-CC	69.39	4.46
N	FO *Ceratolithus acutus*	5.4	1168A-10H-CC	88.20	5.22
D	FO *Fragilariopsis reinholdii*	8.1	1168A-14H-CC	114.20	11.61
R	LO *Stichocorys delmontensis*	5.18-6.9	1168C-13X-CC	115.50	3.00
N	FO *Amaurolithus primus*	7.2	1168A-14X-CC	120.88	4.96
F	FO *Globorotalia conomiozea*	6.9	1168C-15X-CC	129.20	4.34
D	LO *Actinocyclus ingens* var. *ovalis*	6.3	1168A-15H-CC	129.35	3.54
D	FO *Actinocyclus ingens* var. *ovalis*	8.7	1168A-15H-CC	129.35	3.54
R	FO *Stylacontarium aquilonarium*	7.0	1168A-15X-CC	129.40	7.10
F	LO *Paragloborotalia continuosa*	8.0	1168C-16X-CC	137.03	3.49
C	FO *Achomosphaera andalousiensis*	11.6	1168A-18X-CC	145.35	19.54
R	LO *Cyrtocapsella japonica*	9.9	1168A-17X-CC	149.60	9.40
R	FO *Cyrtocapsella japonica*	10.1	1168A-18X-CC	159.60	10.60
F	LO *Paragloborotalia nympha*	10.1	1168C-21X-CC	186.45	4.98
F	LO *Paragloborotalia mayeri*	11.4	1168C-22X-CC	197.55	6.12
N	LO *Cyclicargolithus floridanus*	11.9	1168A-22X-CC	199.87	5.25
F	FO *Paragloborotalia mayeri*	12.1	1168C-24X-CC	217.28	3.39
N	LO *Sphenolithus heteromorphus*	13.6	1168A-26X-CC	238.33	5.21
F	FO *Orbulina suturalis*	15.1	1168A-28X-CC	256.79	3.51
F	FO *Praeorbulina curva*	16.3	1168A-29X-CC	266.32	6.03
N	FO *Calcidiscus premacintyrei*	17.4	1168A-29X-CC	266.32	6.03
F	FO *Globigerinoides trilobus*	18.8	1168A-31X-CC	286.54	5.06
N	FO *Sphenolithus heteromorphus*	18.2	1168A-32X-CC	296.09	4.50
N	LO *Sphenolithus belemnos*	18.3	1168A-32X-CC	296.09	4.50
C	LO *Pyxidinopsis fairhavenensis*	15.5	1168A-34X-CC	300.47	18.99
N	FO *Sphenolithus belemnos*	20.6	1168A-33X-CC	305.28	4.69
F	FO *Globoturborotalita connecta*	20.9	1168A-34X-CC	314.71	4.74
F	FO *Globorotalia woodi*	22.6	1168A-41X-CC	381.81	5.27
F	FO *Globoquadrina dehiscens*	23.2	1168A-43X-CC	401.31	4.70
C	LO *Glaphyrocysta* spp.	25.0	1168A-46X-CC	415.86	19.25
N	LO *Reticulofenestra bisecta*	23.9	1168A-47X-CC	439.66	4.56
N	LO *Chiasmolithus altus*	26.1	1168A-55X-CC	516.45	4.71
F	LO *Chiloguembelina cubensis*	28.5	1168A-60X-CC	564.73	4.41
N	LO *Sphenolithus distentus*	27.5	1168A-70X-CC	658.22	3.28
F	LO *Subbotina angiporoides*	30.0	1168A-75X-CC	696.98	5.36
N	LO *Reticulofenestra umbilica*	31.2	1168A-78X-1, 38	733.60	0.19
N	LO *Isthmolithus recurvus*	32.3	1168A-78X-2, 144	735.74	0.73
F	LO *Globigerinatheka index*	34.3	1168A-78X-CC	738.30	4.89
N	LO *Discoaster saipanensis*	34.2	1168A-80-2, 21	753.44	0.91
N	FO *Isthmolithus recurvus*	36.0	1168A-94X-CC	878.07	0.07

Notes: Lowest sample of event interval is listed. See individual microfossil sections in this chapter for top and bottom samples of event intervals. Depth interval is the distance in meters between the top and bottom sample of the event interval. Group: N = nannofossil, F = planktonic foraminifer, R = radiolarian, D = diatom, C = dinocyst. FO = first occurrence, LO = last occurrence. This table is also available in **ASCII format.**

Table T13. Magnetostratigraphic results of Holes 1168C and 1168A.

Chron	Age (Ma)	Depth (mbsf)
Hole 1168C, 0-50 mbsf:		
Termination C1r1n	0.99	3.75
Onset C1r1n	1.07	9.00
Termination C2n	1.77	28.10
Hole 1168A, 250-350 mbsf:		
Termination C5Cn.1n	16.01	252.60
Onset C5Cn.3n	16.73	257.00
Termination C5Dn	17.28	264.30
Onset C5Dn	17.62	272.30
Termination C5En	18.28	281.90
Onset C5En	18.78	287.60
Termination C6n	19.04	321.50
Onset C6n	20.31	347.30

Table T14. Composite depth section, Site 1168.

Hole, core, section	Depth (mbsf)	Offset (m)	Depth (mcd)
189-1168A-			
1H	0.00	0.42	0.42
2H	7.30	1.36	8.66
3H	16.80	3.70	20.50
4H	26.30	4.92	31.22
5H	35.80	5.40	41.20
6H	45.30	7.58	52.88
7H	54.80	8.45	63.25
8H	64.30	9.81	74.11
9H	73.80	9.81	83.61
10H	83.30	10.87	94.17
11H	92.80	14.22	107.02
12H	102.30	16.34	118.64
13X	111.80	16.34	128.14
14X	118.50	16.34	134.84
15X	128.10	16.34	144.44
16X	137.70	16.34	154.04
17X	147.30	16.34	163.64
18X	156.90	16.34	173.24
19X	166.50	16.34	182.84
20X	176.10	16.34	192.44
21X	185.70	16.34	202.04
22X	195.40	16.34	211.74
23X	205.00	16.34	221.34
24X	214.60	16.34	230.94
25X	224.20	16.34	240.54
26X	233.80	16.34	250.14
27X	243.40	16.34	259.74
28X	253.00	17.28	270.28
29X	262.60	17.28	279.88
30X	272.20	18.75	290.95
31X	281.80	20.04	301.84
32X	291.40	20.04	311.44
33X	300.70	20.04	320.74
34X	310.00	20.04	330.04
35X	319.60	20.04	339.64
36X	329.20	20.04	349.24
37X	338.80	20.04	358.84
38X	348.40	20.04	368.44
39X	358.00	20.04	378.04
40X	367.60	20.04	387.64
41X	377.30	20.04	397.34
42X	386.90	20.04	406.94
43X	396.50	20.04	416.54
44X	406.10	20.04	426.14
45X	415.70	20.04	435.74
46X	425.30	20.04	445.34
47X	434.90	20.04	454.94
48X	444.50	20.04	464.54
49X	454.10	20.04	474.14
50X	463.70	20.04	483.74
51X	473.30	20.04	493.34
52X	482.90	20.04	502.94
53X	492.50	20.04	512.54
54X	502.10	20.04	522.14
55X	511.70	20.04	531.74
56X	521.40	20.04	541.44
57X	531.10	20.04	551.14
58X	540.70	20.04	560.74
59X	550.40	20.04	570.44
60X	560.00	20.04	580.04
61X	569.60	20.04	589.64
62X	579.20	20.04	599.24
63X	588.80	20.04	608.84
64X	598.40	20.04	618.44
65X	608.00	20.04	628.04
66X	617.60	20.04	637.64
67X	627.20	20.04	647.24
68X	636.80	20.04	656.84
69X	646.40	20.04	666.44
70X	656.10	20.04	676.14
71X	665.80	20.04	685.84
72X	675.40	20.04	695.44
73X	685.00	20.04	705.04
74X	694.70	20.04	714.74
75X	704.30	20.04	724.34
76X	713.90	20.04	733.94
77X	723.60	20.04	743.64
78X	733.20	20.04	753.24
79X	742.80	20.04	762.84
80X	752.40	20.04	772.44
81X	762.00	20.04	782.04
82X	771.60	20.04	791.64
83X	781.20	20.04	801.24
84X	790.80	20.04	810.84
85X	800.40	20.04	820.44
86X	809.90	20.04	829.94
87X	819.50	20.04	839.54
88X	829.10	20.04	849.14
89X	838.70	20.04	858.74
90X	848.30	20.04	868.34
91X	855.40	20.04	875.44
92X	861.40	20.04	881.44
93X	867.50	20.04	887.54
94X	873.50	20.04	893.54
95X	877.50	20.04	897.54
189-1168B-			
1H	0.00	0.24	0.24
2H	3.90	3.06	6.96
3H	13.40	3.34	16.74
4H	22.90	4.70	27.60
5H	32.40	4.84	37.24
6H	41.90	5.94	47.84
7H	51.40	6.51	57.91
8H	60.90	8.47	69.37
9H	70.40	9.05	79.45
10H	79.90	8.91	88.81
11H	89.40	9.87	99.27
12H	98.90	11.30	110.20
189-1168C-			
1H	0.00	0.00	0.00
2H	9.50	0.20	9.70
3H	19.00	5.12	24.12
4H	28.50	5.72	34.22
5H	38.00	7.02	45.02
6H	47.50	7.84	55.34
7H	57.00	10.95	67.95
8H	66.50	8.95	75.45
9H	76.00	7.87	83.87
10H	85.50	10.13	95.63
11H	95.00	11.54	106.54
12H	104.50	10.14	114.64
13X	114.00	13.84	127.84
14X	117.70	17.48	135.18
15X	127.30	15.56	142.86
16X	136.90	18.66	155.56
17X	146.50	18.66	165.16
18X	156.10	18.26	174.36
19X	165.70	18.64	184.34
20X	175.30	18.80	194.10
21X	185.00	17.74	202.74
22X	194.70	18.54	213.24
23X	204.30	18.62	222.92
24X	213.90	18.54	232.44
25X	223.50	19.68	243.18
26X	233.20	18.20	251.40
27X	242.50	19.46	261.96
28X	252.10	19.92	272.02
29X	261.70	19.94	281.64
30X	271.30	21.31	292.61
31X	280.90	21.34	302.24

Table T15. Splice tie points, Site 1168.

Hole, core, section, interval (cm)	Depth (mbsf)	Depth (mcd)		Hole, core, section, interval (cm)	Depth (mbsf)	Depth (mcd)
189-				189-		
1168A-1H-5, 20	6.20	6.62	Tie to	1168C-1H-5, 62	6.62	6.62
1168C-1H-7, 68	9.68	9.68	Tie to	1168A-2H-1, 102	8.32	9.68
1168A-2H-7, 30	16.60	17.96	Tie to	1168B-3H-1, 122	14.62	17.96
1168B-3H-5, 26	19.66	23.00	Tie to	1168A-3H-2, 100	19.30	23.00
1168A-3H-5, 68	23.48	27.18	Tie to	1168C-3H-3, 6	22.06	27.18
1168C-3H-7, 60	28.00	33.12	Tie to	1168A-4H-2, 40	28.20	33.12
1168A-4H-6, 22	33.87	38.79	Tie to	1168B-5H-2, 4.5	33.95	38.79
1168B-5H-4, 106	37.96	42.80	Tie to	1168A-5H-2, 10	37.40	42.80
1168A-5H-7, 8	44.78	50.18	Tie to	1168B-6H-2, 84	44.24	50.18
1168B-6H-6, 80	50.20	56.14	Tie to	1168A-6H-3, 26	48.56	56.14
1168A-6H-7, 54	54.79	62.37	Tie to	1168B-7H-3, 146	55.86	62.37
1168B-7H-5, 80	58.20	64.71	Tie to	1168A-7H-1, 146	56.26	64.71
1168A-7H-CC, 8	64.77	73.22	Tie to	1168B-8H-3, 84.5	64.75	73.22
1168B-8H-4, 112	66.52	74.99	Tie to	1168A-8H-1, 88	65.18	74.99
1168A-8H-6, 44	72.24	82.05	Tie to	1168B-9H-2, 110	73.00	82.05
1168B-9H-6, 4	77.94	86.99	Tie to	1168C-9H-3, 12	79.12	86.99
1168C-9H-5, 128	83.28	91.15	Tie to	1168B-10H-2, 84	82.24	91.15
1168B-10H-5, 22	86.12	95.03	Tie to	1168A-10H-1, 86	84.16	95.03
1168A-10H-6, 112	91.92	102.79	Tie to	1168B-11H-3, 68.5	92.92	102.79
1168B-11H-6, 98	97.71	107.58	Tie to	1168A-11H-1, 56	93.36	107.58
1168A-11H-6, 54	100.84	115.06	Tie to	1168B-12H-4, 36	103.76	115.06
1168B-12H-6, 144	107.84	119.14	Tie to	1168A-12H-1, 50	102.80	119.14
1168A-12H-CC, 32	112.03	128.37				

Table T16. Values for inorganic carbon, calcium carbonate, total carbon, total organic carbon, total nitrogen, total sulfur, and hydrogen in sediments, Hole 1168A. (See table notes. Continued on next three pages.)

Hole, core, section	Depth (mbsf)	IC (wt%)	$CaCO_3$ (wt%)	TC (wt%)	TOC (wt%)	N (wt%)	S (wt%)	H (mg H/g)
189-1168A-								
1H-1	0.73	10.48	87.30	NA	NA	NA	NA	NA
1H-3	3.57	10.32	86.00	10.70	0.33	0.02	0.00	0.14
1H-5	6.70	10.31	85.80	NA	NA	NA	NA	NA
2H-1	8.55	9.68	80.70	NA	NA	NA	NA	NA
2H-3	10.99	8.81	73.40	9.09	0.27	0.03	0.01	0.26
2H-5	13.99	10.60	88.30	NA	NA	NA	NA	NA
3H-1	17.49	10.27	85.50	NA	NA	NA	NA	NA
3H-3	20.49	5.86	48.90	6.24	0.37	0.06	0.00	0.59
3H-5	23.49	10.73	89.40	NA	NA	NA	NA	NA
4H-1	27.03	10.04	83.60	NA	NA	NA	NA	NA
4H-3	29.96	9.51	79.30	9.69	0.17	0.02	0.02	0.21
4H-5	32.96	9.89	82.40	NA	NA	NA	NA	NA
5H-1	36.50	9.21	76.70	NA	NA	NA	NA	NA
5H-3	39.50	10.73	89.40	11.00	0.26	0.01	0.03	0.10
5H-5	42.40	10.75	89.60	NA	NA	NA	NA	NA
6H-3	49.04	10.86	90.40	11.00	0.09	0.01	0.01	0.09
6H-5	51.97	10.96	91.30	NA	NA	NA	NA	NA
7H-1	55.56	11.11	92.50	NA	NA	NA	NA	NA
7H-3	58.53	11.21	93.40	11.20	0.03	0.03	0.00	0.06
7H-5	61.53	11.13	92.70	NA	NA	NA	NA	NA
8H-1	65.00	11.15	92.90	NA	NA	NA	NA	NA
8H-3	68.00	10.44	87.00	11.40	0.90	0.00	0.00	0.04
8H-5	71.00	11.30	94.10	NA	NA	NA	NA	NA
9H-1	74.52	10.63	88.50	NA	NA	NA	NA	NA
9H-3	77.52	10.98	91.50	11.30	0.35	0.01	0.02	0.08
9H-5	80.52	11.14	92.80	NA	NA	NA	NA	NA
10H-1	84.02	10.77	89.70	NA	NA	NA	NA	NA
10H-3	87.02	11.02	91.80	10.40	0.00	0.01	0.03	0.07
10H-5	90.02	11.32	94.30	NA	NA	NA	NA	NA
11H-1	93.71	9.74	81.20	NA	NA	NA	NA	NA
11H-3	96.52	11.06	92.10	10.90	0.00	0.00	0.00	0.04
11H-5	99.52	10.34	86.10	NA	NA	NA	NA	NA
12H-1	103.02	10.66	88.80	NA	NA	NA	NA	NA
12H-3	106.02	10.85	90.40	11.20	0.32	0.01	0.00	0.09
12H-5	109.02	10.23	85.20	NA	NA	NA	NA	NA
13X-1	112.52	10.57	88.00	NA	NA	NA	NA	NA
13X-3	115.52	11.09	92.40	11.00	0.00	0.00	0.00	0.08
14X-1	119.22	10.44	87.00	NA	NA	NA	NA	NA
14X-3	122.22	11.22	93.40	11.10	0.00	0.00	0.00	0.08
14X-5	125.22	9.25	77.10	NA	NA	NA	NA	NA
15X-1	128.82	11.30	94.10	NA	NA	NA	NA	NA
15X-3	131.82	11.22	93.50	10.40	0.00	0.00	0.00	0.04
16X-1	138.42	11.59	96.60	NA	NA	NA	NA	NA
16X-3	141.42	11.53	96.10	12.10	0.60	0.00	0.00	0.00
16X-5	144.42	11.28	94.00	NA	NA	NA	NA	NA
17X-1	148.02	11.17	93.10	NA	NA	NA	NA	NA
17X-3	151.02	11.42	95.20	11.30	0.00	0.00	0.00	0.03
17X-5	154.02	11.52	95.90	NA	NA	NA	NA	NA
18X-1	157.62	11.45	95.40	NA	NA	NA	NA	NA
18X-3	160.62	10.33	86.10	11.40	1.10	0.00	0.00	0.05
18X-5	163.62	11.28	93.90	NA	NA	NA	NA	NA
19X-1	167.22	10.87	90.60	NA	NA	NA	NA	NA
19X-3	170.22	10.72	89.30	10.90	0.20	0.00	0.00	0.08
19X-5	173.22	11.03	91.90	NA	NA	NA	NA	NA
20X-1	176.82	10.86	90.50	NA	NA	NA	NA	NA
20X-3	179.82	11.30	94.10	11.50	0.18	0.00	0.00	0.04
20X-5	182.82	11.00	91.60	NA	NA	NA	NA	NA
21X-1	186.42	10.86	90.50	NA	NA	NA	NA	NA
21X-3	189.42	10.24	85.30	10.30	0.05	0.00	0.00	0.08
22X-1	196.12	8.21	68.40	NA	NA	NA	NA	NA
22X-3	199.12	10.87	90.60	10.90	0.05	0.01	0.00	0.11
22X-5	202.12	10.34	86.20	NA	NA	NA	NA	NA
23X-1	205.72	10.88	90.60	NA	NA	NA	NA	NA
23X-3	208.72	11.00	91.70	10.80	0.00	0.00	0.00	0.09
23X-5	211.72	10.88	90.60	NA	NA	NA	NA	NA

Table T16 (continued).

Hole, core, section	Depth (mbsf)	IC (wt%)	$CaCO_3$ (wt%)	TC (wt%)	TOC (wt%)	N (wt%)	S (wt%)	H (mg H/g)
24X-1	215.33	10.74	89.40	NA	NA	NA	NA	NA
24X-3	218.29	10.95	91.20	11.00	0.02	0.01	0.00	0.14
24X-5	221.29	10.96	91.30	NA	NA	NA	NA	NA
25X-1	224.92	10.58	88.20	NA	NA	NA	NA	NA
25X-3	227.92	10.29	85.70	10.40	0.10	0.01	0.00	0.14
25X-5	230.92	10.68	89.00	NA	NA	NA	NA	NA
26X-1	234.52	8.71	72.60	NA	NA	NA	NA	NA
26X-3	237.52	11.11	92.50	11.50	0.39	0.00	0.00	0.06
26X-5	240.52	8.00	66.60	NA	NA	NA	NA	NA
27X-1	244.10	10.61	88.40	NA	NA	NA	NA	NA
27X-3	247.12	10.88	90.60	11.00	0.14	0.00	0.00	0.07
27X-5	250.21	9.83	81.90	NA	NA	NA	NA	NA
28X-1	253.72	6.02	50.20	NA	NA	NA	NA	NA
28X-3	256.64	9.68	80.60	9.76	0.07	0.01	0.00	0.18
28X-5	259.64	8.64	72.00	NA	NA	NA	NA	NA
29X-1	263.32	10.14	84.50	NA	NA	NA	NA	NA
29X-3	266.32	5.14	42.90	5.43	0.28	0.02	0.80	0.62
29X-5	269.32	7.37	61.50	NA	NA	NA	NA	NA
30X-1	272.92	9.68	80.70	NA	NA	NA	NA	NA
30X-3	275.92	8.42	70.10	8.72	0.29	0.01	0.00	0.27
30X-5	278.92	7.69	64.10	NA	NA	NA	NA	NA
31X-1	282.52	7.02	58.50	NA	NA	NA	NA	NA
31X-3	285.52	7.57	63.10	7.68	0.10	0.02	0.00	0.36
31X-5	288.52	7.77	64.70	NA	NA	NA	NA	NA
32X-1	292.12	8.79	73.20	NA	NA	NA	NA	NA
32X-3	295.12	7.09	59.10	7.14	0.04	0.03	0.03	0.37
32X-5	298.12	6.45	53.80	NA	NA	NA	NA	NA
33X-1	301.42	4.21	35.10	NA	NA	NA	NA	NA
33X-3	304.42	4.66	38.80	5.18	0.51	0.03	0.00	0.63
33X-5	307.42	2.08	17.40	NA	NA	NA	NA	NA
34X-1	310.72	6.40	53.40	NA	NA	NA	NA	NA
34X-3	313.72	5.72	47.70	6.03	0.30	0.02	0.00	0.49
34X-5	316.72	5.46	45.50	NA	NA	NA	NA	NA
35X-1	320.32	5.35	44.60	NA	NA	NA	NA	NA
35X-3	323.32	3.51	29.30	3.90	0.38	0.04	0.01	0.67
35X-5	326.32	2.61	21.80	NA	NA	NA	NA	NA
36X-1	329.92	4.12	34.40	NA	NA	NA	NA	NA
36X-3	332.92	4.78	39.90	4.91	0.12	0.04	0.29	0.58
36X-5	335.92	3.25	27.10	NA	NA	NA	NA	NA
37X-1	339.49	4.68	39.00	NA	NA	NA	NA	NA
37X-3	342.07	5.51	45.90	5.50	0.00	0.04	0.00	0.54
38X-1	349.12	4.99	41.60	NA	NA	NA	NA	NA
38X-3	352.12	5.85	48.80	5.86	0.00	0.02	0.00	0.51
38X-5	355.12	5.37	44.80	NA	NA	NA	NA	NA
39X-1	358.72	5.14	42.90	NA	NA	NA	NA	NA
39X-3	361.72	4.68	39.00	4.79	0.10	0.02	0.00	0.57
39X-5	364.72	3.85	32.10	NA	NA	NA	NA	NA
40X-1	368.32	6.39	53.30	NA	NA	NA	NA	NA
40X-3	371.32	5.93	49.40	5.95	0.01	0.02	0.02	0.47
40X-5	374.32	4.27	35.60	NA	NA	NA	NA	NA
41X-1	378.12	5.86	48.90	NA	NA	NA	NA	NA
41X-3	381.01	3.33	27.80	3.47	0.13	0.06	0.00	0.68
41X-5	384.08	5.70	47.60	NA	NA	NA	NA	NA
42X-1	387.62	4.29	35.80	NA	NA	NA	NA	NA
42X-3	390.62	5.07	42.30	5.14	0.06	0.05	0.51	0.61
42X-5	394.08	6.14	51.10	NA	NA	NA	NA	NA
43X-1	397.22	3.53	29.40	NA	NA	NA	NA	NA
43X-3	400.22	4.14	34.50	4.74	0.59	0.05	0.00	0.62
43X-5	403.22	5.12	42.70	NA	NA	NA	NA	NA
44X-1	406.82	4.20	35.00	NA	NA	NA	NA	NA
44X-3	409.88	3.11	25.90	3.36	0.24	0.06	0.42	0.82
44X-5	412.85	3.85	32.10	NA	NA	NA	NA	NA
45X-1	416.42	3.08	25.70	NA	NA	NA	NA	NA
45X-3	419.42	2.30	19.20	2.52	0.21	0.07	0.18	0.85
45X-5	422.42	3.11	25.90	NA	NA	NA	NA	NA
46X-1	425.86	3.40	28.30	NA	NA	NA	NA	NA
46X-3	429.02	3.01	25.10	3.32	0.30	0.05	0.00	0.73
46X-5	432.14	3.50	29.20	NA	NA	NA	NA	NA
47X-1	435.62	2.88	24.00	NA	NA	NA	NA	NA
47X-3	438.62	2.81	23.40	2.95	0.14	0.06	0.00	0.78

Table T16 (continued).

Hole, core, section	Depth (mbsf)	IC (wt%)	$CaCO_3$ (wt%)	TC (wt%)	TOC (wt%)	N (wt%)	S (wt%)	H (mg H/g)
47X-5	441.62	2.96	24.70	NA	NA	NA	NA	NA
48X-1	445.22	2.95	24.60	NA	NA	NA	NA	NA
48X-3	448.22	1.06	8.89	1.44	0.37	0.07	0.68	1.04
48X-5	451.22	1.24	10.40	NA	NA	NA	NA	NA
49X-1	454.82	3.82	31.80	NA	NA	NA	NA	NA
49X-3	457.82	3.03	25.30	3.13	0.09	0.05	0.00	0.82
49X-5	460.82	4.16	34.70	NA	NA	NA	NA	NA
50X-1	464.42	3.68	30.70	NA	NA	NA	NA	NA
50X-3	467.42	2.74	22.90	2.82	0.07	0.05	0.04	0.74
50X-5	470.42	1.64	13.70	NA	NA	NA	NA	NA
51X-1	474.02	1.85	15.40	NA	NA	NA	NA	NA
51X-3	477.34	1.86	15.50	2.27	0.40	0.07	0.00	0.97
51X-5	480.33	1.71	14.30	NA	NA	NA	NA	NA
52X-1	483.62	2.71	22.60	NA	NA	NA	NA	NA
52X-3	486.62	3.42	28.50	3.68	0.25	0.06	0.00	0.85
52X-5	489.62	3.46	28.90	NA	NA	NA	NA	NA
53X-1	493.22	2.30	19.20	NA	NA	NA	NA	NA
53X-3	496.22	3.15	26.30	3.27	0.11	0.06	0.00	0.76
53X-5	499.22	2.05	17.10	NA	NA	NA	NA	NA
54X-1	502.82	2.07	17.30	NA	NA	NA	NA	NA
54X-3	506.06	2.92	24.40	3.10	0.17	0.06	0.58	0.79
54X-5	508.82	2.53	21.10	NA	NA	NA	NA	NA
55X-1	512.42	3.29	27.40	NA	NA	NA	NA	NA
55X-3	515.42	3.36	28.00	3.13	0.00	0.06	0.00	0.79
55X-5	518.52	2.70	22.50	NA	NA	NA	NA	NA
56X-1	522.12	3.30	27.50	NA	NA	NA	NA	NA
56X-3	525.12	2.28	19.00	2.66	0.38	0.07	0.41	0.90
56X-5	528.12	1.91	15.90	NA	NA	NA	NA	NA
57X-1	531.82	3.26	27.20	NA	NA	NA	NA	NA
57X-3	534.82	4.59	38.20	4.40	0.00	0.06	0.13	0.68
57X-5	537.82	3.26	27.20	NA	NA	NA	NA	NA
58X-1	541.42	3.76	31.30	NA	NA	NA	NA	NA
58X-3	544.42	3.95	33.00	4.53	0.57	0.06	1.49	0.72
58X-5	547.42	4.96	41.30	NA	NA	NA	NA	NA
59X-1	551.12	4.01	33.40	NA	NA	NA	NA	NA
59X-3	554.12	3.85	32.10	4.52	0.66	0.06	0.00	0.68
59X-5	557.29	5.00	41.70	NA	NA	NA	NA	NA
60X-1	560.81	3.18	26.50	NA	NA	NA	NA	NA
60X-3	563.82	4.56	38.00	4.83	0.26	0.06	6.77	0.52
60X-5	566.83	5.06	42.20	NA	NA	NA	NA	NA
61X-1	570.32	3.11	26.00	NA	NA	NA	NA	NA
61X-3	573.32	3.62	30.20	4.27	0.64	0.06	0.25	0.68
61X-5	576.32	2.95	24.60	NA	NA	NA	NA	NA
62X-1	579.92	3.84	32.00	NA	NA	NA	NA	NA
62X-3	582.92	2.64	22.00	3.29	0.64	0.07	0.01	0.78
62X-5	585.92	3.39	28.30	NA	NA	NA	NA	NA
63X-1	590.02	3.78	31.50	NA	NA	NA	NA	NA
63X-3	592.52	4.71	39.30	5.07	0.35	0.05	0.70	0.56
63X-5	595.65	2.43	20.30	NA	NA	NA	NA	NA
64X-1	598.95	2.78	23.20	NA	NA	NA	NA	NA
64X-3	602.15	3.48	29.00	4.19	0.71	0.07	0.71	0.73
64X-5	605.21	3.25	27.10	NA	NA	NA	NA	NA
65X-1	608.72	3.73	31.10	NA	NA	NA	NA	NA
65X-3	611.63	4.66	38.90	5.06	0.39	0.06	1.29	0.54
65X-5	614.57	1.98	16.60	NA	NA	NA	NA	NA
66X-1	618.32	4.06	33.80	NA	NA	NA	NA	NA
66X-3	621.32	3.76	31.40	4.37	0.60	0.06	1.62	0.66
66X-5	624.32	4.85	40.40	NA	NA	NA	NA	NA
67X-1	627.91	3.96	33.00	NA	NA	NA	NA	NA
67X-3	630.64	4.16	34.70	5.07	0.90	0.06	0.34	0.65
67X-5	633.27	3.34	27.80	NA	NA	NA	NA	NA
68X-1	637.34	3.35	28.00	NA	NA	NA	NA	NA
68X-3	640.52	3.10	25.90	3.53	0.42	0.05	0.47	0.67
68X-5	643.43	2.07	17.30	NA	NA	NA	NA	NA
69X-1	647.15	4.11	34.30	NA	NA	NA	NA	NA
69X-3	650.12	3.88	32.40	3.98	0.09	0.06	0.41	0.60
69X-5	653.06	3.97	33.10	NA	NA	NA	NA	NA
70X-1	656.82	4.55	37.90	NA	NA	NA	NA	NA
70X-3	659.82	3.45	28.70	3.54	0.08	NA	NA	NA
71X-1	666.52	1.09	9.15	NA	NA	NA	NA	NA

Table T16 (continued).

Hole, core, section	Depth (mbsf)	IC (wt%)	$CaCO_3$ (wt%)	TC (wt%)	TOC (wt%)	N (wt%)	S (wt%)	H (mg H/g)
71X-3	669.52	2.66	22.20	3.01	0.34	0.05	0.03	0.62
71X-5	672.52	1.70	14.20	NA	NA	NA	NA	NA
72X-1	676.09	2.41	20.10	NA	NA	NA	NA	NA
72X-3	679.10	2.27	18.90	2.79	0.51	0.06	0.00	0.69
73X-1	685.72	2.52	21.00	NA	NA	NA	NA	NA
73X-3	688.70	2.21	18.40	2.66	0.44	0.06	1.43	0.69
74X-1	695.08	2.51	20.90	NA	NA	NA	NA	NA
74X-3	698.42	2.40	20.00	2.74	0.34	0.03	0.27	0.73
74X-5	701.40	1.66	13.90	NA	NA	NA	NA	NA
75X-1	705.02	3.99	33.30	NA	NA	NA	NA	NA
75X-3	708.02	2.16	18.00	2.78	0.61	0.05	2.74	0.58
75X-5	711.02	1.21	10.10	NA	NA	NA	NA	NA
76X-1	714.62	2.01	16.80	NA	NA	NA	NA	NA
76X-3	717.62	1.13	9.48	2.83	1.69	0.07	0.73	0.84
76X-5	720.62	1.09	9.08	NA	NA	NA	NA	NA
77X-1	724.32	0.13	1.11	NA	NA	NA	NA	NA
77X-3	727.32	1.76	14.70	2.27	0.50	0.03	0.32	0.59
77X-5	730.32	0.21	1.76	NA	NA	NA	NA	NA
78X-3	735.87	0.82	6.87	2.85	2.02	0.09	0.68	0.96
78X-5	739.00	2.15	18.00	NA	NA	NA	NA	NA
79X-1	743.43	2.76	23.00	NA	NA	NA	NA	NA
79X-3	746.58	4.49	37.40	5.75	1.26	0.03	0.74	0.48
79X-5	749.81	2.07	17.30	NA	NA	NA	NA	NA
80X-1	753.12	0.31	2.65	NA	NA	NA	NA	NA
80X-3	756.12	1.04	8.67	2.65	1.60	0.07	1.16	0.70
80X-5	759.12	0.41	3.44	NA	NA	NA	NA	NA
81X-1	762.72	4.59	38.30	NA	NA	NA	NA	NA
81X-3	765.61	0.00	0.05	1.92	1.91	0.05	1.13	0.34
81X-5	768.20	0.00	0.00	NA	NA	NA	NA	NA
82X-1	772.04	0.81	6.76	NA	NA	NA	NA	NA
82X-3	775.32	0.01	0.12	2.59	2.57	0.05	1.13	0.42
82X-5	778.32	0.01	0.09	NA	NA	NA	NA	NA
83X-1	781.64	0.36	3.05	NA	NA	NA	NA	NA
83X-3	784.80	0.46	3.88	4.04	3.57	0.11	1.98	0.98
83X-5	787.90	0.47	3.97	NA	NA	NA	NA	NA
84X-1	791.52	0.79	6.60	NA	NA	NA	NA	NA
84X-3	794.82	0.40	3.37	4.24	3.83	0.12	1.78	1.01
84X-5	797.56	0.36	3.03	NA	NA	NA	NA	NA
85X-1	801.06	0.61	5.14	NA	NA	NA	NA	NA
85X-3	804.08	0.52	4.34	4.87	4.34	0.14	2.23	1.11
85X-5	807.02	0.54	4.52	NA	NA	NA	NA	NA
86X-1	810.62	0.47	3.97	NA	NA	NA	NA	NA
86X-3	813.62	0.44	3.71	2.66	2.21	0.09	1.71	0.83
86X-5	816.62	0.47	3.96	NA	NA	NA	NA	NA
87X-1	820.22	0.52	4.36	NA	NA	NA	NA	NA
87X-3	823.22	0.38	3.22	5.34	4.95	0.15	1.86	1.11
87X-5	826.21	0.96	8.01	NA	NA	NA	NA	NA
88X-1	829.80	0.18	1.55	NA	NA	NA	NA	NA
88X-3	832.82	1.19	9.94	5.67	4.47	0.15	1.14	1.14
88X-5	835.80	1.04	8.69	NA	NA	NA	NA	NA
89X-1	839.42	1.04	8.73	NA	NA	NA	NA	NA
89X-3	842.42	1.50	12.50	6.71	5.20	0.17	0.16	1.20
89X-5	845.42	1.00	8.36	NA	NA	NA	NA	NA
90X-1	849.02	0.00	0.00	5.01	5.01	0.11	1.40	0.79
91X-1	856.12	0.00	0.00	NA	NA	NA	NA	NA
91X-3	859.12	0.00	0.00	5.65	5.65	0.12	1.29	0.97
91X-5	862.12	0.00	0.00	NA	NA	NA	NA	NA
92X-1	862.11	0.03	0.28	NA	NA	NA	NA	NA
92X-3	865.14	0.19	1.59	4.71	4.52	0.10	0.79	0.77
92X-5	867.97	0.11	0.97	NA	NA	NA	NA	NA
93X-1	868.28	0.00	0.00	NA	NA	NA	NA	NA
93X-3	871.22	0.00	0.00	4.32	4.32	0.10	1.83	0.81
93X-5	874.20	0.00	0.01	NA	NA	NA	NA	NA
94X-1	874.22	0.00	0.00	NA	NA	NA	NA	NA
94X-3	877.05	0.84	7.02	6.52	5.67	0.18	2.18	1.17
95X-1	878.00	0.00	0.00	5.45	5.44	0.12	1.18	0.96

Notes: IC = inorganic carbon, $CaCO_3$ = calcium carbonate, TC = total carbon, TOC = total organic carbon, N = total nitrogen, S = total sulfur, H = hydrogen. NA = not analyzed.

Table T17. Results of Rock-Eval analyses on sediments, Hole 1168A. (See table notes. Continued on next page.)

Hole, core, section	Depth (mbsf)	T_{max} (°C)	S_1	S_2	S_3	TOC (%)	HI	OI
189-1168A-								
1H-4	4.50	360	0.02	0.09	1.49	0.04	225	3725
2H-4	11.80	410	0.05	0.35	1.79	0.23	152	780
3H-4	21.30	372	0.05	0.27	1.58	0.06	442	2633
4H-4	30.75	523	0.06	0.22	1.21	0.04	538	3025
5H-4	40.30	565	0.07	0.11	0.79	0.03	366	2633
6H-4	49.80	482	0.07	0.05	1.29	0.04	125	3225
7H-4	59.30	550	0.11	0.06	0.88	0.06	100	1466
8H-4	68.80	448	0.10	0.19	0.68	0.04	492	1991
9H-4	78.30		0.07	0.00	1.05	0.02	0	5250
10H-4	87.80	400	0.11	0.05	1.17	0.04	125	2925
11H-4	97.30	555	0.07	0.21	0.87	0.10	210	870
12H-4	106.80	507	0.07	0.33	0.87	0.06	553	1356
13X-3	114.80	525	0.04	0.12	0.76	0.03	475	3275
14X-4	123.00	546	0.08	0.07	0.65	0.03	233	2717
15X-4	132.30	541	0.14	0.32	0.52	0.05	613	1775
16X-4	142.20	436	0.05	0.03	0.48	0.02	150	2400
17X-4	151.80	471	0.07	0.10	0.53	0.03	492	2100
18X-4	161.40	512	0.09	0.06	0.41	0.02	300	2050
19X-4	171.10	473	0.13	0.07	0.92	0.04	175	2300
20X-4	180.60	349	0.06	0.03	0.43	0.01	300	4300
21X-4	190.20	510	0.17	0.14	0.74	0.03	450	2725
22X-4	199.90	542	0.14	0.09	0.50	0.03	300	1666
23X-4	209.50	474	0.18	0.09	0.59	0.03	300	1966
24X-4	219.10	473	0.05	0.08	0.84	0.03	266	2800
25X-4	228.70	520	0.07	0.09	0.55	0.03	300	1833
26X-4	238.30		0.09	0.00	0.48	0.01	0	4800
27X-4	247.90		0.11	0.00	0.79	0.08	0	987
28X-5	259.64		0.16	0.00	1.07	0.06	0	1783
29X-4	267.10	526	0.08	0.10	1.00	0.11	82	971
30X-4	276.70	543	0.15	0.24	0.60	0.04	600	1500
31X-4	286.30	506	0.10	0.10	1.00	0.07	142	1428
32X-4	295.90	411	0.09	0.01	1.55	0.07	14	2214
33X-4	305.20	434	0.05	0.02	1.58	0.19	10	831
34X-4	314.50	430	0.09	0.02	1.38	0.14	14	985
35X-4	324.10		0.06	0.00	1.83	0.12	0	1525
36X-4	333.70	441	0.14	0.38	1.42	0.48	78	295
37X-4	343.30	582	0.11	0.36	1.70	0.11	327	1545
38X-4	352.90	573	0.09	0.16	1.35	0.11	145	1227
39X-4	362.50	458	0.11	0.29	1.58	0.14	207	1128
40X-4	372.10		0.11	0.02	1.10	0.10	15	1160
41X-4	381.80	462	0.13	0.39	0.85	0.15	260	566
42X-4	391.40	390	0.08	0.11	1.62	0.21	52	771
43X-4	401.00	530	0.04	0.14	1.15	0.12	116	958
43X-5	403.95	501	0.04	0.15	1.83	0.34	45	546
44X-4	410.60	354	0.12	0.10	1.87	0.21	47	890
45X-4	420.20	428	0.13	0.55	1.23	0.29	168	425
46X-4	429.80	424	0.06	0.14	1.09	0.16	87	681
47X-4	439.40	383	0.09	0.10	1.23	0.18	55	683
48X-4	449.00	530	0.08	0.08	1.14	0.14	57	814
49X-4	458.60	582	0.03	0.10	1.13	0.16	62	706
50X-4	468.20	584	0.04	0.49	1.44	0.22	222	654
51X-4	477.80	522	0.11	0.43	1.69	0.35	131	511
52X-3	485.90	537	0.15	0.22	1.22	0.17	129	717
53X-4	497.00	454	0.05	0.14	1.06	0.19	73	557
54X-4	506.60	567	0.07	0.45	1.45	0.49	91	295
55X-4	516.20	467	0.04	0.21	1.26	0.21	100	600
56X-4	525.90	417	0.16	0.67	1.13	0.57	117	191
57X-4	535.60	474	0.15	0.45	0.83	0.40	112	207
58X-4	545.20	413	0.13	0.48	0.67	0.47	102	142
59X-4	554.90	411	0.14	0.79	0.93	0.69	115	135
60X-4	564.50	416	0.11	0.51	1.08	0.53	96	203
61X-4	574.10	427	0.08	1.04	1.46	0.87	119	167
62X-4	583.70	406	0.11	0.44	1.69	0.69	63	244
63X-4	593.30	406	0.04	0.26	1.06	0.60	125	211
64X-4	602.90	407	0.06	0.22	1.28	0.48	45	266
65X-4	612.50	405	0.09	0.24	1.08	0.63	38	171
66X-4	622.10	419	0.10	0.39	1.25	0.60	65	208

Table T17 (continued).

Hole, core, section	Depth (mbsf)	T_{max} (°C)	S_1	S_2	S_3	TOC (%)	HI	OI
67X-4	631.70	412	0.17	0.62	1.34	0.56	110	239
68X-4	641.30	404	0.10	0.28	1.20	1.00	28	120
69X-4	650.90	413	0.13	0.53	1.14	0.58	91	196
70X-3	659.10	433	0.11	0.36	0.94	0.25	144	376
71X-4	670.30	407	0.05	0.50	0.93	0.46	108	202
72X-3	678.40	418	0.21	0.44	1.38	0.68	64	202
73X-4	689.50	412	0.07	0.63	1.05	0.64	98	164
74X-4	699.20	404	0.17	0.21	0.95	0.65	32	146
75X-4	708.02	423	0.10	0.88	1.04	1.04	84	100
76X-4	718.40	429	0.05	1.74	1.20	2.03	85	59
77X-4	728.10	412	0.06	0.25	0.61	0.60	42	102
78X-4	736.65	429	0.01	1.12	1.07	1.89	59	56
79X-4	747.30	426	0.02	1.90	1.49	2.05	92	72
80X-4	756.90	507	0.05	1.51	1.03	1.69	89	60
81X-4	765.98	589	0.05	1.46	0.42	0.41	363	111
82X-4	776.10	429	0.04	4.17	1.21	3.22	146	40
83X-4	785.70	428	0.07	2.17	1.32	2.50	87	53
84X-4	795.30	430	0.07	3.05	1.32	3.14	97	42
85X-4	804.90	427	0.23	5.81	1.85	4.46	130	41
86X-4	814.40	432	0.21	1.92	1.20	2.37	81	50
87X-4	824.00	433	0.13	5.34	1.54	2.92	182	52
88X-4	833.60	432	0.11	4.39	5.09	4.10	107	124
89X-4	843.20	432	0.07	5.80	6.92	4.54	127	152
90X-1	848.30	426	0.06	6.30	0.99	4.54	138	21
90X-CC	850.24	432	0.08	5.09	5.08	2.86	177	177
91X-4	859.90	424	0.09	5.83	1.21	4.32	134	28
92X-4	865.90	427	0.05	7.31	1.32	4.51	162	29
93X-4	872.00	429	0.06	6.73	1.14	4.85	138	23
94X-2	875.00	429	0.03	8.32	1.33	4.85	171	27
95X-1	877.50	432	0.07	4.01	6.56	2.50	161	264

Notes: T_{max} = temperature (°C) of maximum hydrocarbon generation from kerogen. S_1 = volatile hydrocarbons; S_2 = kerogen-derived hydrocarbons; S_3 = organic CO_2 from kerogen. TOC = total organic carbon obtained by Rock-Eval analysis. HI = hydrogen index, OI = oxygen index. Blanks = no data.

Table T18. Headspace gas composition, Hole 1168A.

Hole, core, section	Depth (mbsf)	C_1 (ppmv)	C_2 (ppmv)	$C_2^=$ (ppmv)	C_3 (ppmv)
189-1168A-					
1H-4	4.50	2417	1	0.0	0
2H-4	11.80	39	0	0.0	0
3H-4	21.30	5	0	0.0	0
4H-4	30.75	3	0	0.0	0
5H-4	40.30	2	0	0.0	0
6H-4	49.80	3	0	0.0	0
7H-4	59.30	4	0	0.0	0
8H-4	68.80	4	0	0.0	0
9H-4	78.30	4	0	0.0	0
10H-4	87.80	6	0	0.0	0
11H-4	97.30	20	0	0.0	0
12H-4	106.80	37	0	0.0	0
13X-3	114.80	58	0	0.0	0
14X-4	123.00	62	0	0.0	0
15X-4	132.30	66	0	0.0	0
16X-4	142.20	74	0	0.0	0
17X-4	151.80	117	0	0.0	0
18X-4	161.40	49	0	0.0	0
20X-4	180.60	172	0	0.0	0
21X-4	190.20	150	0	0.0	0
22X-4	199.90	216	0	0.0	0
23X-4	209.50	182	0	0.0	0
24X-4	219.10	339	0	0.0	0
25X-4	228.70	716	0	0.0	0
26X-4	238.30	2062	0	0.0	0
27X-4	247.90	2240	0	0.0	0
28X-5	259.64	4375	1	0.0	0
29X-4	267.10	6399	1	0.0	0
30X-4	276.70	7655	1	0.0	0
31X-4	286.30	9211	1	0.0	0
32X-4	295.90	7010	1	0.0	0
33X-4	305.20	9575	2	0.0	0
34X-4	314.50	15547	5	0.0	0
35X-4	324.10	14908	7	0.0	0
36X-4	333.70	15806	11	0.0	0
37X-4	343.30	17905	13	0.0	0
38X-4	352.90	26068	22	0.0	0
39X-4	362.50	29122	27	0.0	0
40X-4	372.10	25958	28	0.0	0
41X-4	381.80	28100	30	0.0	0
42X-4	391.40	40075	50	0.0	6
43X-4	401.00	51823	67	0.0	7
43X-5	403.95	25933	39	0.0	4
44X-4	410.60	36626	54	0.0	7
45X-4	420.20	4925	15	0.0	0
46X-4	429.80	9863	15	0.0	0
47X-4	439.40	10520	21	0.0	0
48X-4	449.00	43850	63	0.0	9
49X-4	458.60	39152	61	0.0	10
50X-4	468.20	23740	44	0.0	7
51X-4	477.80	16800	31	0.0	7
52X-3	485.90	38334	63	0.0	9
53X-4	497.00	15316	31	0.0	6
54X-4	506.60	18566	44	0.0	11
55X-4	516.20	11994	26	0.0	5
56X-4	525.90	5209	19	0.0	0
57X-4	535.60	9320	31	0.0	8
60X-4	564.50	3839	14	0.0	0
61X-4	574.10	1715	7	0.0	0
62X-4	583.70	19385	62	0.0	15
63X-4	593.30	6505	17	0.0	4
64X-4	602.90	14423	38	0.0	8
65X-4	612.50	4003	11	0.0	0
67X-4	631.70	7407	21	0.0	7
68X-4	641.30	13694	32	0.0	8
69X-4	650.90	6795	17	0.0	0
70X-3	659.10	4056	7	0.0	0
71X-4	670.30	4179	11	0.0	5
72X-3	678.40	8156	23	0.0	9
73X-4	689.50	7712	16	0.0	10
74X-4	699.20	3294	9	0.0	6
75X-4	708.02	9627	29	0.0	9
76X-4	718.40	8884	27	0.0	7
77X-4	728.10	17820	15	0.0	4
78X-4	736.65	18147	16	0.0	0
79X-4	747.30	6171	11	0.0	0
80X-4	756.90	5825	8	0.0	0
81X-4	765.98	2755	3	0.0	0
82X-4	776.10	9699	53	0.8	3
83X-4	785.70	19735	57	0.0	5
84X-4	795.30	5715	45	0.0	6
85X-4	804.90	8503	105	0.6	15
86X-4	814.40	6767	36	0.0	4
87X-4	824.00	29510	183	0.0	18
88X-4	843.20	4267	177	0.8	17
89X-1	848.30	28673	164	0.0	10
90X-CC	850.24	20452	130	0.0	8
91X-4	859.90	8945	225	1.5	14
92X-4	865.90	8963	121	0.7	6
93X-4	872.00	11564	127	1.5	6
94X-2	875.00	17884	178	0.9	8
95X-1	877.50	24361	264	0.0	23

Note: C_1 = methane, C_2 = ethane, C_3 = propane, ppmv = parts per million by volume.

Table T19. Interstitial water data, Hole 1168A.

Core, section, interval (cm)	Depth (mbsf)	pH	Alkalinity (mM)	Salinity	Cl^- (mM)	SO_4^{2-} (mM)	Na^+ (mM)	Mg^{2+} (mM)	Ca^{2+} (mM)	K^+ (mM)	$H_4SiO_4^0$ (µM)	NH_4^+ (µM)	Sr^{2+} (µM)	Li^+ (µM)
189-1168A-														
1H-3, 145-150	4.45	7.50	3.92	34	559	28.1	485	52.8	10.6	12.2	249	72	157	14
2H-3, 145-150	11.75	7.33	4.41	34	560	25.0	482	50.5	10.6	12.4	385	125	240	14
3H-3, 145-150	21.25	7.07	5.40	34	564	22.7	483	49.1	10.6	12.0	488	250	332	NM
4H-3, 145-150	30.70	7.32	6.00	34	562	20.5	482	47.2	10.6	11.6	430	331	405	16
5H-3, 145-150	40.25	7.32	6.53	34	560	19.3	486	46.4	10.7	11.0	415	357	NM	30
6H-3, 140-150	49.70	7.24	6.75	34	562	17.5	483	45.4	10.7	10.4	432	444	573	31
7H-3, 140-150	59.20	7.23	7.05	34	561	14.1	474	44.7	10.6	10.0	565	488	621	33
8H-3, 140-150	68.70	7.16	7.23	34	558	13.5	476	43.4	10.8	9.9	592	595	674	24
9H-3, 140-150	78.20	7.16	9.11	34	559	13.6	483	42.0	10.6	9.8	586	647	NM	28
10H-3, 140-150	87.70	7.22	7.76	33	559	12.0	485	41.2	11.3	9.7	588	710	781	42
11H-3, 140-150	97.20	7.16	7.47	33	560	10.2	481	41.0	11.6	9.2	614	716	796	45
14X-3, 140-150	122.90	7.39	NM	33	560	8.2	478	39.6	11.7	8.5	804	825	908	46
17X-3, 140-150	151.70	7.13	7.66	32	558	7.2	480	38.1	11.7	8.1	805	952	907	67
20X-3, 140-150	180.50	7.27	8.05	32	557	4.6	478	37.2	11.1	8.8	772	1037	909	75
23X-3, 140-150	209.40	7.29	8.14	32	557	2.9	475	36.3	10.3	7.5	774	1139	873	99
26X-3, 140-150	238.20	7.33	7.43	32	554	0.0	481	35.0	9.7	8.2	448	1275	889	NM
29X-3, 140-150	267.00	7.43	5.91	31	555	0.0	476	33.2	9.9	7.8	324	1299	NM	175
32X-3, 140-150	295.80	7.51	4.37	31	551	0.0	472	31.8	11.1	7.0	468	1305	727	240
35X-3, 140-150	324.00	7.63	3.97	30	550	0.0	456	30.9	12.1	5.8	229	1141	636	324
38X-3, 140-150	352.80	7.53	3.96	30	541	0.0	456	28.9	14.0	6.4	249	1440	NM	426
41X-3, 135-150	381.65	7.43	NM	30	523	0.0	442	26.9	16.6	5.1	425	1355	424	510
44X-3, 135-150	410.45	NM	NM	29	508	0.0	428	24.8	18.1	4.6	591	1438	352	632
47X-3, 135-150	439.25	7.13	5.67	30	526	0.0	436	24.6	20.0	4.6	715	1607	314	712
50X-3, 135-150	468.05	7.20	6.24	29	510	1.0	427	22.6	20.1	4.4	609	1579	267	730
53X-3, 135-150	496.85	NM	NM	30	518	0.0	437	21.6	20.1	4.6	787	1837	251	847
56X-3, 135-150	525.75	NM	NM	29	517	0.0	440	20.4	19.0	4.6	356	1964	233	808
59X-3, 135-150	554.75	7.29	6.98	30	517	0.0	451	20.2	18.7	4.4	462	1888	217	890
62X-3, 135-150	583.55	NM	NM	NM	493	0.0	416	20.1	18.0	3.5	585	1668	216	822
65X-3, 135-150	612.35	NM	NM	28	495	0.0	427	18.8	15.8	3.7	458	1825	NM	767
68X-3, 135-150	641.15	NM	NM	28	505	0.0	439	19.0	14.3	3.7	521	2218	194	739
71X-3, 135-150	670.15	NM	NM	NM	477	0.0	415	17.0	12.3	2.9	462	1839	166	674
74X-3, 135-150	699.05	7.53	4.25	27	486	0.0	431	16.2	12.0	3.1	454	1888	168	623
77X-3, 135-150	727.95	NM	NM	25	447	0.0	402	16.2	10.3	4.2	191	1706	136	568
80X-3, 135-150	756.75	7.39	14.31	27	484	0.0	451	16.3	10.6	3.4	574	2184	135	546
83X-3, 135-150	785.55	NM	NM	28	475	1.1	445	15.9	9.8	3.1	487	2168	118	492
86X-3, 135-150	814.25	8.00	7.61	26	468	0.0	440	14.6	7.8	3.4	248	2259	118	406
89X-3, 135-150	843.05	NM	NM	26	440	0.0	415	15.2	7.1	3.2	297	1789	108	378
92X-3, 135-150	865.75	7.01	19.28	27	463	0.0	452	13.7	5.8	3.8	364	2255	112	277

Note: NM = not measured.

Table T20. *P*-wave velocities measured at discrete intervals, Hole 1168A. (See table notes. Continued on next page.)

Core, section, interval (cm)	Depth (mbsf)	PWS1 (km/s)	PWS2 (km/s)	PWS3 (km/s)
189-1168A-				
1H-1, 21.7	0.22	1.565	1.440	
1H-2, 48.1	1.98	1.586	1.588	
1H-3, 23.4	3.23	1.567	1.562	
1H-4, 46	4.96	1.642	1.679	
1H-5, 47.9	6.48	1.630		1.718
2H-1, 132.4	8.62			1.570
2H-1, 137.3	8.67			1.722
2H-2, 48.3	9.28	1.596	1.608	
2H-2, 49	9.29			1.706
2H-3, 47.5	10.77			1.563
2H-3, 47.7	10.78	1.565		1.661
2H-4, 47.7	12.28	1.590	1.590	1.695
2H-5, 47.6		1.554		
2H-5, 48.1	13.78			1.646
2H-6, 77.1	15.57	1.555	1.581	
2H-6, 77.6	15.58			1.660
3H-1, 99.5	17.80	1.553	1.570	1.641
3H-2, 0.6	18.31	1.573		
3H-2, 21.8	18.52		1.579	1.649
3H-3, 98.9	20.79	1.548	1.466	1.632
3H-4, 95.8	22.26	1.559	1.537	1.672
3H-5, 78.7	23.59	1.588	1.582	1.689
3H-6, 82.4	25.12	1.580	1.598	1.692
3H-7, 5.2	25.85	1.569	1.567	1.665
4H-1, 48	26.78	1.566		
4H-2, 47.9	28.28	1.586		1.679
4H-3, 45.3	29.70	1.567		1.662
4H-4, 48.1	31.23	1.558		1.657
4H-5, 55.2	32.80	1.561		1.632
4H-6, 48	34.13	1.564		1.655
4H-7, 48	35.63	1.546		1.633
5H-1, 48	36.28	1.549	1.520	
5H-2, 48	37.78	1.547	1.538	
5H-3, 48	39.28	1.547	1.544	1.635
5H-4, 47.8	40.78	1.554	1.489	1.650
5H-5, 48	42.18	1.587	1.588	1.683
5H-6, 54.7	43.75	1.629	1.648	1.707
5H-7, 65.5	45.35	1.667	1.651	
5H-7, 65.6	45.36			1.771
6H-2, 48	47.28	1.604	1.587	
6H-3, 48	48.78	1.623	1.642	1.722
6H-4, 48.2	50.28	1.634	1.667	1.790
6H-5, 48.6	51.74	1.637	1.651	1.743
6H-6, 48	53.23	1.635	1.631	2.577
6H-7, 48	54.73	1.601		1.725
7H-1, 48.6	55.29	1.610	1.610	2.497
7H-2, 40.1	56.70	1.595	1.580	1.726
7H-3, 48.9	58.29	1.576		1.675
7H-4, 47.9	59.78	1.618	1.628	1.718
7H-5, 53.4	61.33	1.604	1.605	
7H-5, 112.2	61.92			1.724
7H-6, 48.1	62.78	1.554	1.579	1.668
7H-7, 48.1	64.28	1.563	1.595	1.678
8H-1, 49.8	64.80	1.555		1.707
8H-2, 47.8	66.28			1.743
8H-3, 25.7	67.56	1.608		1.739
8H-4, 37.5	69.18	1.593		1.729
8H-5, 48.1	70.78	1.598	1.567	1.773
8H-6, 48.1	72.28			1.746
8H-7, 48.4	73.28			1.686
9H-1, 48.1	74.28	1.565	1.596	1.664
9H-2, 48.5	75.79	1.582	1.585	1.668
9H-3, 48.4	77.28	1.575	1.594	1.660
9H-4, 49.2	78.79	1.573	1.627	2.024
9H-5, 49.1	80.29	1.599	1.643	1.720
9H-6, 48.7	81.79	1.631	1.601	1.729
10H-1, 48	83.78	1.571	1.595	1.669
10H-2, 55.6	85.36	1.588	1.629	1.675
10H-3, 46.8	86.77		1.647	1.732
10H-4, 48.1	88.28	1.629	1.628	1.731
10H-5, 48.6	89.79	1.612	1.588	1.734
10H-6, 49.2	91.29	1.594	1.622	1.695
10H-7, 48.7	92.79	1.594	1.533	1.707
11H-1, 97.5	93.78	1.543	1.567	1.752
11H-2, 48.1	94.78	1.557	1.560	1.773
11H-3, 48.1	96.28	1.543	1.524	1.769
11H-4, 64.1	97.94	1.553	1.577	1.765
11H-5, 48.1	99.28	1.579	1.594	1.793
11H-6, 48.1	100.78	1.601	1.587	1.831
11H-7, 27.9	102.08	1.566	1.524	1.801
12H-1, 48.2	102.78	1.566	1.551	1.784
12H-2, 48.2	104.28	1.559	1.558	1.789
12H-3, 48.1	105.78	1.561	1.574	1.792
12H-4, 48	107.28	1.562	1.536	1.809
12H-5, 48	108.78	1.549	1.593	1.811
12H-6, 48	110.28			1.791
12H-7, 22.8	111.53			1.889
13X-1, 48.1	112.28	1.580		1.841
13X-2, 48.1	113.78	1.550		1.809
13X-3, 48.1	115.28	1.559	1.539	1.823
14X-1, 48.1	118.98	1.538	1.536	1.802
14X-2, 47.9	120.48	1.558	1.573	1.810
14X-3, 48.1	121.98	1.566	1.566	1.830
14X-4, 48.2	123.48	1.573	1.575	1.855
14X-5, 48.3	124.98	1.582	1.567	1.854
15X-1, 48.1	128.58	1.544	1.534	1.819
15X-2, 48.2	130.08	1.541		1.776
15X-3, 48.1	131.58	1.569		1.879
15X-4, 29	132.59	1.550		1.851
16X-1, 48	138.18	1.551	1.564	1.822
16X-2, 48.1	139.68			1.795
16X-3, 48.1	141.18	1.547	1.559	1.816
16X-4, 47.9	142.68	1.543		1.817
16X-5, 48	144.18	1.549		1.821
17X-1, 48	147.78	1.532	1.536	1.792
17X-2, 48	149.28	1.537		1.792
17X-3, 48.1	150.78	1.524		1.792
17X-4, 47.9	152.28	1.534		1.789
17X-5, 48	153.78	1.537		1.797
18X-1, 48	157.38	1.544		1.816
18X-2, 48	158.88	1.544		1.791
18X-3, 48	160.38	1.548		1.833
18X-4, 48.1	161.88	1.544		1.802
18X-5, 48	163.38	1.545		1.799
19X-1, 48.4	166.98	1.548		1.788
19X-2, 49.1	168.49	1.541		1.783
19X-3, 48.8	169.99	1.543		1.790
19X-4, 48.3	171.48	1.730		1.763
19X-5, 48.6	172.99	1.533		1.789
19X-6, 48.1	174.48	1.531		1.786
20X-1, 48.2	176.58	1.529		1.774
20X-2, 48.5	178.09	1.521		1.763
20X-3, 48.1	179.58	1.532		1.778
20X-4, 48.4	181.08	1.529		1.791
20X-5, 48.1	182.58	1.522		1.772
20X-6, 25.3	183.85	1.524		1.818
21X-1, 48.1	186.18			1.795
21X-2, 48.8	187.69	1.552		1.808
21X-3, 48.1	189.18	1.539		1.803
21X-4, 48.9	190.69	1.536		1.785
21X-5, 49	192.19	1.551		1.800
21X-6, 48.2	193.68	1.539		1.808
22X-1, 48	195.88	1.551		1.828
22X-2, 48.8	197.39	1.567		1.814
22X-3, 51.5	198.91	1.577		1.833

Table T20 (continued).

Core, section, interval (cm)	Depth (mbsf)	PWS1 (km/s)	PWS2 (km/s)	PWS3 (km/s)
22X-4, 48.9	200.39	1.555		1.831
22X-5, 48.2	201.88	1.541		1.805
22X-6, 48.6	203.39	1.569		1.843
22X-7, 17.7	204.58	1.606		1.889
23X-1, 37.4	205.37			1.836
23X-2, 49	206.99			1.787
23X-3, 48	208.48			1.807
23X-4, 48.8	209.99	1.527		1.795
23X-5, 48.8	211.49	1.548		1.824
23X-6, 49.3	212.99	1.545		1.830
23X-7, 18.8	214.19			1.843
24X-1, 49.5	215.10			1.774
24X-2, 49.9	216.60			1.783
24X-3, 51.5	218.12			1.804
24X-4, 48.5	219.59			1.860
24X-5, 48.4	221.08	1.557		1.795
24X-6, 48.7	222.59	1.564		
24X-6, 124.9	223.35			1.824
24X-7, 21.8	223.82	1.566		1.839
25X-1, 48.9	224.69	1.538		1.826
25X-2, 48.3	226.18	1.554		1.851
25X-3, 48.5	227.68	1.551		1.842
25X-4, 48.8	229.19	1.556		1.849
25X-5, 50.3	230.70	1.559		1.839
25X-6, 44.8	232.15	1.557		1.834
26X-1, 48.6	234.29	1.534		1.876
26X-2, 49.5	235.79	1.579		
26X-2, 49.6	235.80			1.866
26X-3, 48.8	237.29	1.557		1.843
26X-4, 48.6	238.79	1.593		1.882
26X-5, 54.3	240.34	1.575		1.857
26X-6, 49.9	241.80			1.904
26X-7, 27.9	243.08			1.868
27X-1, 46.8	243.87			1.918
27X-2, 46.1	245.36			1.917
27X-3, 48.8	246.89			1.959
27X-4, 48.7	248.39			1.900
27X-5, 51	249.91			1.920
27X-6, 62.7	251.53			3.222
27X-6, 68.9	251.59			2.969
27X-7, 18.4	252.58			1.936
28X-1, 52.8	253.53			2.066
28X-2, 50.5	255.01			1.965
28X-3, 50	256.42			2.046
28X-4, 50.2	257.92			2.079
28X-5, 44.9	259.42			1.897
29X-1, 29.4	262.89			1.830
29X-2, 124.3	265.34			1.894
29X-3, 50	266.10			1.917
29X-4, 50.1	267.60			1.881
29X-5, 50.1	269.10			1.942
29X-6, 50.2	270.60			1.971
29X-7, 30.1	271.90			1.974
30X-1, 50	272.70			1.910
30X-2, 50.1	274.20			1.932
30X-3, 50	275.70			1.885
30X-4, 47.2	277.17			2.004
30X-5, 53.9	278.74			2.036
30X-6, 23.1	279.93			1.951
30X-6, 39.3	280.09			1.897
31X-1, 48.1	282.28			1.906
31X-2, 57	283.87			1.957
31X-3, 58.7	285.39			1.955
31X-4, 35.6	286.66			1.891
31X-5, 46.1	288.26			1.905
31X-6, 61.5	289.92			1.926
32X-1, 58.4	291.98			2.108
32X-2, 77.2	293.67			2.009
32X-3, 32	294.72			1.952
32X-4, 48.8	296.39			1.912
32X-5, 42.9	297.83			1.989
32X-6, 44.8	299.35			2.025
33X-1, 133.8	302.04			1.924
33X-2, 55.1	302.75			1.904
33X-3, 47.5	304.17			1.943
33X-4, 50.6	305.71			1.910
33X-5, 78.1	307.48			1.988
33X-6, 53.3	308.73			1.971
34X-1, 47.8	310.48			2.011
34X-2, 54	312.04			1.922
34X-3, 53.3	313.53			1.986
34X-4, 58.5	315.08			1.980
34X-6, 10.9	317.61			1.930
35X-1, 50.1	320.10			1.982
35X-2, 49.5	321.60			2.106
35X-3, 49.8	323.10			2.044
35X-4, 49.5	324.60			2.002
35X-5, 38.2	325.98			1.953
35X-6, 46.8	327.57			2.062
36X-1, 37.2	329.57			1.985
36X-2, 29.6	331.00			2.086
36X-3, 47.4	332.67			2.073
36X-4, 64.8	334.35			2.015
36X-5, 32.1	335.52			2.041
36X-6, 32.9	337.03			2.066
45X-4, 49.1	420.69			2.221
45X-6, 68.5	423.89			2.318
45X-6, 107	424.27			2.527
49X-4, 68.5	459.29			2.292
49X-6, 44	462.04			2.318
51X-1, 121	474.51			2.354
52X-2, 121	485.61			2.290
55X-3, 36	515.06			2.379
56X-1, 132	522.72			2.576
56X-3, 83.2	525.23			2.436
56X-5, 71.1	528.11			2.405
56X-5, 84	528.24			2.584
57X-1, 80	531.90			2.251
57X-2, 73.9	533.34			2.203
75X-6, 65	712.45			5.036
75X-6, 65	712.45			4.900
75X-6, 65	712.45			5.177
75X-6, 65	712.45			4.754
85X-1, 15	800.55			4.928
85X-1, 15	800.55			5.243
85X-1, 15	800.55			4.773

Notes: All *P*-wave velocities measured at discrete intervals. PSW1 = measured along the core, PSW2 = measured perpendicular to the core, PSW3 = measured across the core (Hamilton frame). Blanks = no data.

Table T21. Thermal conductivity measured on whole-core sections, Hole 1168A.

Core, section, interval (cm)	Depth (mbsf)	Thermal conductivity (W/[m·K])
189-1168A-		
2H-3, 75	11.05	0.89
3H-3, 75	20.55	1.09
4H-3, 75	30.00	1.27
5H-3, 75	39.55	1.28
6H-3,75	49.05	1.36
7H-3, 75	58.55	1.29
8H-3, 75	68.05	1.37
9H-3, 75	77.55	1.26
10H-3, 75	87.05	1.34
11H-3, 75	96.55	1.29
12H-3, 75	106.05	1.33

Table T22. Undrained shear strength from miniature vane-shear measurements, Hole 1168A.

Core, section, interval (cm)	Depth (mbsf)	Undrained shear strength (kPa)
189-1168A-		
1H-1,102.4	1.02	21.733
1H-2,100.1	2.50	25.171
1H-3,38.3	3.38	27.056
1H-4, 96.8	5.47	25.393
2H-1, 89.1	8.19	26.058
2H-2,100.1	9.80	24.173
2H-3,100.2	11.30	24.506
2H-4,100.2	12.80	24.284
2H-5, 100	14.30	23.729
2H-6, 100	15.80	25.947
2H-7, 47.4	16.77	25.282
3H-1, 100	17.80	24.395
3H-2,100.2	19.30	44.798
3H-3,100.5	20.81	39.697
3H-4,100.1	22.30	62.539
3H-5,100.3	23.80	36.814
3H-6,100.1	25.30	29.385
3H-7, 26.8	26.07	45.352
4H-2,100.1	28.80	37.59
4H-3, 100	30.25	22.399
4H-4, 97.3	31.72	25.393
4H-5,104.3	33.29	24.395
4H-6, 100	34.65	25.171
4H-7, 54.1	35.69	19.627
5H-1, 100	36.80	29.052
5H-2,100.1	38.30	25.615
5H-3, 99.9	39.80	25.615
5H-4, 100.0	41.30	28.387
5H-5, 99.9	42.70	30.161
5H-6,100.2	44.20	27.5
6H-1, 99.9	46.30	26.28
6H-4,100.1	50.80	30.826
6H-5, 99.9	52.25	27.278
6H-6, 98.9	53.74	37.59
6H-7, 59.5	54.85	37.036
7H-1,103.3	55.83	26.169
7H-2,100.1	57.30	20.847
7H-3, 99.9	58.80	25.171
7H-4,100.6	60.31	33.709
7H-5,100.6	61.81	36.37
7H-6,100.3	63.30	29.828
7H-7, 80.2	64.60	31.602
8H-1,101.4	65.31	24.062
8H-2,100.5	66.81	30.493
8H-3,100.4	68.30	13.861
8H-4, 99.7	69.80	35.927
8H-5,100.3	71.30	25.282
8H-6, 80.6	72.61	16.744
8H-7, 47	73.27	21.955
9H-1, 99.5	74.79	32.157
9H-2, 99.9	76.30	37.368
9H-3,100.1	77.80	58.991
9H-5,100.5	80.81	73.739
9H-6,100.5	82.31	68.749
10H-1, 100	84.30	26.945
10H-2,100.3	85.80	15.302
10H-3, 100	87.30	32.711
10H-4,100.1	88.80	43.134
10H-5, 99.4	90.29	23.729
10H-6,100.3	91.80	20.292
10H-7, 64.1	92.94	41.693
11H-1,123.8	94.04	29.828
11H-3,100.1	96.80	27.5
11H-3,100.2	96.80	36.703
11H-4,100.2	98.30	33.709
11H-5, 100	99.80	53.003
11H-7, 55	102.35	54.445
12H-1, 94.5	103.25	24.617
12H-2,100.1	104.80	37.812
12H-3, 100	106.30	42.469
12H-4,100.1	107.80	40.03
12H-5, 100	109.30	32.6
12H-6,100.1	110.80	42.802
12H-7, 22.6	111.53	42.913
13X-1, 100	112.80	26.28
13X-2 100.2	114.30	26.391
13X-3, 92	115.72	24.506
14X-1, 100	119.50	9.203
14X-2,100.1	121.00	22.177
14X-3, 100	122.50	20.07
14X-4,100.2	124.00	19.627
14X-5, 97.4	125.47	24.838
15X-1, 99.9	129.10	25.725
15X-2, 100	130.60	15.08
15X-3, 100	132.10	17.631
16X-1,100.1	138.70	24.506
16X-2, 100	140.20	24.728
16X-4, 100	143.20	24.617
16X-5, 90	144.60	24.284
17X-1, 100	148.30	28.276
17X-2, 97.1	149.77	23.175
17X-3, 100.0	151.30	24.617
17X-4, 90.1	152.70	47.348
17X-5, 63.2	153.93	48.346
18X-1, 100.0	157.90	23.84
18X-2, 100.0	159.40	24.728
18X-3, 100.0	160.90	24.949
18X-4,100.2	162.40	25.06
18X-5, 100.0	163.90	33.487
19X-1,100.9	167.51	20.957
19X-2,100.5	169.01	13.861
19X-3,100.4	170.50	14.637
19X-4,100.6	172.01	25.725
19X-5, 99.9	173.50	8.871
19X-6,100.2	175.00	19.072
20X-1,100.7	177.11	24.173
20X-2, 100.0	178.60	10.423
20X-3,100.5	180.10	6.32
20X-4, 97.5	181.57	23.175
20X-5, 97.2	183.07	7.984
20X-6, 25.2	183.85	3.77
21X-1, 97.2	186.67	27.943
21X-2, 97.9	188.18	28.276
21X-3, 97.8	189.68	16.855
21X-4, 98.0	191.18	14.526
21X-5, 98.1	192.68	17.076
21X-6, 97.3	194.17	12.974
22X-1, 97.1	196.37	14.637
22X-2, 97.9	197.88	18.961
22X-3,100.6	199.41	27.721
22X-4, 97.9	200.88	31.048
22X-5, 97.3	202.37	29.828
22X-6, 93.3	203.83	41.471
22X-7, 16.0	204.56	49.233
23X-1, 86.5	205.87	29.385
23X-2, 98.1	207.48	17.298
23X-3, 97.1	208.97	32.600
23X-4, 97.9	210.48	21.844
23X-5, 97.9	211.98	18.407
23X-6, 98.4	213.48	28.165
23X-7, 18	214.18	21.068
24X-1, 99.2	215.59	40.473
24X-2, 99.7	217.10	29.163
24X-3, 99.8	218.60	38.477
24X-4, 99.9	220.10	23.729
24X-5,100.2	221.60	36.481
24X-6,121.5	223.32	25.836
24X-7, 21.7	223.82	36.481
25X-1, 103	225.23	17.963
25X-2, 108	226.78	10.867
25X-3, 97.7	228.18	30.715
25X-4, 97.9	229.68	10.312
25X-5, 99.4	231.19	40.695
25X-6, 94	232.64	46.35
26X-1, 97.7	234.78	50.896
26X-2,107.1	236.37	22.953
26X-3, 97.9	237.78	31.048
26X-4, 97.7	239.28	57.217
26X-5,103.4	240.83	42.358
26X-6, 98.9	242.29	29.385
26X-7, 24.9	243.05	33.044
27X-2, 95.2	245.85	46.572
27X-3, 97.9	247.38	53.669
27X-4, 97.8	248.88	76.178
27X-5, 97.3	250.37	56.995
27X-6,119.8	252.10	57.439
27X-7, 22.3	252.62	57.217
29X-1, 100	263.60	40.695

Table T23. Index properties measured at discrete intervals, Hole 1168A. (See table note. Continued on next four pages.)

Core, section, interval (cm)	Depth (mbsf)	Water content (bulk wt%)	Density (g/cm³)		Porosity (%)
			Wet bulk	Dry bulk	
189-1168A-					
1H-1, 71.0-73.0	0.71	35.00	1.71	1.11	58.40
1H-2, 70.0-72.0	2.20	38.80	1.66	1.02	62.90
1H-3, 57.0-59.0	3.57	29.20	1.82	1.29	52.00
1H-4, 70.0-72.0	5.20	33.80	1.75	1.16	57.70
1H-5, 70.0-72.0	6.70	31.70	1.80	1.23	55.70
2H-1, 124.0-126.0	8.54	35.90	1.71	1.09	59.70
2H-2, 70.0-72.0	9.50	36.20	1.69	1.08	59.60
2H-3, 70.0-72.0	11.00	33.60	1.73	1.15	56.90
2H-4, 70.0-72.0	12.50	35.70	1.72	1.11	60.00
2H-5, 70.0-72.0	14.00	34.90	1.72	1.12	58.60
2H-6, 70.0-72.0	15.50	41.00	1.61	0.95	64.60
2H-7, 30.0-32.0	16.60	30.90	1.78	1.23	53.80
3H-1, 70.0-72.0	17.50	33.50	1.75	1.16	57.00
3H-2, 70.0-72.0	19.00	38.20	1.66	1.02	61.90
3H-3, 70.0-72.0	20.50	39.20	1.64	1.00	62.70
3H-4, 70.0-72.0	22.00	32.20	1.77	1.20	55.60
3H-5, 70.0-72.0	23.50	29.90	1.82	1.28	53.20
3H-6, 68.0-70.0	24.98	29.40	1.82	1.28	52.10
3H-7, 56.0-58.0	26.36	32.00	1.78	1.21	55.50
4H-1, 70.0-72.0	27.00	32.00	1.78	1.21	55.50
4H-2, 70.0-72.0	28.50	30.20	1.79	1.25	52.90
4H-3, 70.0-72.0	29.95	34.60	1.73	1.13	58.40
4H-4, 70.0-72.0	31.45	32.20	1.76	1.20	55.30
4H-5, 70.0-72.0	32.95	32.30	1.77	1.20	55.60
4H-6, 70.0-72.0	34.35	33.10	1.76	1.18	56.70
4H-7, 40.0-42.0	35.55	34.00	1.73	1.14	57.60
5H-1, 70.0-72.0	36.50	34.70	1.71	1.12	58.20
5H-2, 70.0-72.0	38.00	32.80	1.76	1.18	56.50
5H-3, 70.0-72.0	39.50	32.20	1.77	1.20	55.50
5H-4, 70.0-72.0	41.00	33.20	1.75	1.17	56.90
5H-5, 70.0-72.0	42.40	31.60	1.78	1.22	55.00
5H-6, 70.0-72.0	43.90	28.80	1.85	1.32	52.10
5H-7, 72.0-74.0	45.42	28.40	1.85	1.33	51.50
6H-2, 70.0-72.0	47.50	31.70	1.77	1.21	54.80
6H-3, 70.0-72.0	49.00	29.50	1.82	1.28	52.20
6H-4, 70.0-72.0	50.50	30.70	1.80	1.25	53.90
6H-5, 70.0-72.0	51.95	29.60	1.81	1.28	52.40
6H-6, 70.0-72.0	53.45	30.20	1.82	1.27	53.70
6H-7, 68.0-70.0	54.93	30.80	1.81	1.25	54.40
7H-1, 73.0-75.0	55.53	30.40	1.80	1.25	53.40
7H-2, 70.0-72.0	57.00	29.40	1.84	1.30	52.80
7H-3, 70.0-72.0	58.50	31.50	1.85	1.27	57.00
7H-5, 70.0-72.0	61.50	31.10	1.83	1.26	55.40
7H-6, 70.0-72.0	63.00	31.00	1.52	1.05	45.90
7H-7, 70.0-72.0	64.50	31.70	1.78	1.22	55.00
8H-1, 70.0-72.0	65.00	31.30	1.79	1.23	54.70
8H-2, 70.0-72.0	66.50	30.70	1.81	1.26	54.40
8H-3, 73.0-75.0	68.03	31.00	1.80	1.24	54.40
8H-4, 70.0-72.0	69.50	29.20	1.82	1.29	52.00
8H-5, 70.0-72.0	71.00	26.90	1.88	1.37	49.40
8H-6, 70.0-72.0	72.50	33.10	1.75	1.17	56.60
8H-7, 63.0-65.0	73.43	31.40	1.77	1.22	54.30
9H-1, 70.0-72.0	74.50	32.80	1.75	1.18	56.10
9H-2, 70.0-72.0	76.00	31.00	1.79	1.24	54.30
9H-3, 70.0-72.0	77.50	31.10	1.78	1.23	54.20
9H-4, 70.0-72.0	79.00	29.70	1.81	1.27	52.60
9H-5, 70.0-72.0	80.50	27.70	1.85	1.34	49.90
9H-6, 70.0-72.0	82.00	28.50	1.84	1.31	51.20
10H-1, 70.0-72.0	84.00	30.70	1.80	1.25	53.80
10H-2, 70.0-72.0	85.50	33.40	1.74	1.16	56.90
10H-3, 70.0-72.0	87.00	30.00	1.81	1.27	53.10
10H-4, 70.0-72.0	88.50	30.80	1.79	1.24	53.90
10H-5, 70.0-72.0	90.00	28.40	1.85	1.32	51.40
10H-6, 70.0-72.0	91.50	30.50	1.79	1.24	53.40
10H-7, 70.0-72.0	93.00	30.30	1.80	1.25	53.30

Table T23 (continued).

Core, section, interval (cm)	Depth (mbsf)	Water content (bulk wt%)	Density (g/cm³)		Porosity (%)
			Wet bulk	Dry bulk	
11H-3, 70.0-72.0	96.50	29.00	1.83	1.30	51.80
11H-5, 70.0-72.0	99.50	30.30	1.80	1.25	53.20
11H-6, 70.0-72.0	101.00	28.70	1.84	1.31	51.40
11H-7, 50.0-52.0	102.30	30.60	1.80	1.25	53.90
12H-1, 70.0-72.0	103.00	31.70	1.79	1.22	55.30
12H-2, 70.0-72.0	104.50	30.00	1.81	1.27	53.10
12H-3, 70.0-72.0	106.00	29.50	1.82	1.28	52.40
12H-4, 70.0-72.0	107.50	30.20	1.82	1.27	53.50
12H-5, 70.0-72.0	109.00	31.40	1.78	1.22	54.60
12H-6, 70.0-72.0	110.50	29.80	1.82	1.28	53.10
12H-7, 30.0-32.0	111.60	30.30	1.80	1.25	53.30
13X-1, 70.0-72.0	112.50	32.90	1.74	1.17	56.00
13X-2, 70.0-72.0	114.00	33.50	1.75	1.16	57.20
14X-1, 70.0-72.0	119.20	36.80	1.67	1.06	60.10
14X-2, 70.0-72.0	120.70	34.20	1.73	1.14	57.70
14X-3, 70.0-72.0	122.20	34.70	1.72	1.12	58.20
14X-4, 70.0-72.0	123.70	34.80	1.72	1.12	58.30
14X-5, 70.0-72.0	125.20	31.60	1.77	1.21	54.50
15X-1, 70.0-72.0	128.80	32.50	1.76	1.19	55.90
15X-2, 70.0-72.0	130.30	35.00	1.71	1.11	58.50
15X-3, 70.0-72.0	131.80	34.50	1.73	1.13	58.20
15X-4, 38.0-40.0	132.68	35.00	1.72	1.12	58.80
16X-1, 70.0-72.0	138.40	32.50	1.76	1.19	56.00
16X-2, 70.0-72.0	139.90	32.60	1.78	1.20	56.50
16X-3, 70.0-72.0	141.40	34.00	1.73	1.14	57.60
16X-4, 70.0-72.0	142.90	34.70	1.72	1.13	58.50
16X-5, 70.0-72.0	144.40	33.80	1.75	1.16	57.80
17X-2, 70.0-72.0	149.50	35.10	1.72	1.12	59.00
17X-4, 70.0-72.0	152.50	33.30	1.73	1.15	56.30
18X-1, 70.0-72.0	157.60	33.30	1.76	1.17	57.10
18X-2, 70.0-72.0	159.10	33.10	1.76	1.17	56.80
18X-3, 70.0-72.0	160.60	33.70	1.75	1.16	57.70
18X-4, 70.0-72.0	162.10	35.20	1.73	1.12	59.40
18X-5, 70.0-72.0	163.60	34.00	1.74	1.15	57.60
19X-1, 70.0-72.0	167.20	34.70	1.73	1.13	58.40
19X-3, 70.0-72.0	170.20	36.20	1.70	1.09	60.10
19X-5, 70.0-72.0	173.20	34.90	1.72	1.12	58.50
20X-1, 70.0-72.0	176.80	36.80	1.68	1.06	60.30
20X-3, 70.0-72.0	179.80	36.20	1.69	1.08	59.70
20X-5, 70.0-72.0	182.80	37.40	1.66	1.04	60.70
21X-1, 70.0-72.0	186.40	34.10	1.73	1.14	57.70
21X-3, 70.0-72.0	189.40	37.20	1.67	1.05	60.70
21X-5, 70.0-72.0	192.40	35.00	1.71	1.11	58.60
22X-1, 70.0-72.0	196.10	34.80	1.71	1.12	58.30
22X-3, 70.0-72.0	199.10	33.30	1.74	1.16	56.80
22X-5, 70.0-72.0	202.10	34.80	1.39	0.91	47.40
23X-1, 70.0-72.0	205.70	33.90	1.74	1.15	57.60
23X-3, 70.0-72.0	208.70	35.90	1.69	1.09	59.40
23X-5, 70.0-72.0	211.70	37.90	1.66	1.03	61.30
24X-1, 74.0-76.0	215.34	32.80	1.76	1.18	56.40
24X-3, 70.0-72.0	218.30	31.20	1.79	1.23	54.60
24X-5, 70.0-72.0	221.30	35.60	1.71	1.10	59.50
25X-1, 70.0-72.0	224.90	35.40	1.72	1.11	59.30
25X-3, 70.0-72.0	227.90	33.90	1.73	1.15	57.40
25X-5, 70.0-72.0	230.90	35.20	1.72	1.12	59.10
26X-1, 70.0-72.0	234.50	34.60	1.73	1.13	58.40
26X-3, 69.0-71.0	237.49	25.10	1.91	1.43	46.80
26X-5, 70.0-72.0	240.50	34.60	1.72	1.12	58.10
27X-1, 71.0-73.0	244.11	30.30	1.81	1.26	53.50
27X-3, 70.0-72.0	247.10	26.00	1.90	1.41	48.30
27X-5, 79.0-81.0	250.19	31.10	1.80	1.24	54.70
28X-1, 70.0-72.0	253.70	27.10	1.88	1.37	49.80
28X-3, 70.0-72.0	256.62	27.30	1.87	1.36	49.70
28X-5, 70.0-72.0	259.62	28.70	1.84	1.31	51.40
29X-1, 70.0-72.0	263.30	30.10	1.81	1.26	53.10
29X-3, 70.0-72.0	266.30	27.40	1.85	1.35	49.60
29X-5, 70.0-72.0	269.30	28.50	1.84	1.31	51.20
30X-1, 70.0-72.0	272.90	31.70	1.78	1.22	55.20

Table T23 (continued).

Core, section, interval (cm)	Depth (mbsf)	Water content (bulk wt%)	Density (g/cm³)		Porosity (%)
			Wet bulk	Dry bulk	
30X-3, 70.0-72.0	275.90	30.10	1.83	1.28	53.60
30X-5, 70.0-72.0	278.90	28.70	1.89	1.35	53.00
31X-1, 70.0-72.0	282.50	28.60	1.85	1.32	51.70
31X-3, 70.0-72.0	285.50	28.70	1.84	1.31	51.50
31X-5, 70.0-72.0	288.50	27.30	1.86	1.36	49.60
32X-1, 70.0-72.0	292.10	25.90	1.89	1.40	47.90
32X-3, 70.0-72.0	295.10	26.70	1.87	1.37	48.70
32X-5, 70.0-72.0	298.10	26.50	1.88	1.38	48.80
33X-1, 70.0-72.0	301.40	26.70	1.88	1.38	48.90
33X-3, 70.0-72.0	304.40	26.40	1.88	1.38	48.50
33X-5, 70.0-72.0	307.40	24.10	1.93	1.47	45.50
34X-1, 70.0-72.0	310.70	26.50	1.88	1.38	48.60
34X-3, 70.0-72.0	313.70	28.00	1.84	1.33	50.50
34X-5, 70.0-72.0	316.70	27.10	1.88	1.37	49.70
35X-1, 70.0-72.0	320.30	24.90	1.92	1.44	46.70
35X-3, 70.0-72.0	323.30	25.60	1.88	1.40	47.10
35X-5, 70.0-72.0	326.30	22.60	1.99	1.54	43.90
36X-1, 72.0-74.0	329.92	25.30	1.91	1.43	47.20
36X-3, 80.0-82.0	333.00	24.70	1.92	1.45	46.30
36X-5, 112.0-114.0	336.32	23.00	1.96	1.51	44.10
37X-1, 67.0-69.0	339.47	25.20	1.90	1.42	46.90
37X-3, 122.0-124.0	343.02	25.90	1.88	1.40	47.60
37X-5, 70.0-72.0	345.50	23.20	1.94	1.49	43.90
37X-6, 70.0-72.0	347.00	22.70	1.95	1.50	43.20
38X-1, 113.0-115.0	349.53	22.60	1.95	1.51	43.00
38X-3, 70.0-72.0	352.10	21.10	1.99	1.57	40.90
38X-5, 84.0-86.0	355.24	23.20	1.94	1.49	43.90
39X-1, 72.0-74.0	358.72	22.30	1.96	1.52	42.70
39X-3, 96.0-98.0	361.96	22.10	1.98	1.54	42.60
39X-5, 57.0-59.0	364.57	22.70	1.95	1.51	43.30
40X-1, 72.0-74.0	368.32	22.80	1.96	1.51	43.60
40X-3, 71.0-73.0	371.31	20.60	2.02	1.60	40.50
40X-5, 71.0-73.0	374.31	21.80	1.96	1.54	41.70
41X-1, 82.0-84.0	378.12	20.70	2.01	1.60	40.70
41X-3, 70.0-72.0	381.00	25.30	1.88	1.41	46.60
42X-1, 70.0-72.0	387.60	25.80	1.87	1.39	47.00
42X-3, 70.0-72.0	390.60	22.80	1.93	1.49	43.00
42X-5, 115.0-117.0	394.05	21.00	2.00	1.58	41.00
43X-1, 70.0-72.0	397.20	22.50	2.04	1.58	44.90
43X-3, 70.0-72.0	400.20	24.20	1.93	1.46	45.50
43X-5, 70.0-72.0	403.20	22.30	1.95	1.51	42.40
44X-1, 70.0-72.0	406.80	27.20	1.85	1.34	49.00
44X-3, 74.0-76.0	409.84	29.00	1.83	1.30	51.90
44X-5, 71.0-73.0	412.81	26.20	1.88	1.39	48.10
45X-1, 71.0-73.0	416.41	25.40	1.89	1.41	46.90
45X-3, 72.0-74.0	419.42	27.70	1.83	1.33	49.70
45X-5, 70.0-72.0	422.40	27.90	1.84	1.33	50.20
46X-1, 55.0-57.0	425.85	25.60	1.91	1.42	47.80
46X-3, 70.0-72.0	429.00	24.00	1.91	1.46	44.80
46X-5, 84.0-86.0	432.14	26.20	1.87	1.38	47.90
47X-1, 70.0-72.0	435.60	25.40	1.90	1.41	47.10
47X-3, 70.0-72.0	438.60	26.10	1.88	1.39	47.80
47X-5, 67.0-69.0	441.57	26.70	1.90	1.39	49.50
48X-1, 72.0-74.0	445.22	24.70	1.93	1.46	46.60
48X-3, 95.0-97.0	448.45	26.80	1.88	1.37	49.10
48X-5, 68.0-70.0	451.18	27.10	1.89	1.38	50.10
49X-1, 68.0-70.0	454.78	26.50	1.88	1.38	48.80
49X-3, 69.0-71.0	457.79	25.30	1.93	1.44	47.50
49X-5, 72.0-74.0	460.82	24.60	1.92	1.45	46.20
50X-1, 70.0-72.0	464.40	24.90	1.91	1.44	46.60
50X-3, 70.0-72.0	467.40	28.20	1.84	1.32	50.60
51X-1, 66.0-68.0	473.96	27.30	1.88	1.37	50.10
51X-3, 99.0-101.0	477.29	23.80	1.96	1.49	45.40
51X-5, 99.0-101.0	480.29	24.10	1.94	1.48	45.70
52X-1, 80.0-82.0	483.70	26.40	1.89	1.39	48.70
52X-3, 70.0-72.0	486.60	25.80	1.90	1.41	47.70
52X-5, 49.0-51.0	489.39	25.30	1.89	1.41	46.70
53X-1, 79.0-81.0	493.29	25.80	1.90	1.41	48.00

Table T23 (continued).

Core, section, interval (cm)	Depth (mbsf)	Water content (bulk wt%)	Density (g/cm³)		Porosity (%)
			Wet bulk	Dry bulk	
53X-3, 40.0-42.0	495.90	24.50	1.93	1.46	46.40
53X-5, 120.0-122.0	499.70	27.80	1.86	1.34	50.60
54X-1, 74.0-76.0	502.84	25.10	1.91	1.43	46.70
54X-3, 96.0-98.0	506.06	25.80	1.90	1.41	47.70
54X-5, 103.0-105.0	509.13	24.70	1.92	1.45	46.30
55X-3, 82.0-84.0	515.52	23.50	1.95	1.49	44.70
55X-5, 73.0-75.0	518.43	25.80	1.89	1.41	47.70
56X-1, 131.0-133.0	522.71	23.60	1.92	1.47	44.20
56X-3, 82.0-84.0	525.22	23.60	1.96	1.49	45.10
57X-1, 68.0-70.0	531.78	22.80	1.96	1.51	43.60
57X-3, 80.0-82.0	534.90	21.80	1.99	1.56	42.40
59X-5, 88.0-90.0	557.28	18.70	2.03	1.65	37.20
60X-1, 81.0-83.0	560.81	21.30	1.98	1.56	41.20
60X-3, 81.0-83.0	563.81	18.40	2.06	1.68	37.10
60X-5, 82.0-84.0	566.82	17.70	2.05	1.69	35.60
61X-1, 68.0-70.0	570.28	26.20	1.87	1.38	47.80
61X-3, 69.0-71.0	573.29	20.60	2.00	1.59	40.10
61X-5, 70.0-72.0	576.30	21.80	1.97	1.54	41.80
62X-1, 70.0-72.0	579.90	20.40	1.98	1.58	39.60
62X-3, 70.0-72.0	582.90	22.30	1.96	1.52	42.60
62X-5, 71.0-73.0	585.91	20.20	1.99	1.59	39.40
63X-3, 71.0-73.0	592.51	19.00	2.03	1.65	37.70
63X-5, 83.0-85.0	595.63	21.80	2.01	1.57	42.80
64X-1, 55.0-57.0	598.95	19.85	1.95	1.57	38.84
64X-3, 74.0-76.0	602.14	22.95	1.93	1.48	45.04
64X-5, 82.0-84.0	605.22	20.45	1.98	1.58	40.44
65X-1, 68.0-70.0	608.68	20.55	1.94	1.54	40.14
65X-3, 60.0-62.0	611.60	22.05	1.93	1.51	43.14
65X-5, 54.0-56.0	614.54	19.95	2.00	1.61	39.54
66X-1, 72.0-74.0	618.32	21.05	2.02	1.61	42.14
66X-3, 66.0-68.0	621.26	20.15	1.97	1.58	39.74
66X-5, 39.0-41.0	623.99	22.15	1.96	1.53	43.84
67X-1, 72.0-74.0	627.92	20.85	1.99	1.58	41.44
67X-3, 44.0-46.0	630.64	21.75	1.93	1.51	42.64
67X-5, 31.0-33.0	633.51	22.35	1.90	1.47	43.44
68X-1, 60.0-62.0	637.40	19.70	2.05	1.65	39.50
68X-3, 46.0-48.0	640.26	20.50	2.01	1.60	40.30
68X-5, 60.0-62.0	643.40	23.00	1.96	1.51	44.00
69X-1, 77.0-79.0	647.17	20.80	1.99	1.57	40.30
69X-5, 66.0-68.0	653.06	22.50	1.98	1.54	43.60
70X-1, 18.0-20.0	656.28	26.90	1.85	1.36	48.70
70X-3, 81.0-83.0	659.91	18.70	2.09	1.70	38.10
71X-1, 70.0-72.0	666.50	22.30	1.99	1.55	43.40
71X-3, 75.0-77.0	669.55	21.20	2.00	1.57	41.30
71X-5, 74.0-76.0	672.54	18.10	2.06	1.69	36.50
72X-1, 67.0-69.0	676.07	20.20	1.99	1.59	39.30
72X-3, 69.0-71.0	679.09	20.20	2.02	1.61	39.80
73X-1, 73.0-75.0	685.73	18.90	2.06	1.67	37.90
73X-3, 71.0-73.0	688.71	19.30	2.05	1.65	38.60
74X-1, 37.0-39.0	695.07	19.60	2.04	1.64	38.90
74X-3, 72.0-74.0	698.42	20.00	2.03	1.62	39.60
74X-5, 70.0-72.0	701.40	19.60	2.05	1.65	39.20
75X-1, 70.0-72.0	705.00	16.90	2.18	1.81	35.90
75X-3, 72.0-74.0	708.02	18.60	2.09	1.70	37.90
75X-5, 70.0-72.0	711.00	17.10	2.11	1.75	35.30
75X-6, 63.0-65.0	712.43	4.10	2.92	2.80	11.70
75X-7, 18.0-20.0	713.48	19.40	2.01	1.62	38.20
76X-1, 72.0-74.0	714.62	17.00	2.10	1.75	35.00
76X-3, 71.0-73.0	717.61	21.10	1.99	1.57	40.90
76X-5, 72.0-74.0	720.62	19.00	2.02	1.64	37.50
77X-1, 70.0-72.0	724.30	18.50	2.10	1.71	38.10
77X-5, 99.0-101.0	730.59	20.40	2.04	1.62	40.60
78X-1, 37.0-39.0	733.57	22.40	1.95	1.51	42.70
78X-3, 72.0-74.0	735.87	21.00	1.98	1.57	40.60
78X-5, 86.0-88.0	739.01	20.10	2.01	1.60	39.40
79X-1, 60.0-62.0	743.40	22.10	1.96	1.53	42.20
79X-3, 76.0-78.0	746.56	24.10	1.92	1.46	45.20
79X-5, 99.0-101.0	749.79	19.70	2.04	1.64	39.30

Table T23 (continued).

Core, section, interval (cm)	Depth (mbsf)	Water content (bulk wt%)	Density (g/cm³)		Porosity (%)
			Wet bulk	Dry bulk	
80X-1, 93.0-95.0	753.33	19.90	1.99	1.59	38.70
80X-3, 58.0-60.0	755.98	19.90	1.98	1.59	38.40
80X-5, 68.0-70.0	759.08	18.60	2.03	1.65	36.90
81X-1, 76.0-78.0	762.76	16.40	2.17	1.82	34.80
81X-3, 100.0-102.0	765.60	15.80	2.07	1.75	31.90
81X-5, 70.0-72.0	768.18	15.40	2.07	1.75	31.00
82X-1, 43.0-45.0	772.03	17.10	2.07	1.71	34.60
82X-3, 71.0-72.0	775.31	16.90	2.04	1.70	33.60
82X-5, 70.0-72.0	778.30	16.60	1.92	1.60	31.10
83X-1, 43.0-45.0	781.63	18.00	2.02	1.65	35.50
83X-3, 59.0-61.0	784.79	17.50	1.84	1.52	31.30
83X-5, 70.0-72.0	787.90	19.70	1.99	1.60	38.20
84X-1, 71.0-73.0	791.51	21.20	1.98	1.56	40.90
84X-3, 102.0-104.0	794.82	18.10	2.02	1.65	35.70
84X-5, 78.0-80.0	797.58	18.20	2.04	1.67	36.30
85X-1, 68.0-70.0	801.08	18.00	2.00	1.64	35.20
85X-3, 66.0-68.0	804.06	19.40	1.80	1.45	34.00
85X-5, 65.0-67.0	807.05	19.90	1.77	1.42	34.40
86X-1, 70.0-72.0	810.60	24.40	1.89	1.43	45.00
86X-5, 71.0-73.0	816.61	19.60	1.98	1.59	37.70
87X-1, 40.0-42.0	819.90	20.90	1.83	1.45	37.50
87X-1, 70.0-72.0	820.20	20.70	1.95	1.55	39.40
87X-3, 71.0-73.0	823.21	19.50	1.95	1.57	37.20
87X-4, 69.0-71.0	824.69	17.90	2.05	1.68	35.80
88X-1, 70.0-72.0	829.80	17.50	2.02	1.67	34.60
88X-3, 71.0-73.0	832.81	19.00	2.00	1.62	37.10
88X-5, 70.0-72.0	835.80	19.50	1.97	1.59	37.50
89X-1, 70.0-72.0	839.40	25.50	1.85	1.37	46.00
89X-3, 69.0-71.0	842.39	22.10	1.91	1.49	41.20
89X-4, 68.0-70.0	843.88	18.70	1.81	1.48	33.00
90X-1, 39.0-41.0	848.69	16.20	2.06	1.72	32.60
91X-1, 73.0-75.0	856.13	16.70	2.00	1.67	32.70
91X-3, 71.0-73.0	859.11	15.10	2.03	1.73	30.00
91X-5, 47.0-49.0	861.87	15.80	2.01	1.69	30.90
92X-1, 71.0-73.0	862.11	16.80	2.00	1.66	32.90
92X-3, 75.0-77.0	865.15	15.40	2.05	1.73	30.90
92X-5, 67.0-69.0	867.92	14.00	2.11	1.81	28.80
93X-1, 78.0-80.0	868.28	15.80	2.03	1.71	31.20
93X-3, 72.0-74.0	871.22	16.30	2.04	1.70	32.40
93X-5, 74.0-76.0	874.20	14.70	2.08	1.77	29.80
94X-1, 72.0-74.0	874.22	15.90	2.03	1.71	31.50
94X-3, 72.0-74.0	877.05	16.40	2.02	1.69	32.50
95X-1, 48.0-50.0	877.98	16.40	2.01	1.68	32.20

Note: Shaded cells = suspect data.

CHAPTER NOTES

N1. 6 July 2001–Errata: After this chapter was published, it was found that the captions for Figures **F9** and **F10** were reversed and that the power spectra curves in Figures **F10** and **F14** were erroneously correlated. The correct captions and figures appear in this version.

*Dates reflect file corrections or revisions.